

# **EXPERIMENTAL STUDY OF SUSPENSION FLOW IN OPEN CHANNELS**

**THÈSE N° 1824 (1998)**

PRÉSENTÉE AU DÉPARTEMENT DE GÉNIE CIVIL

**ÉCOLE POLYTECHNIQUE FÉDÉRALE DE LAUSANNE**

POUR L'OBTENTION DU GRADE DE DOCTEUR ÈS SCIENCES TECHNIQUES

**PAR**

**Massimo CELLINO**

Laurea di Dottore in Ingegneria Idraulica, Politecnico di Torino, Italie  
de nationalité italienne

acceptée sur proposition du jury:

Prof. W.H. Graf, directeur de thèse  
Prof. F. Gallerano, rapporteur  
Dr U. Lemmin, rapporteur  
Prof. D. Lyn, rapporteur  
Prof. P. Monkewitz, rapporteur  
Prof. M. Spreafico, rapporteur

Lausanne, EPFL  
1998

*Alla mia famiglia*

## ACKNOWLEDGMENTS

This thesis was completed at the *Laboratoire de Recherches Hydrauliques* (LRH) of the *Ecole Polytechnique Fédérale de Lausanne* (EPFL). The author wishes to express his thanks to Prof. Walter H. Graf, director of the LRH, for the opportunity to work in his team, for his guidance, and invaluable help.

The author thanks also Dr. U. Lemmin for his encouraging support, constructive suggestions, and critical comments. Many thanks go also to Dr. M. Altinakar for discussion and suggestions about this thesis.

The author is grateful to Prof. F. Gallerano from the *Dipartimento di Idraulica, Trasporti e Strade* of the University of Rome “*La Sapienza*”, Italy, Prof. D. Lyn from the *School of Civil Engineering* of the *Purdue University* at W. Lafayette, USA, Prof. P. Monkewitz from the *Laboratoire de mécanique des fluides* of the *EPFL*, Lausanne, Prof. M. Spreafico from the *Service hydrologique et géologique national*, at Berne, for serving on the doctoral committee, reading the manuscript carefully, and providing useful suggestions on this thesis.

Many thanks go also to Prof. G. Bianco and Prof. G. Pezzoli, from the *Politecnico di Torino, Italy*, for their support and suggestions and for their help.

The author wishes to thank also Ing. C. Perrinjacquet, Ing. Ph. Aviolat, Dr. W.C. Shen, Dr. T. Song, Dr. T. Rolland, and D. Hurther for extraordinary help in the use of the ultrasonic instrument ADVP and APFP.

The author has also benefited from discussions with his colleagues, Dr. B. Yulistiyanto, Dr. Z. Jiang, P. Hamm, K. Blanckaert, I. Istiarto and I. Fer and from the help of Mme Vollichart and Mme Guidetti.

Many thanks also to Dr. M. Bensimon and the staff at GEOLEP who allowed to use their installations and R. Fontanellaz and C. Leiser for their help in the hydraulic laboratory.

Finally, the author would like to express his gratitude to his family who has always supported him, without its help it would have been difficult to finish this thesis.

# Table of contents

ABSTRACT (In English)	IV
RESUMÉ (in French)	VI
RIASSUNTO (in Italian)	VIII
<b>1 INTRODUCTION</b>	
<b>1.1 Motivation of the research</b>	1-1
<b>1.2 Vertical concentration distribution</b>	1-1
<b>1.3 Diffusion coefficients</b>	1-4
<b>1.4 Thesis content</b>	1-5
<b>1.5 Conclusions</b>	1-6
<b>1.6 References</b>	1-6
<b>2 EXPERIMENTAL FACILITIES AND PROCEDURE</b>	
<b>2.1 Introduction</b>	2-1
<b>2.2 Description of the flume and its circuit</b>	2-1
<b>2.3 Flume's bed characteristics</b>	2-4
<b>2.4 Sediment characteristics</b>	2-5
<b>2.5 Experimental procedure</b>	2-5
<b>2.5.1 Set-up of the flume</b>	2-5
<b>2.5.2 Set-up of the APFP instrument</b>	2-6
<b>2.5.3 Suction method</b>	2-10
<b>2.6 Determination of the hydraulic parameters</b>	2-10
<b>2.6.1 Velocity and resistance parameters</b>	2-11
<b>2.6.2 Concentration parameters</b>	2-13
<b>2.6.3 Diffusion parameters</b>	2-13
<b>2.7 Conclusions</b>	2-15
<b>2.8 References</b>	2-15
<b>3 MEASUREMENTS OF SUSPENSION FLOW</b>	
<b>3.1 Introduction</b>	3-1
<b>3.2 Presentation of data</b>	3-3
<b>3.3 Velocity profiles</b>	3-7
<b>3.4 Turbulence intensity</b>	3-11
<b>3.5 Reynolds-stress distribution</b>	3-12
<b>3.6 Energy spectra distribution</b>	3-14

<b>3.7</b>	Turbulence scale	3-16
<b>3.8</b>	Concentration profiles	3-26
<b>3.9</b>	Diffusion coefficients	3-28
<b>3.10</b>	Experimental $\beta(y)$ -values	3-30
<b>3.11</b>	Practical use of $\bar{\beta}$ -values	3-31
<b>3.12</b>	Verification of the hypothesis of <i>Fortier</i> , 1967	3-35
<b>3.13</b>	Conclusions	3-38
<b>3.14</b>	References	3-38

## **4 CONCLUSIONS**

<b>4.1</b>	Introduction	4-1
<b>4.2</b>	Conclusions	4-1
<b>4.3</b>	Further research topics	4-5
<b>4.4</b>	References	4-6

## **APPENDIX A The Sonar ADVP/APFP Instrument**

<b>A 1</b>	Introduction	A-1
<b>A 2</b>	Doppler effect	A-1
<b>A 3</b>	Monostatic mode	A-4
<b>A 4</b>	Bistatic mode	A-9
<b>A 5</b>	Tristatic mode	A-13
<b>A 6</b>	APFP mode (Acoustic Particle Flux Profiles)	A-14
<b>A 7</b>	Conclusions	A-19
<b>A 8</b>	References	A-20

## **APPENDIX B CONCENTRATION DISTRIBUTION; ANALYSIS OF LITERATURE DATA**

<b>B 1</b>	Introduction	B-1
<b>B 2</b>	Analysis procedure	B-3
<b>B 3</b>	Remarks on the concentration distribution data used	B-6
<b>B 4</b>	Other types of experiments	B-8
<b>B 5</b>	Discussion	B-11
<b>B 6</b>	Conclusions	B-13
<b>B 7</b>	References	B-17

## APPENDIX C VELOCITY AND CONCENTRATION PROFILES IN NON-CAPACITY CONDITION

<b>C1</b>	Introduction	C-1
<b>C2</b>	Experimental procedure	C-2
<b>C3</b>	Velocity and turbulence-intensity profiles	C-5
<b>C4</b>	Turbulence spectra	C-6
<b>C5</b>	Micro and Macro turbulence scale	C-7
<b>C6</b>	Concentration profiles	C-10
<b>C7</b>	Diffusion coefficients	C-11
<b>C8</b>	Conclusions	C-13
<b>C9</b>	References	C-14

## APPENDIX D SUSPENSION FLOW OVER BED FORMS

<b>D1</b>	Introduction	D-1
<b>D2</b>	Experimental facilities and flow conditions	D-2
<b>D3</b>	Velocity measurements	D-5
<b>D4</b>	Spatial evolution of the flow structure	D-8
<b>D5</b>	Concentration measurements	D-13
<b>D6</b>	Conclusions	D-17
<b>D7</b>	References	D-18

## APPENDIX E VELOCITY-CONCENTRATION CORRELATIONS

<b>E1</b>	Introduction	E-1
<b>E2</b>	Four-quadrant analysis	E-4
<b>E3</b>	Filtration of the instantaneous velocity	E-5
<b>E4</b>	Filtration of the longitudinal mean velocity	E-8
<b>E5</b>	Filtration of the fluctuating velocities	E-10
<b>E6</b>	Filtration of the Reynolds stress	E-13
<b>E7</b>	Filtration of the sediment flux	E-14
<b>E8</b>	Mean event intervals	E-15
<b>E9</b>	Visual correlation between velocity and suspended concentration	E-17
<b>E10</b>	Conclusions	E-19
<b>E11</b>	References	E-29

## CURRICULUM VITAE

## ABSTRACT

The study of the sediment transport in open-channel as well as in river flow is of great importance for fluvial hydraulics. While the transport of sedimentary particles at the bed, as the bed-load, has been the subject of much research, less attention has been paid to the transport of sediments in suspension. This thesis is a contribution to our knowledge of the transport of sediments in suspension.

The most important theory on the vertical distribution of the mean sediment concentration in suspension flows is the diffusion-convection theory, given by the Rouse equation. This equation is rather simple and contains few parameters. About one of these parameters, the  $\beta$ -value, there is little known, despite its importance and physical meaning. One of the main aims of this thesis is to experimentally measure the  $\beta$ -values for different suspension flow configurations.

The major objective was to investigate suspension flows over moveable beds without bed forms and this in capacity condition. Since flows are at times not in capacity, i.e. the flows are not saturated with sediments, an additional study (see Appendix C) was also performed. Furthermore, two special runs were done (see Appendix D), where the bed was covered with artificial bed forms.

In order to evaluate the  $\beta$ -values, the vertical profiles of the mean velocity and its fluctuations as well as the mean concentration and its fluctuations had to be measured. This could only be done by using the new ultrasonic instrument (Acoustic Particle Flux Profiler, APFP), developed and assembled at the *Laboratoire de Recherches Hydrauliques* (LRH).

Suspension flows were investigated focusing on the possible modification of the clear-water turbulence by suspended sediments. The concentration was carefully measured and interpreted by the Rouse equation. In particular, the ratio of the sediment,  $\epsilon_s(y)$ , and momentum,  $\epsilon_m(y)$ , diffusion coefficients, being the  $\beta(y)$ -value, was for the first time, directly measured.

The strongest effect of particles on the flow was noticed on the vertical component of the turbulence intensity,  $\sqrt{v'^2}/u_*$ , which was considerably suppressed, when compared to clear-water flow. The longitudinal velocity,  $\bar{u}(y)$ , its turbulence intensity component,  $\sqrt{u'^2}/u_*$ , and the Reynolds stress,  $-\rho\bar{u}'\bar{v}'$ , were only slightly affected.

By using the APFP instrument, the instantaneous sediment concentrations,  $c_s$ , were, for the first time, directly measured. The calibration of the APFP instrument was achieved by measuring the mean concentration profiles,  $\bar{c}_s$ , with the suction method. The largest measured fluctuating concentrations,  $\sqrt{c_s'^2}$ , and sediment flux,  $\bar{c}_s'\bar{v}'$ , profiles were observed close to the bed, where the mean concentration is also very large.

The sediment,  $\epsilon_s$ , and the momentum,  $\epsilon_m$ , diffusion coefficients, which represent the “ability” of sediment and fluid particles to be diffused in the flow by turbulence, were computed from the APFP measurements. For suspension flows over plane-bed, the sediment diffusion-coefficient profiles are always smaller than the momentum ones,  $\epsilon_s < \epsilon_m$ . This indicates that

sediment particles undergo less diffusion than fluid particles; consequently the  $\beta$ -values are less than unity,  $\beta < 1$ . Thus, the usual assumption of  $\varepsilon_s = \varepsilon_m$ , that leads to  $\beta = 1$ , is not justified for the present measurements.

The Rouse equation gives a better agreement to the concentration distributions measured with the suction method, by using the experimental obtained  $\beta$ -values,  $\overline{\beta_{APFP}}$ , rather than by using  $\beta = 1$ .

For practical use, the experimental  $\overline{\beta_{APFP}}$ -values and the ones obtained by a best-fit (least-squares method) of the Rouse equation to some concentration distributions taken from the literature are summarized in a plot. It seems that the  $\overline{\beta}$ -values increase with either scaling parameters,  $v_{ss}/u_*$ , and  $(v_{ss}/u_*) \cdot (C_s/\bar{c}_{sa})$ .

The effects of suspended particles on the clear-water turbulence was also investigated in non-capacity suspension flows having increasing concentrations. The measurements show that, the suppression (damping) of the vertical component of the turbulence intensity – caused by suspended particles – increases with the depth-averaged concentration. The tendency of the  $\overline{\beta_{APFP}}$ -values to decrease approaching the capacity condition, i.e. increasing the concentration, was also found.

Suspension flows over bed forms were also investigated; in this study special attention was paid to the evolution of the flow structure behind the bed-form crest as well as the effect of bed forms on the  $\overline{\beta}$ -values. The bed-form crest seems to generate a high-turbulence region with consequent peaks in both the longitudinal and vertical turbulence-intensity profiles as well as in the Reynolds-stress profiles. This high-turbulence region enhances the sediment diffusion coefficient but suppresses the momentum one. As a consequence, we found that for suspension flows over beds with bed forms,  $\varepsilon_s > \varepsilon_m$ , leading to  $\overline{\beta} > 1$ .

The most important result of this thesis is a recommendation that the Rouse equation with an improved  $\overline{\beta}$ -value – itself to be estimated from the experimental plots obtained in this study – can be used to establish the dimensionless concentration profile of suspension flows. For beds without bed forms the  $\overline{\beta}$ -values are  $\overline{\beta} < 1$ , while for beds with bed forms the  $\overline{\beta}$ -values are  $\overline{\beta} > 1$ .

The correlation between the velocity fluctuations, associated with coherent structures (burst cycle), and the concentration was also investigated. From this study it becomes evident that the ejection event, being the most important phase of a burst cycle, is responsible of the erosion of sediment on the bed, behaving as an “injector” of sediments into the main flow.

# RESUMÉ

L'étude du transport de sédiments dans les écoulements à surface libre et dans les rivières est primordiale pour l'hydraulique fluviale. Si le transport de sédiments au fond a largement été étudié, l'étude du transport de sédiments en suspension a suscité moins d'attention. Cette thèse a pour but d'améliorer les connaissances du transport de sédiments en suspension.

La théorie de convection-diffusion est la plus importante sur la distribution verticale de la concentration moyenne de sédiments en suspension. Grâce à cette théorie l'équation de Rouse, largement utilisée en pratique, avait été obtenue. Cette équation est facile à utiliser tout en contenant peu de paramètres. Parmi ces derniers, le paramètre  $\bar{\beta}$  est peu connu malgré son importance. Un des buts de ce travail consiste à mesurer expérimentalement la valeur de  $\beta$  ( $\bar{\beta}$  représente sa valeur moyennée sur la profondeur) pour différents types d'écoulement.

L'objectif majeur était d'étudier les écoulements en suspension sur fond mobile sans formes de fond et en condition de capacité (saturation). Dans la mesure où les écoulements peuvent également exister en condition de non capacité, i.e. l'écoulement n'est pas saturé par les sédiments, une étude supplémentaire (Appendix C) a été prévue. De plus, d'autres expériences ont été effectuées (Appendix D) dans lesquelles le fond du canal était couvert de formes artificielles.

Pour l'évaluation des valeurs de  $\bar{\beta}$ , les profils verticaux de vitesse et ses fluctuations ainsi que la concentration et ses fluctuations doivent être mesurés. La vitesse bidimensionnelle instantanée,  $u(y, t)$  et  $v(y, t)$ , et la concentration instantanée,  $c_s(y, t)$ , ont été mesurées à l'aide d'un nouvel instrument, l'APFP (Acoustic Particle Flux Profiler), développé et construit au *Laboratoire de Recherches Hydrauliques* (LRH).

La concentration a été mesurée soigneusement et a été interprétée à l'aide de l'équation de Rouse. En particulier, le rapport du coefficient de diffusion de sédiments,  $\varepsilon_s$ , et de quantité de mouvement,  $\varepsilon_m$ , qui définit la valeur de  $\beta$ , a été mesuré pour la première fois. Une attention particulière a également été consacrée à la modification de la turbulence en eau claire produite par les particules suspendues.

Les écoulements en suspension montrent une forte diminution de la composante verticale de l'intensité de turbulence,  $\sqrt{v'^2}/u_*$ , par rapport aux écoulements en eau claire. La vitesse longitudinale,  $\bar{u}(y)$ , la composante longitudinale de l'intensité de turbulence,  $\sqrt{u'^2}/u_*$ , et la tension de Reynolds,  $-\rho\bar{u}'\bar{v}'$ , sont peu affectées.

Le calibrage de l'APFP a été effectué en mesurant les profils de concentration moyenne,  $\bar{c}_s$ , avec la méthode de succion. La concentration fluctuante,  $\sqrt{c'_s{}^2}$ , et les flux de sédiments,  $\bar{c}'_s\bar{v}'$ , maximaux, ont été observés au voisinage du fond où la concentration est également maximale.

Les coefficients de diffusion de sédiments,  $\varepsilon_s$ , et de quantité de mouvement,  $\varepsilon_m$ , qui représentent les taux de diffusion des particules solides et fluides dus à la turbulence, ont été calculés à partir des mesures faites avec l'APFP. Pour les écoulements sur fond plat le coefficient

de diffusion des particules est toujours inférieur à celui de quantité de mouvement,  $\varepsilon_s < \varepsilon_m$ . Cela signifie que les particules solides sont moins diffusées que les particules "fluides", donc  $\beta$  est inférieur à l'unité, i.e.  $\beta < 1$ . Par conséquent, l'hypothèse classique  $\varepsilon_s = \varepsilon_m$ , qui mène à  $\beta = 1$ , n'est pas justifiée par nos mesures.

L'équation de Rouse comparée avec les profils de concentration mesurés par succion donne de meilleurs résultats si on utilise les valeurs expérimentales moyennées sur la profondeur,  $\overline{\beta}_{APFP}$ , plutôt que  $\bar{\beta} = 1$ .

Pour une utilisation pratique, les valeurs expérimentales de  $\overline{\beta}_{APFP}$  et celles obtenues avec la méthode des moindre carrés appliquée à quelques distributions de concentration reportées dans la littérature, ont été résumées dans un graphique. Les valeurs de  $\overline{\beta}$  sont proportionnelles aux paramètres  $v_{ss}/u_*$ , et  $v_{ss}/u_* \cdot C_s/\bar{c}_{sa}$ .

Les effets des particules sur la turbulence en eau claire ont également été examinés dans le cas des écoulements en suspension en condition de non-capacité pour des concentrations croissantes. Les résultats montrent que la diminution de l'intensité de turbulence, provoquée par les particules, augmente avec la concentration moyenne. De plus, les valeurs de  $\overline{\beta}_{APFP}$ , diminuent en se rapprochant de la condition de capacité, c'est à dire en augmentant la concentration.

Dans cette thèse on a également étudié les écoulements en suspension sur des formes de fond. En particulier, nous avons examiné l'évolution de la structure turbulente derrière la crête d'une de ces formes de fond. L'effet des formes de fond sur les valeurs de  $\overline{\beta}$  a également été déterminé. Les résultats montrent que la crête des formes génère une région de haute turbulence qui se traduit par des pics observés dans les composantes longitudinales et verticales de l'intensité de turbulence ainsi que dans les profils de tension de Reynolds. Cette région accroît également le coefficient de diffusion des sédiments et, au même temps, diminue le coefficient de diffusion de quantité de mouvement. Par conséquent, pour les écoulements en suspension sur des formes de fonds, on obtient:  $\varepsilon_s > \varepsilon_m$ , ce qui implique,  $\overline{\beta} > 1$ .

Le résultat majeur de cette thèse est représenté par la détermination des valeurs correctes de  $\overline{\beta}$ , qui peuvent être obtenues aisément à l'aide de graphiques expérimentaux, pour l'établissement des profils de concentration moyenne. Pour des écoulements sur fond plat les valeurs de  $\overline{\beta}$  sont petites,  $\overline{\beta} < 1$ , mais pour des écoulements sur des formes de fond on obtient  $\overline{\beta} > 1$ .

Dans ce travail on a aussi étudié les corrélations existantes entre les fluctuations des vitesses reliées aux structures cohérentes (comme les bursts) et la concentration. On observe que la phase la plus importante d'un cycle de burst, appelée éjection, est responsable de l'érosion des sédiments au fond du canal. Cette phase représente une sorte d'injecteur de sédiments dans l'écoulement.

## RIASSUNTO

L'attenzione della ricerca scientifica nel campo del trasporto solido in idraulica fluviale è sempre stata rivolta prevalentemente al trasporto di sedimenti al fondo (bed-load). In questa tesi si è cercato di dare un contributo significativo all'altro possibile modo di trasporto solido: il trasporto di sedimenti in sospensione.

L'approccio teorico probabilmente più importante nello studio delle correnti in sospensione è rappresentato dalla teoria di convezione-diffusione. Da questa deriva l'equazione di Rouse, ampiamente utilizzata per la determinazione del profilo verticale della concentrazione media di sedimenti in sospensione. Nell'equazione di Rouse compare un parametro, usualmente denominato  $\beta$ , del quale poco si conosce nonostante la sua importanza ed il suo significato fisico. Uno degli obiettivi di questa tesi è la misura sperimentale del corretto valore di  $\beta$  per diverse configurazioni delle correnti in sospensione.

Lo studio sperimentale è stato effettuato principalmente su correnti saturate di sedimenti, su di un letto mobile ed in assenza di forme di fondo (fondo piatto). In appendice sono anche riportati i risultati di un ulteriore studio effettuato su correnti non saturate (appendice C) e su correnti in presenza di forme di fondo (Appendice D).

Per una corretta valutazione del valore di  $\beta$ , sono stati misurati i profili sperimentali della velocità, della concentrazione e delle rispettive fluttuazioni intorno al valore medio. Questo tipo di misura è stato possibile grazie all'utilizzo di un nuovo strumento (Acoustic Particle Flux Profiler, APFP) concepito e sviluppato al *Laboratoire de Recherches Hydrauliques* (LRH).

I profili di concentrazione sono stati interpretati per mezzo dell'equazione di Rouse. In particolare, il rapporto fra il coefficiente di diffusione dei sedimenti,  $\varepsilon_s(y)$ , e della quantità di moto,  $\varepsilon_m(y)$ , che rappresenta il valore di  $\beta(y)$ , è stato per la prima volta ottenuto sperimentalmente.

Nello studio si è anche cercato di valutare l'influenza dei sedimenti in sospensione sulla turbolenza del fluido portante (acqua dolce). L'effetto più consistente è stato osservato nel profilo della componente verticale dell'intensità di turbolenza,  $\sqrt{v'^2}/u_*$ , che risulta considerabilmente diminuito rispetto a quello normalmente osservato in caso di correnti di acqua limpida. I profili della velocità longitudinale media,  $\bar{u}(y)$ , della relativa intensità di turbolenza,  $\sqrt{u'^2}/u_*$ , e della tensione di Reynolds,  $-\rho\bar{u}'v'$ , risultano invece modificati solo debolmente.

Utilizzando il suddetto strumento (APFP) è stato possibile misurare per la prima volta, ed in modo diretto, la concentrazione istantanea di sedimenti,  $c_s$ . La necessaria calibratura dello strumento APFP è stata ottenuta deducendo la concentrazione media con il classico metodo per suzione. I valori più elevati della concentrazione fluttuante,  $\sqrt{c_s'^2}$ , e del flusso di sedimenti,  $\bar{c}'v'$ , sono stati registrati in vicinanza del letto, dove maggiore è la concentrazione media.

I coefficienti di diffusione dei sedimenti,  $\varepsilon_s$ , e della quantità di moto,  $\varepsilon_m$ , che indicano rispettivamente la facilità con la quale le particelle solide (sedimenti) e liquide (acqua) sono

diffuse dalla corrente ad opera della turbolenza, sono state calcolate a partire dalle misure effettuate dallo strumento APFP. Per le correnti in sospensione su fondo piano, il coefficiente di diffusione dei sedimenti è sempre minore del coefficiente di diffusione della quantità di moto,  $\varepsilon_s < \varepsilon_m$ . Questo indica che i sedimenti si diffondono meno facilmente delle particelle liquide; conseguentemente i valori di  $\beta$  risultano inferiori all'unità,  $\beta < 1$ . La pratica corrente di porre  $\varepsilon_s = \varepsilon_m$  e di conseguenza ipotizzare  $\beta = 1$ , non sembra quindi giustificata.

L'aderenza fra l'equazione di Rouse ed i profili di concentrazione media misurati per suzione risulta notevolmente migliorata utilizzando i valori sperimentali di  $\beta$ ,  $\overline{\beta_{APFP}}$ , piuttosto che il valore classico di  $\beta$ ,  $\beta=1$ .

Per un utilizzo pratico, i valori sperimentali di  $\beta$ ,  $\overline{\beta_{APFP}}$ , e quelli ottenuti adattando (metodo dei minimi quadrati) l'equazione di Rouse ai profili di concentrazione disponibili in letteratura, sono stati riassunti in un unico grafico. Il valore di  $\overline{\beta}$  sembra direttamente proporzionale ai parametri:  $v_{ss}/u_*$  e  $(v_{ss}/u_*) \cdot (C_s/\bar{c}_{sa})$ .

L'effetto delle particelle in sospensione sulla turbolenza dell'acqua limpida è stata studiata anche per correnti non saturate di sedimenti aventi crescenti livelli di concentrazioni medie. Le misure mostrano che la diminuzione (soppressione) della componente verticale dell'intensità di turbolenza, causata dalle particelle sospese, è proporzionale alla concentrazione media. È stata anche evidenziata la tendenza dei valori sperimentali di  $\overline{\beta}$ ,  $\overline{\beta_{APFP}}$ , a diminuire avvicinandosi alla condizione di saturazione della corrente.

Nello studio sperimentale delle correnti in sospensione, in presenza di forme di fondo, si è cercato di evidenziare l'evoluzione spaziale del flusso in vicinanza delle creste delle forme di fondo. L'effetto globale delle forme di fondo stesse sul valore di  $\overline{\beta_{APFP}}$  è stato ugualmente quantificato. Le creste sembrano generare nella loro scia dei picchi di entrambe le componenti, orizzontale e verticale, dell'intensità di turbolenza come pure della tensione di Reynolds. In questa scia il coefficiente di diffusione dei sedimenti,  $\varepsilon_s$ , è incrementato mentre quello della quantità di moto,  $\varepsilon_m$ , risulta diminuito. Nella sezione in cui sono state effettuate le misure si è ottenuto che  $\varepsilon_s > \varepsilon_m$ . Si è potuto quindi affermare che in presenza di forme di fondo il valore di  $\overline{\beta_{APFP}}$  è probabilmente superiore all'unità,  $\overline{\beta} > 1$ .

Il risultato principale di questa tesi è rappresentato dal miglioramento dell'equazione di Rouse ottenuto per mezzo dei valori sperimentali di  $\overline{\beta}$ . Detti valori possono essere valutati facilmente con l'ausilio dei grafici proposti in questo studio. Per correnti in sospensione in presenza di forme di fondo si ha  $\overline{\beta} > 1$ , mentre in presenza di fondo piano si ha  $\overline{\beta} < 1$ .

La correlazione fra le fluttuazioni di velocità associate a strutture coerenti, come il ciclo di burst, e la concentrazione istantanea di sedimenti è stata anche oggetto di indagine (appendice E). Si è osservato che l'eiezione (fase principale del ciclo di burst, caratterizzata da un rapido allontanamento dal letto,  $v' > 0$ , di un fluido lento,  $u' < 0$ ) è la principale responsabile dell'erosione e messa in sospensione dei sedimenti altrimenti giacenti sul letto.

# 1. Introduction

## 1.1 Motivation of the research

The hydraulics of sediment transport represents an intensively studied topic (see *Graf*, 1984, *Yang*, 1996). In particular, the sediment transport at the bed – the bed-load – has been the subject of innumerable works. Less attention has been paid to the transport of sediment in suspension. In the last decade great interest has been aroused in the study of the complex interaction between turbulence and suspended particles. This interest lead to a massive investigation on suspended-laden flows using sophisticated instruments such as Laser Doppler Velocimeter (*Muste and Patel*, 1997), Particle Image Velocimeter (*Garcia et al.*, 1996), or Sonar Doppler Velocimeter (*Thorne et al.*, 1996). The importance of the coherent structures on the diffusion of suspended particles in the flow as well as the effect of sediment particles on the turbulence intensity, has been pointed out. Much work must be still done to clearly describe the processes of interaction between the solid (sediment particles) and the fluid (water flow) phase for different conditions of flow and of concentration.

The most important theory on the vertical mean distribution of suspended concentration in sediment-laden flow is the diffusion-convection one. By this theory, the well-known equations, the Rouse or Hunt equations, have been derived. These equations have the merit to be rather simple and to contain few parameters. One of this parameter, the  $\beta$ -value, is little known even if it is important and physically meaningful.

This thesis represents an effort, undertaken to fill the existing knowledge gap on the interaction of suspended sediment particles and the fluid. The experimental measurement of the  $\beta$ -values has also been performed to improve the Rouse and Hunt equations by providing a criterion to choose better the parameters to use in these formulae.

## 1.2 Vertical concentration distribution

The distribution of sediment as suspended load is commonly obtained by consideration of the diffusion-convection equation, (see *Graf*, 1984, §8.3). In its general formulation it is expressed as:

$$\frac{\partial \bar{c}_s}{\partial t} = -\bar{u} \frac{\partial \bar{c}_s}{\partial x} - \bar{v} \frac{\partial \bar{c}_s}{\partial y} - \bar{w} \frac{\partial \bar{c}_s}{\partial z} + \frac{\partial}{\partial x} \left( \epsilon_{sx} \frac{\partial \bar{c}_s}{\partial x} \right) + \frac{\partial}{\partial y} \left( \epsilon_{sy} \frac{\partial \bar{c}_s}{\partial y} \right) + \frac{\partial}{\partial z} \left( \epsilon_{sz} \frac{\partial \bar{c}_s}{\partial z} \right) \quad (1.1)$$

where  $\bar{c}_s(y) = c_s - c'_s$ : mean suspended sediment concentration

$c_s$ ,  $c'_s$ : instantaneous and fluctuating concentration

$t$ : time

$x$ ,  $y$ ,  $z$ : streamwise, vertical and lateral coordinate

$u$ ,  $\bar{u}$ ,  $u'$ : streamwise instantaneous, mean and fluctuating velocities;  $u = \bar{u} + u'$

$v$ ,  $\bar{v}$ ,  $v'$ : vertical instantaneous, mean and fluctuating velocities;  $v = \bar{v} + v'$

$w$ ,  $\bar{w}$ ,  $w'$ : transversal instantaneous, mean and fluctuating velocities;  $w = \bar{w} + w'$   
 $\varepsilon_{sx}$ ,  $\varepsilon_{sy}$ ,  $\varepsilon_{sz}$ : streamwise, vertical and lateral sediment turbulent diffusion coefficients

Eq. 1.1 is valid for incompressible, turbulent flows in which the turbulent diffusion coefficients – predominant over the molecular ones - do not vary with concentration.

Assuming a steady-state condition, one-dimensionality – no change of concentration with respect to the time,  $t$ , to the longitudinal,  $x$ , and to the lateral,  $z$ , direction – eq 1.1 leads to the following equation:

$$v_{ss} \cdot \bar{c}_s + \varepsilon_{sy} \frac{\partial \bar{c}_s}{\partial y} = Cte = 0 \quad (1.2)$$

In this equation the velocity of the suspension flow is assumed equal to the liquid and to the sediment particle ones. It is customary to assume that the vertical mean velocity of the sediment particles represents the settling velocity of the particles in the fluid,  $\bar{v} = -v_{ss}$ . To simplify the computation the settling velocity is assumed in pure still clear water,  $v_{ss}$ . The constant of integration is taken as  $Cte=0$ , which does imply that at the water surface  $\bar{c}_s = 0$  for  $\varepsilon_{sy} = 0$ . Eq. 1.2 can be rewritten on the form:

$$v_{ss} \cdot \bar{c}_s + \varepsilon_s \frac{\partial \bar{c}_s}{\partial y} = 0 \quad (1.2bis)$$

where  $v_{ss}$  is settling velocity (assumed in still clear water) and  $\varepsilon_s = \varepsilon_{sy}$  is the sediment diffusion coefficient along the vertical direction.

Note, that eq. 1.2bis remains reasonably valid for small concentrations, say  $\bar{c}_s < 0.05 \text{ [m}^3/\text{m}^3\text{]} \cong 132 \text{ [kg/m}^3\text{]}$ .

Above eq. 1.2bis implies that the downward flux due to the gravitational settling,  $v_{ss}\bar{c}_s$ , and the upward sediment flux due to the turbulence of the flow,  $\bar{c}'_s v'$ , are in equilibrium; the latter is commonly expressed as:

$$\bar{c}'_s v' = -\varepsilon_s \frac{\partial \bar{c}_s}{\partial y} \quad (1.3)$$

Usually, it is assumed that the sediment diffusion coefficient,  $\varepsilon_s$ , and the momentum diffusion coefficient, which is nothing else than the turbulent (eddy) viscosity,  $\varepsilon_m = v_t$ , are closely related, such as:

$$\varepsilon_s = \beta \cdot \varepsilon_m \quad (1.4)$$

where  $\varepsilon_m$  is defined using the shear stress,  $-\rho \cdot \bar{u}'v'$ , by:

$$\bar{u}'v' = -\varepsilon_m \frac{\partial \bar{u}}{\partial y} \quad (1.5)$$

For uniform and unidirectional open-channel flow the vertical distribution of the momentum diffusion coefficient is given (see *Graf*, 1984, p. 173) by:

$$\varepsilon_m = \kappa \cdot u_* \cdot \frac{y}{h} (h - y) \quad (1.6)$$

where  $h$  is the flow depth,  $u_*$  is the shear velocity. The Karman constant,  $\kappa$ , has been assumed to be  $\kappa = 0.4$  for both clear-water and suspension flows according to Coleman's findings (Coleman, 1981).

Upon substitution of eq. 1.4 and eq. 1.6 into the diffusion-convection equation, eq. 1.2, after separation of the variables and upon integration in parts between the limits,  $a < y < h$ , the well known solution – often referred to as Rouse equation – is obtained:

$$\frac{\bar{c}_s}{\bar{c}_{sa}} = \left( \frac{h-y}{y} \frac{a}{h-a} \right)^z \quad (1.7)$$

where the Rouse number is defined such as:

$$z = \frac{v_{ss}}{\kappa u_*} \quad \text{or} \quad z' = \frac{v_{ss}}{\bar{\beta} \kappa u_*} = \frac{z}{\bar{\beta}} \quad \text{where: } \bar{\beta} = \frac{1}{h-a} \int_a^h \beta(y) dy \quad (1.8)$$

The reference concentration,  $\bar{c}_{sa}$ , is usually evaluated at  $a = 0.05 \cdot h$ , which represents a vertical position in the flow. For  $y > a$  the sediments are supposed to be transported in suspension while for  $y < a$  the sediments are part of the bed load. With such a definition of the reference concentration, the resulting sediment transport as suspended load is in full *capacity* (saturation).

A sediment-laden flow is defined as *capacity* flow when a layer of sediment, composed of the same sediment as is in suspension, is present on the bed. When flow transports the full capacity of sediment – at saturation – one may consider the flow to be in a sedimentary equilibrium, this means that deposited particles can be readily replaced by eroded ones. Any further addition of sediments to the flow leads to a deposition of sediments on the channel bed without an increase of the suspended sediment concentration. If a flow is in *non-capacity* condition there is no active sediment layer on the bed. All the sediments added to the flow are kept suspended. A further addition of sediment to the flow leads to an increase of the sediment concentration without a deposition on the bed.

If the concentration can not be considered small, say  $\bar{c}_s > 0.05 \equiv 132 \text{ [kg/m}^3]$ , the following equation – firstly given by Hunt (see Graf, 1984, p.185) – must be used instead of eq. 1.2bis, such as:

$$v_{ss} \bar{c}_s (1 - \bar{c}_s) + [\varepsilon_s + \bar{c}_s (\varepsilon_m - \varepsilon_s)] \frac{\partial \bar{c}_s}{\partial y} = 0 \quad (1.9)$$

Eq. 1.9 is a general differential equation for the vertical distribution of suspended matter; this equation is valid for every value of suspended concentration taking into account the volume of sediment particles,  $\bar{c}_s$ , and the volume of water,  $(1 - \bar{c}_s)$ , per unit volume of mixture. If the solid concentration can be considered small, eq. 1.9 is reduced to eq. 1.2bis. Note, that eq. 1.9

do not take into account the interactions among particles and between fluid and particles. These interactions could be important for hyperconcentrated flows when the concentration is very high,  $\bar{c}_s > 10\%$ . Introducing eqs. 1.4 and 1.6 into the eq. 1.9 one obtains the following equation:

$$\frac{\kappa \cdot u_*}{v_{ss}} \cdot \frac{y}{h} (h - y) \cdot \frac{\partial \bar{c}_s}{\partial y} + \frac{(1 - \bar{c}_s) \cdot \bar{c}_s}{\beta + \bar{c}_s \cdot (1 - \beta)} = 0 \quad (1.10)$$

Upon integration in parts between the limits,  $a < y < h$ , eq. 1.10 gives the so-called Hunt equation:

$$\frac{\bar{c}_s}{c_{sa}} = \left( \frac{1 - \bar{c}_s}{1 - c_{sa}} \right)^{\frac{1}{\beta}} \left( \frac{h - y}{y} \frac{a}{h - a} \right)^z \quad (1.11)$$

Note that eq. 1.11 is an implicit equation. The plot and the fit of eq. 1.11 to the measured vertical mean concentration profile has to be done in a numerical way.

### 1.3 Diffusion coefficients

One of the key aspects of the theory on the vertical concentration distribution is the relation between the turbulent sediment and momentum diffusion coefficients. It is customary to correlate them by using a coefficient, usually called  $\beta$ , by the following equation:

$$\varepsilon_s = \beta \cdot \varepsilon_m \quad (1.4)$$

The  $\beta$ -value represents the difference in the diffusion of a sediment particle and the diffusion of a liquid (water) particle in the flow. If  $\beta > 1$ , this means that the solid particles diffuse more readily than the liquid ones; this is usually the case in sediment-laden jet (and open channel) flows in which the solid particles are “ejected” from turbulent eddies by centrifugal forces. If  $\beta = 1$ , this means that the solid particles follow readily the movement of the fluid; this is the case for very small particles or particles with density,  $\rho_s$ , close to the density of the water,  $\rho_w$ . If  $\beta < 1$ , this means that the solid particles are diffused less readily than fluid particles; this is possible if solid particles follow the turbulent eddies only for a part of their lifetime or if the turbulence is so strong for the solid particles to follow the high intensity fluid movements.

The turbulent Schmidt number,  $Sc$ , is usually defined as the ratio of the momentum diffusion coefficient and the molecular transport coefficient (Hinze, 1975, p. 293). Analogously, some authors introduced the turbulent Schimdt number defined as  $Sc = \varepsilon_m / \varepsilon_s$ . The relation of  $Sc$  with the  $\beta$ -value used here is simple:  $Sc = 1/\beta$ .

In this thesis using a Sonar instrument – Acoustic Particle Flux Profiler (APFP) – it has been possible to measure *at the same time* both the profiles of the *instantaneous suspended sediment concentration* and the *instantaneous longitudinal and vertical velocities* (see Appendix A). Thus, the sediment flux profile,  $\bar{c}_s v'(y)$ , has been measured directly and the vertical profile of the sediment diffusion coefficient,  $\varepsilon_s(y)$ , could be computed by its definition, see eq. 1.3, such as:

$$\varepsilon_s(y) = -\frac{\overline{c'_s v'(y)}}{\frac{\partial \bar{c}_s(y)}{\partial y}} \quad (1.12)$$

The velocity covariance,  $\overline{u'v'}$ , has been measured using the same APFP instrument. This led to the evaluation of the Reynolds-stress profile,  $-\rho \cdot \overline{u'v'}(y)$ . The longitudinal mean velocity profile,  $\bar{u}(y)$ , has also been measured, therefore the momentum diffusion coefficient profile, see eq. 1.5, could be calculated, such as:

$$\varepsilon_m(y) = -\frac{\overline{u'v'(y)}}{\frac{\partial \bar{u}(y)}{\partial y}} \quad (1.13)$$

The depth-averaged values of the sediment and momentum diffusion coefficient can also be computed:

$$\overline{\varepsilon_s} = \frac{1}{h-a} \int_a^h \varepsilon_s(y) dy ; \quad \overline{\varepsilon_m} = \frac{1}{h} \int_0^h \varepsilon_m(y) dy \quad \text{where } h: \text{flow depth} \quad (1.14)$$

Since both the sediment and the momentum diffusion coefficient profiles were known, also the vertical distribution of the measured  $\beta$ -value could be calculated. In fact, by its definition, see eq. 1.4, it is possible to write:

$$\beta(y) = \frac{\varepsilon_s(y)}{\varepsilon_m(y)} = \frac{\overline{c'_s v'(y)}}{\overline{u'v'(y)}} \quad (1.15)$$

The depth-averaged value of the  $\beta(y)$ -value has been calculated, such as:

$$\overline{\beta} = \frac{1}{h-a} \int_a^h \beta(y) dy \quad (1.16)$$

Using the definition of eq. 1.16 the  $\beta(y)$ -values have been evaluated experimentally (see Appendix A and §3.22) using the APFP instrument. The  $\beta(y)$ -values have also been obtained by a best-fitting technique of the Rouse equation, eq. 1.11, to the vertical mean concentration profiles measured by the suction method (see Appendix B).

## 1.4 Thesis content

The diffusion-convection approach has been used to interpret the results of the experimental investigation of suspension flows in capacity condition over plane bed. Two kinds of sediments have been used, namely sand I ( $d_{50} = 0.135$  [mm]) and sand II ( $d_{50} = 0.230$  [mm]); the results

can be found in ch. 3. The description of the installation facilities and the APFP instrument is presented in ch. 2 and Appendix A, respectively.

Suspension flows (sand I) in non-capacity condition over plane bed have been investigated as well. The results are shown in Appendix C.

A literature review (see Appendix B) put into evidence a substantial difference between the  $\bar{\beta}$ -values obtained investigating suspension flows in capacity condition over plane bed and over bed forms.

For sake of comparison, an investigation of suspension flows (using sand I) in capacity condition over bed with bed forms has been performed (see Appendix D).

As underlined in section 1.1, the coherent structures (especially the bursting cycle) are thought to be responsible for the suspension mechanics. A study of the complex mutual interaction between bursting cycles and suspended sediments (sand I and sand II) is presented in the Appendix E.

## 1.5 Conclusions

In this chapter the diffusion-convection theory is presented and the resulting equation – the Rouse equation, eq. 1.7 – is discussed. In case of very large suspended concentration,  $\bar{c}_s > 0.05 \cong 132 \text{ [kg/m}^3\text{]}$ , one should use the Hunt equation, eq. 1.11, instead of eq. 1.7. The Rouse and Hunt equations express the vertical suspended concentration distribution, for  $a < y < h$ , in case of suspension flows in uniform condition. Close to the bed, for  $y < a$ , the sediments are thought to be part of the bed load. Note, that the reference concentration,  $c_{sa}$ , is defined at  $y = a$  and represents, thus, the largest concentration of sediments transported in suspension.

The experimental determination of the  $\bar{\beta}$ -values to be used in the Rouse equation is one of the major goals of this thesis. The APFP instrument, able to measure simultaneously the instantaneous suspended concentration and velocity, has been used to obtain the sediment flux,  $\bar{c}_s v(y)$ , the momentum,  $\varepsilon_m(y)$ , and the sediment,  $\varepsilon_s(y)$ , diffusion coefficient. Subsequently, the  $\beta(y)$ -value has been computed by its definition  $\beta(y) = \varepsilon_s(y)/\varepsilon_m(y)$  and its depth-averaged value,  $\bar{\beta}$ , used in the Rouse or Hunt equation.

## 1.6 References

- COLEMAN, N. L. (1981). "Velocity profiles with suspended sediment." *J. Hydr. Res.*, vol. 19, N° 3, pp. 211-229.
- GARCIA, M., NINO, Y. and LOPEZ, F. (1996). "Laboratory Observations of Particle Entrainment into Suspension by Turbulent Bursting", in *Coherent Flow Structures in Open Channels*, Wiley & Sons Ltd, Chichester, UK.
- GRAF, W. H. (1984). *Hydraulics of Sediment Transport*, Water Resource Publications, Littleton, CO (USA).
- HINZE, J. O. (1975). *Turbulence*. McGraw-Hill, New York.

MUSTE, M. and PATEL, V. C. (1997). "Velocity profiles for Particles and Liquid in open-channel flow with suspended sediment." *J. Hydr. Engr.*, vol. 123, No. 9, pp. 742-751.

THORNE, P. D., HARDCASTLE, P. J. and HOGG, A. (1996). "Observation of Near-bed Suspended Sediment Turbulence Structures using Multifrequency Acoustic Backscattering" in *Coherent Flow Structures in Open Channels*, Wiley & Sons Ltd, Chichester, UK.

YANG, C. T. (1996). *Sediment Transport: Theory and Practice*, McGraw-Hill, New York.



## **2. Experimental facilities and procedure**

### **2.1 Introduction**

In this chapter are described the flume used in the experiments and the flow circuit. Subsequently, the bed and sediment characteristics and the measuring equipment are presented. The methods to reduce the measured time series into hydraulic parameters which characterize the flow are also discussed.

### **2.2 Description of the flume and its circuit**

The measurements were done in a 16.8 [m] long, 0.60 [m] wide and 0.80 [m] high flume at the Laboratoire de Recherches Hydrauliques (LRH) at the Ecole Polytechnique Fédérale de Lausanne (EPFL). The flume can be tilted around a pivoting point, from slopes of -1 [%] up to + 9 [%]. The flume has glass walls and a smooth steel floor which can be modified according to the purpose of the investigation. In Fig. 2.1 a view of the channel is shown. A detailed description can be found in *Suszka, 1988*.

In Fig. 2.2 a sketch (not to scale) of the flume and the flow circuit is presented. A grid (1) and a straightener (2) were placed at the entrance of the channel to attenuate flow irregularities. The first 3 [m] of the channel have a rigid bed made of concrete cubes (3) to generate a fully-developed turbulence. A floating polystyrene plate (4), fixed to the channel structure, attenuates waves due to the entrance in the channel.

The measuring section (8) is located 13 [m] from the entrance of the channel; in this section both the suction equipment and the sonar instrument (APFP) operate. The suction equipment is used to draw samples from the suspension flow. It is composed by a pipette (5) connected by flexible tubes to an air-compressed pump (6) that draws mixture samples (7) from the flow. The pipette can be regulated vertically in order to sample at different levels. The pump can be regulated to draw samples in an isokinetic condition, i.e. the velocity of the flow into the pipette top is equal to the velocity of the flow surrounding it. This condition is important to avoid a perturbation of the flow.

The sonar instrument (Acoustic Particle Flux Profiler, APFP) (9) operates in the measuring section (8). By emitting and receiving ultrasonic waves this instrument measures both the instantaneous velocity profiles – exploiting the Doppler effect (see *Rolland, 1994*) – and the instantaneous suspended concentration profiles – exploiting the proportionality between the suspended concentration and the ultrasonic echo intensity (see *Shen, 1997*).



Fig. 2.1: View of the channel

The APFP instrument has been calibrated, for each run, by comparing the mean echo-intensity profile (measured with the APFP) and the mean sediment concentration profile (measured with the suction method) in the same measuring section (8). In this way, a calibration curve could be obtained. A detailed description of the instrument principle can be found in Appendix A; for more information about the instrument electronics see *Shen*, 1997, and *Shen and Lemmin*, 1996. The APFP instrument is connected to a Macintosh computer (10) that controls the acquisition and records the velocity and echo-intensity profiles. The sonar transducers (11) emitting and receiving ultrasonic waves are installed above the flow surface and below the channel bed; this instrument does not perturb the flow except very close to the free surface.

At the end of the channel, a control weir (12) can be regulated to adjust the uniformity of the flow; subsequently, the flow falls in a collection tank (13). A hydrocyclone (14) was used, at the end of every run, to separate a part of the sediment particles from the water. In this way it was possible to recycle some sediments.

Two pumps, P1 (45 [kW]) and P2 (15 [kW]), were connected to the collection tank. They can be used separately or in parallel according to the discharge needed. The recirculation is generated, closing V7, with pump P1 or P2, opening the valve M1, and the valves M4-V3-V1 or M2-V2 respectively. The other valves were closed.

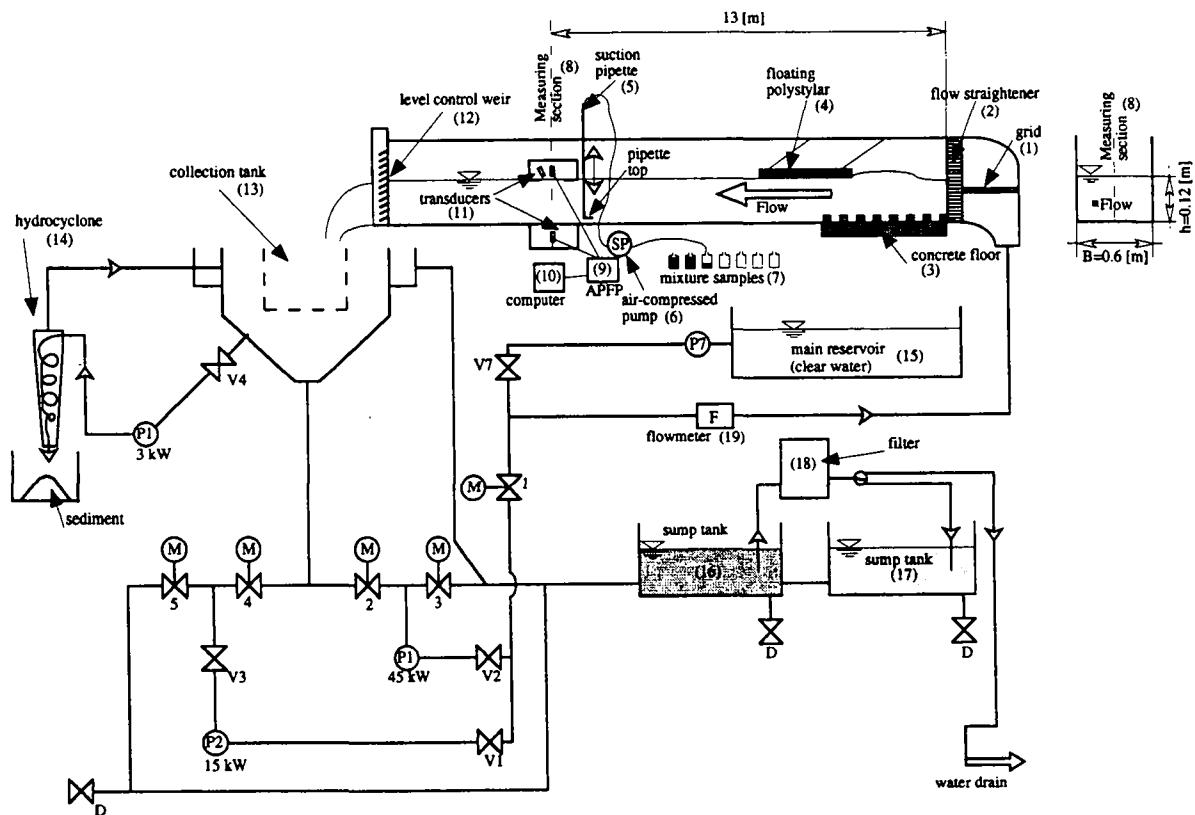


Fig. 2.2: Schematic of the flume and water circuit (not to scale)

Clear water was taken from the main reservoir (15) of the LRH (Laboratoire de Recherches Hydrauliques) by using the pump P7 and keeping open the manual valve V7. Once part of suspended sediments was separated using the hydrocyclone (14), the sediment-laden water was stocked in two sump tanks (16), (17) in which coarser particles settled down. A filter (18) was normally used to eliminate the finest particles. A magnetic flowmeter (19) measured continuously the discharge flowing in the circuit.

### 2.3 Flume's bed characteristics

The original steel floor of the channel was covered by rough plates. Each plate was waterproofed using putty to avoid infiltration of sediments on the steel floor. In Fig. 2.3 is shown a schematic of the rough plate installation. To simulate flow with bed forms, some artificial sand waves were also glued on the rough plate (see Appendix D).

A mean height of roughness,  $k_s = 0.0048 \text{ [m]}$ , was obtained by averaging the measured height of 40 individual elements randomly selected on the surface layer of the plate.

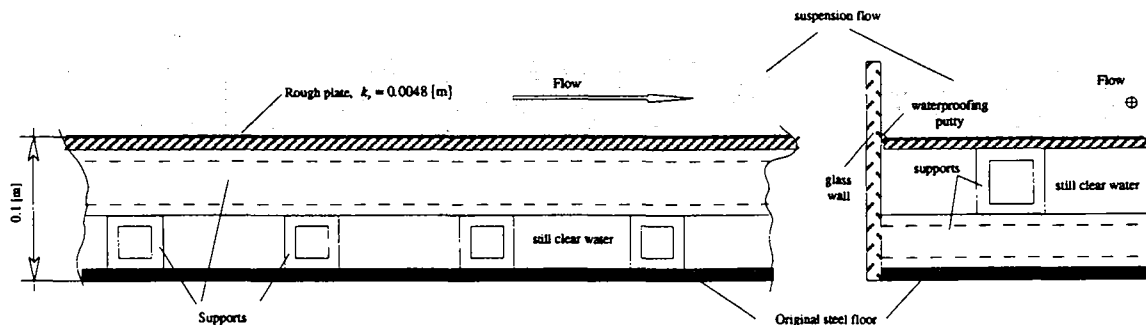


Fig. 2.3: Rough plate and original steel floor

Most of the research deals with flows in *capacity* condition. In this condition the rough plate was covered with a layer of the same sediment as is in suspension. The existence of the sediment layer on the bed was verified optically by observing if the orange colored rough plates were covered by the white sediment layer. Subsequently, the thickness of the sediment layer was measured by limnimeters. Usually, the sediment layer thickness was constant along the channel,  $\approx 2 \text{ [mm]}$ ; in this case the bed slope,  $S_b$ , was equal to the channel slope,  $S_f$ . The latter was read on a graded scale, previously calibrated using a precise optical instrument.

Some flow in *non-capacity* condition were also investigated (see Appendix C). In this condition all the sediments injected to the flow were kept suspended and no accumulation of sediment on the plate were observed.

## 2.4 Sediment characteristics

Two types of sediment were used in this study: sand I and sand II. Their principal characteristics are summarized in Table 2.1.

Type	Commercial name	Diameter			Density $\rho_s$	Settling vel. $v_{ss}$
		$d_{50}$ [mm]	$d_{30}$ [mm]	$d_{80}$ [mm]		
Sand I	DPTF AFA 96 ±6	0.135	0.121	0.171	2650	12.0
Sand II	Molochite™ 50-80DD	0.230	0.180	0.280	2650	21.0

Table 2.1: Summary of sediment characteristics

The sediment sand I was natural sand normally used as aggregate in several applications. Sand II (Molochite™) is a hard, abrasion resistant alumino-silicate refractory aggregate material produced by the calcination of specially selected china clays. Characteristic diameters as well as density were furnished by the producer, G. Gauthier (GE, Switzerland) and ECC International (UK) respectively, and checked by a granulometric analysis made in the Rock Mechanic Laboratory at the EPFL.

The settling velocity in still clear water was evaluated from the characteristic diameter,  $d_{50}$  (see *Graf*, 1984, p.45).

The sediment particles chosen fulfilled the requisites imposed by the Author:

- i) Particles small enough to follow the high-frequency movements of the flow,
- ii) Particles large enough to avoid diffraction of the emitted ultrasonic waves,
- iii) non-cohesive particles

## 2.5 Experimental procedure

In this section all the procedures, the set-up of the flume and of the capacity flow, the performance of the suction method, the set-up and the calibration of the APFP instrument, are discussed.

### 2.5.1 Set-up of the flume

To obtain a suspension flow it is firstly necessary to generate a clear water flow having the same channel slope,  $S_f$ , and flow depth,  $h$ . Firstly, the channel slope,  $S_f$ , was fixed mechanically and its value was read on a graded scale, previously calibrated using a precise optical instrument. Fresh water was then taken from the main reservoir (see Fig. 2.2) and recirculated adjusting the discharge by manually operating the pumps P1 or P2. The value

of the discharge,  $Q$  [ $\text{m}^3/\text{s}$ ], given by a magnetic flowmeter installed in the recirculating circuit, was chosen in a way to give the flow depth,  $h$ , equal to  $h=0.12$  [m]. This depth permits to investigate efficaciously the flow using the APFP instrument (see Appendix A).

The uniformity of the flow was obtained by adjusting the level control weir (12) and was verified by measuring the flow depth in some sections along the channel by using limnimeters. Only after the uniformity of the flow was assured, sediments were added slowly to the recirculating flow until the capacity flow was achieved. The capacity condition of the flow was verified observing if the white-colored sediment layer covered the orange-colored rough plates (see § 2.4). The measurements started after 4 [h] of flow recirculation in capacity condition. In Appendix C the results of an investigation of flows in *non-capacity* condition are presented while in Appendix D are reported the results of the investigation of suspension flow over bed form in capacity condition.

### 2.5.2 Set-up of the APFP instrument

The operation and installation of the APFP instrument are widely described in Appendix A. Here, the procedure followed to use the APFP are reported.

The APFP instrument was set-up only after that the suspension flow, having the assigned bed slope,  $S_b$ , and flow depth,  $h$ , was verified to be in the required conditions. The set-up of the APFP instrument consists of two parts, namely: i) transducers' installation and ii) elimination of acoustic noises.

The first part of the set-up deals with the installation of the transducers in their correct position (see Appendix A). It is important to verify the coaxiality of the vertical transducers and the position of the tilted transducer, but also to verify that the mylar-film – plastic film normally used to separate the transducers' housing and the flow (see Appendix A) – of the surface housing is permanently in contact with the water flow surface. If the contact is not assured the ultrasonic waves cannot propagate along the flow column.

More difficult is the control of the contact between the flow and the mylar film at the channel bed. The mylar film is acoustically transparent: almost all the acoustic energy passes through this film, but if the film is dirty or if air bubbles are present, see Fig. 2.4, the waves can not penetrate into the flow because of reflection by air bubbles. It is sufficient to clean the film and eliminate the air bubbles to solve the problem.

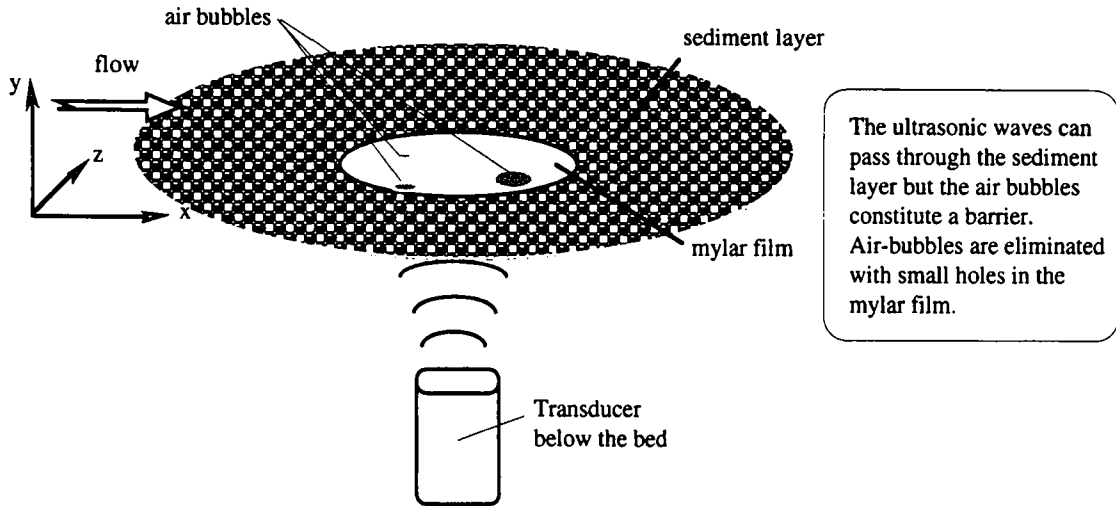


Fig. 2.4: Air bubbles below the bed mylar film

The APFP instrument emits and receives high-frequency ultrasonic waves. Good sound-proofing is then very important to avoid fixed ultrasonic echoes due to acoustic multi-reflections. A fixed ultrasonic echo in fact can affect seriously the measurements of both velocity and concentration if it is superimposed on the useful signal coming from the flow. The fixed echoes affecting the measurements are produced by a wrong installation of the APFP instrument. Here, the three main causes of fixed ultrasonic echoes are presented.

### 1) Multi-reflection of ultrasonic waves

If the transducer installed below the bed is exactly vertical, the emitted ultrasonic wave can be multi-reflected (see Fig. 2.5). For this reason the bed transducer is tilted on the vertical (along the transversal direction) by an angle of nearly  $1^\circ$ . In this way the emitted ultrasonic wave, reflected by the sediment layer, can not be recorded more than once, see Fig. 2.5.

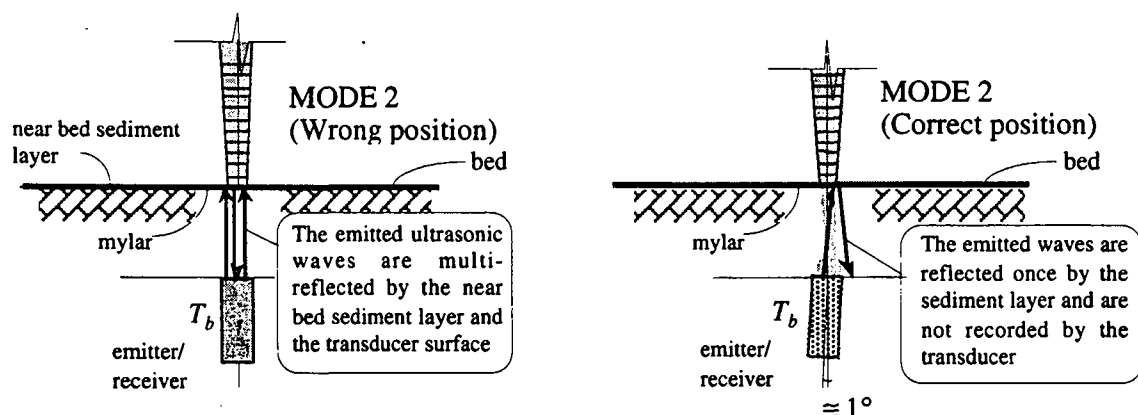


Fig. 2.5: Wrong and correct position of the bed vertical transducer

## 2) Not correct sound-proofing of the water filled housing

Ultrasonic waves are also reflected by the housing walls. The consequent multi-reflection can be attenuated by glueing a layer of soundproof material on the housing walls. In Fig. 2.6 a sketch of the possible path of multi-reflected waves is presented.

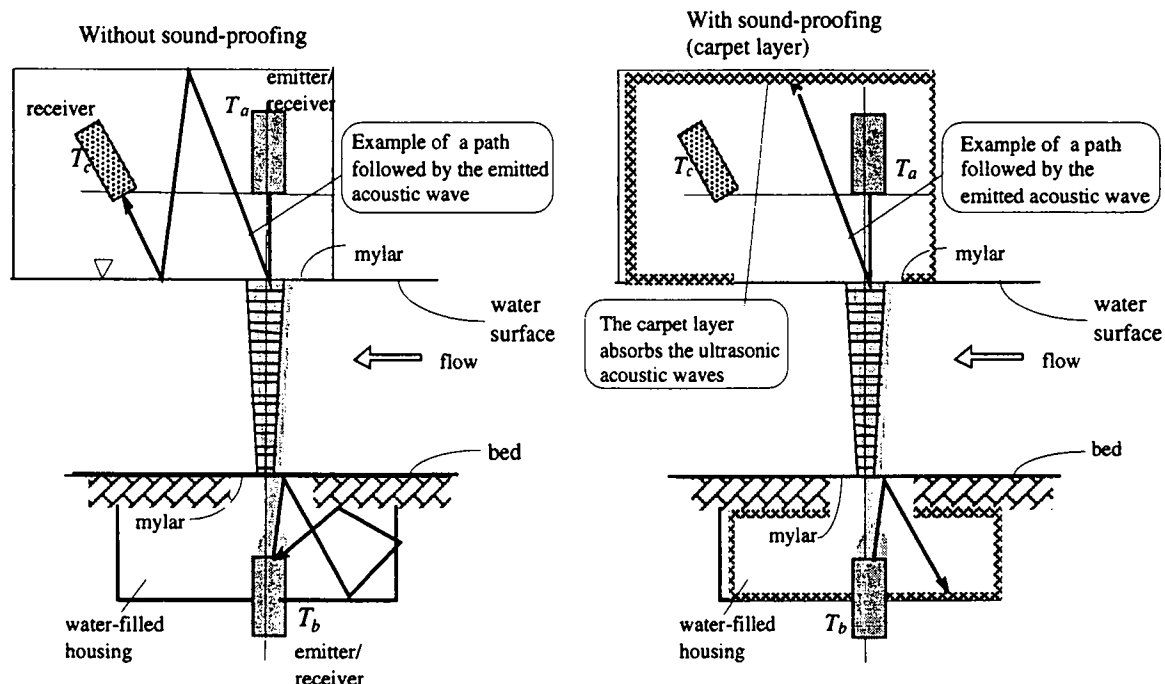


Fig. 2.6: Housing with and without sound-proofing

Generally a layer of carpeting leads to good results especially if the Pulse Repetition Frequency (PRF) is not too high ( $PRF \approx 1000$  [Hz], see Appendix A).

## 3) APFP energy level

The intensity of the emitted wave can be adjusted by operating on the power of the electronic ultrasonic wave generator. The emitted wave intensity should not be too high because the electronic device converting the ultrasonic echo signal into electric signals would be saturated. On the other hand, the signal must be strong enough to dominate the inevitable electronic noise.

The final check of the APFP instrument is performed with an oscilloscope visualizing the ultrasonic signal. As described in Appendix A the APFP instrument works alternatively into two modes. In mode 1 the surface transducer works alternatively as emitter and receiver while the bed transducer receives only the forward scattered signal. In Fig. 2.7 is presented a typical (correct) echo-intensity signal observed on the oscilloscope in mode 1. The backscattered signal recorded by the surface transducer represents the echo intensity

that is proportional to the suspended concentration. In the signal of Fig. 2.7 the two mylar echoes and the echo due to the sediment layer on the bed are clearly evident. The part of the signal recorded on a magnetic support is the one corresponding to the gates shown in the upper part of the oscilloscope screen.

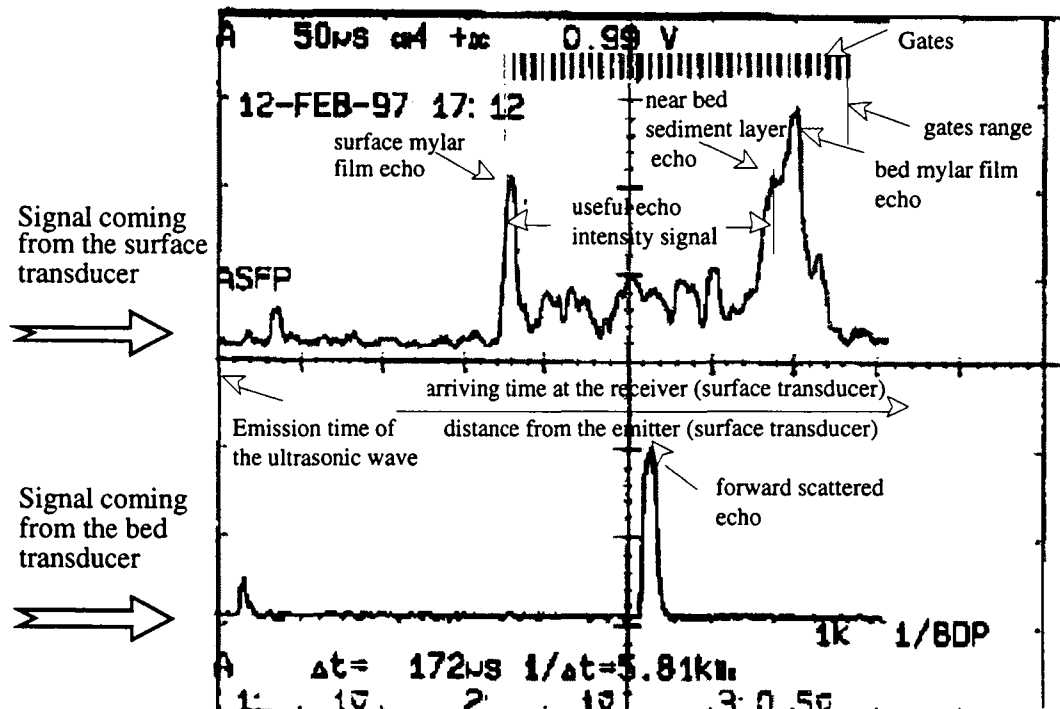


Fig. 2.7: Correct APFP signal (mode 1)

The signal recorded by the bed transducer, forward-scattered echo, represents the reception of the emitted wave that has traveled from the surface transducer (emitter) to the bed transducer (receiver). Since the emitted wave is an ultrasonic pulse, the received forward-scattered signal will also be an ultrasonic pulse. The signal between the surface mylar echo and the sediment layer echo is the useful signal recorded to compute – after the calibration of the APFP – the instantaneous vertical suspended concentration profiles.

In Fig. 2.8 is presented a typical signal visualized on an oscilloscope during the mode 2. The signal coming from the bed transducer shows the two mylar echoes and the echo due to the sediment layer. Note the parasite echo close to the surface mylar film: this echo has no physical meaning but does not perturb the measurements being not recorded (out of the gates range).

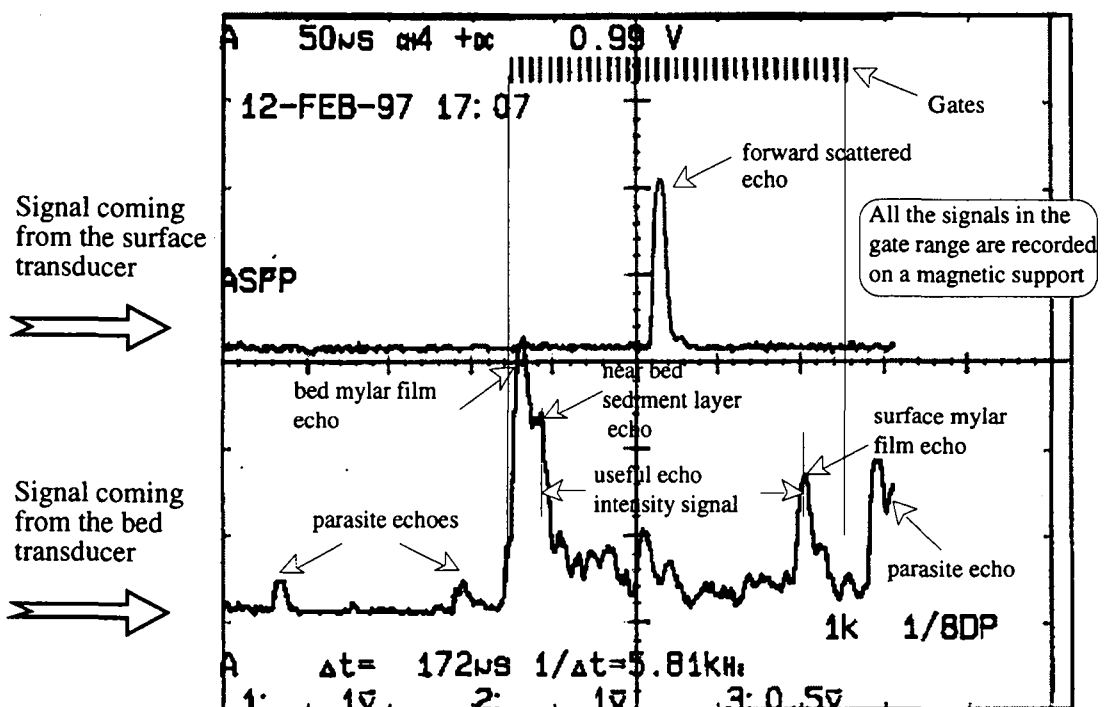


Fig. 2.8: Correct APFP signal (mode 2)

### 2.5.3 Suction method

The vertical mean suspended sediment concentration profile is directly measured by the suction method. A total of 12 samples were drawn at the following depths:  $y/h=0.05, 0.075, 0.1, 0.125, 0.15, 0.175, 0.2, 0.25, 0.5, 0.7, 0.9, 0.95$ . The samples were collected in 2-liters' bottles. As shown in Fig. 2.2, the pipette top, having a diameter of 4.8 [mm], draws samples directly from the flow. The suction velocity, regulated by operating on the air-compressed pump, was equal to the velocity of the fluid surrounding the pipette head. This condition, known as isokinetic condition, assures a minimal perturbation on the flow. Subsequently, the samples were filtered to obtain the suspended sediment concentration. The filtration was performed under pressure using special filters.

The calibration of the APFP instrument (see Appendix A) is performed comparing the vertical mean-echo intensity profile and the vertical mean concentration profile measured by the suction method. The vertical mean concentration profile was also used to compute the best-fit  $\beta$ -values using the Rouse or the Hunt equations (see Appendix B).

## 2.6 Determination of the hydraulic parameters

The measurements of the instantaneous velocity and concentration profiles have been performed using the APFP instrument. The definition of the hydraulic parameters measured and computed are described next.

## 2.6.1 Velocity and resistance parameters

The following parameters were measured or computed using the APFP instruments.

- 1) Longitudinal and vertical instantaneous velocity profiles:  $u(y, t)$  [m/s],  $v(y, t)$  [m/s]
- 2) Longitudinal and vertical mean velocity profiles:  $\bar{u}(y)$  [m/s],  $\bar{v}(y)$  [m/s]
- 3) Longitudinal and vertical rms. velocity profiles:  $\sqrt{\bar{u}^2}(y)$  [m/s],  $\sqrt{\bar{v}^2}(y)$  [m/s]  
where the fluctuating velocities are defined as:  

$$u'(y, t) = u(y, t) - \bar{u}(y)$$

$$v'(y, t) = v(y, t) - \bar{v}(y)$$
- 4) Velocity covariance (also called Reynolds stress):  $\overline{u'v'}(y)$  [m<sup>2</sup>/s<sup>2</sup>]
- 5) Depth-averaged velocity (bulk velocity),  $U$  [m/s]: obtained by integrating the profile of the longitudinal velocity, such as: 
$$U = \frac{1}{h} \int_0^h \bar{u}(y) \cdot dy$$
- 6) Maximum velocity,  $\bar{u}_c$  [m/s]: observed at the height  $y = \delta$ .
- 7) Shear velocity,  $u_*$  [m/s]

Several methods for the determination of the shear velocity are found in the literature (see *Nezu* and *Nakagawa*, 1993). The following methods were used:

- i) Energy-gradient method,  $u_{*s}$  [m/s]

Using the energy slope,  $S_e$ , – equal to the bed slope,  $S_b$ , in case of uniform flow– and the flow depth,  $h$ , the shear velocity can be calculated as:  

$$u_{*s} = \sqrt{ghS_e} = \sqrt{ghS_b}$$

- ii) Reynolds-stress method,  $u_{*r}$  [m/s]

The measured Reynolds-stress profiles,  $-\rho \cdot \overline{u'v'}(y)$ , extrapolated towards the bed give the value  $-\rho \cdot u_{*r}^2$ . Thus, the shear velocity can be evaluated.

Usually this is the value of the shear velocity used in computation.

- 8) Coles' wake strength,  $\Pi$  [-]: as given in Coles' velocity-defect law, is defined as the deviation of the mean velocity profile from the log-law.

In the defect form their expressions are:

$$\text{log-law: } \frac{\bar{u}_c - \bar{u}}{u_*} = -\frac{1}{\kappa} \ln\left(\frac{y}{\delta}\right)$$

$$\text{Coles' law: } \frac{\bar{u}_c - \bar{u}}{u_*} = -\frac{1}{\kappa} \ln\left(\frac{y}{\delta}\right) + \frac{2\Pi}{\kappa} \cos^2\left(\frac{\pi \cdot y}{2 \cdot \delta}\right)$$

where:  $\bar{u}_c$ : maximum velocity measured at  $y = \delta$

$$\kappa = 0.4 [-]: \text{Karman constant (for clear and sediment-laden flow)}$$

$$u_* = (u_{*S}, u_{*T})$$

The Coles wake strength,  $\Pi$ , was obtained by best-fitting the Coles' law to the measured velocity-defect profile,  $\bar{u}(y)$ .

9) Constants of integration,  $Br$  [-],  $Bs$  [-],  $Bt$  [-]: appearing in the logarithmic velocity law, they were computed according to the flow regime. The classical forms of the log-law for each regime are:

$$\frac{\bar{u}}{u_*} = \frac{1}{\kappa} \ln \left( \frac{y}{k_s} \right) + Br : \text{for rough bed, where } k_s [\text{m}] \text{ is the equivalent bed roughness}$$

$$\frac{\bar{u}}{u_*} = \frac{1}{\kappa} \ln \left( \frac{u_* y}{v} \right) + Bs : \text{for smooth bed, where } u_* = (u_{*S}, u_{*T})$$

$$\frac{\bar{u}}{u_*} = \frac{1}{\kappa} \ln \left( \frac{y}{k_s} \right) + Bt : \text{for transitional bed}$$

The criterion to chose the integration constant was:

$$\text{if } Re_* = \frac{k_s u_*}{v} < 5 \text{ then the bed was hydraulically smooth: } Bs = 5.5.$$

$$\text{if } 5 < Re_* = \frac{k_s u_*}{v} < 70 \text{ then the bed was hydraulically in transitional condition: } Bt$$

was deduced graphically (see *Graf and Altinakar*, 1991, pp. 427).

$$\text{if } Re_* = \frac{k_s u_*}{v} > 70 \text{ then the bed was hydraulically rough: } Br = 8.5 .$$

10) Friction factor,  $f$  [-]: calculated using:  $f = 8(u_*/U)^2$ .

11) Equivalent bed roughness,  $k_s$  [m]: calculated using the Colebrook and White relation:  $\sqrt{\frac{1}{f}} = -2 \cdot \log \left( \frac{k_s/R_h}{a_f} + \frac{b_f}{Re \sqrt{f}} \right)$  where:  $a_f = 11.5$ ,  $b_f = 3$  (see *Silberman et al.*, 1963, pp. 97-143) and  $R_h$  [m] is the hydraulic radius.

## 2.6.2 Concentration parameters

The following parameters were obtained from the APFP instrument after calibration with the vertical mean concentration profile measured by the suction method.

- 1) Instantaneous suspended concentration profile:  $c_s(y, t)$  [ $\text{m}^3/\text{m}^3$ ], represents the volume of suspended sediment per volume of mixture; the concentration can be also defined as massic,  $c_s^m(y, t)$  [ $\text{kg}/\text{m}^3$ ], in this case it represents the mass of suspended sediment per volume of mixture.
- 2) Mean concentration profiles:  $\bar{c}_s^m(y)$  [ $\text{kg}/\text{m}^3$ ], were measured by the suction method to calibrate the APFP instrument and to deduce the best fitting  $\beta$ -values,  $\bar{\beta}_{SM}$ .
- 3) rms. fluctuating concentration profile:  $\sqrt{\bar{c}'_s^2}$  [ $\text{m}^3/\text{m}^3$ ], where the fluctuating concentration is defined as:  $c'_s(y, t) = c_s(y, t) - \bar{c}_s(y)$
- 4) Reference concentration,  $\bar{c}_{sa}^m$  [ $\text{m}^3/\text{m}^3$ ], measured by the suction method, is defined as the one at the height:  $y = a = 0.05 \cdot h$ .
- 5) Depth-averaged suspended concentration (bulk concentration),  $C_s$  [ $\text{m}^3/\text{m}^3$ ], was obtained by depth-integrating the mean concentration profile, such as:  

$$C_s = \frac{1}{h-a} \int_a^h \bar{c}_s(y) \cdot dy.$$

## 2.6.3 Diffusion parameters

The following parameters were calculated using the data obtained with the APFP instrument.

- 1) Sediment flux:  $\bar{c}'_s v'(y)$  [ $\text{m}/\text{s}$ ], was calculated knowing the instantaneous suspended concentration and the vertical velocity measured simultaneously by the APFP instrument, or:  

$$\bar{c}'_s v'(y) = (\bar{c}_s(y, t) - \bar{c}_s(y)) \cdot (v(y, t) - \bar{v}(y))$$
- 2) Momentum diffusion coefficients:  $\varepsilon_m(y)$  [ $\text{m}^2/\text{s}$ ], also known as the eddy viscosity,  $v_t$ , is given by:  

$$\varepsilon_m(y) = - \frac{\overline{u'v'}(y)}{\partial \bar{u} / \partial y}$$

- 3) Sediment diffusion coefficient:  $\varepsilon_s(y)$  [m<sup>2</sup>/s], is defined as:

$$\varepsilon_s(y) = -\frac{\overline{c'_s v'(y)}}{\partial \bar{c}_s / \partial y}$$

- 4)  $\beta$ ,  $\bar{\beta}$  [-]-values: are important parameters in the diffusion-convection theory, being the ratio of the sediment and the momentum diffusion coefficients:

$$\beta(y) = \frac{\varepsilon_s(y)}{\varepsilon_m(y)} = \frac{\overline{c'_s v'(y)}}{\overline{u' v'(y)}} \text{ from which: } \bar{\beta} = \frac{1}{h-a} \int_a^h \beta(y) \cdot dy$$

Note that:  $\overline{\beta_{APFP}}$ :  $\bar{\beta}$ -value obtained using the APFP instrument,

$\overline{\beta_{SM}}$ :  $\bar{\beta}$ -value obtained by best-fitting the Rouse or Hunt equation to the vertical mean concentration profile measured with the suction method.

- 5) Richardson number:  $Ri$  [-], characteristic of stratified fluids, was calculated using the definition of *Coleman*, 1981, such as:

$$Ri = \frac{g \cdot h \cdot [\rho_m(y=a) - \rho_m(y=h)]}{\bar{\rho}_m \cdot u_*^2}$$

where:  $\rho_m(y=a) = \rho_w + (\rho_s - \rho_w) \cdot \bar{c}_{sa}$  : mixture density close to the bed

$\rho_m(y=h) = \rho_w + (\rho_s - \rho_w) \cdot \bar{c}_s(y=h)$  : mixture density at the surface

$\rho_w, \rho_s$  : water and sediment density

$$\bar{\rho}_m = \frac{1}{h-a} \int_a^h \rho_m(y) \cdot dy \text{ : depth-averaged mixture density}$$

- 6) Rouse number:  $z$  [-], is defined as:  $z = \frac{v_{ss}}{\kappa \cdot u_*}$

- 7) Modified Rouse number:  $z'$  [-], is defined as:  $z' = \frac{z}{\bar{\beta}} = \frac{v_{ss}}{\bar{\beta} \cdot \kappa \cdot u_*}$

## 2.7 Conclusions

The channel, the sediment particles and the procedure to create the suspension flows have been described. While the APFP instrument, used to measure the velocity and concentration, has been widely described in Appendix A, here the procedure followed to perform the measurements are discussed. All the velocity and concentration and diffusion parameters used in this thesis have been defined and discussed.

## 2.8 References

- COLEMAN, N. L. (1981). "Velocity profiles with suspended sediment." *J. Hydr. Res.*, vol. 19, N°3, pp. 211-229.
- GRAF, W. H. (1984). *Hydraulics of Sediment Transport*, Water Resource Publications, Littleton, CO, USA.
- GRAF, W. H. and ALTINAKAR, M. S. (1991). *Hydrodynamique*, Eyrolles, Paris.
- NEZU, I. and NAKAGAWA, H. (1993). *Turbulence in open-channel flows*. A. A. Balkema, Rotterdam.
- ROLLAND, T. (1994). "Developpement d'une instrumentation Doppler ultrasonore adaptée a l'étude hydraulique de la turbulence dans les canaux" *Thèse de doctorat N° 1281*, Ecole Polytechnique Fédérale, Lausanne.
- SHEN, W. (1997). "An acoustic instantaneous sediment flux profiler for turbulent flow," *Doctoral dissertation, No. 1630*, Ecole Polytechnique fédérale, Lausanne.
- SHEN, W. and LEMMIN, U. (1996). "Ultrasonic measurements of suspended sediments. A concentration profiling system with attenuation compensation." *Meas. Sci. Technol.*, Vol. 7, pp. 1191-1194.
- SILBERMAN, E. et al. (1963). "Friction Factors in Open Channels." *Proc. Am. Soc. Civil Engrs.*, vol. 90, N° HY1, USA.
- SUSZKA, L. (1988). "Sediment transport at steady and unsteady flow; a laboratory study," *Doctoral dissertation, No. 704*, Ecole Polytechnique fédérale, Lausanne.



### **3. Measurements of Suspension Flow**

#### **3.1 Introduction**

The total load of sediment, transported by open-channel flows, is composed of a bed load, transported close to the bed, and the suspended load, transported in suspension. For the determination of the suspended load knowledge of the vertical distribution of the concentration of the suspended particles is of importance. It is a common procedure to determine this distribution by solving the diffusion-convection equation under appropriate boundary conditions (see ch. 1).

In natural alluvial channels and waterways the sediment-laden flow is usually in *capacity* (saturation) condition, implying that the flow will charge (saturate) itself with particles, which are available in the bed load and/or on the bed itself. Thus, it is fundamental to investigate the laboratory flows under the same (capacity) condition because only in such a case the flows are in a sediment equilibrium reflecting a natural condition, i.e.: deposited particles can be readily replaced by eroded particles. The results of experimental investigations of flows in under-capacity condition should not be used for natural alluvial channels (see Appendix C).

Another interesting aspect of suspension flows is the mutual interaction between suspended particles and the carrying fluid (water). The Navier-Stokes equations, representing the classical theoretical approach to clear-water flow, have to be modified because of the bi-phasic nature of suspension flow. One should re-write the equations of mass conservation as well as the equations of motion for both the fluid and solid phases taking into account the relative interactions (see *Cao et al.*, 1995, pp. 726). Regrettably, the resulting system of equations becomes so complicated to discourage every analytical or numerical resolution. In order to give simple, but reasonably correct, theoretical-empirical tools to investigate suspension flows, it is a common procedure to still apply the clear-water equations also for suspension flows (see *Itakura and Kishi*, 1980, and *Coleman*, 1981). This approach leads to good results if the size of the particles and the suspended concentration are small enough to be able to neglect the interactions among particles. In addition, the sediments should not be cohesive otherwise the clear-water rheological law (Newtonian law) has to be modified.

If the theory of suspension flow is complicated due to the presence of suspended particles, also the experimental investigation of suspension flows renders itself as difficult. The moving suspended particles can destroy sophisticated but fragile

measuring apparatus such as hot film or hot wire. Non-intrusive instrument, such as Laser-Doppler velocimeter has been used with success to measure high-frequency instantaneous velocities but for very low concentrations due to the problems of laser wave propagation (see *Muste and Patel*, 1997). In the past *Einstein and Chien*, 1955, used Pitot tubes to measure the velocity profiles without investigating high frequency velocity fluctuation. To sum up, a key problem is the presence of suspended particles that, to measure instantaneous velocity, obliges the experimenter to use a non-intrusive instrument and, at the same time, forms a barrier for the instrument itself.

Another key problem deals with the experimental measurement of the suspended concentration. The frequently used method to measure the mean suspended concentration is the suction method. More difficult is the measurement of the instantaneous suspended concentration. The importance of measuring the instantaneous – and also of evaluating the fluctuating – suspended concentrations is related to the need of high-frequency correlations between velocity and concentration fields to study the suspension-flow dynamics.

An answer to the problem concerning the simultaneous measurement of both the high-frequency velocities and concentrations in suspension flows is, for the moment, obtained using ultrasonic instruments such as the Acoustic Particle Flux Profiler (APFP), conceived and developed at the Hydraulics Laboratory (LRH) of the Ecole Polytechnique Fédérale de Lausanne (EPFL), by dr. C. Shen and dr. U. Lemmin. This instrument permits the measurement of the instantaneous velocity profiles by measuring the back-scattered echo signals (see *Lhermitte and Lemmin*, 1994) generated by the emission of high-frequency sonar pulses. In addition, by measuring the forward and backward-echo signals, an echo intensity can be measured (see *Shen and Lemmin*, 1996 and *Shen*, 1997) which is indicative of the sediment concentration. However, to obtain the concentration a calibration – using the suction-sampling method – has to be performed. Since the sonar transducers of the APFP are placed above the water surface and/or below the channel bed, this instrument does not perturb the flow.

In this chapter we report on experiments performed in the laboratory on suspension flows using the above-mentioned APFP instrument. The experiments have been done by using two kinds of sand particles, (sand I, having  $d_{50} = 0.135$  [mm] and sand II, having  $d_{50} = 0.230$  [mm]). The flows were **steady** and **uniform** carrying sediment particles – **at capacity** – over a bed where a layer composed by the same sediment was available. The size of the sediment particles and the suspended concentrations

were small enough to justify the use of clear-water formulation. The accuracy of this hypothesis will be verified at the end of this chapter.

A detailed description of the ADVP/APFP instrument can be found in the Appendix A. The results presented in this chapter refer to flow in capacity condition in presence of a plane bed. In the Appendix B some data on suspension flows found in the literature are presented, summarized and compared to the results of this study. The results of the investigation of flow in non-capacity condition are presented in the Appendix C, while the results of the measurements conducted on flows over bed forms can be found in the Appendix D. In ch. 1 the diffusion-convection theory applied to suspension flows has been presented while in ch. 2 the experimental facilities as well as the investigation procedures have been described.

### 3.2 Presentation of data

The measurements were made in a recirculating tilting channel, 16.8 [m] long and 0.60[m] wide. The measuring section was located 13 [m] from the entrance at the channel, where the boundary layer is assumed to be established; all measurements were performed at the centerline of the cross section. The measurements started at 4[h] after the injection of the amount of sediment ( $\approx 120$  [kg]) that can be transported by the flow *at its capacity*. This amount was added slowly until an uniform layer of sediments, ( $\approx 2$  [mm] thick) was observed on the channel bed. If additionally particles were added, the thickness of the bed layer would be simply increased. The velocity and concentration measurements were made with a sonar instrument, the APFP. The experimental facilities and the procedure followed to create the suspension flow are described respectively in ch. 2.2 and ch. 2.5. The detailed description of the APFP instrument can be found in the Appendix A. The details of each run are given in Appendix B.

In Table 3.1 for sand I and Table 3.2 for sand II, are summarized all the hydraulic and sediment parameters and the results of the runs, namely:

Flow discharge:  $Q$  [ $m^3/s$ ], was adjusted to maintain constant the flow depth. A magnetic flowmeter measured continuously the discharge. Since the presence of suspended sediments perturbed the flowmeter readings, the discharge has been posed to be:  $Q \equiv U \cdot h \cdot B$

Flow depth:  $h$  [m]=0.12 [m], being fixed for all runs

$\delta$  [m] is the height where the maximum velocity,  $\bar{u}_c$  [m/s], has been measured

Aspect ratio:  $B/h$  [-] = 5.0, where  $B=0.6$  [m] is the channel width

Depth-averaged longitudinal velocity:  $U \text{ [m/s]} = \frac{1}{h} \int_0^h \bar{u}(y) \cdot dy$ , where  $\bar{u}(y)$  is the

longitudinal mean velocity measured at the centerline by the APFP

Bed slope:  $S_b \text{ [-]}$ , read on a graded scale, previously calibrated using a precise optical instrument

Reynolds number:  $Re \text{ [-]} = \frac{4 \cdot U \cdot R_h}{v_m}$

where  $R_h \text{ [m]}$  is the hydraulic radius and  $v_m \text{ [m}^2/\text{s]}$  is the mixture kinematic viscosity,  $v_m \text{ [m}^2/\text{s]} = v \cdot \frac{\rho_w \cdot (1 + 2.5 \cdot C_s)}{\rho_w + (\rho_s - \rho_w) \cdot C_s}$ . The water

viscosity is  $v \text{ [m}^2/\text{s]}$ , the water and sediment density are, respectively,  $\rho_w \text{ [kg/m}^3]$  and  $\rho_s \text{ [kg/m}^3]$ , while  $C_s \text{ [m}^3/\text{m}^3]$  is the depth-averaged concentration. Since the detected highest depth-averaged concentration was  $C_s^m = 6.29 \text{ [kg/m}^3]$  giving  $v_m/v = 1.002$ , it has been posed  $v_m \equiv v$

Froude number:  $Fr \text{ [-]} = U / \sqrt{gh}$

Shear velocity:

$u_* \text{ [m/s]}$ , obtained by extrapolating the measured Reynolds-stress profile towards the bed

$u_* \text{ [m/s]}$ , obtained by the energy method,  $u_* = \sqrt{ghS_f}$ , where:

$S_f \text{ [-]}$  (energy slope) =  $S_w \text{ [-]}$  (water slope) =  $S_b \text{ [-]}$  (bed slope)  
(uniform-flow condition)

In this chapter only the shear velocity obtained by the Reynolds-stress profile,  $u_*$ , has been used in the computation, such as:  $u_* \equiv u_{*r}$ .

Friction factor:  $f \text{ [-]} = 8(u_*/U)^2$

Equivalent roughness:  $k_s \text{ [mm]}$ , computed by Colebrook & White formula

Particle Reynolds number:  $Re_p \text{ [-]} = \frac{u_* k_s}{v_m}$

Integration constant:  $Bs$ ,  $Bt \text{ [-]}$ , if the bed was hydraulically smooth, or  $u_* k_s / v_m < 5$ ,  $Bs = 5.5$  was taken; if the bed was hydraulically in transition, or  $70 > u_* k_s / v_m > 5$ ,  $Bt$  was deduced graphically (see *Graf and Altinakar, 1991, p. 427*)

Coles wake strength:  $\Pi \text{ [-]}$ , obtained by best-fitting the Coles' velocity-defect law to the measured velocity profile

Karman constant:  $\kappa \text{ [-]} = 0.4$  taken as a constant

Nominal particle diameter:  $d_{50} \text{ [mm]}$  of the sediment particles in suspension

Sediment density:  $\rho_s \text{ [kg/m}^3]$  of quartz sand

Settling velocity:  $v_{ss}$  [m/s], taken in still, clear water (see *Graf*, 1984, p. 45)

Depth-averaged concentration:  $C_s^m$  [kg/m<sup>3</sup>], computed from the suction method measurements

Reference concentration:  $\bar{c}_{sa}^m$  [kg/m<sup>3</sup>], measured with the suction method at the reference height  $y = a = 0.05 \cdot h$ .

Depth-averaged mixture density:  $\bar{\rho}_m$  [kg/m<sup>3</sup>] =  $\rho_w + (\rho_s - \rho_w) \cdot C_s$

$$\text{Richardson number: } Ri [-] = \frac{gh[\rho_m(y=a) - \rho_m(y=h)]}{\bar{\rho}_m u_*^2}$$

where:  $\rho_m(y) = \rho_w + (\rho_s - \rho_w) \cdot \bar{c}_s(y)$ ,  $\bar{c}_s(y)$  is the local mean suspended concentration

$$\text{Rouse number: } z [-] = \frac{v_{ss}}{\kappa \cdot u_*}$$

Modified Rouse number:  $z'[-] = \frac{v_{ss}}{\kappa \cdot u_* \cdot \bar{\beta}} = \frac{z}{\bar{\beta}}$ , obtained best-fitting the Rouse equation to the concentration profile measured with the suction method

$$\bar{\beta} \text{- values} \begin{cases} \overline{\beta_{SM}} [-] & , \text{ depth - averaged } \bar{\beta} \text{- values, best - fit using suction method} \\ \overline{\beta_{APP}} [-] & , \text{ depth - averaged } \bar{\beta} \text{- values, measured with APPF} \end{cases}$$

run	$Q$	$h$	$\delta$	$\bar{u}_c$	$B/h$	$U$	$S_b$	$Re \cdot 10^5$	$Fr$	$u_{*r}$	$u_{*s}$	$f$	$k_s$	$\frac{u_s k_s}{V_m}$	$B_s$	$B_t$	$\Pi$
	[m³/s]	[m]	[m]	[m/s]	[-]	[m/s]	[%]	[-]	[-]	[m/s]	[m/s]	[-]	[mm]	[-]	[-]	[-]	[-]
Q40S003	0.049	0.120	0.105	0.786	5.0	0.680	0.030	2.330	0.63	0.028	0.019	0.014	0.050	1.4	5.5	0.555	
Q45S005	0.058	0.120	0.103	0.902	5.0	0.806	0.050	2.761	0.74	0.034	0.024	0.014	0.063	2.2	5.5	0.467	
Q48S0075	0.060	0.120	0.103	0.941	5.0	0.829	0.075	2.840	0.76	0.037	0.030	0.016	0.108	4.0	5.5	0.556	
Q50S010	0.057	0.120	0.108	0.930	5.0	0.792	0.100	2.712	0.73	0.039	0.034	0.019	0.175	6.8	5.5	0.548	
Q53S0125	0.059	0.120	0.114	0.951	5.0	0.824	0.125	2.822	0.76	0.040	0.038	0.019	0.148	5.9	5.5	0.543	
Q55S015	0.062	0.120	0.099	1.008	5.0	0.858	0.150	2.938	0.79	0.043	0.042	0.020	0.222	9.5	9.92	0.538	
Q57S0175	0.062	0.120	0.109	0.968	5.0	0.855	0.175	2.927	0.79	0.044	0.045	0.021	0.292	12.8	9.98	0.528	
Q60S020	0.065	0.120	0.097	1.045	5.0	0.905	0.200	3.098	0.83	0.045	0.049	0.020	0.207	9.3	9.92	0.459	
Q65S0225	0.066	0.120	0.099	1.046	5.0	0.916	0.225	3.135	0.84	0.046	0.051	0.020	0.231	10.6	9.97	0.558	
Q70S025	0.066	0.120	0.103	1.084	5.0	0.917	0.250	3.138	0.85	0.049	0.054	0.023	0.422	20.6	9.97	0.552	
Q75S03	0.065	0.120	0.110	1.064	5.0	0.897	0.300	3.069	0.83	0.055	0.059	0.030	1.234	67.8	9.14	0.542	

run	$d_{so}$	$\rho_s$	$v_{ss}$	$C_s^n$	$\bar{C}_{sa}^n$	$\bar{\rho}_m$	$Ri$	$z = \frac{v_{ss}}{k \cdot u_*}$ (best fit)	$z'$ (best fit)	$\beta_{sm}$ (best fit)	$\beta_{apfp}$ (APFP)
	[mm]	[kg/m³]	[mm/s]	[kg/m³]	[kg/m³]	[kg/m³]	[-]	[-]	[-]	[-]	[-]
Q40S003	0.135	2650	12.0	2.05	24.62	1001.28	21.364	1.071	2.15	0.498	0.728
Q45S005	0.135	2650	12.0	2.81	28.62	1001.75	17.563	0.882	1.35	0.652	0.469
Q48S0075	0.135	2650	12.0	2.94	31.62	1001.83	16.872	0.811	1.48	0.548	0.422
Q50S010	0.135	2650	12.0	3.61	39.33	1002.25	18.830	0.769	1.72	0.447	0.534
Q53S0125	0.135	2650	12.0	3.32	36.04	1002.07	16.450	0.750	1.51	0.498	0.499
Q55S015	0.135	2650	12.0	4.41	46.05	1002.75	18.120	0.698	1.60	0.436	0.532
Q57S0175	0.135	2650	12.0	4.73	49.41	1002.95	18.610	0.682	1.45	0.471	0.464
Q60S020	0.135	2650	12.0	4.91	48.58	1003.06	17.380	0.667	1.56	0.427	0.568
Q65S0225	0.135	2650	12.0	5.08	50.82	1003.16	17.490	0.652	1.38	0.472	0.519
Q70S025	0.135	2650	12.0	5.98	50.04	1003.72	14.990	0.612	1.26	0.486	0.563
Q75S03	0.135	2650	12.0	6.29	62.47	1003.92	14.960	0.545	1.46	0.373	0.514

Table 3.1: Summary of data (sand I)

run	$Q$	$h$	$B/h$	$\delta$	$\bar{u}_c$	$U$	$S_b$	$Re \cdot 10^5$	$Fr$	$u_{*r}$	$u_{*s}$	$f$	$k_s$	$\frac{u_s k_s}{V_m}$	$B_s$	$B_t$	$\Pi$
	[m³/s]	[m]	[-]	[m]	[m/s]	[m/s]	[%]	[-]	[-]	[m/s]	[m/s]	[-]	[mm]	[-]	[-]	[-]	[-]
Q50S01_II	0.058	0.120	5.0	0.109	0.916	0.801	0.100	2.743	0.74	0.039	0.034	0.019	0.153	6.0	5.5	0.220	
Q55S015_II	0.060	0.120	5.0	0.109	0.959	0.833	0.150	2.855	0.77	0.044	0.042	0.022	0.334	14.5	9.99	0.263	
Q57S0175_II	0.060	0.120	5.0	0.105	0.953	0.836	0.175	2.864	0.77	0.043	0.045	0.021	0.290	12.5	9.97	0.206	
Q60S02_II	0.061	0.120	5.0	0.105	0.971	0.850	0.200	2.911	0.78	0.045	0.049	0.023	0.425	19.3	9.95	0.222	
Q65S0225_II	0.062	0.120	5.0	0.105	0.997	0.865	0.225	2.964	0.80	0.047	0.051	0.023	0.444	20.6	9.93	0.310	
Q70S025_II	0.063	0.120	5.0	0.105	0.994	0.868	0.250	2.974	0.80	0.048	0.054	0.024	0.524	24.9	9.86	0.197	

run	$d_{so}$	$\rho_s$	$v_{ss}$	$C_s^n$	$\bar{C}_{sa}^n$	$\bar{\rho}_m$	$Ri$	$z = \frac{v_{ss}}{k \cdot u_*}$ (best fit)	$z'$ (best fit)	$\beta_{sm}$ (best fit)	$\beta_{apfp}$ (APFP)
	[mm]	[kg/m³]	[mm/s]	[kg/m³]	[kg/m³]	[kg/m³]	[-]	[-]	[-]	[-]	[-]
Q50S01_II	0.230	2650	21	1.57	21.31	1000.98	10.25	1.346	2.009	0.670	0.809
Q55S015_II	0.230	2650	21	2.30	28.07	1001.43	10.87	1.207	1.717	0.703	0.659
Q57S0175_II	0.230	2650	21	2.01	24.77	1001.25	9.80	1.221	1.724	0.708	0.680
Q60S02_II	0.230	2650	21	1.90	23.29	1001.18	8.26	1.154	1.766	0.654	0.685
Q65S0225_II	0.230	2650	21	2.78	34.36	1001.73	11.37	1.128	1.796	0.628	0.561
Q70S025_II	0.230	2650	21	2.84	33.83	1001.77	10.91	1.103	1.667	0.662	0.586

Table 3.2: Summary of data (sand II)

### 3.3 Velocity profiles

The longitudinal mean velocity profiles,  $\bar{u}(y)$ , – measured with the APFP instrument – for 11 flows with sand I and 6 with sand II, are shown in Fig. 3.1.

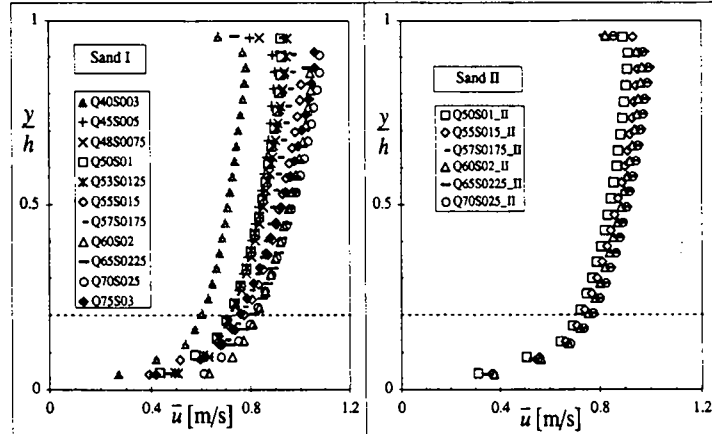


Fig. 3.1: Longitudinal mean velocity profiles for sand I and sand II

Some typical dimensionless velocity profiles,  $\bar{u}/u_*$ , – for sand I and sand II – are plotted in Fig. 3.2 in smooth,  $y \cdot u_*/v_m$ , and rough,  $y/k_s$ , dimensionless coordinates. Velocity measurements performed within the inner region, limited to  $y/h < 0.2$ , can be discussed in the framework of the universal law of the wall (log-law):

$$\frac{\bar{u}}{u_*} = \frac{1}{\kappa} \ln \left( \frac{u_* y}{v_m}, \frac{y}{k_s} \right) + (B_s, B_t) \quad (3.1)$$

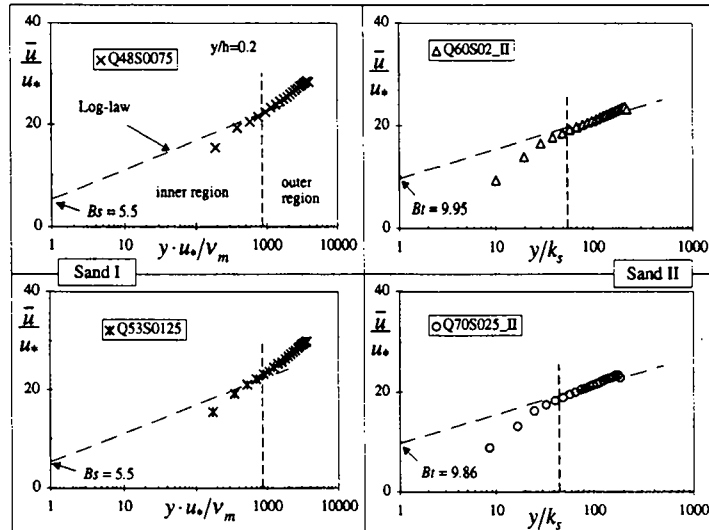


Fig. 3.2: Dimensionless mean velocity profiles for sand I and sand II

For six flows (5 with sand I and 1 with sand II) the roughness Reynolds number was small,  $u_*k_s/v_m < 5$ , indicating that the bed (represented by the sediment layer on the channel bed) was hydraulically smooth. The other flows investigated were in transitional condition,  $70 > u_*k_s/v_m > 5$ . Four typical dimensionless velocity profiles, two having a smooth and two having a transitional bed, are plotted in Fig. 3.2; also shown are the log-laws (dashed lines, eq. 3.1), plotted by using the hydraulic parameters, specified of each run, as shown in Table 3.1 and 3.2.

For all the mean velocity profiles, only 4 measuring points were usually available in the inner region. This means that the integration constants,  $Bs$ ,  $Bt$ , deduced by best fitting the log-law profile in the inner region, see eq. 3.1, may be affected by errors. For this reason the values of the integration constants in Table 3.1 were obtained by the following equations:

if  $Re_* = \frac{k_s u_*}{\nu} < 5$  (smooth bed)  $Bs = 5.5$  was taken, and

if  $5 < Re_* = \frac{k_s u_*}{\nu} < 70$  (transitional bed)  $Bt$  was deduced graphically (see *Graf*

and *Altinakar*, 1991, pp. 427)

The distinction between a smooth and a transitional bed condition is not sharp; a flow having  $3 < u_*k_s/v_m < 8$  can be modeled indifferently using smooth or rough coordinates; in this case the coordinates leading to a better agreement of the theoretical profiles to the experimental points have been chosen. Note, that the log-laws in Fig. 3.2 (dashed lines, eq. 3.1) were not fitted to the measured velocity profiles but are only plotted for the sake of comparison. The two measuring points closest to the bed deviate from the theoretical profile (log-law). This is probably due to the vicinity of the sediment layer where the exchange between eroded and deposited particles occur, but could also be due to ultrasonic echo (noise) caused by the vicinity of the bed.

In the outer region,  $y/h > 0.2$ , another deviation from the standard log-law is evident. It is customary to formulate this deviation as being a wake-like function of  $y/\delta$ . The law of the wake, also known as Coles' law, is formulated for smooth and rough boundaries as follows:

$$\frac{\bar{u}}{u_*} = \frac{1}{\kappa} \ln \left( \frac{u_* y}{v_m}, \frac{y}{k_s} \right) + (Bs, Bt) + \frac{2\pi}{\kappa} \sin^2 \left( \frac{\pi}{2} \cdot \frac{y}{\delta} \right) \quad (3.2)$$

where:  $\Pi$ : Coles' wake strength

$y = \delta$ : height where the maximum velocity has been measured

The Coles' law can be advantageously written in the defect form, as follows:

$$\frac{\bar{u}_c - \bar{u}}{u_*} = -\frac{1}{\kappa} \ln\left(\frac{y}{\delta}\right) + \frac{2\pi}{\kappa} \cos^2\left(\frac{\pi \cdot y}{2 \cdot \delta}\right) \quad (3.3)$$

where:  $\bar{u}_c$ : maximum velocity measured at  $y = \delta$ .

Note that the relation, eq. 3.3, is valid in both the inner and outer region for both smooth and rough beds. Furthermore it is independent of the bed roughness,  $k_s$ . The Coles' wake strength,  $\Pi$ , was determined by best fitting the Coles' defect form, eq. 3.3, to the measured defect velocity profile. Only data in the outer region,  $y/\delta > 0.2$ , are used, since in the inner region the data are probably of questionable quality. In Fig. 3.3 the velocity profiles are plotted in defect form:

$$\frac{\bar{u}_c - \bar{u}}{u_*} = f\left(\frac{y}{\delta}\right)$$

The wake-strength values,  $\Pi$ , obtained with the fitting technique are given in Table 3.1 for sand I and Table 3.2 for sand II. In Fig. 3.3 the defect velocity profiles are compared with the Coles defect law, eq. 3.3, using average  $\Pi$ -values computed from Table 3.1 and Table 3.2, namely  $\Pi=0.50$  for sand I and  $\Pi=0.24$  for sand II. The agreement is judged satisfactory.

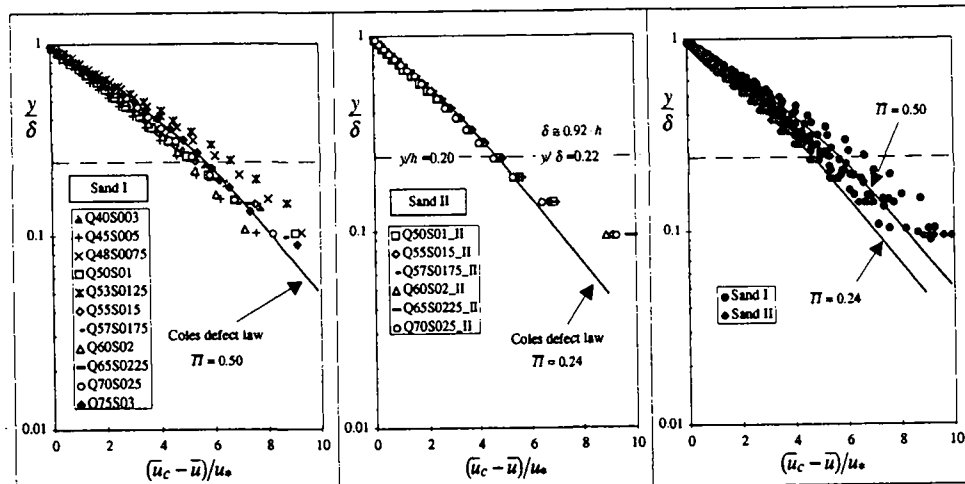


Fig. 3.3: Longitudinal velocity profiles in defect form

The values of Coles' wake strength,  $\Pi$ , measured for sand I are larger than the ones measured for sand II. In both cases the  $\Pi$ -values are larger than the clear-water values obtained by *Kironoto*, 1992,  $\Pi \approx 0.1$ . *Cioffi* and *Gallerano*, 1991 also found large values of  $\Pi$ ,  $\Pi=0.3$ . *Coleman*, 1981, investigating velocity profiles of

sediment-laden flows, found an useful correlation between the Coles' wake strength,  $\Pi$ , and the Richardson number,  $Ri$ . The values obtained in the present study (gray symbols) are compared in Fig. 3.4 with the Coleman results (black symbols). The agreement is satisfactory only for the sand I results. For sand II the experimental points fall below. However, the overall trend of the  $\Pi$ -values to increase with larger values of the Richardson number is confirmed.

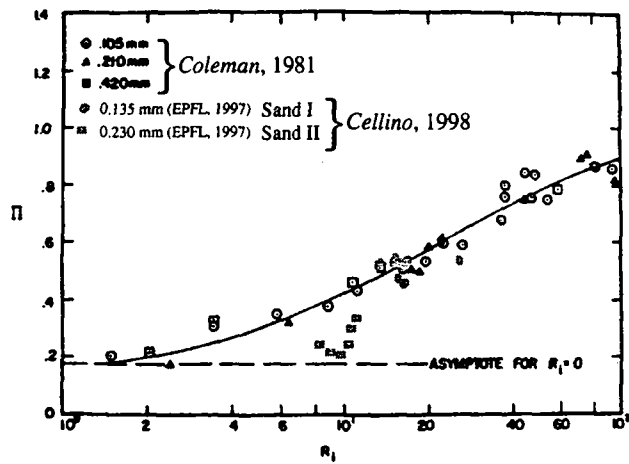


Fig. 3.4: Coles wake strength as a function of the Richardson number

The profiles of the vertical component of the velocity, normalized using the shear velocity,  $\bar{v}/u_*$ , are shown in Fig. 3.5. Note that a positive value of the vertical velocity means that the velocity is directed upwards (towards the water surface). The vertical velocities are very small, especially for sand II, when compared to the longitudinal component. The largest (downwards) vertical velocities,  $\bar{v}/u_* \approx -0.7$ , have been observed – for both sand I and sand II – close to the surface.

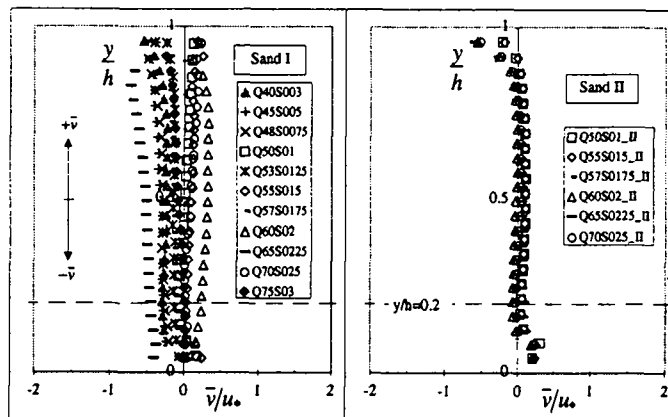


Fig. 3.5: Dimensionless profiles of the vertical velocity

### 3.4 Turbulence intensity

For uniform clear-water open-channel flow the turbulence intensity profiles have been extensively investigated. *Nezu* and *Nakagawa*, 1993, p. 53, suggested that the turbulence intensity is distributed according to an universal exponential law. *Kironoto's*, 1992, experiments show that for a rough bed, the turbulence-intensities distributions can be expressed as:

$$\frac{\sqrt{u'^2}}{u_*} = 2.04 \cdot \exp\left(-0.97 \frac{y}{\delta}\right) \quad (3.4)$$

$$\frac{\sqrt{v'^2}}{u_*} = 1.14 \cdot \exp\left(-0.76 \frac{y}{\delta}\right) \quad (3.5)$$

The measured longitudinal and vertical turbulence intensity profiles for sand I and II have been plotted in Fig. 3.6a,c and Fig. 3.6b,d respectively.

The measured longitudinal turbulence-intensity profiles (symbols in Fig. 3.6a,c) are comparable to the experimental clear-water profiles measured by *Song, Graf* and *Lemmin*, 1994, (gray lines) and the ones, eq. 3.4, (black lines) proposed by *Kironoto*, 1992. In the inner region,  $y/h < 0.2$ , the measured profiles are lower, probably due to the effect of the concentration of suspended sediments. On the other hand, in the outer region,  $y/h > 0.2$ , it is somehow evident that the experimental profiles are slightly enhanced. Both for sand I and II the vertical trends are rather similar, which means that the longitudinal component of the turbulence intensity is apparently independent of the size of the particles investigated.

The experimental vertical turbulence-intensity profiles (gray symbols, see Fig. 3.6b,d) do not agree with the experimental profiles measured by *Song, Graf* and *Lemmin*, 1994, and the ones proposed by *Kironoto*, 1992. It is rather obvious that the presence of suspended sediments suppresses the vertical turbulence intensity. Note that in the inner region,  $y/h < 0.2$ , the clear-water turbulence intensity profile proposed by *Song, Graf* and *Lemmin*, 1994, (gray lines) deviates from the universal profile proposed by *Nezu* and *Nakagawa*, 1993. The present data show the same kind of deviation in the inner region. Comparing the profiles measured by *Song, Graf* and *Lemmin*, 1994, in clear water (gray lines) and the present profiles (symbols) it becomes evident that the presence of suspended sediments operates an uniform suppression of the turbulence over the entire flow depth.

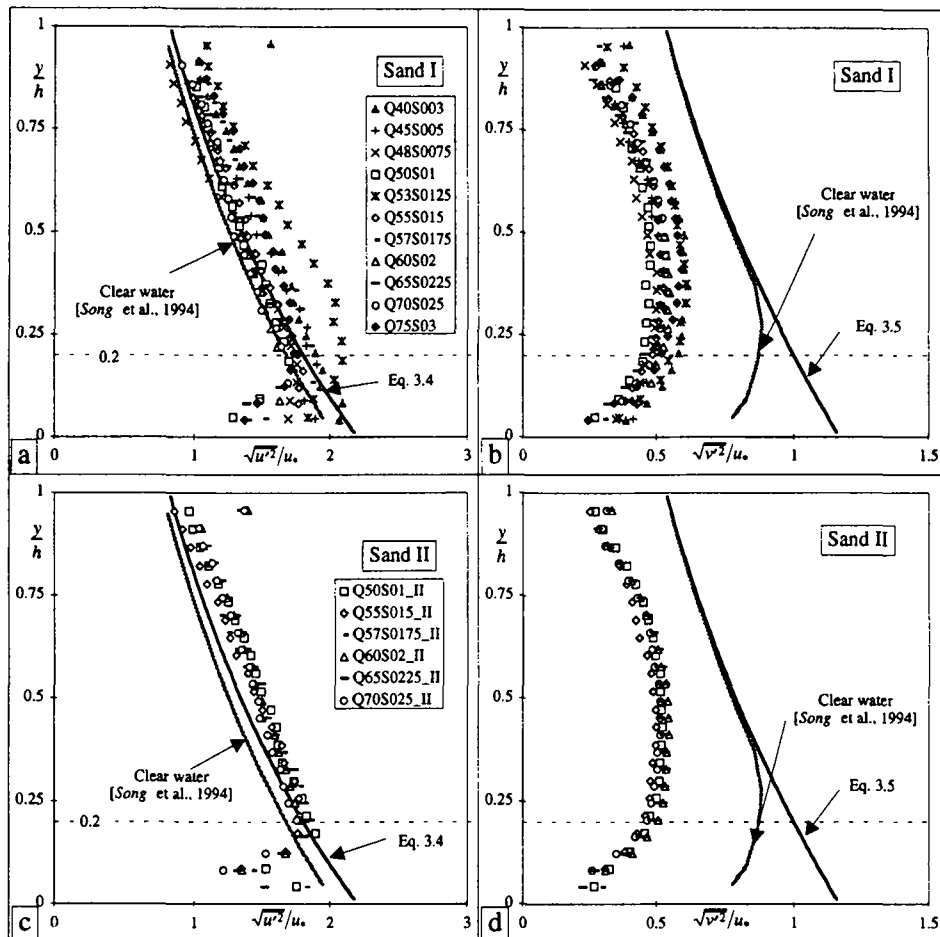


Fig. 3.6a,b,c,d: Longitudinal and vertical turbulence intensity profiles

Investigating non-capacity flows (see Appendix C) it has been shown that the turbulence damping increases approaching the capacity condition (see Fig. C2a,b). This means that the turbulence damping increases when the concentration increases. Other researchers observed the same phenomenon using sand (see Muste and Patel, 1997, p. 749) and also using polymer (see Best, 1993).

### 3.5 Reynolds-stress distribution

The determination of the shear-stress profiles in open channel flow is important for theoretical and practical considerations. From the measured shear-stress distribution the wall shear stress,  $\tau_0$ , can be obtained. The total shear stress,  $\tau$ , is expressed as an addition of the viscous stress and the turbulent (Reynolds) stress, such as:

$$\frac{\tau}{\rho} = \nu \frac{\partial \bar{u}}{\partial y} + (-\bar{u}'v') \quad \text{where } \nu [\text{m}^2/\text{s}] \text{ is the kinematic viscosity} \quad (3.6)$$

It is well known that the viscous stress is maximum at the bed and decreases very rapidly with the distance from the bed, becoming negligible as compared with the Reynolds stress at  $y/h > 0.05$ . Thus, the total shear stress,  $\tau$ , is well approximated by the Reynolds stress, over a large distance from the bed.

It is also known that in uniform flow the total shear stress decreases linearly from the bed, where it is equal to the bed shear stress,  $\tau_0$ , towards the surface, where it is equal to zero, such as:

$$\frac{\tau}{\rho} = -\overline{u'v'} = u_*^2 \left( 1 - \frac{y}{h} \right) \quad (3.7)$$

Extrapolating the Reynolds stress profiles – measured with the APFP instrument – towards the bed, the shear velocity,  $u_*$ , can be evaluated (see eq. 3.7). This shear velocity, denominated  $u_* = u_{*\tau}$ , has been used for all computations. The Reynolds-stress profiles, normalized using  $u_*$ , are presented in Fig. 3.7.

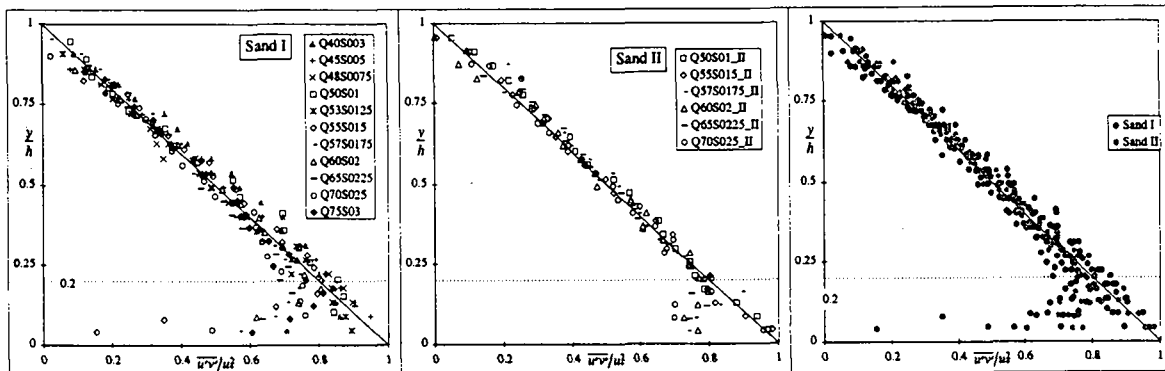


Fig. 3.7: Reynolds-stress profiles

The Reynolds-stress profiles – measured by the APFP instrument – show some scatter, while it is evident that these profiles retain their linear trend implying that the flow is a uniform one. In the inner region,  $y/h < 0.2$ , the experimental Reynolds-stress profiles deviate from the linear trend falling to zero rather rapidly. This deviation is probably due to the region close to the bed where the sediment layer interacts with the flow (erosion and deposition of particles) and where the local suspended concentration is very high. Also the vicinity of the bed can generate ultrasonic echoes affecting the APFP measurements (see Appendix A). The linearity of the Reynolds stress profiles in suspension flows has also been observed by *Muste and Patel*, 1997, p. 749, by *Lyn*, 1988, p. 12, and by *Tsujimoto and Gotoh*, 1995, p. 5.

### 3.6 Energy spectra distribution

The turbulence spectra,  $E(n)$ , of the fluctuating components of the velocity,  $u'$ ,  $v'$ ,  $w'$ , represent the distribution of the turbulent energy,  $\overline{u'^2}$ ,  $\overline{v'^2}$ ,  $\overline{w'^2}$ , with respect to the frequency,  $n$ , of the turbulent eddies. The spectra analysis is an useful tool to understand how the energy is distributed with respect to the frequency,  $n$ , of the turbulent eddies and how it is modulated by the introduction of sediment particles to the flow. The spectra have been obtained by taking the Fourier transform of the complex random wave form of the turbulent motion.

The integral of the turbulence spectra is equal to the mean square value of the fluctuating velocity. For the vertical direction, for example, one can write:

$$\int_0^{\infty} E_v(n) dn = \overline{v'^2}$$

The spectra is usually normalized such as:

$$\int_0^{\infty} F(n) dn = 1$$

In our analysis the spectra have been computed analyzing *only the vertical fluctuating velocity* signal at three locations: near the bed, near the surface and in the middle of the flow depth. Amongst the three regions of the spectra, i.e. production, inertial and dissipation subranges, the APPF instrument is capable of detecting only the first two.

In Fig. 3.8 are shown the spectra of 4 typical runs for sand I (Q50S01, Q55S015, Q60S02, Q70S025, black symbols) and 4 spectra for sand II (Q50S01\_II, Q55S015\_II, Q60S02\_II, Q70S025\_II, gray symbols) and 4 spectra measured in clear-water flows (Q50S01\_CW, Q55S015\_CW, Q60S02\_CW, Q70S025\_CW, open symbols). The spectra refer to flows having the same bed slope,  $S_b$ . The spectral distribution in the inertial subrange follows the form of  $F(n) \propto n^{-5/3}$ , as was suggested by Kolmogoroff for locally-isotropic turbulence (see Hinze, 1975, p. 228). It is not possible to observe the spectral distribution for frequencies larger than 39 [Hz] in the dissipation subrange.

Differences between the spectral distribution observed using sand I and the ones using sand II are not evident. The influence of the suspended-sediment size on the spectral distribution is not discernible either. Similar spectral distributions have been measured in the Conwy Estuary by West and Oduyemi, 1989, p. 463. The modulation

of the turbulence due to suspended particles and in particular the diminution of the turbulent energy associated to largest eddies (small frequencies), as shown investigating the energy spectra of non-capacity flows (see Appendix C), is confirmed comparing the spectra measured in clear-water flows. In fact, also in this case it has been found that increasing the concentration the energy spectra decreases only towards small frequencies.

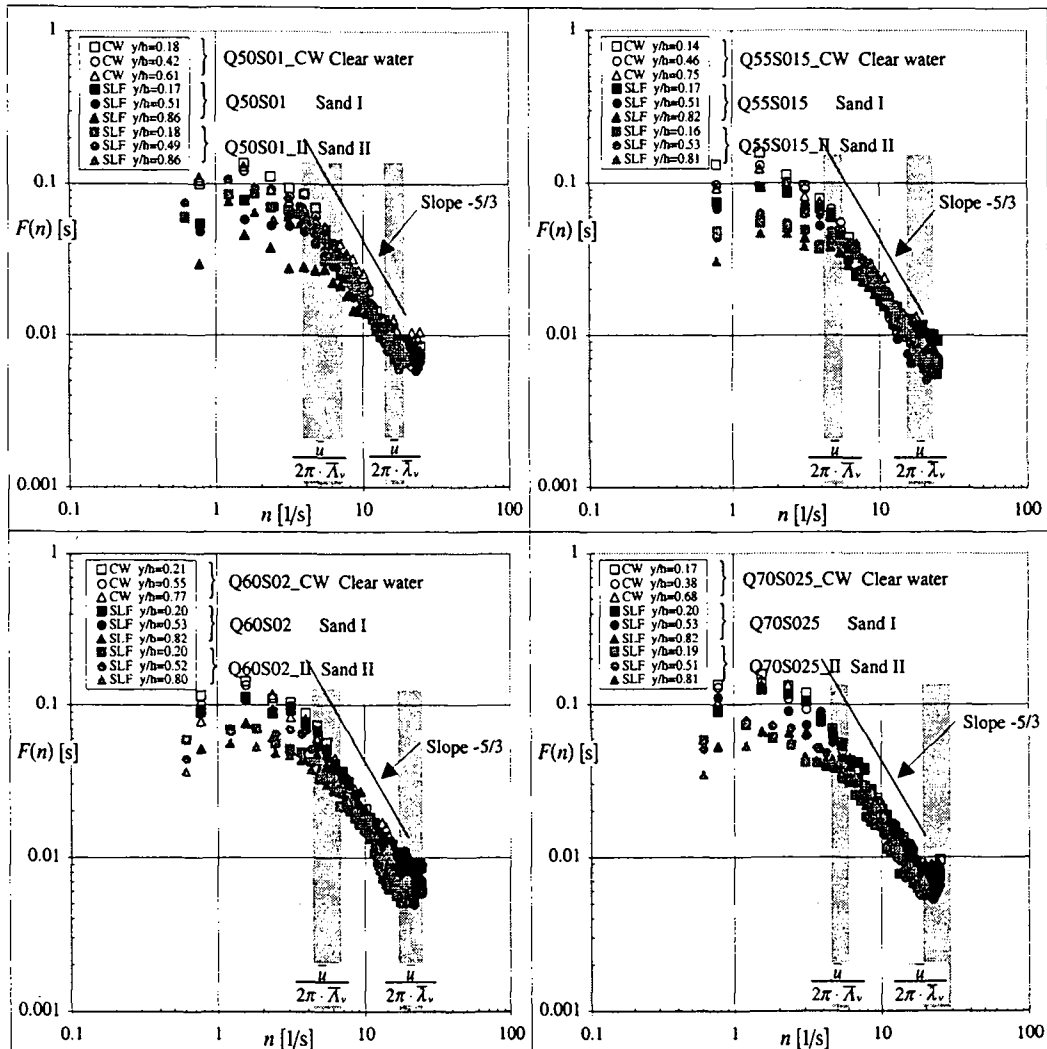


Fig. 3.8: Typical energy spectra for suspension flows using sand I (black symbols) and sand II (gray symbols)

### 3.7 Turbulence scale

The turbulence may be thought of as a group of various scales of eddies. It is customary to identify two characteristic scales of turbulence, namely the micro scale,  $\lambda$ , and the macro scale,  $\Lambda$ . The micro scale,  $\lambda$ , represents the size of the eddies responsible of the energy dissipation, while the macro scale,  $\Lambda$ , represents the characteristic size of the eddies containing the turbulent energy. Since the turbulence is not isotropic, the turbulence scales along the longitudinal and vertical directions have to be distinguished. In this way the both scales have been divided into longitudinal,  $\lambda_u$  and  $\Lambda_u$ , and vertical,  $\lambda_v$  and  $\Lambda_v$ , components. The turbulence scales along the longitudinal and vertical directions are empirically related as follows (see *Graf and Altinakar, 1991, p. 271*):

$$\lambda_u = \sqrt{2} \cdot \lambda_v \quad \text{and} \quad \Lambda_u = 2 \cdot \Lambda_v \quad (3.8)$$

It is possible to compute these scales knowing the correlation coefficients of a time series of the longitudinal or vertical velocity fluctuations. The correlation coefficients are computed measuring in two points – a distance of  $r$  apart – both the fluctuating longitudinal and vertical velocities (see Fig. 3.9). In eq. 3.9 and 3.10 are presented the expression of the longitudinal and vertical correlation coefficients, respectively:

$$R_u(r) = \frac{\overline{u'_1 \cdot u'_2}}{\sqrt{\overline{u'^2_1} \cdot \sqrt{\overline{u'^2_2}}} \quad (3.9)$$

$$R_v(r) = \frac{\overline{v'_1 \cdot v'_2}}{\sqrt{\overline{v'^2_1} \cdot \sqrt{\overline{v'^2_2}}} \quad (3.10)$$

The correlation coefficient for the same point, when  $r = 0$ , is equal to unity. The correlation coefficient is equal to zero if the fluctuating velocities are not correlated, this is the case if  $r \rightarrow \infty$ . An example of the correlation profiles is plotted in Fig. 3.10.

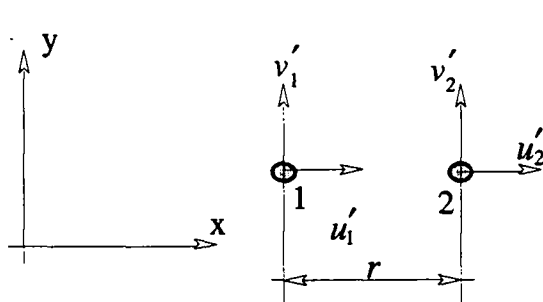


Fig. 3.9: Measurements points

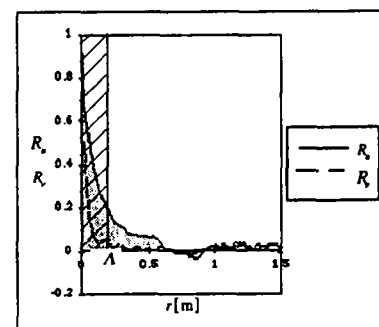


Fig. 3.10: Characteristic trend of the correlation coefficients

The integral of the correlation coefficients (equal to the gray surface in Fig. 3.10) gives the macro (integral) scale of the turbulence,  $\Lambda$ ; the longitudinal and vertical macro scales are defined as:

$$\Lambda_u = \int_0^\infty R_u(r)dr; \quad \Lambda_v = \int_0^\infty R_v(r)dr \quad (3.11)$$

The longitudinal and vertical micro scales are defined as:

$$\frac{1}{\lambda_u^2} = -\frac{1}{2} \cdot \frac{\partial^2}{\partial r^2} R_u(r)|_{r \rightarrow 0}; \quad \frac{1}{\lambda_v^2} = -\frac{1}{2} \cdot \frac{\partial^2}{\partial r^2} R_v(r)|_{r \rightarrow 0} \quad (3.12)$$

Since it is difficult to compute the micro scales according to these relations, a definition given by *Nezu and Nakagawa*, 1993, p. 73, will be used:

$$\lambda_u = \frac{\sqrt{u'^2}(y)}{\sqrt{(\partial u / \partial x)^2}}; \quad \lambda_v = \frac{\sqrt{v'^2}(y)}{\sqrt{(\partial v / \partial x)^2}} \quad (3.13)$$

Invoking the Taylor frozen turbulence hypothesis, eq. 3.13 can be written as:

$$\lambda_u = \bar{u} \cdot \frac{\sqrt{u'^2}}{\sqrt{\left(\frac{\partial u}{\partial t}\right)^2}}; \quad \lambda_v = \bar{u} \cdot \frac{\sqrt{v'^2}}{\sqrt{\left(\frac{\partial v}{\partial t}\right)^2}} \quad (3.14)$$

The macro-scale profiles, computed with eq. 3.11, for suspension flows carrying sand I and sand II, are presented in Fig. 3.11. For the sake of comparison, also the macro-scale profiles measured in a clear-water flow (run CW\_S015, see Appendix C) are shown. The longitudinal macro-scale profiles,  $\Lambda_u$ , for both sand I and sand II, increase in the inner region ( $y/h < 0.2$ ) with the distance from the bed (see Fig. 3.11a,c) while in the upper part of the flow ( $y/h > 0.2$ ) they remain rather constant. The vertical macro-scale profiles,  $\Lambda_v$ , also increase near the bed reaching a maximum value around  $y/h = 0.2$ , they decrease towards the flow surface. In both cases the profiles reach a maximum value at the height  $y/h \approx 0.3$ . Note, that the longitudinal macro scales are always larger than the vertical ones. The longitudinal and vertical macro-scale profiles measured in clear-water are larger than the ones measured using sand II whereas, for sand I, the profiles are similar.

The longitudinal and vertical micro-scales distributions for sand I and sand II are plotted respectively in Fig. 3.12a,b and Fig. 3.12c,d. The tendency of the micro-scale profiles is rather evident. All the profiles, for both sand I and sand II, increase with the distance from the bed reaching the maximum value close to the water surface,  $y/h \approx 0.8$ . Very close to the flow surface,  $y/h > 0.9$ , the profiles slightly decrease;

this effect is probably due to the vicinity of the water surface. For both sand I and sand II it is evident that, increasing the depth-averaged concentration, the micro scales increase. This is confirmed by the profiles measured in clear-water flow (run CW\_S015), which are smaller than the suspension flow ones. This tendency will be examined later. The longitudinal micro scales are slightly larger than the vertical ones. For sand II, both the longitudinal and vertical micro scales, are larger than the ones measured in case of sand I.

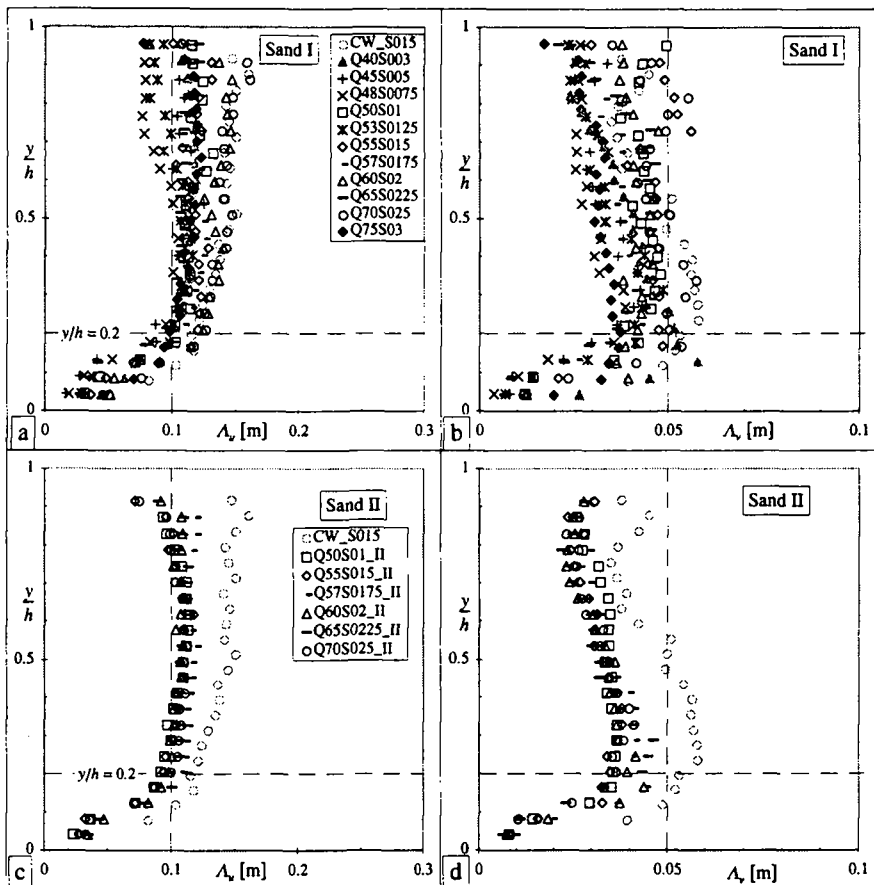


Fig. 3.11a,b,c,d: Macro-scales distributions (sand I and sand II)

The depth-averaged values of the micro and macro scales were calculated as well, such as:

$$\bar{\lambda}_u = \frac{1}{h} \int_{y=0}^{y=h} \lambda_u dy, \quad \bar{\lambda}_v = \frac{1}{h} \int_{y=0}^{y=h} \lambda_v dy; \quad \bar{\Lambda}_u = \frac{1}{h} \int_{y=0}^{y=h} \Lambda_u dy \text{ and } \bar{\Lambda}_v = \frac{1}{h} \int_{y=0}^{y=h} \Lambda_v dy \quad (3.15)$$

Their values are summarized for the different runs in Table 3.3. The turbulence scale range (for both sand I and sand II), in the form  $\frac{\bar{u}}{2\pi \cdot (\bar{\lambda}_v, \bar{\Lambda}_v)}$ , have been superimposed on the turbulence spectra (gray surface, see Fig. 3.8).

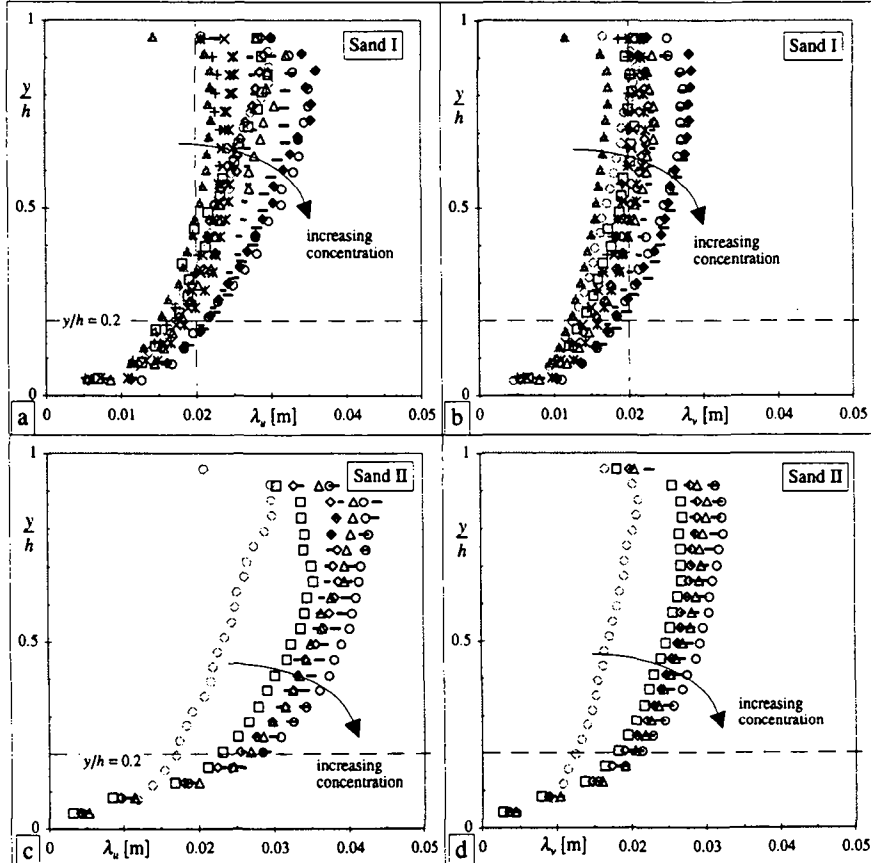


Fig. 3.12a,b,c,d: Micro-scales distributions (sand I and sand II)

The average value of the ratio between the depth-averaged longitudinal and vertical macro-scale lengths,  $\bar{\Lambda}_u/\bar{\Lambda}_v = 2.96$  for sand I and  $\bar{\Lambda}_u/\bar{\Lambda}_v = 3.18$  for sand II (see Table 3.3), are larger than the empirical one (see eq. 3.8), or  $\Lambda_u/\Lambda_v = 2$ . The average ratios of the micro-scale lengths,  $\bar{\lambda}_u/\bar{\lambda}_v = 1.20$  for sand I and  $\bar{\lambda}_u/\bar{\lambda}_v = 1.31$  for sand II, are close to the empirical one (see eq. 3.8), or  $\lambda_u/\lambda_v = \sqrt{2} = 1.41$ . This result confirms the reliability of the scale length – especially the micro-scale one – profiles measured by the APFP instrument. The longitudinal macro-scale profiles are always larger than the vertical ones (see Fig. 3.11); this means that the largest eddies are not circular being stretched by the longitudinal velocity. On the contrary, the longitudinal and vertical

micro-scale profiles are similar (see Fig. 3.12) showing that the smallest eddies are close to be circular even in presence of suspended particles.

run Clear water	$\bar{\Lambda}_u$	$\bar{\Lambda}_v$	$\bar{\Lambda}_u/\bar{\Lambda}_v$	$\bar{\lambda}_u$	$\bar{\lambda}_v$	$\bar{\lambda}_u/\bar{\lambda}_v$	Clear water flows		$\frac{\sqrt{v'^2}}{u_*}$	$\Delta\sqrt{v'^2}$
	[cm]	[cm]	[--]	[cm]	[cm]	[--]	Song , Graf and Lemmin , 1994	[--]	[%]	
CW_S015	13.40	4.60	2.91	2.17	1.60	1.36		0.740	0.00	
run Sand I	$\bar{\Lambda}_u$	$\bar{\Lambda}_v$	$\bar{\Lambda}_u/\bar{\Lambda}_v$	$\bar{\lambda}_u$	$\bar{\lambda}_v$	$\bar{\lambda}_u/\bar{\lambda}_v$	$C_s^m$	$\bar{c}_{sa}^m$	$\frac{\sqrt{v'^2}}{u_*}$	$\Delta\sqrt{v'^2}$
	[cm]	[cm]	[--]	[cm]	[cm]	[--]	[kg/m³]	[kg/m³]	[--]	[%]
Q40S003	10.60	3.75	2.82	1.81	1.42	1.28	2.05	24.62	0.512	-30.71
Q45S005	9.72	3.05	3.19	1.99	1.71	1.17	2.81	28.62	0.444	-40.02
Q48S0075	8.45	2.78	3.04	2.11	1.78	1.19	2.94	31.62	0.399	-46.11
Q50S01	10.77	4.09	2.63	2.21	1.74	1.27	3.61	39.33	0.415	-43.92
Q53S0125	9.47	3.18	2.98	2.19	1.94	1.13	3.32	36.04	0.505	-31.67
Q55S015	10.99	4.30	2.55	2.25	1.89	1.19	4.41	46.05	0.436	-41.05
Q57S0175	10.66	3.27	3.26	2.38	1.90	1.25	4.73	49.41	0.434	-41.33
Q60S02	12.15	4.03	3.02	2.39	1.96	1.22	4.91	48.58	0.449	-39.32
Q65S0225	9.98	3.57	2.79	2.60	2.26	1.15	5.08	50.82	0.411	-44.38
Q70S025	12.87	4.48	2.87	2.67	2.28	1.17	5.98	50.04	0.433	-41.52
Q70S03	10.51	3.06	3.44	2.79	2.32	1.21	6.29	62.47	0.473	-36.00
average	10.56	3.60	2.96	2.31	1.93	1.20	4.19	42.51	0.446	-39.64
run Sand II	$\bar{\Lambda}_u$	$\bar{\Lambda}_v$	$\bar{\Lambda}_u/\bar{\Lambda}_v$	$\bar{\lambda}_u$	$\bar{\lambda}_v$	$\bar{\lambda}_u/\bar{\lambda}_v$	$C_s^m$	$\bar{c}_{sa}^m$	$\frac{\sqrt{v'^2}}{u_*}$	$\Delta\sqrt{v'^2}$
	[cm]	[cm]	[--]	[cm]	[cm]	[--]	[kg/m³]	[kg/m³]	[--]	[%]
Q50S01_II	9.01	2.98	3.02	2.74	2.15	1.27	1.57	21.31	0.433	-41.59
Q55S015_II	8.99	2.86	3.14	3.02	2.30	1.32	2.30	28.07	0.436	-45.27
Q57S0175_II	9.71	3.09	3.14	2.98	2.28	1.31	2.01	24.77	0.448	-39.54
Q60S02_II	9.36	2.92	3.20	3.13	2.40	1.30	1.90	23.29	0.446	-39.86
Q65S0225_II	9.65	2.86	3.37	3.28	2.47	1.33	2.78	34.36	0.434	-41.41
Q70S025_II	9.16	2.85	3.22	3.34	2.56	1.31	2.84	33.83	0.418	-43.53
average	9.31	2.93	3.18	3.08	2.36	1.31	2.23	27.61	0.44	-41.87

Table 3.3: Depth-averaged micro and macro scales (sand I and sand II)

Also shown in Table 3.3 are the depth-averaged concentrations,  $C_s^m$ , and the reference concentrations,  $\bar{c}_{sa}^m$ , measured with the suction method (see Table 3.1 and Table 3.2). The measurements of the concentration will be discussed later. There is a weak increasing trend discernible observing the longitudinal,  $\bar{\Lambda}_u$ , and vertical,  $\bar{\Lambda}_v$ , depth-averaged macro scales, plotted against the depth-averaged concentration,  $C_s^m$ , for sand I (see Fig. 3.13a,b). No tendencies are discernible observing the sand II measurements (see Fig. 3.13c,d). The longitudinal and vertical macro scales measured in clear water,  $C_s^m = 0$ , are the largest ones. In Fig. 3.13e,f the longitudinal and vertical depth-averaged macro scales, measured using sand I and II, are compared.

Apart the clear-water runs, an overall tendency of the turbulence macro scales to increase with the concentration is somehow evident.

In Fig. 3.14 for clear water and for both sand I and sand II, are shown the dimensionless depth-averaged longitudinal,  $\bar{\lambda}_u/h$ , and vertical,  $\bar{\lambda}_v/h$ , micro-scale ones plotted against the depth-averaged concentration,  $C_s^m$ . There is a clear, but weak tendency of  $(\bar{\lambda}_u, \bar{\lambda}_v)/h$  to increase with the concentration. In Fig. 3.14e,f the results, for sand I and II, are compared. Both the dimensionless longitudinal micro and macro scales, measured in presence of sand II, are larger than the ones measured with sand I and clear water. This is probably due to the size of sand II ( $d_{50} = 0.230$  [mm]) which is larger than the sand I one ( $d_{50} = 0.135$  [mm]). The larger particles (sand II) are probably partially ejected away by the smallest eddies – by centrifugal forces – increasing the apparent micro-scale length (see Fig. 3.14e,f). For sand I this effect is weaker leading to values similar to the clear-water ones. This “centrifugal” effect is not important for larger eddy scales (macro scale, see Fig. 3.13e,f).

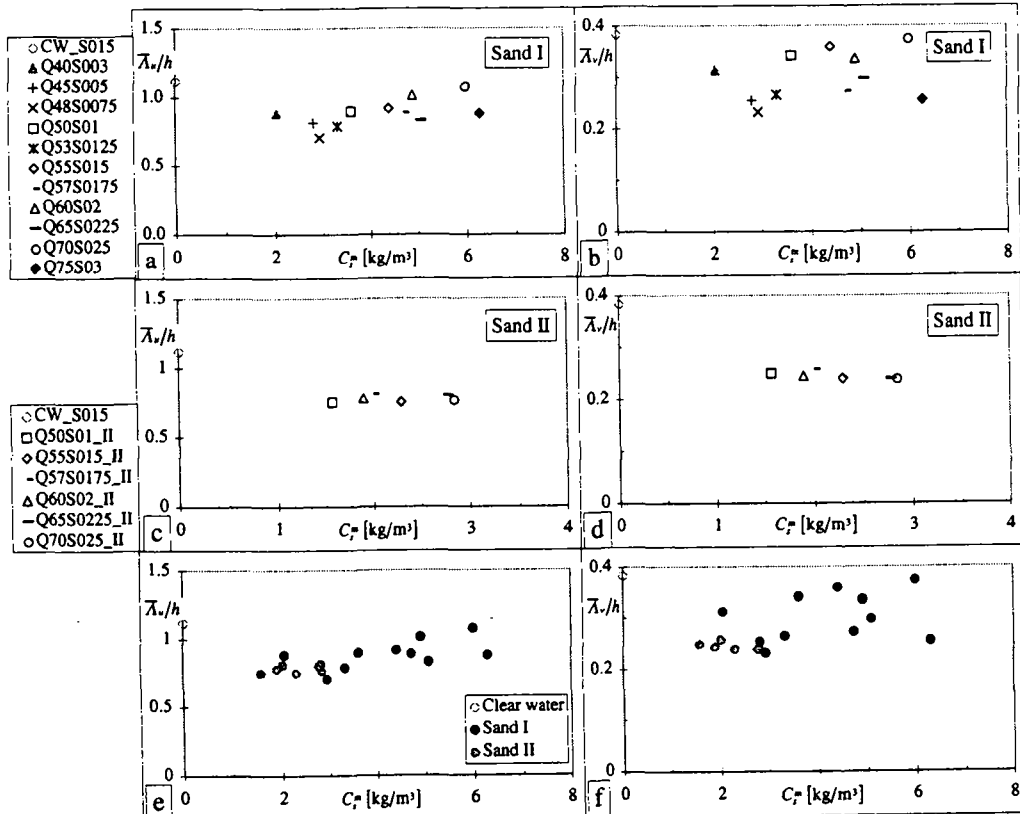


Fig. 3.13a,b,c,d,e,f: Influence of depth-averaged concentration on macro scales

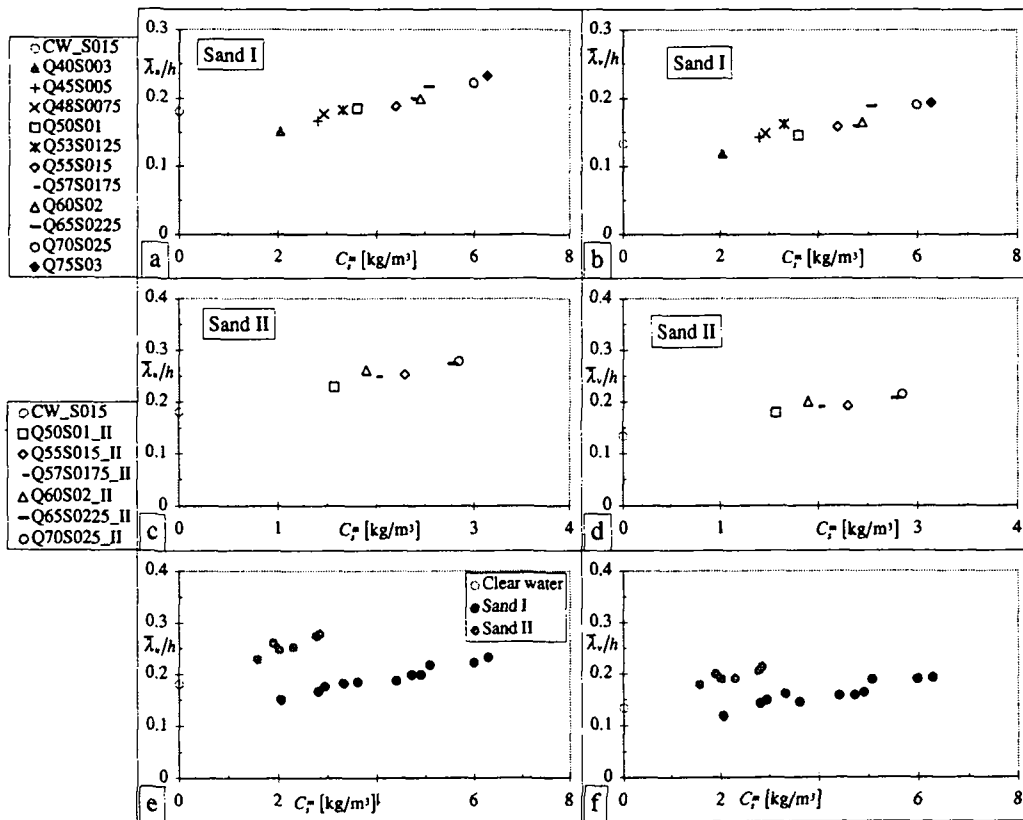


Fig. 3.14a,b,c,d,e,f: Influence of depth-averaged concentration on micro scales

*Gore and Crowe, 1989*, summarized experimental data – taken from the literature – on the turbulence modulation due to the addition of particles to the flow and proposed for scaling the turbulence modulation (expressed as  $\left( \sqrt{u'_s} - \sqrt{u'_w} \right)$ , where  $u'_s$  and  $u'_w$  are the fluctuation of the velocity of mixture and correspondent clear-water flow, respectively) the ratio of particle diameter,  $d$ , to the integral length scale,  $\Lambda$ , such as:

$$\frac{\sqrt{u'_s} - \sqrt{u'_w}}{\sqrt{u'_w}} \cdot 100 = f\left(\frac{d}{\Lambda}\right) \quad (3.16)$$

The data collected by *Gore and Crowe, 1989*, are shown in Fig. 3.15. These results refer to air-solid, liquid-solid and liquid-air suspensions. Even for such a variety of different mixture flows it was evident that for values of  $d/\Lambda < 0.1$  the turbulence is suppressed whereas for  $d/\Lambda > 0.1$  an enhancement of the turbulence takes place.

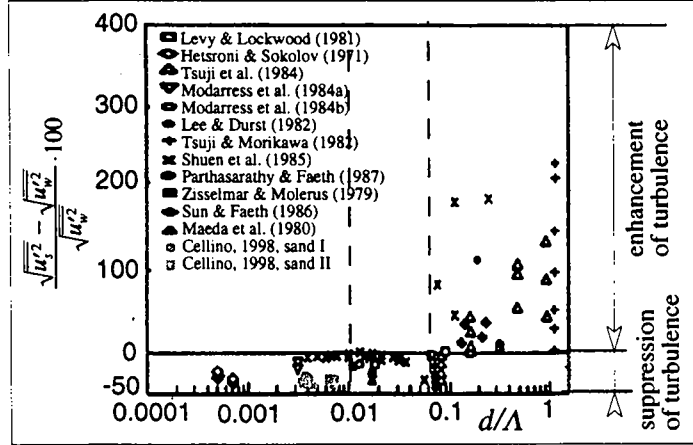


Fig. 3.15: Relationship between turbulence damping and macro scale

The relation given with eq. 3.16 shall be used to try to explain our data. In case of suspension flows we shall compute the left-hand side of eq. 3.16, such as:

$$\Delta \overline{\sqrt{v'^2}} = \frac{\sqrt{\overline{v'^2}_{SF}} - \sqrt{\overline{v'^2}_{CW}}}{\sqrt{\overline{v'^2}_{CW}}} \cdot 100 \quad (3.17)$$

where:  $\sqrt{\overline{v'^2}_{SF}}$ , depth-averaged value of the rms. fluctuating vertical velocity measured in suspension flow:  $\sqrt{\overline{v'^2}_{SF}} = \frac{1}{h} \int_{y=0}^{y=h} \sqrt{v'^2}(y) dy$

$\sqrt{\overline{v'^2}_{CW}}$ , depth-averaged value of the rms. fluctuating vertical velocity measured in clear water flow:  $\sqrt{\overline{v'^2}_{CW}} = \frac{1}{h} \int_{y=0}^{y=h} \sqrt{v'^2}(y) dy$  (the measurements presented by *Song, Graf and Lemmin, 1994*, have been used for computation).

In Table 3.3 (sand I) and in Table 3.4 (sand II) the depth-averaged values of the vertical turbulence-intensity profiles,  $\sqrt{v'^2}/u_*$ , are reported. The difference between these values and the ones measured by *Song, Graf and Lemmin, 1994*, in clear-water flows,  $\Delta \overline{\sqrt{v'^2}} [\%]$ , represents the modulation of the vertical turbulence intensity due to suspended particles. An average modulation of  $\Delta \overline{\sqrt{v'^2}} \approx 40 [\%]$  was found for sand I and  $\Delta \overline{\sqrt{v'^2}} \approx 42 [\%]$  for sand II; these values are compared with *Gore and Crowe's, 1989*, results, in Fig. 3.15. The results obtained with sand I (gray circles) and sand II (gray box) confirm the suppression of turbulence for values of  $d/\Lambda < 0.1$ . The tendency of the turbulence modulation,  $\Delta \overline{\sqrt{v'^2}}$ , to increase with  $d/\Lambda$  is evident only for non-capacity flows (open gray circles, see Appendix C). Enhancement of the turbulence would be observed if, for the given flow and its characteristic value of the

vertical macro scale, namely:  $\bar{A}_v = 0.03$  [m], the diameter of the sand particles was:  $d > 0.1 \cdot \bar{A}_v = 3$  [mm].

The relation between the turbulence modulation,  $\Delta\sqrt{v'^2}$ , and the parameters,  $d_{50}/(\bar{\lambda}_u, \bar{\lambda}_v)$  (called here dimensionless micro scale) and  $d_{50}/(\bar{A}_u, \bar{A}_v)$  (called here dimensionless macro scale), shall be investigated more closely. The respective plots are shown in Fig. 3.16 (macro scale) and in Fig. 3.17 (micro scale).

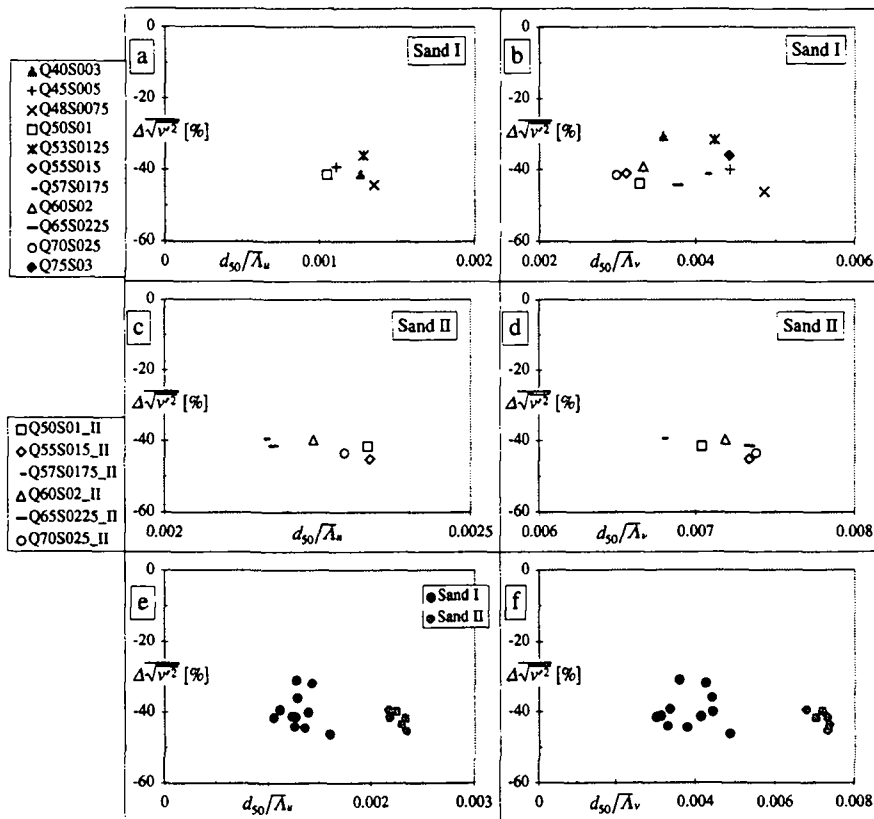


Fig. 3.16a,b,c,d,e,f: Turbulence modulation against macro scales (sand I and sand II)

In Fig. 3.16a,b (sand I) a correlation between the turbulence modulation and the dimensionless macro scale,  $d_{50}/(\bar{\lambda}_u, \bar{\lambda}_v)$ , is not discernible. On the contrary, for sand II (see Fig. 3.16c,d), the turbulence modulation seems to decrease for increasing values of the dimensionless macro scale. By comparing the results of sand I and sand II (see Fig. 3.16e,f), an overall weak tendency of the turbulence modulation to decrease for increasing values of the dimensionless macro scale becomes somehow evident. This result is in contrast with the overall tendency shown in Fig. 3.15.

The turbulence modulation, plotted against the dimensionless micro scale,  $d_{50}/(\bar{\lambda}_u, \bar{\lambda}_v)$ , using sand I (see Fig. 3.17a,b) and sand II (see Fig. 3.17c,d), seems to increase weakly. In Fig. 3.17e,f, the turbulence modulations, measured using sand I and sand II, are compared. Again, a very weak tendency of the turbulence modulation to increase with the dimensionless micro scale can be observed. By investigating non-capacity flow (see Appendix C, Fig. C9), the same tendency has been observed much more clearly.

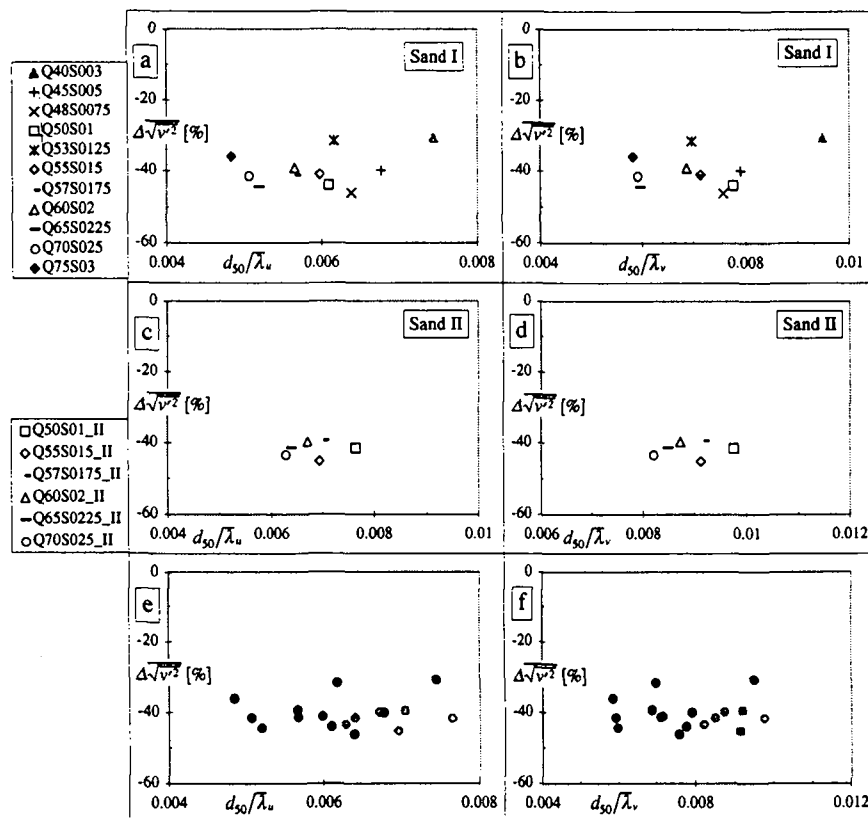


Fig. 3.17a,b,c,d,e,f: Turbulence modulation against micro scales

To sum up, the dimensionless macro scale,  $d/\Lambda$ , can be used as a discriminant parameter to judge whether suspended particles enhance or suppress the turbulence of the carrying fluid. Gore and Crowe, 1989, showed that for value of  $d/\Lambda > 0.1$  the suspended particles enhances the turbulence while for  $d/\Lambda < 0.1$  the turbulence is partially suppressed. This tendency has been confirmed by our measurements. In other words, if the particles are small, compared to the size of the macro eddies,  $d/\Lambda < 0.1$ , the suspended particles operate as a turbulence suppresser. On the contrary, if the

particles can be considered large, a turbulence enhancement takes place. Some researchers tried to explain the latter effect as a consequence of the wake region generated behind these “large” particles (see *Hetsroni*, 1989).

### 3.8 Concentration profiles

The APFP instrument has been used to measure simultaneously the instantaneous velocities,  $u(y, t)$  and  $v(y, t)$ , and concentration profiles,  $c_s(y, t)$ . The mean concentration profiles,  $\bar{c}_s(y)$ , have also been measured by the suction method to calibrate the APFP instrument (see *Shen and Lemmin*, 1996). Comparing the vertical mean echo-intensity profile, measured by the APFP instrument, and the vertical mean concentration profile, measured by the suction method, a calibration curve was obtained. Since a calibration is very important to obtain precise results, it has been performed for every run investigated. In Fig. 3.18 are presented some typical calibration curves, being linear fits.

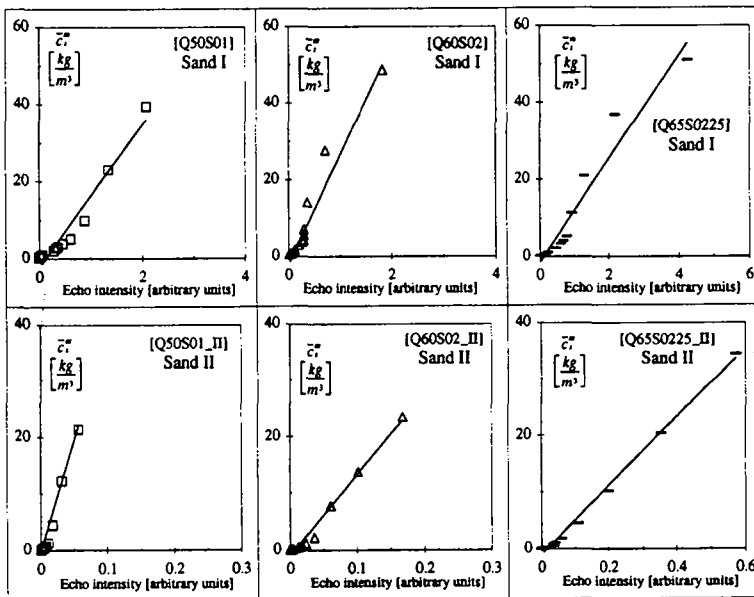


Fig. 3.18: Typical calibration curves

The mean concentration profiles,  $\bar{c}_s^m(y)$  – measured with the suction method – as well as the profiles of the dimensionless fluctuating concentration,  $\sqrt{\bar{c}_s'^2}/\bar{c}_{sa}^m$  – measured with the APFP instrument – are plotted in Fig. 3.19. The reference concentration,  $\bar{c}_{sa}^m$  [kg/m<sup>3</sup>] evaluated at  $a = 0.05 \cdot h$ , as well as the depth-averaged concentrations,  $C_s^m$  [kg/m<sup>3</sup>] – both measured with the suction method – are given in Table 3.1 and Table 3.2.

The dimensionless fluctuating concentration profiles,  $\sqrt{c_s'^2}/\bar{c}_{sa}^m$ , (see Fig. 3.19) have their maximum values close to the bed ( $y/h < 0.2$ ) for both sand I and sand II; in the upper part of the flow the fluctuating concentrations remain rather constant. These profiles are rather similar to the ones measured by Thorne et al., 1996, p. 351.

The sediment-flux profiles,  $\bar{c}'v'$ , are also shown in Fig. 3.19, being normalized with their values at  $y=a$ . Some scattering is present, but globally all profiles (for sand I and sand II) are of similar shape.

The dimensionless mean concentration profiles,  $\bar{c}_s^m/\bar{c}_{sa}^m$  – measured with the suction method – are plotted in Fig. 3.19; they are used to obtain the  $\bar{\beta}_{SM}$ -values, computed by best-fitting (least-squares method) to the Rouse equation, eq. 1.7. The resulting  $\bar{\beta}_{SM}$ -values are listed in Table 3.1 and Table 3.2, being considerably different from the “theoretical” value of  $\bar{\beta} = 1$ . These results will be further discussed later.

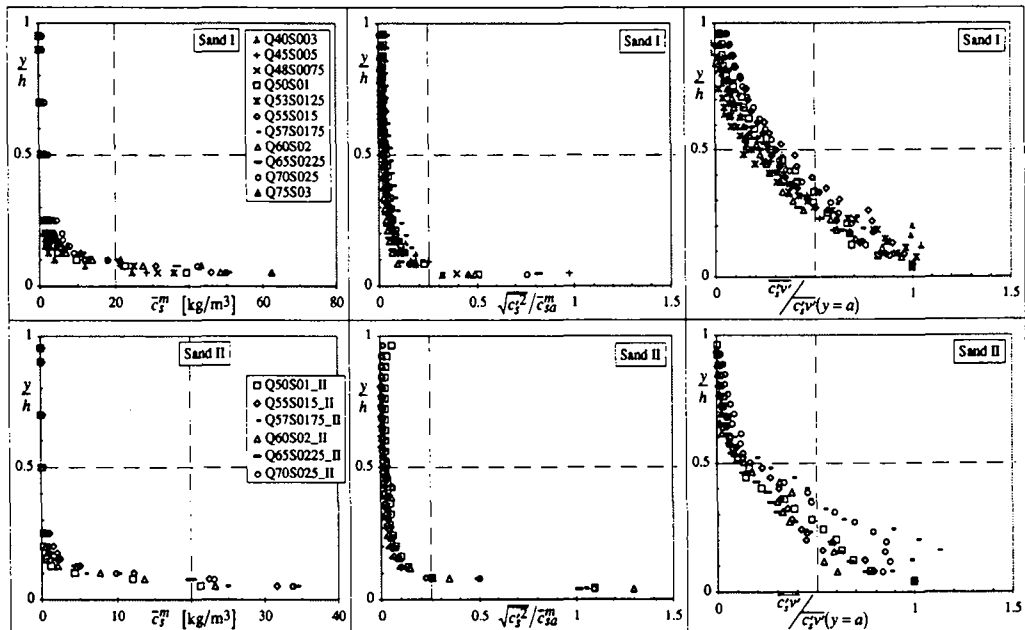


Fig. 3.19: Mean concentration profiles measured by the suction method, fluctuating concentration and sediment-flux profiles measured by the APFP instrument

### 3.9 Diffusion coefficients

The simultaneous measurements of both the instantaneous velocity and concentration permitted a direct calculation of both the momentum and sediment diffusion coefficient profiles, according to their respective definitions:

$$\text{sediment diffusion coefficients: } \varepsilon_s(y) [\text{m}^2/\text{s}] = -\frac{\overline{c'_s v'}}{\partial \bar{c}_s / \partial y} \quad (1.12)$$

$$\text{in dimensionless form: } \frac{\varepsilon_s(y)}{u_* h} [-]$$

$$\text{momentum diffusion coefficients } \varepsilon_m(y) [\text{m}^2/\text{s}] = -\frac{\overline{u' v'}}{\partial \bar{u} / \partial y} \quad (1.13)$$

$$\text{in dimensionless form: } \frac{\varepsilon_m(y)}{u_* h} [-]$$

$$\beta\text{-value: } \beta(y) = \frac{\varepsilon_s(y)}{\varepsilon_m(y)} = \frac{\overline{c'_s v'} / (\partial \bar{c}_s / \partial y)}{\overline{u' v'} / (\partial \bar{u} / \partial y)}(y) \quad (1.6)$$

In Fig. 3.20 the dimensionless form of the experimental – obtained with the APFP instrument – sediment diffusion coefficient,  $\varepsilon_s$ , profiles (black points) are compared with the experimental (gray points) and the theoretical (full line) clear-water momentum diffusion,  $\varepsilon_m$ , coefficient profiles. The shapes of the sediment and momentum diffusion coefficient profiles of the different runs for both sands are rather similar. However, scattering is large and even the dimensionless form does not take care of this; apparently the concentration and the sand size should still be considered.

Close to the bed, where the concentration is high, the momentum diffusion coefficients are always larger than the sediment diffusion coefficients for both sands. In the middle of the flow depth the difference is still very large, but in the upper part of the flow, where the concentration is small, the two diffusion coefficients become rather similar. Near the bed and near the water surface the momentum diffusion coefficient profiles (gray points) are similar to the theoretical (full line) clear-water one, while in the middle of the flow depth the difference is rather large.

Despite the scatter, there is sufficient evidence, that the sediment diffusion coefficients,  $\varepsilon_s(y)$ , are always smaller than the momentum diffusion coefficients,  $\varepsilon_m(y)$ ; the latter is almost always smaller than the theoretical value, eq. 1.6, postulated for clear-water flows.

In Fig. 3.21 the experimental momentum diffusion coefficient profiles,  $\varepsilon_m(y/h)$ , are compared to the corresponding sediment diffusion coefficient profiles,  $\varepsilon_s(y/h)$ , for some typical runs. From the bed – where the concentration is very high – to  $y/h \approx 0.8$ , the momentum diffusion coefficient is always larger than the sediment diffusion one.

This means that the sediment particles are less diffused than the momentum ones. The diffusion coefficients profiles become similar close to the flow surface (see Fig. 3.20 and Fig. 3.21).

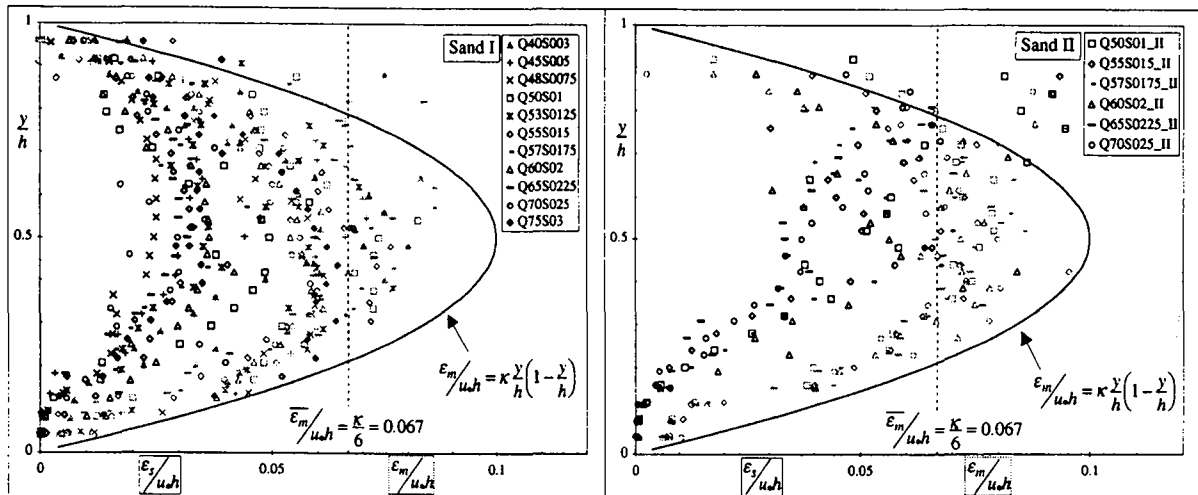


Fig. 3.20: Dimensionless sediment and momentum diffusion coefficient profiles

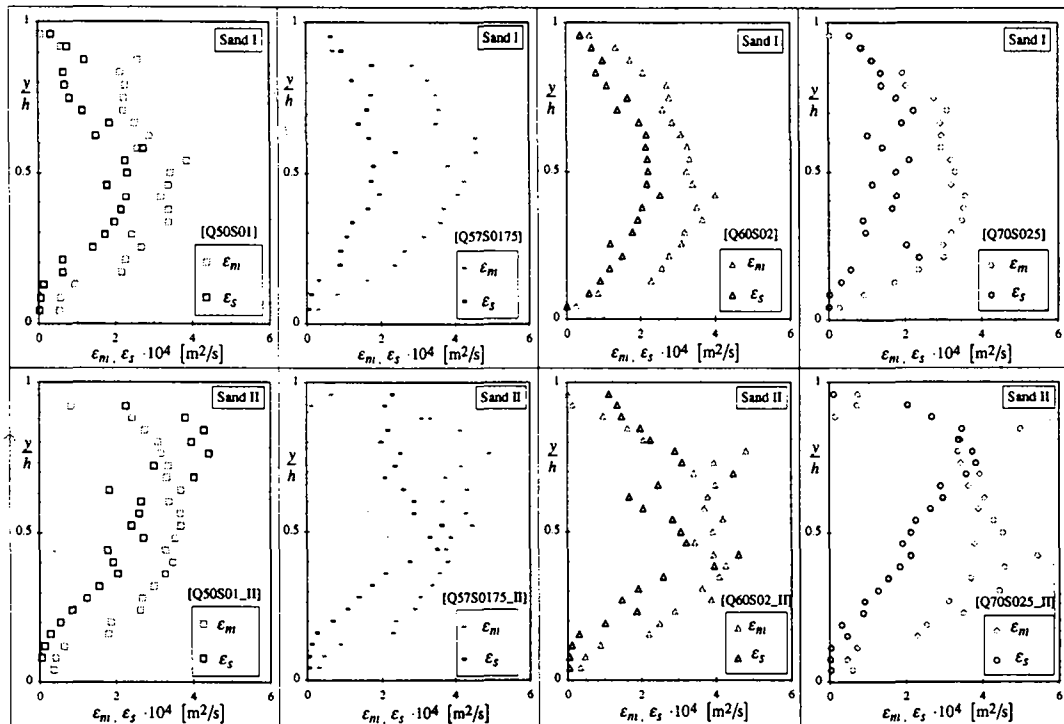


Fig. 3.21: Some typical sediment (gray points) and momentum (black points) diffusion coefficient profiles (sand I and sand II)

### 3.10 Experimental $\bar{\beta}$ -values

The ratio of the sediment and momentum diffusion coefficient defines the  $\beta(y)$ -value, given with eq. 1.15. Some typical vertical distributions of the  $\beta_{APFP}$ -values – the index recalls that the data are taken with the APFP instrument – are plotted in Fig. 3.22.

The  $\beta_{APFP}$ -values are close to zero at the bed and increase with the distance from the bed, up to  $y/h < 0.5$ . Above the mid-depth and towards the water surface, the  $\beta_{APFP}$ -values reach their maximum, but a clear tendency is not evident. From these plots it becomes also clear, that the higher the concentration,  $\bar{c}_s^m$  (see Fig. 3.19), the lower are the  $\beta_{APFP}$ -values. In Fig. 3.22 are also shown the depth-averaged values,  $\bar{\beta}_{APFP}$  (see Table 3.1 and Table 3.2), which are always smaller than the “theoretical” value of  $\bar{\beta} = 1$ .

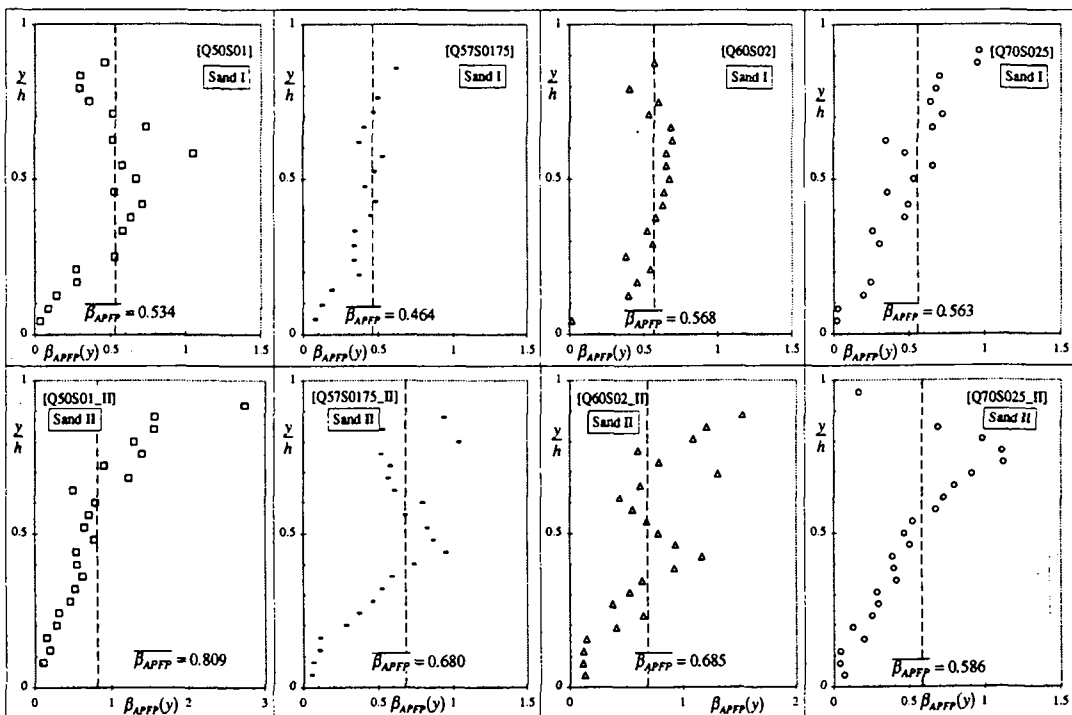


Fig. 3.22: Vertical profiles of the  $\beta_{APFP}$ -values (sand I and sand II)

Another way of obtaining a  $\bar{\beta}_{SM}$ -value – the index recalls that the data are taken with the suction method – is by best-fitting (least-squares method) the Rouse equation to the concentration profiles directly measured with the suction method. The  $\bar{\beta}$ -values obtained with these two independent methods,  $\bar{\beta}_{APFP}$  and  $\bar{\beta}_{SM}$ , shall be compared, as seen in

Table 3.1 and Table 3.2, being both smaller than unity,  $\overline{\beta}_{APFP}, \overline{\beta}_{SM} < 1$ . Such a comparison is also shown in Fig. 3.23 for some selected runs; while agreement is not perfect, it is considered to be reasonable. Also shown is the Rouse equation, using a value of  $\overline{\beta} = 1$  and the measured data points, used to obtain the  $\overline{\beta}_{SM}$ -values. In either cases, it is rather obvious that the  $\overline{\beta}$ -values for suspension flow of small particles, should be taken to be  $\overline{\beta} < 1$ . This conclusion is in agreement with *Jobson and Sayre*, 1970, p. 706 and *Graf*, 1984, p. 177.

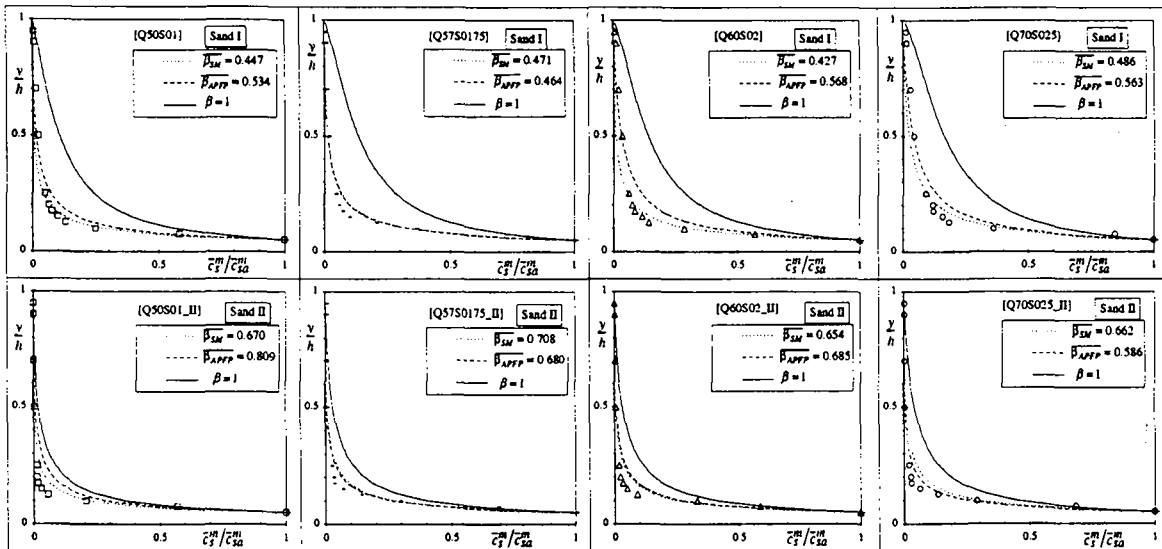


Fig. 3.23: Dimensionless concentration profiles.

### 3.11 Practical use of $\overline{\beta}$ -values

In the laboratory, where the experiments were performed, the suspension flows can be well established and their hydraulic parameters are thus well known. In field situations (river, waterways) the direct investigation of the sediment concentration profile is generally problematic. Therefore, it is useful to correlate the experimental  $\overline{\beta}$ -values with a parameter easily obtainable in situ. An important parameter involved in the diffusion of sediments is the settling velocity,  $v_{ss}$ . On the other hand, another important parameter involved in the momentum diffusion is the shear velocity,  $u_*$ . Thus, it seems reasonable to scale the experimental  $\overline{\beta}$ -values,  $\overline{\beta}_{APFP}$ , with the parameter  $v_{ss}/u_*$ ; this is shown in Fig. 3.24a.

In a second approximation also the sediment concentration affects the diffusion of fluid and sediment particles (see the effects of the high-concentration region on the

diffusion coefficient profiles, see Fig. 3.22 and Appendix C). For this reason the scaling parameter,  $v_{ss}/u_* \cdot C_s/\bar{c}_{sa}$ , has also been used.

The plot of  $\overline{\beta}_{APFP} = f(v_{ss}/u_*)$  is presented in Fig. 3.24a, while the plot of  $\overline{\beta}_{APFP} = f(v_{ss}/u_* \cdot C_s/\bar{c}_{sa})$  is presented in Fig. 3.24b.

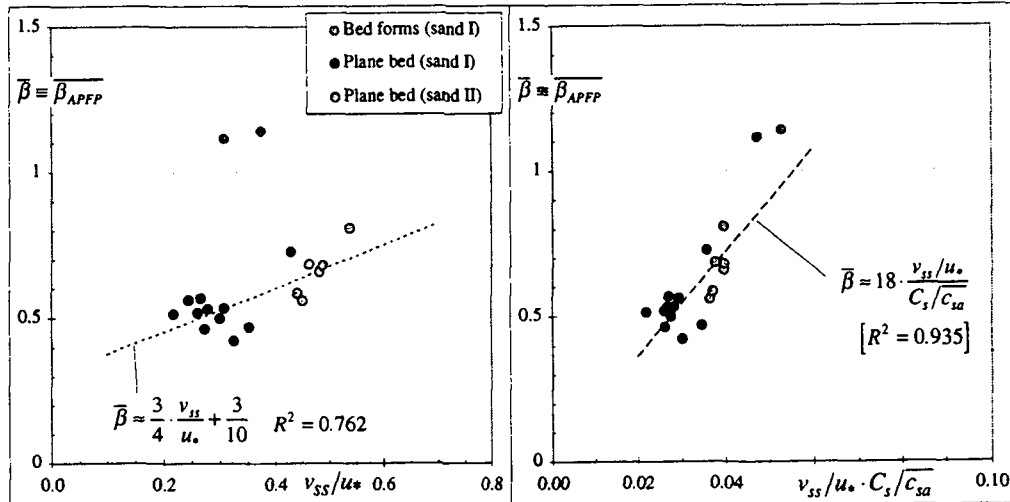


Fig. 3.24a,b: Correlation between the  $\overline{\beta}$ -values and the scaling parameters

For both sand I and sand II a tendency of the  $\overline{\beta}_{APFP}$ -values to increase with the scaling parameters,  $v_{ss}/u_*$ , is evident. For the sake of comparison the  $\overline{\beta}_{APFP}$ -values measured over bed forms (see Appendix D) are shown; note that in this case  $\overline{\beta}_{APFP} > 1$ . A linear relationship using a regression line might be suggested (taking only the plane bed values), such as:

$$\overline{\beta} \equiv \overline{\beta}_{APFP} \approx \frac{3}{4} \cdot \frac{v_{ss}}{u_*} + \frac{3}{10} \quad [R^2 = 0.762] \quad (3.18a)$$

$$\overline{\beta} \equiv \overline{\beta}_{APFP} \approx 18 \cdot \frac{v_{ss}/u_*}{C_s/\bar{c}_{sa}} \quad [R^2 = 0.935] \quad (3.18b)$$

Even if agreement is not excellent, eq. 3.18a or Fig. 3.24a can be used to obtain an approximated  $\overline{\beta}$ -value if the settling velocity of the suspended sediment,  $v_{ss}$ , and the shear velocity of the flow,  $u_*$ , are known. If the depth-averaged concentration,  $C_s$ , and the reference concentration,  $\bar{c}_{sa}$ , are also known, eq. 3.18b or Fig. 3.24b can be used.

In the literature, there has also been reported evidence, that  $\overline{\beta} \geq 1$  (see Appendix B, Nordin and Dempster, 1963, Coleman, 1970 and Rijn, 1984, p. 1621). Carefully study of this, points to the fact that the bed forms on the moveable bed might be responsible for these large  $\overline{\beta}$ -values. In the investigation reported in Appendix D, we

address this question. In Fig. 3.25, are shown two runs, each one having a plane bed and (hydraulically equivalent) beds with bed forms. Here, it is evident that the  $\bar{\beta}$ -values in the presence of bed forms are always larger. Such large values are mainly due to the effect of the high turbulence region, generated by the bed-form crest, where the sediment diffusion coefficient is considerably enhanced and the momentum diffusion coefficient is suppressed, leading to an augmentation of the  $\bar{\beta}$ -values.

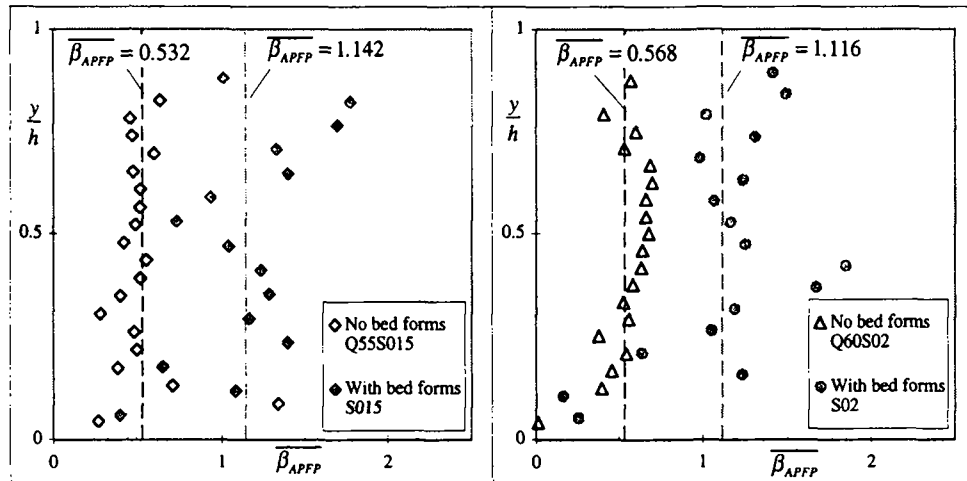


Fig. 3.25a,b: Profiles of  $\bar{\beta}_{APFP}$ -values for plane bed and bed forms

Several suspension flows over beds with bed forms taken from the literature, have been evaluated in Appendix B. The results refer to both channel and river data. Here is to be observed that the  $\bar{\beta}$ -values are always large,  $\bar{\beta} > 1$  (see Fig. 3.26), and have a tendency to increase with both the parameters,  $v_{ss}/u_*$  and  $v_{ss}/u_* \cdot C_s/\bar{c}_{sa}$ .

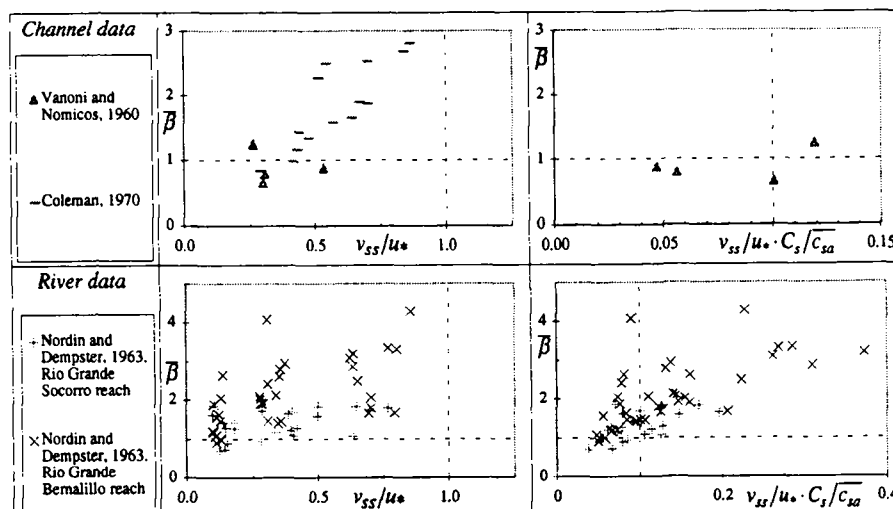


Fig. 3.26a,b,c,d: Data of the literature on flows over bed forms

All the data (channel with plane bed, channel with bed forms and river data) taken from the literature and analyzed in Appendix B as well as the results of this thesis are summarized in Fig. 3.27. Also shown are the regression line obtained by best-fitting (least-squares method) the data referring to flows over beds with bed forms (channels and river) as well as the one for the flows investigated in this thesis (beds without bed forms), eq. 3.18. Here it is particularly evident that for the suspension flows over beds without bed forms:  $\bar{\beta} < 1$ , while for the ones over beds with bed forms:  $\bar{\beta} > 1$ .

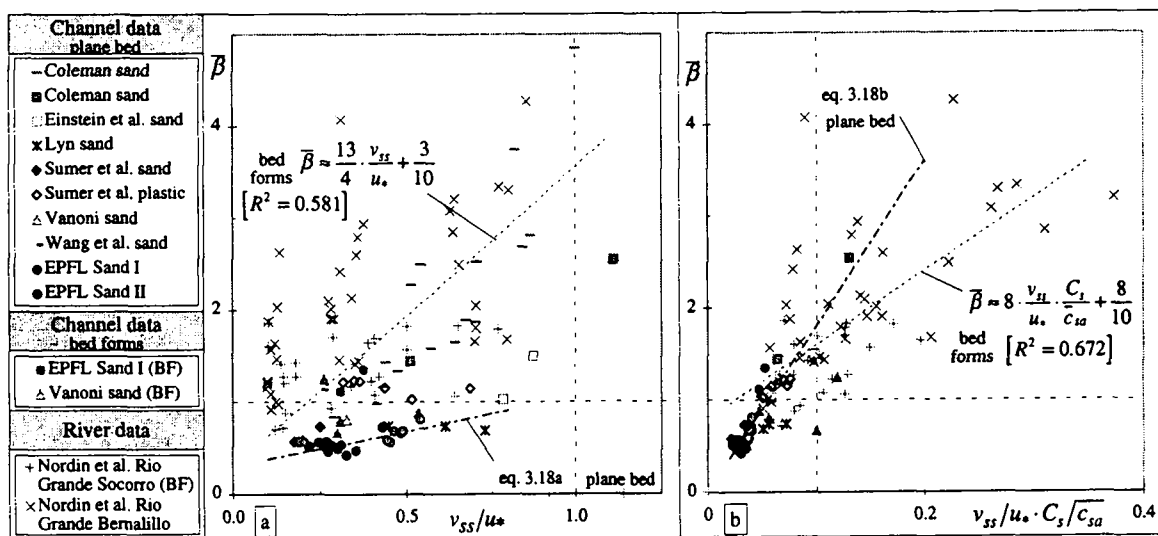


Fig. 3.27: Summary of all data considered

Figs. 3.24, 3.26 and 3.27 or the regression lines of eq. 3.18a,b can be used to obtain an approximated  $\bar{\beta}$ -value to establish the dimensionless concentration profile using the Rouse equation when few flow parameters are known, namely  $v_{ss}$  and  $u_*$  ( $v_{ss}/u_*$ ) or  $v_{ss}$ ,  $u_*$ ,  $C_s$  and  $\bar{c}_{sa}$  ( $v_{ss}/u_* \cdot C_s/\bar{c}_{sa}$ ). This is typically the case of natural rivers. Note, that the reference concentration,  $\bar{c}_{sa}^m$  [ $\text{kg/m}^3$ ], measured at  $a = 0.05h$ , must be known to compute the sediment concentration profile in dimensional form, in fact:

$$\frac{\bar{c}_s^m}{\bar{c}_{sa}^m} = \left( \frac{h-y}{y} \frac{a}{h-a} \right)^z \Rightarrow \bar{c}_s^m(y) [\text{kg/m}^3] = \bar{c}_{sa}^m(y) [\text{kg/m}^3] \cdot \left( \frac{h-y}{y} \frac{a}{h-a} \right)^{z'=\frac{v_{ss}}{\bar{c}_{sa}^m}=\frac{z}{\bar{\beta}}}$$

If the longitudinal velocity profiles,  $\bar{u}(y)$  [ $\text{m/s}$ ], and the suspended concentration profiles,  $\bar{c}_s^m(y)$  [ $\text{kg/m}^3$ ], are known, the suspended load can be easily calculated as follows (see *Graf*, 1984, p. 173):

$$g_{ss} \left[ \frac{\text{kg}}{\text{ms}} \right] = \int_{y=a}^{y=h} u(y) \cdot \bar{c}_s^m(y) dy$$

where  $g_{ss} \left[ \frac{\text{kg}}{\text{ms}} \right]$  is the suspended-load rate in weight per unit time and width.

### 3.12 Verification of the hypothesis of *Fortier*, 1967

In this thesis it has been supposed that the particles are small enough to justify the use of the clear-water formulation. This supposition is basically correct if the suspended particles have the same velocity than the surrounding fluid. Other conditions to be satisfied are related to the particle size and concentration that should not to be too large.

The local velocity of a suspension flow is usually defined as the weighted average of the local velocity of the fluid and of the sediment particles (see *Fortier*, 1967, p. 20), such as:

$$(u_m, v_m) = \frac{\rho_s c_s (u_s, v_s) + \rho_w (1 - c_s) (u_w, v_w)}{\rho_s c_s + \rho_w (1 - c_s)} \quad (3.19)$$

where:  $\rho_s$  [kg/m<sup>3</sup>]: density of sediment particles

$\rho_w$  [kg/m<sup>3</sup>]: density of the water

$c_s$  [m<sup>3</sup>/m<sup>3</sup>]: local instantaneous suspended-sediment concentration

$(u_m, v_m)$  [m/s]: longitudinal and vertical instantaneous velocity of suspension

$(u_s, v_s)$  [m/s]: longitudinal and vertical instantaneous velocity of the sediment

$(u_w, v_w)$  [m/s]: longitudinal and vertical instantaneous velocity of clear water

In this thesis only suspension flows in which suspended particles have the same instantaneous velocity than the surrounding fluid are investigated. In this way eq. 3.19 is simplified as follows:

$$(u_m, v_m) = (u_s, v_s) = (u_w, v_w) \quad (3.20)$$

The velocity of suspended particles can be assumed equal to the surrounding fluid (water) one if the relaxation time<sup>1</sup> of suspended particles is very small compared to the characteristic time of turbulence. This can be verified with the following expression proposed by *Fortier*, 1967, p. 92, reads:

$$\frac{\sqrt{(v'_w - \bar{v}_w)^2}}{\sqrt{v'_w^2}} \cong \frac{2}{9} \cdot \left| 1 - \frac{\rho_s}{\rho_w} \right| \cdot \frac{(d/2)^2}{v \cdot \tau_*} \ll 1 \quad (3.21)$$

where:  $\tau_*$  [s]: characteristic time of turbulence

$v'_w = v_w - \bar{v}_w$  [m/s]: vertical fluctuating velocity of the fluid (clear water)

<sup>1</sup> The relaxation time of a particle represents the time that the particle spend to adapt its velocity to the new one produced by a sudden acceleration of the surrounding fluid.

$v'_s = v_s - \bar{v}_s$  [m/s]: vertical fluctuating velocity of the sediment

$\rho_w$  [kg/m<sup>3</sup>]: density of the water

$d$  [m]: sediment diameter

$\nu$  [m<sup>2</sup>/s]: viscosity of the water

If the right-hand term of eq. 3.21 is very small, say < 0.01, it is possible to confuse the sediment and the fluid fluctuating velocities, such as:

$$\frac{\sqrt{(v'_w - v'_s)^2}}{\sqrt{v'^2}} < 0.01 \Rightarrow v'_m \approx v'_w \approx v'_s \quad (3.22)$$

If the sediment particles are smaller than the micro scale of turbulence,  $\lambda$ , they can follow the smallest eddies (having the highest frequency movements). This condition is verified by comparing the radius of the characteristic sediment particle,  $d$ , and the micro-scale of the fluid,  $\lambda$ . Thus, the expression to evaluate is:

$$\frac{d/2}{\lambda} \ll 1 \quad (3.23)$$

If eqs 3.21 and 3.23 are verified, the suspension flow can be treated as it was mono-phase. In addition, if the fluid is also Newtonian – as usually the case if the sediment is not Kaolin and if the concentration is not large ( $\bar{C}_s < 1\% \Rightarrow \bar{C}_s^m < 26.5$  [kg/m<sup>3</sup>], (see *Graf and Altinakar, 1996, p.104*) – it becomes possible to use the clear-water formulation also for suspension flows. The only corrections to do concern the suspension viscosity,  $\nu_m$ , and density  $\rho_m$ .

In the first condition, expressed by eq. 3.21, the characteristic time of the turbulence can be calculated as being the ratio of the characteristic vertical micro-scale,  $\lambda_v$ , and the characteristic fluctuating vertical velocity,  $\sqrt{v'^2}$  (the movement of sediment particles along the vertical direction is supposed to be the most representative):

$$\tau_* = \lambda_v / \sqrt{v'^2} \quad (Fortier, 1967, p. 92) \quad (3.24)$$

The evaluation of eq. 3.21 has been made in Table 3.4. In all the cases the criterion is satisfied.

The geometrical condition expressed in eq. 3.23, that reflects the possibility of the suspended particles to follow the micro-scale eddies, and the concentration condition, that limits the depth-averaged concentration,  $\bar{C}_s < 1\% \Rightarrow \bar{C}_s^m < 26.5$  [kg/m<sup>3</sup>], are shown in Table 3.4. In all cases the criteria proposed by *Fortier, 1967*, are widely

verified. Thus, the suspension flows investigated in this chapter can be treated as monophase and newtonian; the clear-water formulation can be applied.

run Sand I	$\tau_* = \frac{\sqrt{(v_f - v_p)^2}}{\sqrt{v_f^2}}$	Eq. 3.20	$\frac{d_{s0}/2}{\bar{\lambda}_v}$	Eq. 3.22	$C_s^m$	
	[s]	[--]		[--]		[kg/m³]
Q40S003	0.991	0.0017	<<1 verified	0.0047	<<1 verified	2.05
Q45S005	1.132	0.0015	<<1 verified	0.0040	<<1 verified	2.81
Q48S0075	1.207	0.0014	<<1 verified	0.0038	<<1 verified	2.94
Q50S01	1.076	0.0016	<<1 verified	0.0039	<<1 verified	3.61
Q53S0125	0.958	0.0017	<<1 verified	0.0035	<<1 verified	3.32
Q55S015	1.008	0.0017	<<1 verified	0.0036	<<1 verified	4.41
Q57S0175	0.997	0.0017	<<1 verified	0.0035	<<1 verified	4.73
Q60S02	0.972	0.0017	<<1 verified	0.0034	<<1 verified	4.91
Q65S0225	1.195	0.0014	<<1 verified	0.0030	<<1 verified	5.08
Q70S025	1.075	0.0016	<<1 verified	0.0030	<<1 verified	5.98
Q70S03	0.889	0.0019	<<1 verified	0.0029	<<1 verified	6.29

average	1.045	0.0016	0.0036	4.19
---------	-------	--------	--------	------

run Sand II	$\tau_* = \frac{\sqrt{(v_f - v_p)^2}}{\sqrt{v_f^2}}$	Eq. 3.20	$\frac{d_{s0}/2}{\bar{\lambda}_v}$	Eq. 3.22	$C_s^m$	
	[s]	[--]		[--]		[kg/m³]
Q50S01_II	1.275	0.0032	<<1 verified	0.0049	<<1 verified	1.57
Q55S015_II	1.212	0.0033	<<1 verified	0.0029	<<1 verified	2.30
Q57S0175_II	1.185	0.0034	<<1 verified	0.0030	<<1 verified	2.01
Q60S02_II	1.185	0.0034	<<1 verified	0.0028	<<1 verified	1.90
Q65S0225_II	1.223	0.0033	<<1 verified	0.0027	<<1 verified	2.78
Q70S025_II	1.284	0.0031	<<1 verified	0.0026	<<1 verified	2.84

average	1.227	0.0033	0.0032	2.23
---------	-------	--------	--------	------

Table 3.3: Verification of the Fortier criteria (sand I and sand II)

### 3.13 Conclusions

Suspension flows have been investigated by using an ultrasonic instrument (APFP) that allowed the simultaneous measurements of the instantaneous concentration and two-dimensional velocities. The direct evaluation of both the sediment,  $\bar{c}_s \bar{v}$ , and the momentum flux,  $\bar{u} \bar{v}$ , allowed the computation of the ratio,  $\beta(y)$ , of the sediment,  $\epsilon_s(y)$ , and of the momentum,  $\epsilon_m(y)$ , diffusion coefficients. The experimentally obtained  $\beta(y)$ -values — sensibly smaller than the unity (see Fig. 3.22) — have been correlated with the parameter  $v_{ss}/u_*$  (see Fig. 3.27 or eqs. 3.18) leading to a graphic of practical use. For beds without bed forms the  $\bar{\beta}$ -values are  $\bar{\beta} < 1$ , while for beds with bed forms the  $\bar{\beta}$ -values are  $\bar{\beta} > 1$ .

The profiles of the longitudinal component of the turbulence intensity,  $\sqrt{u'^2}/u_*$  (see Fig. 3.6a,c), measured in suspension flows are reasonably comparable to the clear-water ones. However the profiles of the vertical component of the turbulence intensity,  $\sqrt{v'^2}/u_*$  (see Fig. 3.6b,d), are clearly lower than the clear-water ones. The correspondent change of turbulence intensity,  $\Delta\sqrt{v'^2}$ , has been scaled by using the particle diameter / turbulence macro-scale ratio (see Figs. 3.15, 3.16 and 3.17) according to the popular diagram proposed by Gore and Crowe (1989). Our results confirm the tendency that “small” particles,  $d/\Lambda_v < 0.1$ , operate as turbulence suppressors.

### 3.14 References

- BEST, J. L. (1993). “On the interactions between turbulent flow structure, sediment transport and bedform development: some considerations from recent experimental research”, in *Turbulence, Perspectives on Flow and Sediment Transport* Wiley & Sons Ltd. Chichester, UK, pp. 61-92.
- CAO, Z., WEI, L. and XIE, J. (1995). “Sediment-laden Flow in Open-channels from two-phase Flow viewpoint.” *J. Hydr. Engr.*, Vol. 121, N° 10, pp. 725-735.
- CIOFFI, F. And GALLERANO, F. (1991). “Velocity and concentration profiles of solid particles in a channel with movable and erodible bed” *J. Hydr. Res.*, vol. 29, N.° 3, pp. 387-401.
- COLEMAN, N. L. (1970). “Flume Studies of the Sediment Transfer Coefficient.” *Water Resources Research*, vol. 6, N.° 3, pp. 801-809.
- COLEMAN, N. L. (1981). “Velocity profiles with suspended sediment.” *J. Hydr. Res.*, vol. 19, N° 3, pp. 211-229.

- EINSTEIN, H. A. and CHIEN, N. (1955). "Effects of Heavy Sediment Concentration Near the Bed on the Velocity and Sediment Distribution." Uni. of Cal., Berkeley, US Army Corps of Engr., Missouri River Div.
- FORTIER, A. (1967). *Mécanique des suspension*, Masson, Paris.
- GORE, R. A. and CROWE, C. T. (1989). "Effect of Particle size on modulating turbulent intensity." *J. Fluids Engnr.*, vol. 111, pp. 304-307.
- GRAF, W. H. (1984). *Hydraulics of Sediment Transport*, Water Resource Publications, Littleton, CO, USA.
- GRAF, W. H. and ALTINAKAR, M. S. (1991). *Hydrodynamique*, Eyrolles, Paris.
- GRAF, W. H. and ALTINAKAR, M. S. (1996). *Hydraulique fluviale Tome 2*, Presses Polytechniques et Universitaires Romandes, Lausanne.
- HETSRONI, G. (1989). "Particles-Turbulence interaction." *J. Multiphase Flow*, vol. 15, N° 5, pp.735-746.
- HINZE, J. O. (1975). *Turbulence*, McGraw-Hill, New York.
- ITAKURA, T. and KISHI, T. (1980). "Open channel flow with suspended sediments", *J. Hydr. Div.*, vol. 106, N° HY8, pp. 1325-1343.
- JOBSON, H. E. and SAYRE, W. W. (1970). "Vertical Transfer in Open Channel Flow." *Proc. Am. Soc. Civil Engrs.*, vol. 96, N° HY3, pp. 703 - 724.
- KIRONOTO, B. (1992). "Turbulence characteristics of non-uniform Flow in rough Open-channel", *Doctoral dissertation n° 1094*, Ecole Polytechnique Fédérale, Lausanne.
- LHERMITTE, R. and LEMMIN, U. (1994). "Open-Channel Flow and Turbulence Measurements by High-Resolution Doppler Sonar." *J. Atm. Oceanic Tech.*, vol. 11, No. 5, pp. 1295-1308.
- LYN, D. A. (1988). "A similarity approach to turbulent sediment-laden flows in open channels" *J. Fluid Mech.*, vol. 193, pp. 1-26.
- MUSTE, M. and PATEL, V. C. (1997). "Velocity profiles for Particles and Liquid in open-channel flow with suspended sediment" *J. Hydr. Engr.*, vol. 123, N°. 9, pp. 742-751.
- NEZU, I. and NAKAGAWA, H. (1993). *Turbulence in open-channel flows*, A.A. Balkema, Rotterdam.
- NORDIN, C. F. and DEMPSTER, G. R. (1963). "Vertical Distribution of Velocity and Suspended Sediment Middle Rio Grande New Mexico.", U.S. Geol. Survey; Professional Paper 462-B.

- RIJN, L. C. van (1984). "Sediment transport, part II: Suspended Load Transport." *J. Hydr. Engr.*, vol. 110, N°. 11, pp. 1613-1641.
- SHEN, W. (1997). "An acoustic instantaneous sediment flux profiler for turbulent flow." *Doctoral dissertation No. 1630*, Ecole Polytechnique fédérale, Lausanne.
- SHEN, W. and LEMMIN, U. (1996). "Ultrasonic measurements of suspended sediments. A concentration profiling system with attenuation compensation." *Meas. Sci. Tecn.*, vol. 7, pp. 1191-1194.
- SONG, T., GRAF, W. H. and LEMMIN, U. (1994). "Uniform flow in open channels with movable gravel bed", *J. of Hydr. Res.*, Vol. 32, N° 6, pp. 861-876.
- THORNE, P. D., HARDCASTLE, P. J. and HOGG, A. (1996). "Observation of Near-bed Suspended Sediment Turbulence Structures using Multifrequency Acoustic Backscattering", in *Coherent Flow Structures in Open Channels*, Wiley & Sons Ltd., Chichester, UK.
- TSUJIMOTO, T. and GOTOH, H. (1995). "Turbulent Structure of Open-channel Flow with Suspended Sediment", KHL Progressive Report, December 1995, Hydraulics Laboratory, Kanazawa University.
- WEST, J. R. and ODUYEMI, K. O. K. (1989). "Turbulence Measurements of Suspended Solids Concentration in Estuaries." *J. Hydr. Engr.*, vol. 115, N°4, pp.457-474.

## 4. Conclusions

### 4.1 Introduction

The main object of this thesis was to investigate (experimentally) the turbulence and concentration characteristics of suspension flows in open channels. Two sediments (sand particles) were used, namely sand I ( $d_{50} = 0.135$  [mm]) and sand II ( $d_{50} = 0.230$  [mm]) respectively. The suspension flows investigated were in capacity condition i.e. the flows were saturated with suspended sediments. A few runs in non-capacity condition were also performed. Both flows over plane beds and beds with bed forms were investigated.

The instantaneous two-dimensional velocity as well as the instantaneous suspended concentration were measured using a new ultrasonic instrument (Acoustic Particle Flux Profiler, APFP) developed and assembled at the *Laboratoire de Recherches Hydrauliques* (LRH) of the *Ecole Polytechnique Fédérale de Lausanne* (EPFL) by Dr. U. Lemmin and Dr. C. Shen.

The turbulence characteristics of suspension flows were studied focusing the attention on the modification of the clear-water turbulence induced by suspended sediments. The instantaneous concentration was also carefully measured and interpreted by the classic diffusion-convection approach (Rouse equation). The ratio of the sediment and the momentum diffusion coefficients, labeled  $\bar{\beta}$ , was, for the first time, directly measured. This led to a significant improvement of the agreement between the Rouse equation and the measured concentration distributions. A correlation (of practical use) between the corrected  $\bar{\beta}$ -values and two parameters, namely  $v_{ss}/u_*$ , and  $v_{ss}/u_* \cdot C_s/\bar{c}_{sa}$ , is proposed. Note that the first parameter,  $v_{ss}/u_*$ , is easily obtainable in situ.

The main conclusions of the present study are summarized next.

### 4.2 Conclusions

The well-known Rouse equation, eq. 1.7, obtained with the diffusion-convection theory and expressing the dimensionless concentration profile,  $\bar{c}_s/\bar{c}_{sa}$ , was applied to suspension flows in capacity and non-capacity condition over beds with and without bed forms. The Rouse equation contains a parameter,  $\bar{\beta}$ , that is little known.

In our study the  $\bar{\beta}$ -values were obtained, for the first time, by measuring the momentum,  $\varepsilon_m(y)$ , and the sediment,  $\varepsilon_s(y)$ , diffusion coefficients. The diffusion coefficients were obtained by measuring the vertical profile of the velocity,  $\bar{u}(y)$ , and of the concentration,  $\bar{c}_s(y)$ , as well as of the momentum flux,  $\overline{u'v'}(y)$ , and of the sediment flux,  $\overline{c'_sv'}(y)$ .

These measurements were successfully performed by using the APFP instrument (see Appendix A). A calibration of the APFP instrument, performed by measuring the mean concentration profiles with the suction method was necessary. The longitudinal and vertical instantaneous velocities were extracted from the frequency shift between the emitted and the received ultrasonic waves (Doppler effect); in this case the calibration was not needed.

In all, 17 suspension flows in capacity condition over plane beds were investigated (11 runs for sand I, and 6 runs for sand II). In addition, 8 flows in non-capacity condition over plane beds and 2 flows in capacity condition over beds with bed forms were also investigated (in both cases sand I was used).

The following conclusions can be drawn:

- i) The most important result of this study is a recommendation, that the Rouse equation, eq. 1.7, with an improved  $\bar{\beta}$ -value – itself to be estimated from Fig. 3.27 or eqs. 3.18 – can be used to establish the dimensionless concentration profile,  $\bar{c}_s/\bar{c}_{sa}$ . For beds without bed forms the  $\bar{\beta}$ -values are  $\bar{\beta} < 1$ , while for beds with bed forms the  $\bar{\beta}$ -values are  $\bar{\beta} > 1$ .
- ii) The longitudinal mean velocity profiles,  $\bar{u}(y)$ , measured with the APFP instrument, plotted in defect form, can be described reasonably well by the Coles' law; the agreement is good in the upper part of the flow,  $y/\delta > 0.2$ , while the agreement is not satisfactory close to the bed,  $y/\delta < 0.2$ . The values of the Coles wake strength,  $\Pi$ , are larger than the ones measured by *Kironoto*, 1992, in clear-water flow; this is in agreement with the data obtained by *Coleman*, 1981. The tendency of the wake strength,  $\Pi$ , to increase with the Richardson number,  $Ri$  (see Fig. 3.4), is confirmed by both sand I and II measurements. To sum up, the stratification effect of the flow, due to suspended particles and expressed by the Richardson number,  $Ri$ , influences the outer region of the flow.
- iii) The vertical mean velocity profiles,  $\bar{v}(y)$ , are always very small compared to the longitudinal ones. The largest vertical velocities, usually observed near the surface, are directed towards the bed (see Fig. 3.5); they are probably associated to weak large-scale movements or secondary currents.
- iv) The profiles of the longitudinal component of the turbulence intensity,  $\sqrt{u'^2}/u_*$ , measured with the APFP instrument, show reasonable agreement with the profiles measured by several researchers in clear-water flow (see Fig. 3.3a). However, the presence of suspended sediment particles seem to enhance slightly the turbulence intensity.
- v) For both sand I and sand II, the profiles of the vertical component of the turbulence intensity,  $\sqrt{v'^2}/u_*$ , are clearly suppressed by sediment particles (see Fig. 3.3b,d). The link between turbulence suppression (also called turbulence damping) and suspended particles has been clarified by measuring the turbulence-intensity profiles in suspension flows for increasing sediment concentrations (see Appendix C). The results clearly show that the larger is the suspended concentration, the larger will be the turbulence suppression (see Fig. C2). In the case of suspension flow in capacity condition a turbulence suppression of nearly 40 [%] has been observed for both sand I and sand II (see Fig. 3.3b,d and Table 3.3).
- vi) The Reynolds-stress profiles,  $\bar{u}'v'$ , measured in suspension flows, for both sand I and sand II, retain the same linear trend observed in clear-water flows (see Fig. 3.7). However, in the inner region,  $y/h < 0.2$ , the experimental profiles deviate from the linear trend, falling to zero

rather rapidly. A physical phenomenon as the interaction between flow and sediment layer on the bed (erosion and deposition of particles) and/or the instrumental ultrasonic noise generated by the vicinity of the bed can explain this deviation.

vii) The energy spectra of the vertical fluctuating velocity show the diminution of the turbulence energy, associated to smaller frequency (larger eddies), due to the presence of suspended sediments. Note, that only the vertical velocity fluctuation has been taken in consideration being the one mainly responsible of the suspension of particles in the flow. Regrettably, it was not possible to investigate high-frequency (small eddies) fluctuating velocities due to the instrument restrictions.

viii) In the inner region,  $y/h < 0.2$ , the longitudinal and vertical macro-scale profiles,  $\Lambda_u(y)$ ,  $\Lambda_v(y)$ , increase going from the bed towards the water surface. In the upper part of the flow,  $y/h > 0.2$ , the longitudinal macro scales remain rather constant while the vertical ones slightly decrease (see Fig. 3.11a,b). These profiles are similar to the ones measured in clear-water flows; this means that the suspended particles investigated do not influence the size of the largest eddies.

ix) The longitudinal and vertical micro-scale,  $\lambda_u(y)$ ,  $\lambda_v(y)$ , profiles increase monotonously going from the bed towards the surface. Also in this case the profiles are similar to the ones measured in clear-water flows. A proportionality between the depth-averaged micro scales and the depth-averaged concentration (see Fig. 3.12, 3.14 and Table 3.3) is rather evident. This is probably due to the smallest (micro) eddies, characterized by high bending radius of the fluid trajectories, that partially eject – by centrifugal forces – the suspended particles. The ejection leads to an apparent augmentation of the micro-scale lengths; this effect increases with the concentration and with the size of the particles. The same phenomenon is weaker in the case of macro scales due to the small value of the bending radius of the largest (macro) eddies.

x) The suppression of the vertical component of the turbulence intensity,  $\Delta\sqrt{v'^2}$ , has been correlated to the dimensionless macro,  $d_{50}/(\Lambda_u, \Lambda_v)$ , and micro,  $d_{50}/(\lambda_u, \lambda_v)$ , scales. There are no evident tendency of  $\Delta\sqrt{v'^2}$  to vary with the dimensionless scales. However, our results corroborates with the findings of *Gore and Crowe, 1989*, (see Fig. 3.15) who suggested the use of the parameter  $d_{50}/\Lambda < 0.1$  (where  $\Lambda$  is the characteristic integral turbulence scale equal to the vertical macro scale,  $\Lambda_v$ , in our measurements) as discriminant to judge whether the turbulence is enhanced,  $d_{50}/\Lambda > 0.1$ , or suppressed,  $d_{50}/\Lambda < 0.1$ , by the suspended particles.

xi) By comparing the mean concentration profiles – measured with the suction method – to the echo-intensity profiles – measured with the APFP instrument – the calibration curves have been obtained (see Fig. 3.18) being linear fits.

xii) The dimensionless mean concentrations,  $\bar{c}_s/\bar{c}_{sa}$ , measured with the suction method (see Fig. 3.19) are, as expected, very high close to the bed and they decrease rapidly towards the

surface. The dimensionless fluctuating concentration profiles,  $\sqrt{c_s'^2}/\bar{c}_{sa}$ , (see Fig. 3.19) have their maximum values close to the bed ( $y/h < 0.25$ ). In the upper part of the flow the fluctuating concentrations remain rather constant. The same tendency has been observed by *Thorne et al.*, 1996, p. 351.

xiii) The sediment-flux profiles,  $\bar{c}'v'$ , (plotted in Fig. 3.19) being normalized with their value at  $y=a$ , present some scatters but globally all profiles are of similar shape. The largest sediment fluxes have been observed, as expected, close to the bed where the suspended concentration is large.

xiv) The sediment diffusion coefficient profiles,  $\varepsilon_s(y)$ , have been computed according to the definition of eq. 1.12. In the same way, the momentum diffusion coefficient profiles,  $\varepsilon_m(y)$ , have been computed using eq. 1.13. Despite the scatter, there is sufficient evidence, that the sediment diffusion coefficients,  $\varepsilon_s(y)$ , are always smaller than the momentum,  $\varepsilon_m(y)$ , ones; the latter are always smaller than the theoretical value, eq. 1.6, postulated for clear-water flows.

xv) The ratio of the sediment and momentum diffusion coefficient defines the  $\beta(y)$ -value, given with eq. 1.15. The experimental  $\beta_{APFP}$ -values, are close to zero at the bed and increase with the distance from the bed, up to  $y/h < 0.5$ . Above the mid-depth and towards the water surface, the  $\beta_{APFP}$ -values reach their maximum, but a clear tendency is not evident. From these plots it becomes also clear, that the higher the concentration,  $\bar{c}_s''$  (see Fig. 3.19), the lower are the  $\beta_{APFP}$ -values. In Fig. 3.22 are also shown the depth-averaged values,  $\overline{\beta_{APFP}}$  (see Table 3.1 and Table 3.2), which are always smaller than unity,  $\overline{\beta} = 1$ .

xvi) Another way of obtaining a  $\overline{\beta_{SM}}$ -value – the index recalls that the data are taken with the suction method – is by best-fitting (least-squares method) the Rouse equation to the concentration profiles directly measured with the suction method. The  $\overline{\beta}$ -values obtained with these two independent methods,  $\overline{\beta_{APFP}}$  and  $\overline{\beta_{SM}}$ , shall be compared, as seen in Table 3.1 and Table 3.2, being both smaller than unity,  $\overline{\beta_{APFP}}, \overline{\beta_{SM}} < 1$ .

xvii) The concentration profiles,  $\bar{c}_s/\bar{c}_{sa}$ , measured with the suction method agree well with the Rouse equation, eq. 1.7, using the  $\overline{\beta_{APFP}}$ -values – obtained with the diffusion coefficients, eq. 1.15 – as well as the best-fit  $\overline{\beta_{SM}}$ -values. Again, the usual value of  $\overline{\beta} = 1$  is not justified for the present measurements.

xviii) The  $\overline{\beta_{APFP}}$ -values have been scaled using two parameters:  $v_{ss}/u_*$  and  $v_{ss}/u_* \cdot C_s/\bar{c}_{sa}$ ; the former is reasonably easy to compute/measure in practical situations. In both cases a reasonable correlation has been found (see Fig. 3.24a,b); consequently, two regression lines have been computed (eq. 3.18a,b).

xix) The analysis of the results, taken from the literature (see Appendix B), of some suspension flows over bed with bed forms (see Fig. 3.26) and the results (see Fig. 3.25) of the investigation reported in Appendix D, clearly indicates that in case of flows over bed with bed

forms the  $\bar{\beta}$ -values are always large,  $\bar{\beta} > 1$  (see Figs. 3.25 and 3.26). These values have a tendency to increase with both the parameters  $v_{ss}/u_*$  and  $v_{ss}/u_* \cdot C_s/\bar{c}_{sa}$ . This corroborates with the conclusion drawn by *Rijn*, 1984, p. 1621.

xx) All the data taken from the literature (see Appendix B) as well as the results of this thesis are summarized in Fig. 3.27. The regression lines computed by using the results of the present investigation (eqs. 18a,b) agree reasonably only with the data referring to plane bed. On the contrary, the regression lines obtained by using the data of flows over bed forms (channel and river data) give a poor correlation (see Fig. 3.27).

### 4.3 Further research topics

In this thesis suspension flows in capacity and non-capacity condition over plane bed and over beds with bed forms were investigated in detail. However, further research topics can be suggested to add to our understanding of the structure of suspension flows.

The measuring frequency of the APFP instrument was of 16 [Hz] for concentration and velocity measurements. The measuring frequency could be increased up to 39 [Hz] for the velocity only. The development of an ultrasonic instrument capable to measure both concentration and velocity at high frequency ( $> 50$  [Hz]) could help to investigate the influence of suspended particles on very small turbulence eddies. Moreover, the effect of suspended particles on the high-frequency energy spectra could be also investigated.

A new ultrasonic instrument, characterized by focused transducers, has been recently developed. This instrument will be able to measure the instantaneous three-dimensional velocity profiles reducing the dimension of the measuring volume. With this instrument it would be interesting to investigate the generation region (where the most part of the turbulence generation and dissipation takes place) by using a 8-quadrants filtration technique. In this way our knowledge on the complex interactions between coherent structures and suspended transport could be improved.

This new ultrasonic instrument could be refined to discriminate the solid and the liquid velocity by extracting the Doppler signal coming from the suspended particles and the one coming from the surrounding water. This would allow to investigate larger particles and to analyze the bi-phasic nature of suspension flows.

Suspension flows with small ( $d_{50} < 0.1$  [mm]) and large particles ( $d_{50} > 0.3$  [mm]) can be investigated to supplement the present results. The summary plot, relating the  $\bar{\beta}$ -values to the hydraulic parameter,  $v_{ss}/u_*$  (see Fig. 3.27) could be useful for practical use.

The study of suspension flows over bed forms should be refined by measuring the concentration in several sections located along an entire bed-form wave length. Only then it would be possible to take the non-uniformity of the flow into account. It is obvious that the convection-diffusion theory should be re-formulated to integrate the spatial-dependent terms as  $\partial \bar{c}_s / \partial x$ .

#### 4.4 References

- COLEMAN, N. L. (1981). "Velocity profiles with suspended sediment." *J. Hydr. Res.*, vol. 19, N° 3, pp. 211-229.
- GORE, R. A. and CROWE, C. T. (1989). "Effect of particle size on modulating turbulent intensity." *Int. J. Multiphase Flow*, Vol. 15, No. 2, pp. 279-285.
- HETSRONI, G. (1989). "Particles-Turbulence interaction." *J. Multiphase Flow*, vol. 15, N° 5, pp.735-746.
- KIRONOTO, B. (1992). "Turbulence characteristics of non-uniform Flow in rough Open-channel", *Doctoral dissertation n° 1094*, Ecole Polytechnique Fédérale, Lausanne.
- RIJN, L. C. van (1984). "Sediment transport, part II: Suspended Load Transport." *J. Hydr. Engr.*, vol. 110, N°. 11, pp. 1613-1641.
- SHEN, W. and LEMMIN, U. (1996). "Ultrasonic measurements of suspended sediments: a concentration profiling system with attenuation compensation." *Meas. Sci. Technol.*, Vol. 7, pp. 1191-1194.
- SHEN, W. (1997). "An acoustic instantaneous sediment flux profiler for turbulent flow." *Doctoral dissertation, No. 1630*, Ecole Polytechnique Fédérale, Lausanne.
- THORNE, P. D., HARDCASTLE, P. J. and HOGG, A. (1996). "Observation of Near-bed Suspended Sediment Turbulence Structures using Multifrequency Acoustic Backscattering", in *Coherent Flow Structures in Open Channels*, Wiley & Sons Ltd., Chichester, UK.

# APPENDIX A

## The Sonar ADVP/APFP Instrument

### A 1 Introduction

The ADVP (Acoustic Doppler Velocity Profiler) is a non-intrusive sonar instrument that measures the instantaneous velocity profiles of the water in open-channel flows. It is not necessary to calibrate the instrument because the velocity is extracted directly from the Doppler-frequency shift. Subsequently, the ADVP instrument was modified to simultaneously measure the instantaneous velocity and the instantaneous sediment concentration in suspension flows; the resulting instrument was called Acoustic Particle Flux Profiler (APFP). These instruments were developed at the Hydraulic Laboratory of the Ecole Polytechnique Fédérale de Lausanne (Switzerland) by Dr. U. Lemmin (*Lhermitte and Lemmin, 1994, Lemmin and Rolland, 1997, Rolland and Lemmin, 1997*), Dr. T. Rolland (*Rolland, 1994*) and W.C. Shen (*Shen, 1997*).

### A 2 Doppler effect

The ADVP instrument can measure the instantaneous velocity of flow, exploiting the Doppler shift of the ultrasonic waves introduced in the medium by transducers. The ultrasonic waves are reflected by "targets" moving with the flow. These targets may be suspended particles, air bubbles dissolved in the medium (water) or density fronts due to temperature gradients resulting from turbulent dissipation.

Let us imagine a target, having a velocity,  $\vec{V}$ , in the acoustic field of two acoustic transducers: one emitter and one receiver (see Fig. A1). The emitter transducer emits ultrasonic sound waves with a certain frequency,  $f_e$ , and speed,  $c$ , (sound speed in the medium).

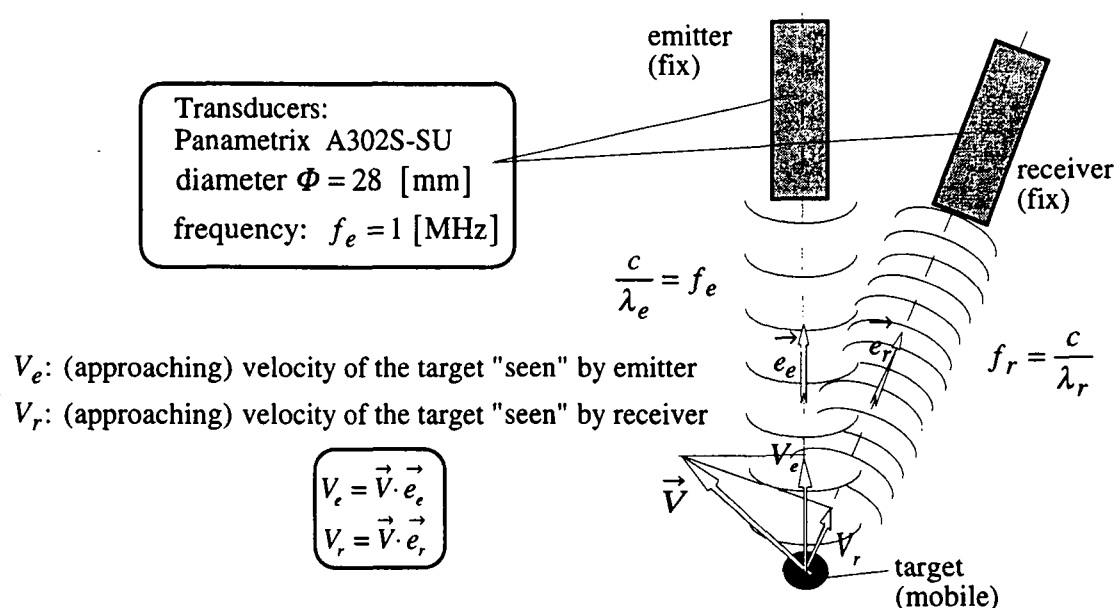


Fig. A1: Doppler effect

The axial components of the velocity are defined as:

$$V_e = \vec{V} \cdot \vec{e}_e \quad (A1)$$

$$V_r = \vec{V} \cdot \vec{e}_r \quad (A2)$$

where  $\vec{e}_e$  and  $\vec{e}_r$  are two unit vectors whose direction is from the target to the emitter and receive transducers respectively.

The target receives the sound waves with a frequency,  $f_t$ , different from the emitted one,  $f_e$ , because of the axial component of the velocity,  $V_e$ . The frequency of the wave received by the target is:

$$f_t = f_e + \frac{\vec{V} \cdot \vec{e}_e}{c} f_e = f_e \left( \frac{c + \vec{V} \cdot \vec{e}_e}{c} \right) \quad (A3)$$

The target represents, for the transducer receiver, a sound source moving with a velocity  $V_r$ . For the receiver, the frequency of the sound waves coming from the target is:

$$f_r = f_t \frac{c}{c - \vec{V} \cdot \vec{e}_r} \quad (A4)$$

Substituting eq. A3 into eq. A4, one obtains:

$$f_r = \left( f_e + \frac{\vec{V} \cdot \vec{e}_e}{c} f_e \right) \frac{c}{c - \vec{V} \cdot \vec{e}_r} = f_e \left( \frac{c + \vec{V} \cdot \vec{e}_e}{c - \vec{V} \cdot \vec{e}_r} \right) \quad (A5)$$

The Doppler frequency,  $f_D$ , defined as the difference between the received frequency and the emitted one, is:

$$f_D = f_r - f_e = f_e \left[ \frac{\vec{V} \cdot \vec{e}_e + \vec{V} \cdot \vec{e}_r}{c - \vec{V} \cdot \vec{e}_r} \right] \quad (A6)$$

Since the target velocity is very small compared to the speed of the sound in the medium, above eq. A6 becomes:

$$f_D = f_e \left[ \frac{\vec{V} \cdot \vec{e}_e + \vec{V} \cdot \vec{e}_r}{c} \right] = f_e \left[ \frac{V_e + V_r}{c} \right] \quad (A7)$$

Eq. A7 is the formula used to extract the target velocity from the signal recorded by the ADVP instrument.

The transducers used (in our experiment) to emit and receive the sound waves are piezoelectric ceramics, produced by Panametrics, model A302S-SU, (see Fig. A1). Their diameter is  $\Phi = 28$  [mm] and the nominal frequency is 1 [MHz]. The space ensonified by the

transducer has an irregular shape in the first 10 [cm] behind the transducer surface (near field). For larger distances (far field) the acoustic beam is conical with an angle of  $\theta = 3.4^\circ$  (see Fig. A2).

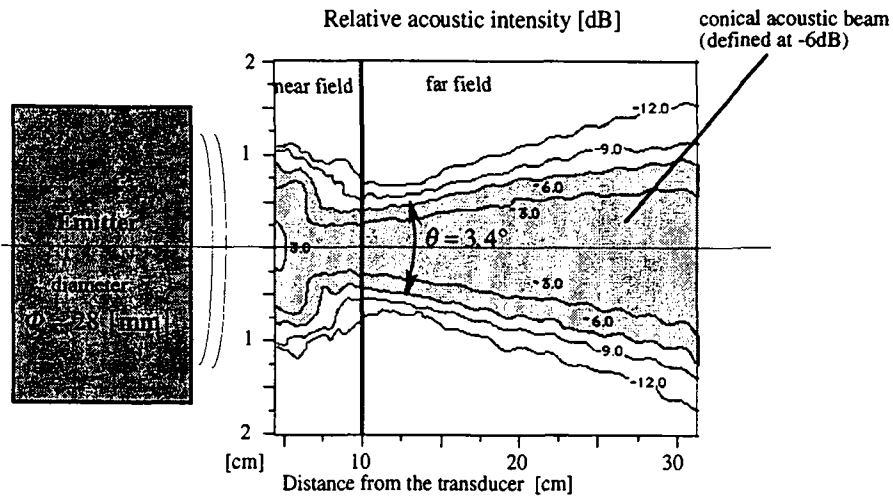


Fig. A2: Acoustic Beam

The acoustic beam represents the water column that will be investigated by the ADVP instrument. The transducer has been mounted in a water-filled housing to avoid measurements in the near field. The contact between the housing and the flow is made by a Mylar film, being a plastic film transparent to acoustic waves, (see Fig. A3).

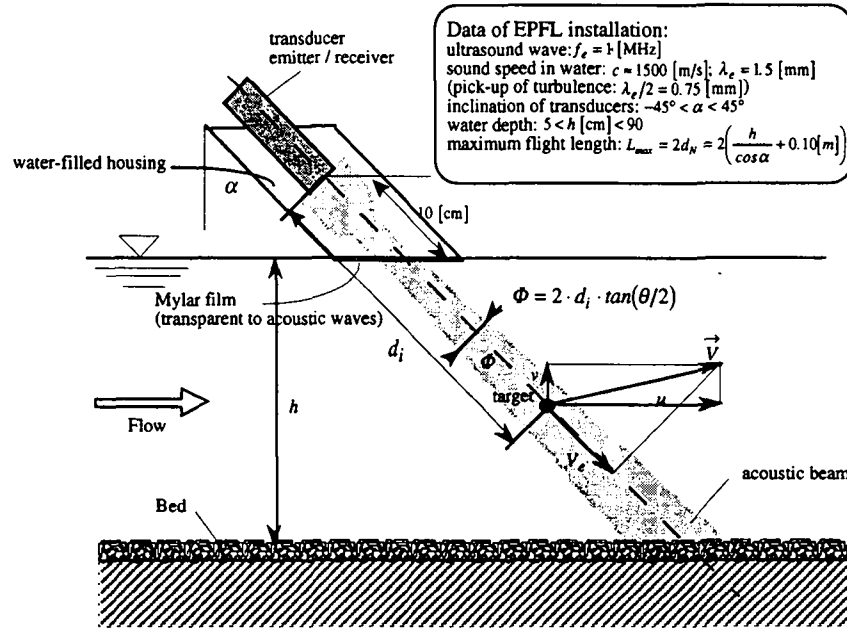


Fig. A3: Transducer installation

In Fig. A3 is presented the installation scheme of one transducer operating as emitter and/or receiver. The dimension of the ultrasonic beam can be calculated by the experimental formula:

$$\Phi_i = 2 \cdot d_i \cdot \tan(\theta/2) \quad (A8)$$

The ADVP instrument can be used in different configurations according to the number of transducers available. The four configurations presented here have been used with success to measure the instantaneous bidimensional velocity and concentration profiles in open-channel flow. They are:

- Monostatic mode (Velocity), (*Lhermitte and Lemmin*, 1994, and *Lemmin and Rolland*, 1997): The transducer is both emitter and receiver of the sound waves.
- Bistatic mode (Velocity), (*Rolland*, 1994, and *Rolland and Lemmin*, 1997): One transducer is both emitter and receiver, the second one is only receiver.
- Tristatic mode (Velocity), (*Rolland*, 1994): One transducer is emitter, while there are two transducers receivers.
- APFP (Acoustic Particle Flux Profiler) (Velocity and concentration), (*Shen and Lemmin*, 1996 and *Shen*, 1997): Two transducers are emitter and receiver to measure the sediment concentration, one of them measures the vertical velocity as well. A third transducer, tilted on the vertical, measures the longitudinal component of the velocity.

### A 3 Monostatic mode

As mentioned before, one single transducer is both emitter and receiver of the sonar waves. The same transducer is used three times consecutively to detect the vertical component of the velocity and two tilted ones. The transducer emits short trains of several sinusoidal waves (pulses) at regular intervals (the pulse-repetition frequency, PRF). Between two pulses the transducer operates as a receiver. An electronic system detects the difference between the emitted and received frequency, the Doppler frequency,  $f_D$ , computing the velocities of the target, according to eq. A7.

The backscattered signal, coming from the targets, is gated in time,  $T_i$ , where  $i = 1, \dots, N$ ;  $N$  is the number of gates needed to cover the measured water depth. Each gate corresponds to a certain time needed for the wave to propagate from the emitter to the target and back to the receiver. Thus the distance,  $d_i$ , from the transducer to the target,  $t_i$ , is (see Fig. A4):

$$d_i = (c \cdot T_i)/2 \quad (\text{A9})$$

Each single target, that corresponds to a certain gate, can be positioned spatially by eq. A9. Furthermore, the distance across a target is:

$$\Delta d = d_{i+1} - d_i = c \cdot (T_{i+1} - T_i)/2 = c \cdot \Delta T/2 \quad (\text{A10})$$

By fixing  $\Delta T = 6\mu s$ , the height of the measuring volume (target) is:

$$\Delta d = c \cdot \Delta T/2 = 1500 \cdot 6 \cdot 10^{-6}/2 = 4.5 \cdot 10^{-3} [\text{m}]$$

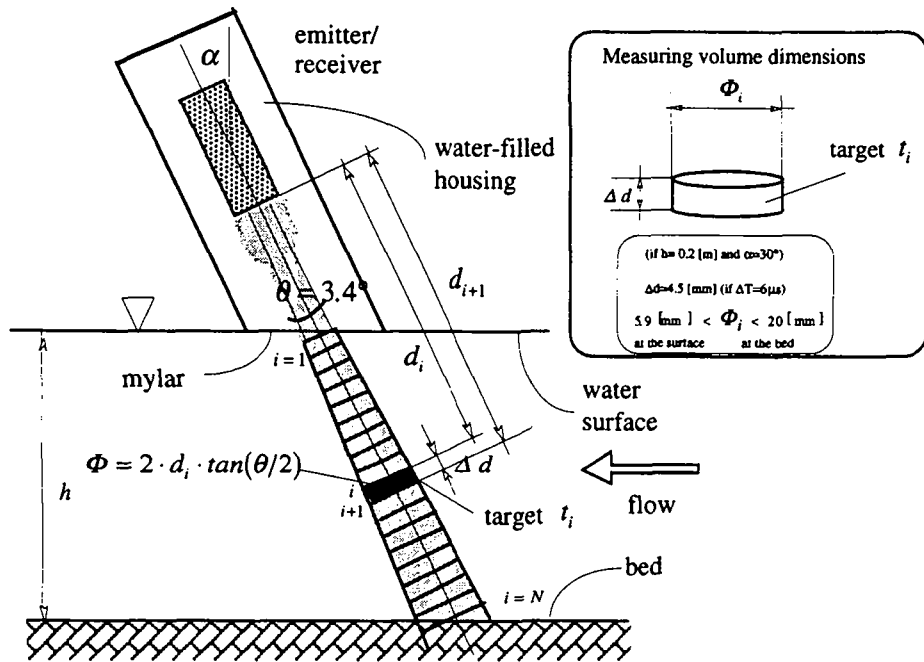


Fig. A4: Position of the target

A conical water column is covered by the sound waves. The measuring volume, positioned at a distance  $d_i$  from the transducer and containing the target  $t_i$ , has a diameter given by the relation:  $\Phi = 2 \cdot d_i \cdot \tan(\theta/2)$ . The angle  $\theta = 3.4^\circ$  is the span of the conical water column ensonified by the transducer: this region is delimited by an attenuation of -6 [dB] of the emitted ultrasonic intensity, (see Fig. A2). The first target ( $i=1$ ) positioned near the mylar, where the mylar is located 0.10 [m] below the transducer, has the measuring volume  $\Phi_1 = 5.9 \text{ [mm]} \times \Delta d = 4.5 \text{ [mm]}$ . The last target, in case of a flow depth of  $h = 0.2 \text{ [m]}$  and transducer inclination of  $\alpha = 30^\circ$ , has the measuring volume  $\Phi_N = 20 \text{ [mm]} \times \Delta d = 4.5 \text{ [mm]}$ .

In Fig. A5 is presented the configuration used to measure the velocity and turbulence characteristics using the monostatic mode.

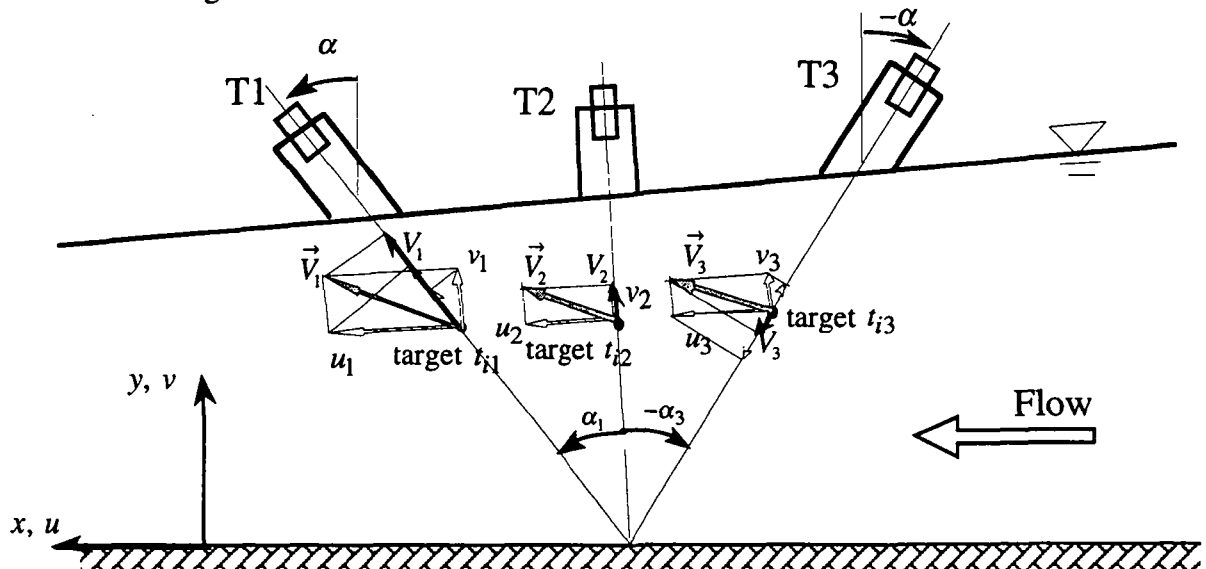


Fig. A5: Velocity decomposition in monostatic mode

The measurements are made by three acquisitions, made consecutively by the use of the same transducer. First, the transducer is placed in the position, called T1. At a certain position the target,  $t_{i1}$ , has an instantaneous velocity,  $\vec{V}_1(u_1, v_1)$ . The instantaneous velocity seen and recorded by the transducer,  $V_1$ , is the projection along the transducer axis. Applying eq. A1 one has:

$$\left( V_e = \vec{V} \cdot \vec{e}_e \right) \equiv \left( V_r = \vec{V} \cdot \vec{e}_r \right) = V_1$$

The velocity can be calculated, see eq. A7, knowing the Doppler frequency,  $f_{D_1}$ , recorded by the transducer T1, such as:

$$V_1 = \frac{c \cdot f_{D_1}}{2 \cdot f_e} \quad (\text{A11})$$

where  $f_e$  is the frequency emitted by the ADVP. The geometrical relationship among  $V_1$  and the unknowns velocity components,  $\vec{V}_1(u_1, v_1)$  is:

$$V_1 = u_1 \sin(\alpha_1) + v_1 \cos(\alpha_1) \quad (\text{A12})$$

Subsequently, the transducer is placed in the vertical position, called T2. For the target  $t_{i2}$ , the velocity seen and measured is  $V_2$ , where  $V_2$  is calculated in the same way as  $V_1$ , or:

$$V_2 = \frac{c \cdot f_{D_2}}{2 \cdot f_e}$$

Note, that a positive vertical velocity is directed from the channel bed to the flow surface. The geometrical relationship among  $V_2$  and the instantaneous velocity components,  $\vec{V}_2(u_2, v_2)$ , is:

$$V_2 = v_2 \quad (\text{A13})$$

In the position T3 the transducer measures the velocity  $V_3$ . Applying eq. A7 one has:

$$V_3 = \frac{c \cdot f_{D_3}}{2 \cdot f_e}$$

The geometrical relationship among  $V_3$  and the instantaneous velocity components,  $\vec{V}_3(u_3, v_3)$ , is:

$$V_3 = u_3 \sin(-\alpha_3) + v_3 \cos(-\alpha_3) \quad (\text{A14})$$

For the mean quantities one can write, by taking  $\alpha_1 = \alpha_3 = \alpha$ :

$$\overline{V}_1 = \overline{u}_1 \sin(\alpha) + \overline{v}_1 \cos(\alpha) \quad (\text{A15})$$

$$\overline{V}_2 = \overline{v}_2 \quad (\text{A16})$$

$$\overline{V}_3 = -\overline{u}_3 \sin(\alpha) + \overline{v}_3 \cos(\alpha) \quad (\text{A17})$$

For the fluctuating components, defined with the Reynolds decomposition, one obtains:

$$V_i = \bar{V}_i + V'_i ; \quad u_i = \bar{u}_i + u'_i ; \quad v_i = \bar{v}_i + v'_i \quad i = 1, 2, 3 \quad (\text{A18})$$

and therefore:

$$\overline{V'^2} = \overline{u'^2} \sin^2(\alpha) + \overline{u'_1 v'_1} \sin(2\alpha) + \overline{v'^2} \cos^2(\alpha) \quad (\text{A19})$$

$$\overline{V'^2} = \overline{v'^2} \quad (\text{A20})$$

$$\overline{V'^2} = \overline{u'^2} \sin^2(\alpha) - \overline{u'_3 v'_3} \sin(2\alpha) + \overline{v'^2} \cos^2(\alpha) \quad (\text{A21})$$

In case of fully developed uniform flow the turbulence is horizontally homogeneous and stationary; the time averaged quantities such as the mean velocity, turbulence intensities and Reynolds stress are function of the vertical position only. Thus, it is possible to write,:.

$$\bar{u}_1 = \bar{u}_2 = \bar{u}_3 = \bar{u} ; \quad \bar{v}_1 = \bar{v}_2 = \bar{v}_3 = \bar{v} \quad (\text{A22a})$$

$$\sqrt{\overline{u'^2}} = \sqrt{\overline{u_1'^2}} = \sqrt{\overline{u_2'^2}} = \sqrt{\overline{u_3'^2}} ; \quad \sqrt{\overline{v'^2}} = \sqrt{\overline{v_1'^2}} = \sqrt{\overline{v_2'^2}} = \sqrt{\overline{v_3'^2}} \quad (\text{A22b})$$

$$\overline{u'_1 v'_1} = \overline{u'_2 v'_2} = \overline{u'_3 v'_3} = \overline{u'_i v'_i} = \overline{u' v'} \quad (\text{A22c})$$

By subtracting and adding eqs. A15 and A17 and eqs. A19 and A21 it is possible to deduce the formulae useful to compute the mean velocity, turbulence intensities and Reynolds stress from the three consecutively measurements made by the transducers:

$$\bar{u} = \frac{\bar{V}_1 - \bar{V}_3}{2 \sin(\alpha)} \quad (\text{A23})$$

$$\bar{v} = \frac{\bar{V}_1 + \bar{V}_3}{2 \cos(\alpha)} \quad \text{or} \quad \bar{v} = \bar{V}_2 \quad (\text{A24})$$

$$\sqrt{\overline{u'^2}} = \sqrt{\frac{\overline{V'^2} + \overline{V'^2} - 2 \overline{V'^2} \cos^2(\alpha)}{2 \sin^2(\alpha)}} \quad (\text{A25})$$

$$\sqrt{\overline{v'^2}} = \sqrt{\overline{V'^2}} \quad (\text{A26})$$

$$-\overline{u' v'} = -\frac{\overline{V'^2} - \overline{V'^2}}{2 \sin 2\alpha} \quad (\text{A27})$$

The Pulse Repetition Frequency, PRF, should not be too small otherwise the number of velocity profiles measured per second would not be enough to detect the high-frequency turbulent movement. On the other hand, it exists an upper limit for the PRF; in fact between two emissions the transducers operate as receivers and the sonar waves must have the time to propagate until the last target ( $i = N$ ) and to be reflected to the receiver.

By assuming a flow depth of  $h=0.2$  [m], a distance from the emitter to the water surface of 0.10 [m] and an angle  $\alpha = 30^\circ$ , the longest path made by the sonar waves is:

$$L_{max} = 2d_N = 2 \left( \frac{h}{\cos(\alpha)} + 0.1[m] \right) = 2 \left( \frac{0.2[m]}{\cos(30^\circ)} + 0.1[m] \right) = 0.662[m]$$

The time needed for the wave to propagate, to be reflected and to be received by the transducer is:

$$T_N = \frac{L_{max}}{c} = \frac{0.662[m]}{1500[m \cdot s^{-1}]} = 4.413 \cdot 10^{-4}[s]$$

and thus the maximum PRF allowed is:

$$PRF_{max} = \frac{1}{T_N} = 2266[\text{Hz}]$$

In reality it is not possible to choose a PRF larger than 1500 [Hz] because of the noise that would affect the backscattered signal. Accurate measurements can be made with a 1 [MHz] transducer having a PRF of 1000 [Hz] and gate width of  $\Delta T = 6 [\mu s]$  (it means one measure every 4.5 [mm] along the vertical). By using a gate width of  $\Delta T = 6 [\mu s]$  and investigating a flow having a depth of  $h=0.20$  [m], one obtains a velocity profile composed by a number of points,  $N$ , equal to the number of gates in the water columns:  $N$ ; this can be calculated as:

$$N = \frac{h/\cos(\alpha)}{\Delta d} = \frac{0.20[m]/\cos(30)}{4.5 \cdot 10^{-3}[m]} = 51 \text{ gates or measuring points}$$

The maximum longitudinal velocity that can be measured by the ADVP in monostatic mode is limited by the frequency PRF. By using an algorithm eliminating the aliasing ambiguity the maximum Doppler frequency that can be measured is:

$$f_{D_{MAX}} = PRF$$

Thus, by eqs. A11 and A12, neglecting the vertical velocity, one obtains:

$$u_{i_{MAX}} = \frac{c \cdot PRF}{2 \cdot f_e \cdot \sin(\alpha)}$$

By assuming  $PRF = 1000$  [Hz],  $c = 1500$  [m/s],  $f_e = 1000000$  [Hz] and  $\alpha = 30^\circ$  one obtains that the maximum longitudinal velocity measurable with the ADVP is 1.5 [m/s].

Some results obtained with the monostatic configuration can be found in *Song, 1995*.

#### A 4 Bistatic mode

In this mode two transducers work simultaneously. The vertical transducer, placed on the surface or below the bed, emits a pulse of ultrasonic waves with a frequency PRF (Pulse Repetition Frequency) and operates as receiver of the backscattered signals the remaining time. A wide angle transducer, tilted on the vertical, receives all the time the backscattered signals. In Fig. A6 is presented a possible configuration of the bistatic mode.

The backscattered signal is gated in time,  $T_i$ , where  $i = 1, \dots, N$ ; where  $N$  is the number of gates needed to cover the measuring volume over the water depth. The determination of the spatial position of the targets is more complex than in the monostatic case because of the angle  $\alpha_i$  that exists between the transducers and the target (see Fig. A6).

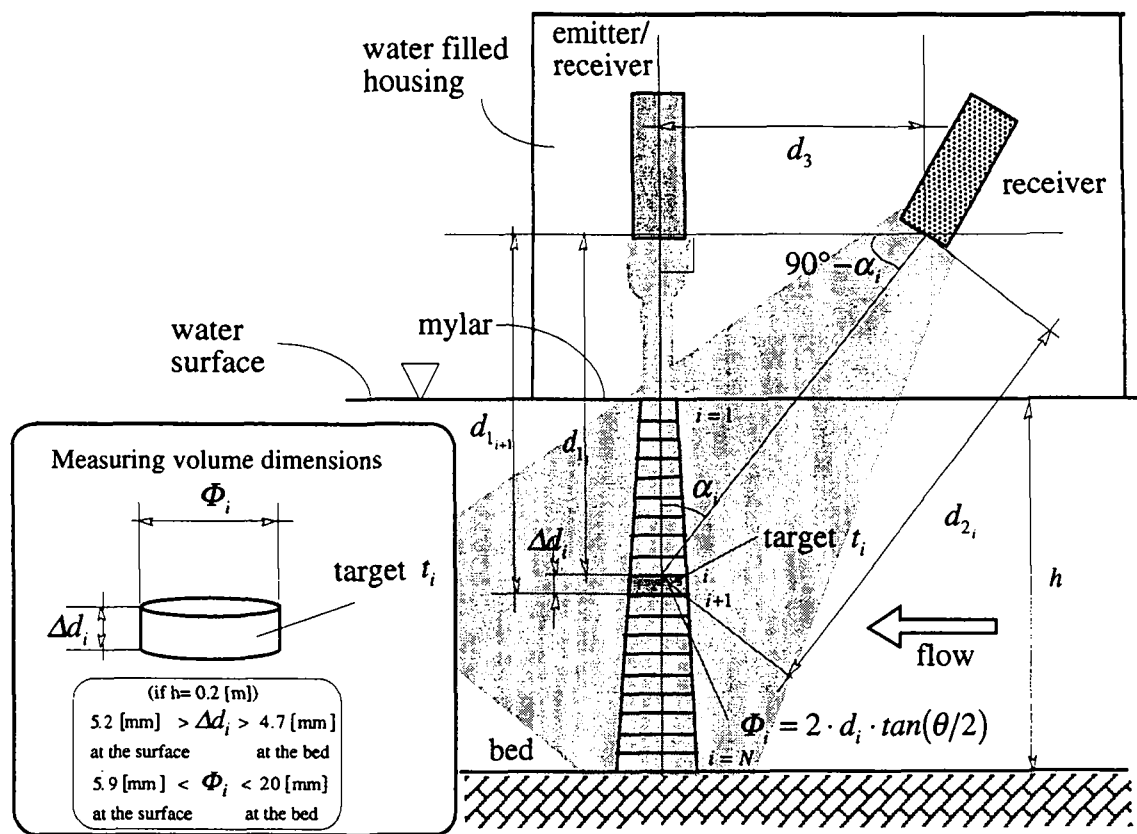


Fig. A6: Position and dimension of the target

The distance covered by the waves can be calculated:

$$d_{1,i} + d_{2,i} = c \cdot T_i \quad (A28)$$

where  $d_{1,i}$  and  $d_{2,i}$  are the distances from the emitter to the target and from the target to the receiver, respectively. According to geometrical considerations (see Fig. A6), one can write:

$$\frac{d_{1,i}}{\sin(90^\circ - \alpha_i)} = \frac{d_{2,i}}{\sin(90^\circ)} = \frac{d_3}{\sin(\alpha_i)} \quad (A29)$$

which leads to:

$$d_{1_i} = d_{2_i} \cdot \cos(\alpha_i) \text{ and } d_{2_i} = \frac{d_3}{\sin(\alpha_i)} \quad (\text{A30})$$

Substituting eqs. A29 and A30 into eq. A28, one obtains:

$$c \cdot T_i = d_{1_i} + d_{2_i} = d_{2_i} \cdot \cos(\alpha_i) + d_{2_i} = \frac{d_3}{\sin(\alpha_i)} \cdot \cos(\alpha_i) + \frac{d_3}{\sin(\alpha_i)} = d_3 \left[ \frac{1 + \cos(\alpha_i)}{\sin(\alpha_i)} \right]$$

this renders:

$$\frac{d_3}{c \cdot T_i} = \frac{\sin(\alpha_i)}{1 + \cos(\alpha_i)} \quad (\text{A31})$$

According to eq. A29 one can write:

$$d_{1_i} = \frac{d_3}{\tan(\alpha_i)} \quad (\text{A32})$$

The angle  $\alpha_i$  can be calculated at gate time  $T_i$  by eq. A31, and then the vertical position of the target,  $d_{1_i}$ , is obtained with eq. A32. The distance between two consecutive targets, being the height of the measuring volume, can be computed as:

$$\Delta d_i = d_{1_{i+1}} - d_{1_i} = (c \cdot T_{i+1} - d_{2_{i+1}}) - (c \cdot T_i - d_{2_i})$$

subsequently, one can write:

$$\Delta d_i = c \cdot \Delta T - \left( \frac{d_3}{\sin(\alpha_{i+1})} - \frac{d_3}{\sin(\alpha_i)} \right) \quad \text{where : } \Delta T = T_{i+1} - T_i \quad (\text{A33})$$

Use of eq. A33 shows that the height of the measuring volume depends on the position of the target with respect to the emitter.

The width of the acoustic beam that represents the width of the measuring volume, can be obtained from eq. A8, namely:

$$\Phi_i = 2 \cdot d_i \cdot \tan(\theta/2) \quad (\text{A8})$$

The range of  $\Delta d_i$  and  $\Phi_i$  values are shown in Fig. A6 for a flow depth of  $h=0.20$  [m].

In Fig. A7 is presented the decomposition scheme of the velocity of the target. Let us consider a target having an instantaneous velocity of  $\vec{V}$ . The emitter-receiver transducer,  $T_1$ , measures the vertical component of the velocity,  $\vec{V} \cdot \vec{e}_1 = V_1$ , whereas the tilted transducer,  $T_2$ , measures the velocity, (see eq. A7):

$$\left( \vec{V} \cdot \vec{e}_1 + \vec{V} \cdot \vec{e}_2 \right) = (V_1 + V_2)$$

Geometrical relationships among the components of  $\vec{V}(u_i, v_i)$  and the projection velocities,  $V_1$  and  $V_2$ , are:

$$\vec{V} \cdot \vec{e}_2 = V_2 = u_i \sin(-\alpha_i) + v_i \cos(-\alpha_i) = -u_i \sin(\alpha_i) + v_i \cos(\alpha_i) \quad (\text{A34})$$

$$\vec{V} \cdot \vec{e}_1 = V_1 = v_i \quad (\text{A35})$$

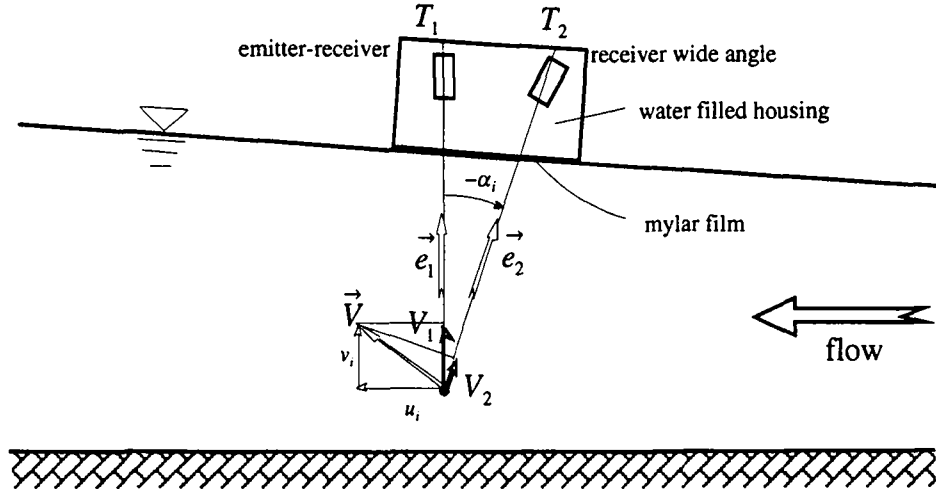


Fig. A7: Schematic of the bistatic mode

Firstly, the velocity,  $V_1 = \vec{V} \cdot \vec{e}_1$ , is calculated with eq. A11 knowing the Doppler frequency measured by the transducer  $T_1$ ,  $f_{D_1}$ . Subsequently, the velocity  $V_2 = \vec{V} \cdot \vec{e}_2$  is deduced by applying eq. A7 to the bistatic case, such as:

$$f_{D_2} = f_e \left[ \frac{\vec{V} \cdot \vec{e}_1 + \vec{V} \cdot \vec{e}_2}{c} \right]$$

this leads to:

$$\vec{V} \cdot \vec{e}_2 = \frac{f_{D_2}}{f_e} c - \vec{V} \cdot \vec{e}_1 \quad (\text{A36})$$

Introducing eq. A11 in eq. A36 one obtains the formula to calculate  $V_2$ :

$$\vec{V} \cdot \vec{e}_2 = V_2 = \frac{c}{f_e} \left( f_{D_2} - \frac{f_{D_1}}{2} \right) \quad (\text{A37})$$

where  $f_{D_2}$  is the Doppler frequency measured by the transducer  $T_2$ .

Once the projection velocities,  $V_1 = \vec{V} \cdot \vec{e}_1$  and  $V_2 = \vec{V} \cdot \vec{e}_2$ , are calculated, it is possible to compute the velocity  $\vec{V}(u, v)$ , using eqs. A34 and A35, such as:

$$u_i = \frac{-\vec{V} \cdot \vec{e}_2 + \vec{V} \cdot \vec{e}_1 \cdot \cos \alpha_i}{\sin \alpha_i} = \frac{-V_2 + V_1 \cos \alpha_i}{\sin \alpha_i} = \frac{c}{f_e \sin \alpha_i} \left[ -f_{D_2} + \frac{f_{D_1}}{2} (1 + \cos \alpha_i) \right] \quad (\text{A38})$$

$$v_i = \vec{V} \cdot \vec{e}_1 = V_1 = \frac{c \cdot f_{D_1}}{2 f_e} \quad (\text{A39})$$

From the instantaneous velocity profiles the mean quantities can be computed, such as:

$$\bar{u}_i = \bar{u}_i(y) = \frac{1}{T_{MEAS}} \sum_{t=0}^{t=T_{MEAS}} u_i(y, t) \cdot \Delta t_{MEAS} \quad (\text{A40a})$$

$$\bar{v}_i = \bar{v}_i(y) = \frac{1}{T_{MEAS}} \sum_{t=0}^{t=T_{MEAS}} v_i(y, t) \cdot \Delta t_{MEAS} \quad (\text{A40b})$$

where  $T_{MEAS}$  is the measurement time length, (usually  $T_{MEAS} = 180$  [s]), and  $\Delta t_{MEAS} = 1/PRF$  is the time lag between two consecutive velocity acquisitions.

The fluctuating velocities are defined in the following way:

$$u'_i(y, t) = u_i(y, t) - \bar{u}_i(y) \quad \text{for the longitudinal direction} \quad (\text{A41a})$$

$$v'_i(y, t) = v_i(y, t) - \bar{v}_i(y) \quad \text{for the vertical direction} \quad (\text{A41b})$$

Therefore, the turbulent quantities as turbulence intensity and Reynolds stress can be calculated, such as:

$$\overline{u'^2}(y) = \frac{1}{T_{MEAS}} \sum_{t=0}^{t=T_{MEAS}} u'^2(y, t) \cdot \Delta t_{MEAS} = \frac{1}{T_{MEAS}} \sum_{t=0}^{t=T_{MEAS}} [u_i(y, t) - \bar{u}_i(y)]^2 \cdot \Delta t_{MEAS} \quad (\text{A42a})$$

$$\overline{v'^2}(y) = \frac{1}{T_{MEAS}} \sum_{t=0}^{t=T_{MEAS}} v'^2(y, t) \cdot \Delta t_{MEAS} = \frac{1}{T_{MEAS}} \sum_{t=0}^{t=T_{MEAS}} [v_i(y, t) - \bar{v}_i(y)]^2 \cdot \Delta t_{MEAS} \quad (\text{A42b})$$

$$\overline{u'_i v'_i}(y) = \frac{1}{T_{MEAS}} \sum_{t=0}^{t=T_{MEAS}} \{[u_i(y, t) - \bar{u}_i(y)] \cdot [v_i(y, t) - \bar{v}_i(y)]\} \cdot \Delta t_{MEAS} \quad (\text{A42c})$$

Assuming that the flow depth is equal to  $h=0.2$  [m], a distance from the emitter to the water surface of 0.10 [m] and an angle  $\alpha_N = 21^\circ$ , the longest path covered by the sonar waves is:

$$L_{max} = d_{1_N} + d_{2_N} \quad \text{with} \quad d_{2_N} = \frac{d_3}{\sin \alpha_N} \quad \text{and} \quad d_3 = 0.117 \text{ [m]} \text{ (fixed)}$$

this leads to:

$$d_{1_N} = 0.20 \text{ [m]} + 0.10 \text{ [m]} = 0.30 \text{ [m]}; \quad d_{2_N} = \frac{0.117 \text{ [m]}}{\sin 21^\circ} = 0.326 \text{ [m]}$$

$$L_{max} = 0.30 \text{ [m]} + 0.326 \text{ [m]} = 0.626 \text{ [m]}$$

The time needed for the wave to propagate, to be reflected and to be received by the transducer is:

$$T_N = \frac{L_{max}}{c} = \frac{0.626 \text{ [m]}}{1500 \text{ [m} \cdot \text{s}^{-1}]} = 4.173 \cdot 10^{-4} \text{ [s]}$$

and thus the maximum PRF allowed is:

$$PRF_{max} = \frac{1}{T_N} = 2396 \text{ [Hz]}$$

An advantage of the bistatic configuration is the possibility to investigate the flow close to obstacles as wall or cylinders because of the vertical shape of the water column ensonified.

## A 5 Tristatic mode

In the tristatic configuration the vertical transducer emits the sound waves while the wide angle transducers receive the backscattered signals. In Fig. A8 is presented a scheme of the velocity decomposition in case of tristatic mode. The formulae used to deduce the vertical position of the targets are the same as the ones presented for the bistatic case.

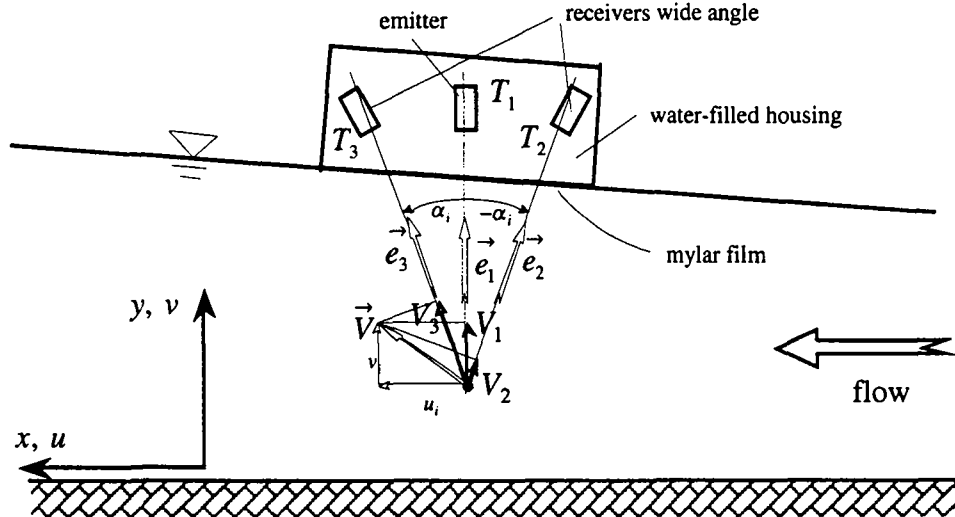


Fig. A8: Schematic of the tristatic configuration

Using geometrical relationships it is possible to write (see Fig. A8):

$$\vec{V} \cdot \vec{e}_1 = V_1 = v_i \quad (A43)$$

$$\vec{V} \cdot \vec{e}_2 = V_2 = u_i \sin(-\alpha_i) + v_i \cos(-\alpha_i) = -u_i \sin(\alpha_i) + v_i \cos(\alpha_i) \quad (A44)$$

$$\vec{V} \cdot \vec{e}_3 = V_3 = u_i \sin(\alpha_i) + v_i \cos(\alpha_i) \quad (A45)$$

$$\vec{V} \cdot \vec{e}_1 = \frac{\vec{V} \cdot \vec{e}_2 + \vec{V} \cdot \vec{e}_3}{2 \cos(\alpha_i)} = V_1 = \frac{V_2 + V_3}{2 \cos(\alpha_i)} \quad (A46)$$

The tilted transducers,  $T_2$  and  $T_3$ , measure respectively the Doppler frequencies,  $f_{D_2}$  and  $f_{D_3}$ , and permit to calculate, according to eq. A36, the velocities  $V_2 = \vec{V} \cdot \vec{e}_2$  and  $V_3 = \vec{V} \cdot \vec{e}_3$  by the equations:

$$\vec{V} \cdot \vec{e}_2 = -\vec{V} \cdot \vec{e}_1 + \frac{c \cdot f_{D_2}}{f_e} = V_2 = -V_1 + \frac{c \cdot f_{D_2}}{f_e} \quad (A47)$$

$$\vec{V} \cdot \vec{e}_3 = -\vec{V} \cdot \vec{e}_1 + \frac{c \cdot f_{D_3}}{f_e} = V_3 = -V_1 + \frac{c \cdot f_{D_3}}{f_e} \quad (A48)$$

The instantaneous vertical velocity,  $v_i$ , is obtained introducing eqs. A48 and A47 in eq. A46, the result is:

$$v_i = \vec{V} \cdot \vec{e}_i = V_i = \frac{c}{2 \cdot f_e} \cdot \frac{(f_{D_2} + f_{D_3})}{[1 + \cos(\alpha_i)]} \quad (\text{A49})$$

Subtracting eqs. A44 and A45 one obtains the equation to compute the longitudinal instantaneous velocity along the whole depth.

$$u_i = \frac{\vec{V} \cdot \vec{e}_3 - \vec{V} \cdot \vec{e}_2}{2 \sin(\alpha_i)} = \frac{c(f_{D_3} - f_{D_2})}{2 f_e \sin(\alpha_i)} \quad (\text{A50})$$

From the instantaneous velocity profiles the mean and fluctuating quantities can be computed with eqs. A40a, A40b, A41a and A41b. Subsequently, the turbulence intensity and Reynolds stress can be calculated with eqs. A42a, A42b and A42c. The calculation of the maximum PRF allowed,  $PRF_{max}$ , is the same than the one presented for the bistatic case, (see page A-12).

In this study the tristatic mode was applied when the instantaneous velocities at high-frequency were required (velocity profiles, energy spectra and micro and macro-scale profiles); in this case the measuring frequency was approximately of 39 [Hz].

## A 6 APFP mode (Acoustic Particle Flux Profiler)

This configuration has been set up to measure simultaneously the velocity and the suspended sediment concentration profiles (see *Shen*, 1997). The transducer below the bed and the tilted transducer measure the instantaneous velocity profiles in the same manner than the ADVP in bistatic configuration. To measure the instantaneous suspended sediment concentration profiles the vertical transducers record alternatively the intensity of the ultrasonic echo coming from the targets in the water columns ensonified. *Shen* and *Lemmin*, 1996, showed that the local sediment concentration is proportional to the intensity of the ultrasonic echo.

In Fig. A9 is presented the scheme of the APFP. The instrument works alternatively in two modes: one time the transducer  $T_a$  works as emitter and, with  $T_c$ , receiver of the backscattered signal while  $T_b$  works as receiver of the forward-scattered signal only (Mode 1); after, is the transducer  $T_b$  that emits and receives the backscattered signal while  $T_a$  receives the forward-scattered signal (Mode 2). This alternate working makes, as shown afterwards, possible the compensation of the ultrasonic-intensity attenuation.

For the measurement of the velocity, as shown in Fig. A9, the APFP works one time as bistatic instrument (Mode 1) and one time as simply monostatic (Mode 2). The measurement of the concentration is made by the vertical transducers.

The position of the targets can be easily deduced by the formulae already presented. In Mode 1, similar to the bistatic mode, the position of the target  $i$  is calculated by the equation:

$$d_{a_i} = \frac{d_3}{\tan(\alpha_i)} \quad (\text{A51})$$

with the angle  $\alpha_i$  calculated by eq. A31, see Fig. A10.

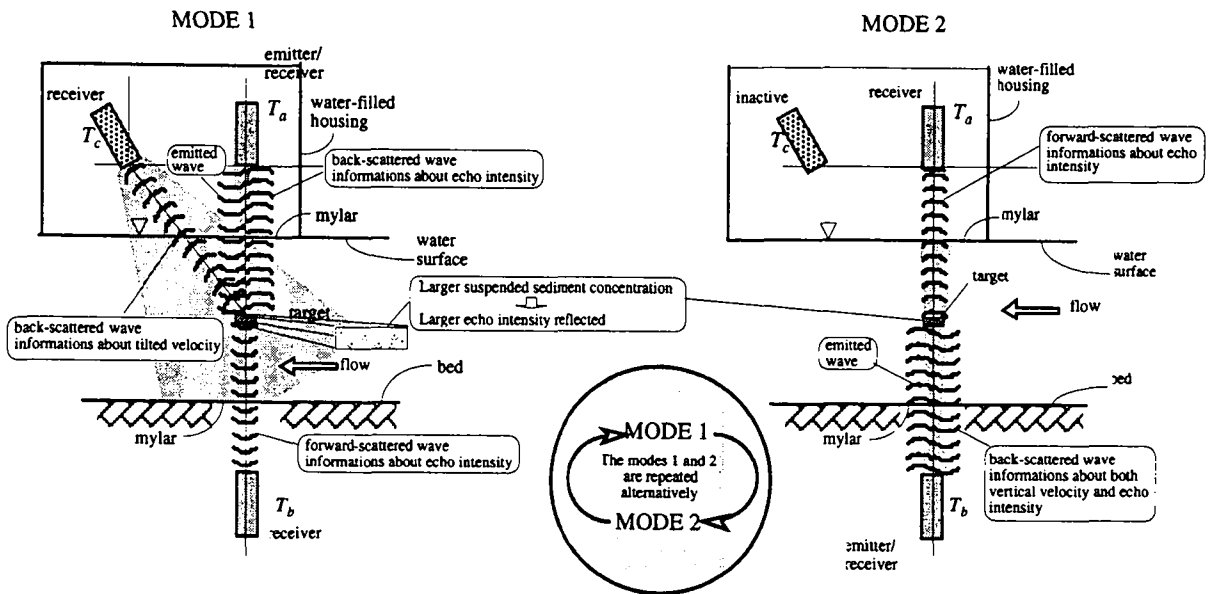


Fig. A9: Scheme of the alternative working of the APPF

In Mode 2, similar to the monostatic mode, the position of the target  $i$  is deduced by:

$$d_{b_i} = \frac{c \cdot T_i}{2} \quad (\text{A52})$$

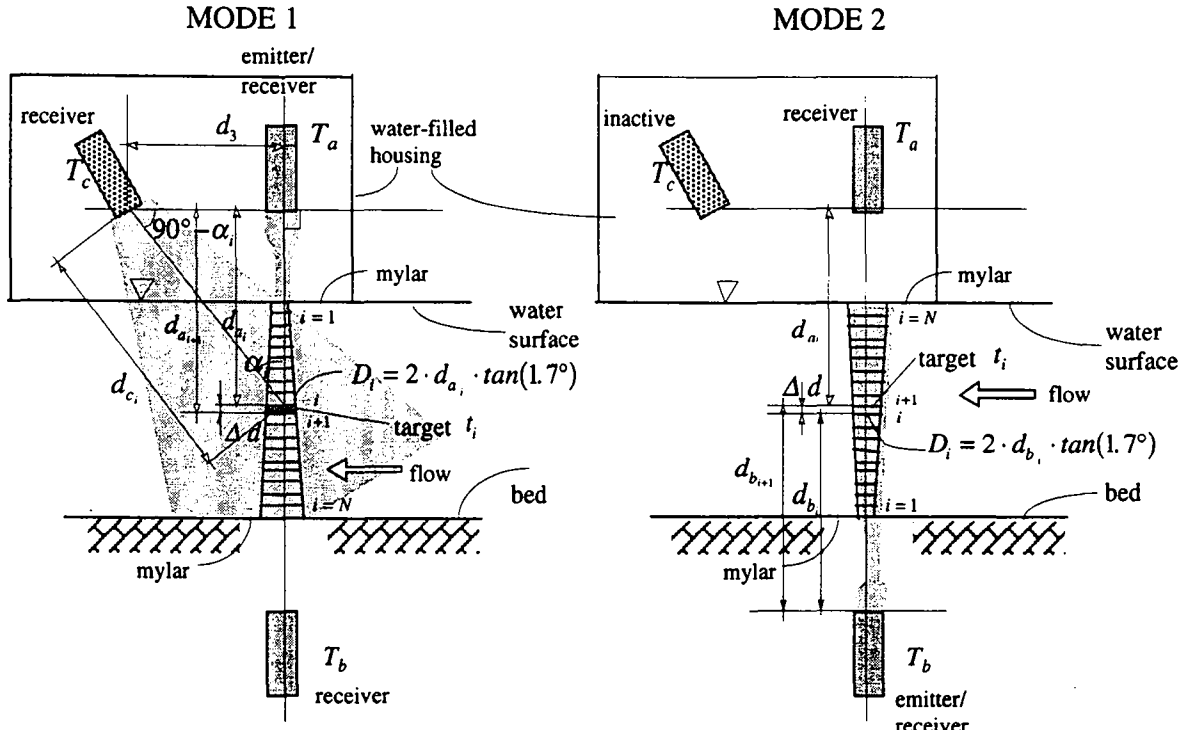


Fig. A10: Position of targets

In Fig. A11 is presented the decomposition of the velocity. The wide angle transducer  $T_c$  works always as receiver of the Doppler signal to measure the velocity  $(V_1 + V_2)$  such as, (see bistatic mode):

$$V_1 + V_2 = \frac{c \cdot f_{D,c}}{f_e} \quad (\text{A53})$$

where  $f_{D,c}$  and  $f_e$  are respectively the Doppler frequency measured by the transducer  $T_c$  and the frequency of the wave emitted by  $T_a$ .

The vertical velocity  $V_1$  is measured in Mode 2 by the transducer  $T_b$  (see monostatic mode):

$$V_1 = -\frac{c \cdot f_{D,b}}{2f_e} \quad (\text{A54})$$

The sign in eq. A54 comes from the convention about the vertical velocity: positive if directed from the bed to the surface.

The instantaneous velocity,  $\vec{V}(u_i, v_i)$ , can thus be obtained.

$$u_i = \frac{V_2 - V_1 \cos(\alpha_i)}{\sin(\alpha_i)} = \frac{c}{f_e \sin(\alpha_i)} \left[ f_{D,c} + \frac{f_{D,b}}{2} (1 + \cos(\alpha_i)) \right] \quad (\text{A55})$$

$$v_i = V_1 = -\frac{c \cdot f_{D,b}}{2f_e} \quad (\text{A56})$$

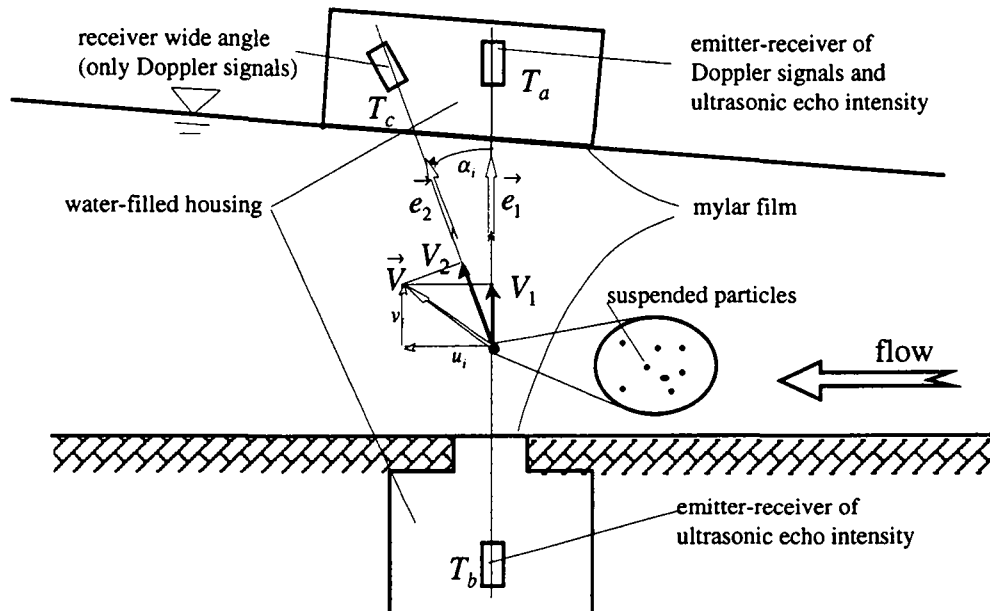


Fig. A11: Velocity decomposition

In suspension flow, the intensity of the back-scattered waves is attenuated by the presence of the sediment particles. By an iterative procedure, considering the echo-intensity profiles obtained from the two transducers,  $T_a$  and  $T_b$ , the attenuation has been corrected numerically. The water column between the vertical transducers is segmented into  $N$  volumes at position  $i$  (targets), see Fig. A12. Let  $\mu_i$  be the attenuation coefficient of volume  $t_i$ , defined as the ratio of the outgoing acoustic intensity to the incident intensity at  $t_i$ , and let  $\beta_i$  be its back-scattering cross section, defined as the ratio of the backscattered intensity to the incident intensity at  $t_i$ . When the  $T_a$  and  $T_b$  work in Mode 1, one finds :

$$\mu_1 \mu_2 \dots \mu_N = K_0 I_{B0} \quad (\text{A57})$$

$$\beta_i \mu_1^2 \mu_2^2 \dots \mu_{i-1}^2 = K_1 I_{Ai} \quad (\text{A58})$$

When  $T_b$  works in Mode 2, one obtains :

$$\beta_i \mu_{i+1}^2 \mu_{i+2}^2 \dots \mu_N^2 = K_2 I_{Bi} \quad (\text{A59})$$

$I_{B0}$  is the signal power of the sound pulse emitted by  $T_a$  and received by  $T_b$ .  $I_{Ai}$  and  $I_{Bi}$  are the backscattered intensities received by  $T_a$  and  $T_b$  respectively. Since the emitted sound is not an ideal plane wave, its intensity is attenuated along its propagation path. Therefore  $I_{Ai}$  and  $I_{Bi}$  have to be corrected by a factor  $I_i^\circ$ , given by :

$$I_i^\circ = \sin^2 \left[ \frac{\pi}{\lambda_0} \left( \sqrt{a_i^2 + d_i^2} - d_i \right) \right] \quad (\text{A60})$$

where  $\lambda_0$  is the acoustic wavelength.  $a_i$  is the radius of the transducer and  $d_i$  is the distance from the investigated region,  $t_i$ , to the transducer from which the sound is emitted.

The iteration solution for eqs. A57, A58 and A59 is:

$$\mu_i^2 = \frac{I_{Ai} I_{Bi-1}}{I_{Ai-1} I_{Bi}} \mu_{i-1}^{-2} \quad i = 2, N \quad (\text{A61})$$

$$\beta_i = \frac{K_1 K_2 I_{Ai} I_{Bi-1}}{K_0^2 I_{B0}^2} \beta_{i-1}^{-1} \quad i = 2, N \quad (\text{A62})$$

with the initial values  $\beta_1 = K_1 I_{A1}$  and  $\mu_1^2 = \beta_1^2 K_0^2 I_{B0}^2 / K_2 I_{B1}$ . Constants  $K_0$ ,  $K_1$  and  $K_2$  are sensitive to this iteration algorithm and have to be determined precisely. They are found by a calibration with a rigid sphere of known scattering cross section.

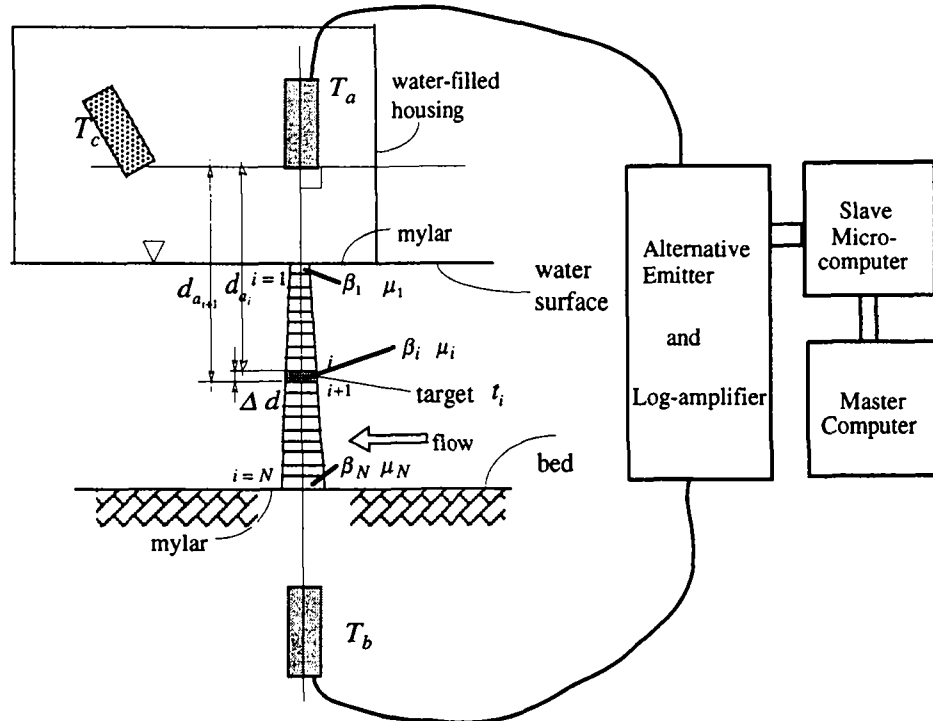


Fig. A12 Schematic of the APFP echo-intensity attenuation

In a dilute suspension, multiple scattering is negligible. Hence, the volume scattering cross section is proportional to its concentration,  $c_{s,i} = K \cdot \beta_i$ . The constant  $K$  can be obtained in situ by measuring the vertical mean intensity profile and the vertical mean concentration profile. In this study the vertical mean concentration profile has been measured by suction with the installation shown in Fig. A13.

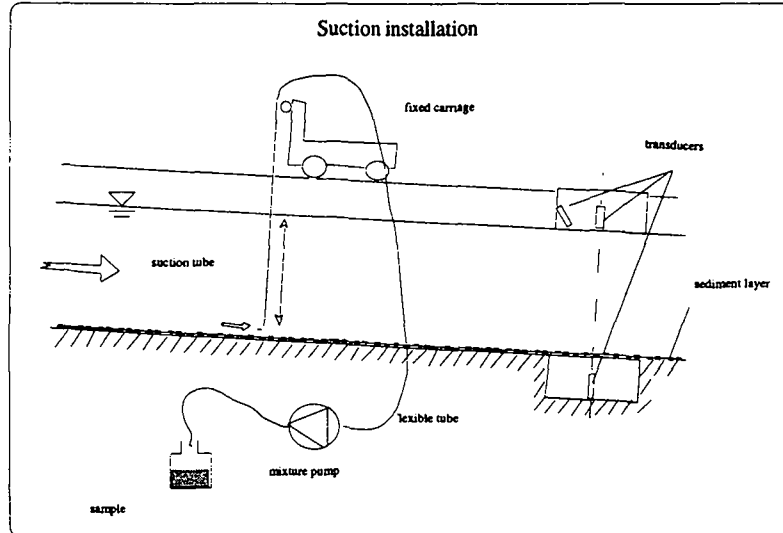


Fig. A13: Schematic of the suction installation

After this calibration on averaged values, the instantaneous concentration profile can be calculated from the instantaneous intensity profile. The vertical velocity profile  $v_i$  is measured by  $T_b$  working in Mode 2. Doppler information from this transducer is demodulated and then computed by a "pulse-pair" (PP) algorithm (see *Lhermitte and Lemmin, 1994*). Since  $v_i$  and  $c_{s,i}$  are measured at the same time, the vertical sediment flux,  $F_i$ , can be obtained:

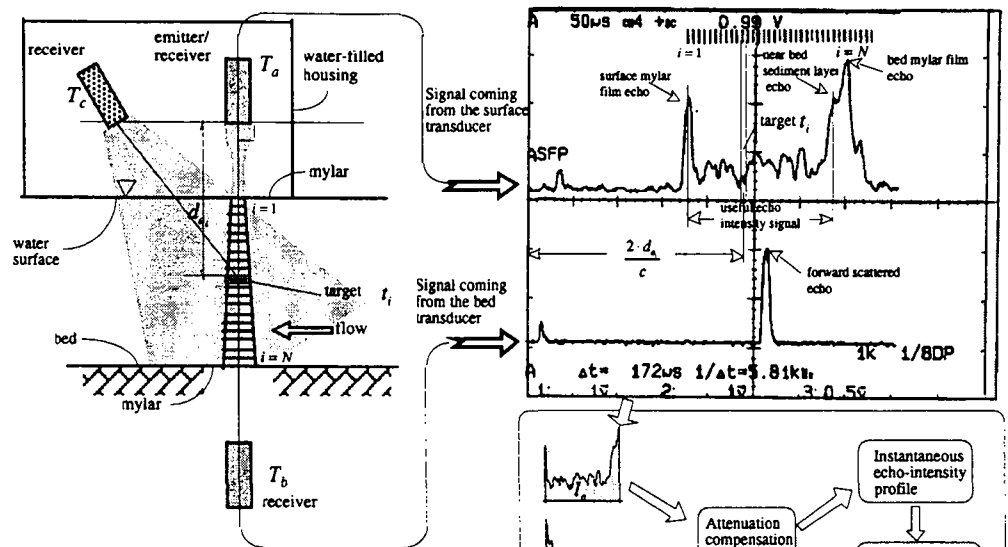
$$F_i = \overline{v'_i c'_{s,i}} \quad i = 1, N \quad (\text{A63})$$

In Fig. A14 is shown a typical signal visualized by the oscilloscope always connected with the APFP in order to check the presence of ultrasonic parasite echoes.

It is interesting to note that all the components of a typical signal are evident on the oscilloscope screen. The signal containing the information about the echo intensity is delimited by the two mylar echoes. The gates track shows the portion of the signal that will be recorded on magnetic support. The parasite echoes, usually present, do not disturb the measurements because they will not be recorded. The signal recorded in Mode 1 and 2 are then used to compensate the attenuation giving the vertical profile of the echo intensity; multiplying it by the constant  $K$  one obtains the suspended sediment concentration profile.

In this study the APFP instrument could be used reaching a measuring frequency of 19 [Hz].

### MODE 1



### MODE 2

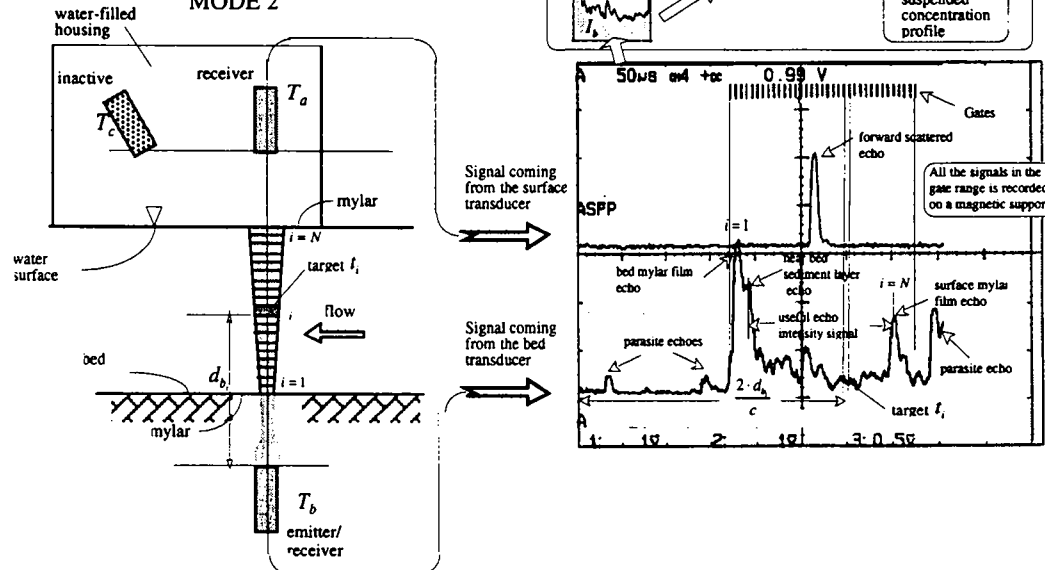


Fig. A14: Typical echo-intensity signal recorded by the APFP

## A 7 Conclusions

In this Appendix, the ultrasonic instrument measuring the velocity, called ADVP (Acoustic Doppler Velocity Profiler), and the one measuring simultaneously the velocity and concentration, called APFP (Acoustic Particle Flux Profiler), have been described. Special attention has been paid on the physical principles exploited to extract the velocity (Doppler effect) and the concentration (back and forward-scattered signals).

In this study the ADVP instrument, in tristatic configuration, was used when the velocity measurements at high-frequency were required (velocity profiles, energy spectra and micro and macro-scale profiles); in this case the measuring frequency was of 39 [Hz]. When using the APFP instrument (measurements of the simultaneous velocity and concentration, fluctuating concentration, sediment flux) the measuring frequency was of 19 [Hz].

## A 8 References

- LEMMIN, U. and ROLLAND, T. (1997). "Acoustic Velocity Profiler for Laboratory and Field Studies." *J. Hydr. Engr.*, vol. 123, N°. 12.
- LHERMITTE, R. and LEMMIN, U. (1994). "Open-Channel Flow and Turbulence Measurements by High-Resolution Doppler Sonar" *J. Atm. Oceanic Tech.*, vol. 11, N°. 5, pp. 1295-1308.
- ROLLAND, T. (1994). "Developpement d'une instrumentation Doppler ultrasonore adaptée a l'étude hydraulique de la turbulence dans les canaux" *These de doctorat N° 1281*, Ecole Polytechnique Fédérale, Lausanne.
- ROLLAND, T. and LEMMIN, U. (1997). "A two-component acoustic velocity profiler for use in turbulent open-channel flow." *J. Hydr. Res.*, vol. 35, N°. 4.
- SHEN, C. (1997). "An acoustic instantaneous particle flux profiler for turbulent flow" *These de doctorat N° 1630*, Ecole Polytechnique Fédérale, Lausanne.
- SHEN, W. and LEMMIN, U. (1996). "Ultrasonic measurements of suspended sediments. A concentration profiling system with attenuation compensation", *Meas. Sci. Tech.*, Vol. 7, pp. 1191-1194.
- SONG, T. (1995). "Velocity and Turbulence Distribution in Non-Uniform and Unsteady Open-Channel Flow", *These de doctorat N° 1324*, Ecole Polytechnique Fédérale, Lausanne.

## APPENDIX B

### Concentration distribution; Analysis of literature data

#### B 1 Introduction

This Appendix presents and summarizes available data on suspension flows as found in the literature. Only data which are considered to be capacity or near-capacity flow data will be analyzed. The flow has been defined as *capacity* flow when a layer of sediment, composed of the same sediment which is in suspension, is also present on the bed. Any further addition of sediments to the flow leads to a deposition of sediments on the channel bed without increment of the suspended sediment concentration. If a flow is in *non-capacity* condition there is no sediment layer on the bed. All the sediments injected to the flow are kept suspended. A further addition of sediment to the flow leads to an increment of the sediment concentration without deposition on the bed.

The data have been drawn from the following publications:

- 1) *Einstein and Chien*, 1955
- 2) *Coleman*, 1986
- 3) *Lyn*, 1988
- 4) *Wang and Qian*, 1989
- 5) *Sumer, Kozakiewicz, Fredsøe and Deigaard*, 1996
- 6a) *EPFL*, 1997 (Results of this thesis)
- 6b) *EPFL*, 1998 (Results of this thesis)
- 7) *Vanoni*, 1946
- 8) *Vanoni and Nomicos*, 1960
- 9) *Coleman*, 1970
- 10) *Nordin and Dempster*, 1963

Table B1 summarizes the important hydraulic and sedimentary characteristics of the experiments which provide the concentration distributions (publications 1-5). Other types of experiments (publications 7-10) are summarized in Table B2a and B2b. They still refers to near-capacity or capacity flows but do not provide the concentration distributions.

The equations used in this Appendix are the following:

Rouse eq.: 
$$\frac{\bar{c}_s}{c_{sa}} = \left( \frac{h-y}{y} \cdot \frac{a}{h-a} \right)^z \quad \text{with: } z [-] \text{ Rouse number}; z = \frac{v_{ss}}{\kappa \cdot u_*}$$

Modified Rouse eq.: 
$$\frac{\bar{c}_s}{c_{sa}} = \left( \frac{h-y}{y} \cdot \frac{a}{h-a} \right)^{z'} \quad \text{with: } z' [-] \text{ modified Rouse number}; z' = \frac{z}{\beta}$$

Hunt eq.:

$$\frac{\bar{c}_s}{\bar{c}_{sa}} = \left( \frac{1 - \bar{c}_s}{1 - \bar{c}_{sa}} \right)^{\frac{1}{\bar{\beta}}} \cdot \left( \frac{h - y}{y} \cdot \frac{a}{h - a} \right)^{z'}$$

Momentum diffusion coefficient:  $\varepsilon_m = \frac{\overline{u'v'}}{\partial u / \partial y}$

Sediment diffusion coefficient:  $\varepsilon_s = \frac{\overline{c'_s v'}}{\partial c'_s / \partial y}$  or  $\varepsilon_s = \beta \cdot \varepsilon_m$

$\bar{\beta}$ -value:  $\bar{\beta} = \frac{z'}{z'} = \frac{1}{h-a} \int_a^h \beta(y) dy$

When flow transports the full capacity of sediment – at saturation – one may consider the flow to be in a sediment equilibrium, i.e.: deposited particle can be readily replaced by eroded particle.

The channel and river data have been divided into three categories:

a) Capacity condition

This group includes the runs made in capacity condition. The criterion used to consider the flow saturated was the presence of a sediment layer on the bottom, composed of the sediment in suspension.

b) Near-capacity condition

In this group have been included all the runs in which the near-bed concentration was the largest possible without a presence of sedimentation on the bottom.

c) Non-capacity condition

All the runs that were not in the above conditions have been considered in non-capacity condition.

The capacity condition group has also been divided into two sub-categories:

a-1) Plane bed

In this category have been included the sediment flow, in capacity condition, in which the sediment layer on the bed was plane.

a-2) Bed forms

In this category are included saturated flows over a sediment layer having bed forms.

In order to make evident the importance of saturation (capacity) on the concentration distribution – parametrized by the  $\bar{\beta}$ -value – we shall show experimental runs performed by *Coleman* (1986, p. 1378) where sediment was added to the flow till “near-capacity” flow is achieved. It is evident that by increasing the concentration, thus approaching the capacity condition (going from Run 2 to

Run 20 and from Run 22 to Run 31), the  $\bar{\beta}$ -value that best fits the Rouse equation to the experimental points, decreases (see Fig. B1a,b). Thus, the  $\bar{\beta}$ -value would be over-estimated, if the flow was in non-capacity condition.

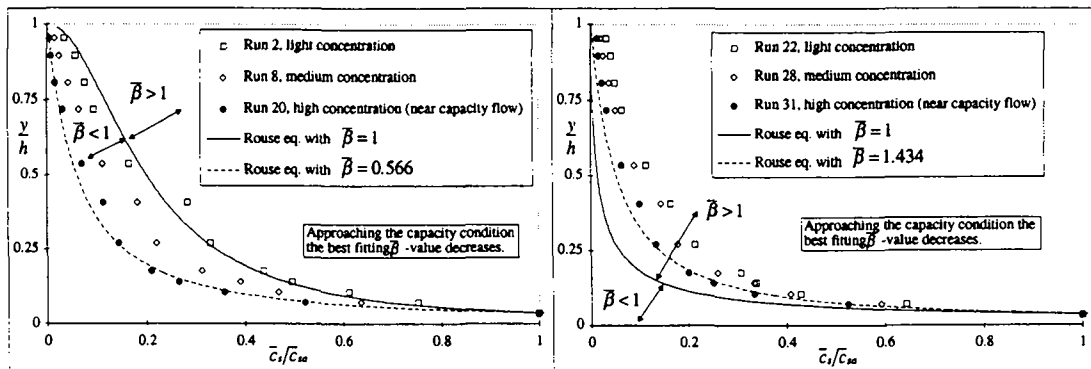


Fig. B1a,b: Importance of saturation on concentration

## B 2 Analysis procedure

The following analysis procedure was performed on experiments which provided the concentration distributions; the data are summarized in Table B1.

- The data considered are classed in one of the categories presented above.

Sometimes it has been difficult to judge if the flow was saturated or only in near-capacity condition. In this case, by comparing similar flows, the one having the largest reference concentration is considered in near-capacity condition. In case of doubt the run is assumed to be in non-capacity condition. The analysis has been made only for runs falling in categories a and b.

- The next step is to determinate the reference level,  $a$  [m], and the concentration,  $\bar{c}_{sa}^m$  [ $\text{kg}/\text{m}^3$ ], measured at the reference level.

The reference level is defined as the upper limit of the bed-load layer. Due to the difficulty of measuring this layer it is usually assumed that the reference level,  $a$ , is the 5% of the depth:  $a = 0.05 \cdot h$ . If measurements on this level were not available the reference concentration has been taken equal to the one measured closest to  $0.05 \cdot h$ .

- The hydraulic characteristics are taken from the publications (numbers written in *italic*) or computed by the author of this thesis (numbers written in regular).

Flow discharge:  $Q$  [ $\text{m}^3/\text{s}$ ]

Flow depth:  $h$  [m]

Aspect ratio:  $B/h$  [-], where  $B$  is the channel width

Depth-averaged streamwise velocity:  $U$  [m/s], if taken from the publication

$$U \text{ [m/s]} = Q/(B \cdot h), \text{ if computed}$$

Bed slope:  $S_b$  [%]

Reynolds number:  $Re [-] = \frac{4 \cdot U \cdot R_h}{\nu_m}$ , where  $R_h$  [m] is the hydraulic radius and  $\nu_m$  [ $m^2/s$ ]

is the mixture kinematic viscosity,  $\nu_m = \nu \cdot (1 + 2.5 \cdot C_s) \frac{\rho_w}{\rho_m}$

Froude number:  $Fr [-] = U / \sqrt{gh}$

Shear velocity:  $u_*$  [m/s], usually taken as:  $u_* = \sqrt{gR_h S_b}$

Friction factor:  $f [-] = 8(u_*/U)^2$

Equivalent roughness:  $k_s$  [mm], computed by the Colebrook and White formula

Reynolds particle number:  $Re_p [-] = \frac{u_* k_s}{\nu_m}$

Karman constant:  $\kappa [-] = 0.4$

- iv) The sedimentary characteristics are taken from the publications (numbers written in *italic*) or computed by the author of this thesis (numbers written in regular).

Nominal particle diameter:  $d_{50}$  [mm]

Sediment density:  $\rho_s$  [kg/m<sup>3</sup>]

Settling velocity:  $v_{ss}$  [mm/s], taken in still, clear water

Depth-averaged volumetric suspended concentration:  $C_s$  [m<sup>3</sup>/m<sup>3</sup>]

massic suspended concentration:  $C_s^m$  [kg/m<sup>3</sup>]

Reference concentration volumetric:  $\bar{c}_{sa}$  [m<sup>3</sup>/m<sup>3</sup>]

massic:  $\bar{c}_{sa}^m$  [kg/m<sup>3</sup>]

Depth-averaged mixture density:  $\bar{\rho}_m$  [kg/m<sup>3</sup>] =  $\rho_w + (\rho_s - \rho_w) \cdot C_s$

Richardson number:  $Ri [-] = \frac{gh[\rho_m(y=a) - \rho_m(y=h)]}{\bar{\rho}_m u_*^2}$

Rouse number:  $z [-] = \frac{v_{ss}}{\kappa \cdot u_*}$

modified Rouse number:  $z' [-] = \frac{v_{ss}}{\kappa \cdot u_* \cdot \bar{\beta}} = \frac{z}{\bar{\beta}}$

- v) Subsequently, the Rouse equation for  $\bar{c}_{sa} < 0.05$  [m<sup>3</sup>/m<sup>3</sup>] or the Hunt equation for  $\bar{c}_{sa} > 0.05$  [m<sup>3</sup>/m<sup>3</sup>] are evaluated by a best-fitting (least-square method) to obtain the  $\bar{\beta}$ -values. The corresponding Rouse number is  $z' [-] = z/\bar{\beta}$ .

- vi) The relative dimensionless sediment concentration profile,  $\bar{c}_s / \bar{c}_{sa}$  vs.  $y/h$ , has been plotted. For sake of comparison the Rouse equation with  $\bar{\beta} = 1$  is also plotted.

The scheme of the procedure is presented in Fig. B2.

The data of each investigation are commented on the following pages and are summarized in Table B1. The data of each run are found on individual worksheets which are put at the end of this Appendix.

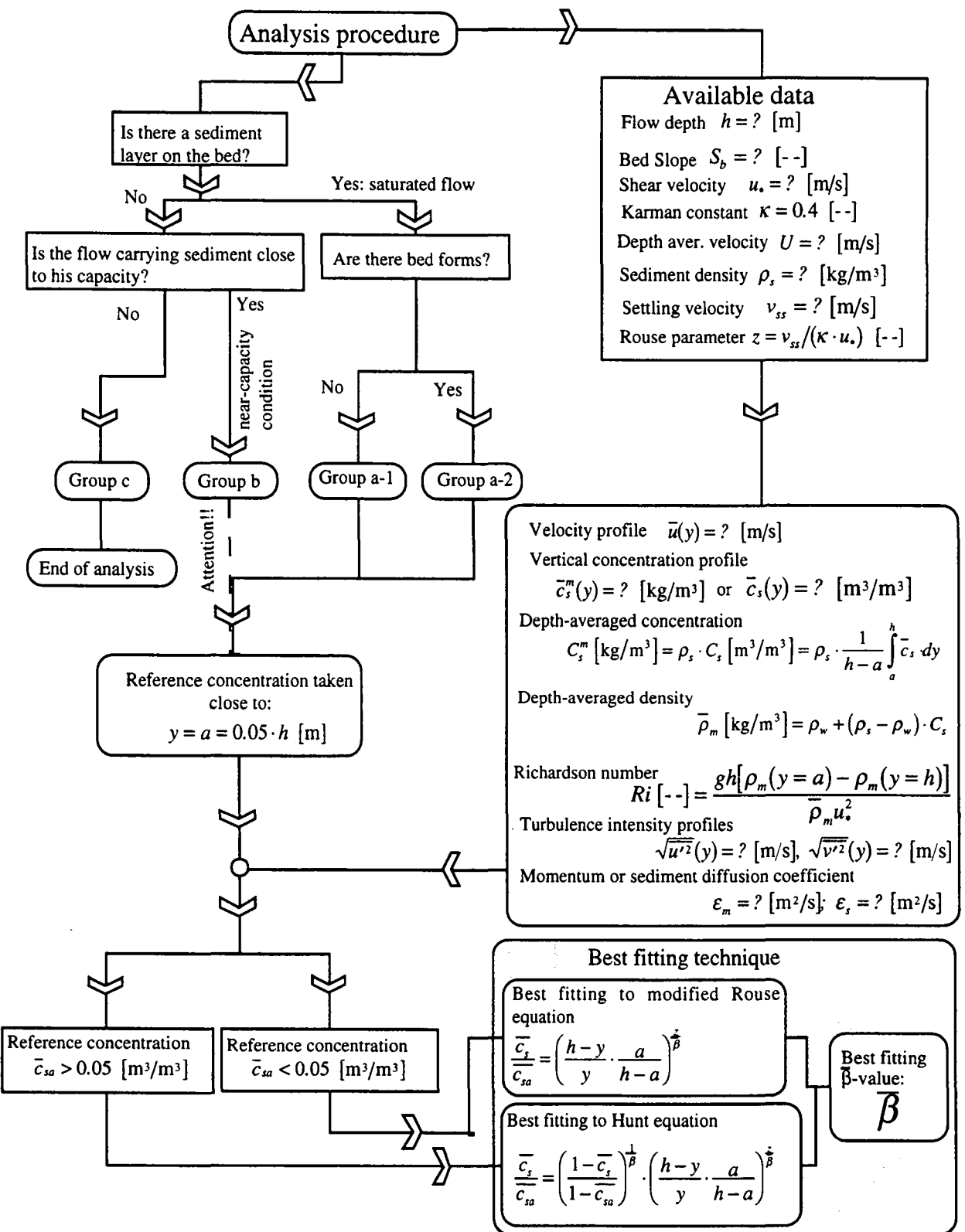


Fig. B2: Block diagram of the analysis procedure

### **B 3 Remarks on the concentration distribution data used**

The experimental installations in which the experimenters performed the runs (whose hydraulic characteristics are summarized in Table B1) are described as follows:

#### **1) Einstein and Chien, 1955**

The experiments were conducted in a recirculating steel flume, 31 [cm] wide by 36 [cm] deep and 12 [m] long. The velocity distribution was measured by a Pitot-tube special conceived to operate very close to the bottom. The concentration distribution was measured by point integrating samples siphoned from the flow through an iso-kinetic sampling tube. The water was separated from the sediment and returned to the flume while the particles were dried, weighted and sieved to determine the composition.

The bed roughness was composed by glued sand of the same kind of the suspended load. After that a certain amount of sediment was added to the flow the measurement of velocity and concentration was performed. Three sands were used: coarse,  $d_{50} = 1.30$  [mm], medium,  $d_{50} = 0.94$  [mm], and fine,  $d_{50} = 0.274$  [mm]. The run was terminated when the amount of sediment in the flow reached the saturation point and further increase in supply induced excessive sediment deposition to the bed. All the flows investigated were supercritical ones.

A total of 16 runs was made but only 3 runs are considered as near-capacity flows.

#### **2) Coleman, 1986**

The recirculating flume was a rectangular Plexiglas channel 35.6 [mm] wide and 15 [m] long. Velocity profiles were measured with a Pitot-static tube. Suspended concentration profiles were obtained by a suction technique using an iso-kinetic pipette. When the clear-water uniform flow is established, sand was added in 0.91 [kg] increments; measurements being made after each addition. The sand was injected at the upstream end of the flume. Experiments were continued until a highly concentrated continuously moving sheet of sand was observed on the flume bottom. The experiments were repeated with three sands with nominal diameters of 0.105, 0.210 and 0.420 [mm]. A total of 40 runs were performed, but only three were in near-capacity condition: run 20, 31 and 40. All flows were subcritical ones.

#### **3) Lyn, 1988**

Experiments were performed in a 13 [m] long, 26.7 [cm] wide, tiltable recirculating flume. The velocity profile was obtained with a laser Doppler velocimeter while the concentration profile was measured by a suction method. The bottom was covered by a layer of erodible sand 2 [cm] thick. The flow was thus a capacity flow. The lower boundary was defined as the point at which the bed is found after the cessation of the flow. The runs performed were 10 but only 4 had a bed in equilibrium. The 3 flows investigated were all subcritical ones.

4) *Wang and Qian, 1989*

The experimental installation was composed by a recirculating tilting flume 20 [m] long, 30 [cm] wide and 40 [cm] high. The bottom was hydraulically smooth. Only a 1% bed slope was investigated. The velocity was measured using a total pressure probe. The concentration was measured with the suction method. The longitudinal turbulence-intensity profile, shown in the paper, is smaller than the clear-water one. The loss of turbulent energy is attributed by the authors to collisions between suspended particles and turbulent eddies. No information about the vertical turbulence intensity is reported. All the flows investigated were supercritical ones. A total of 12 runs were performed but only one was considered as near-capacity flow.

5) *Sumer et al., 1996*

Experiments were carried out in a recirculating tilting flume, 10 [m] long, 0.3 [m] deep and 0.3 [m] wide. Some tests were performed with a free surface and some with a flat lid on the surface to avoid perturbation of the surface. The velocity profile was obtained with a Pitot tube while the concentration was measured with a Delft-Hydraulics conductivity-type concentration meter. The maximum concentration that this instrument can measure is nearly 50% in volume. A stationary sediment bed, of the same composition as the sediment load, was present on the bottom assuring the saturation of the flow. The authors provided the vertical concentration profiles for 9 of the 158 runs made, which are considered as capacity flow. Since the data are all duct-flow data and the definition of the y-axis is not too clear, they must be considered with reservation.

6a,b) *EPFL, 1997; EPFL, 1998*

The recirculating flume was a rectangular channel 60 [cm] wide and 16.8 [m] long. The flume had glass walls and a steel bottom on which an artificial roughness was glued by adequate supports, see Ch. 2. The measurement of instantaneous velocity and concentration profiles was made with an ultrasonic (APFP) instrument described in Appendix A. A calibration by suction was made to calibrate the ultrasonic instrument. Sediments were added slowly to the flow; the measurements started only after 4 [h] of flow circulation when the presence of a sediment layer ( $\approx 2$  [mm] thick) on the bed is assured. Two kinds of sediments were used: Sand I (*EPFL, 1997*) with characteristic diameter of  $d_{50} = 0.135$  [mm] and Sand II (*EPFL, 1998*) with  $d_{50} = 0.230$  [mm]. The measuring section is 13 [m] from the entrance of the channel, where the boundary layer is assumed to be established. All flows were subcritical and considered as capacity flows.

In the same flume used to investigate uniform suspension flows (*EPFL, 1997, 1998*), two runs (capacity flows) were performed over bed forms (*EPFL, 1997*) using Sand I. The complete description of the installation and the results can be found in Appendix D.

## B 4 Other types of experiments

Here we evaluated experiments, which do not give concentration distribution directly but still refer to capacity or near-capacity flows. They are commented in the following page and are summarized in Table B2a,b. The data have been drawn from the following publications:

- 7) *Vanoni, 1946*
- 8) *Vanoni and Nomicos, 1960*
- 9) *Coleman, 1970*
- 10) *Nordin and Dempster, 1963*
- 7) *Vanoni, 1946*

The experiments were performed in a channel 84.5 [cm] wide and 18.3 [m] long in which both the bed slope and the discharge could be varied. The bottom of the channel was a steel plate artificially roughened with sand. Water depths were measured with a point gage with a precision up to 0.305 [mm]. Velocities were measured with a pitot static tube having a diameter of 4.8 [mm] of the standards Prandtl design. The sediment distribution was determined by suction with an iso-kinetic pipette having a diameter of 7.9 [mm]. The 1 liter sample was filtered, dried and weighted to compute the mean concentration. Sediments used as suspended load were graded sand whose settling velocity in clear water was calculated theoretically.

In the first series of experiments the bed slope was kept constant and the discharge was varied. The bottom roughness was composed of sand different from the one used as suspended load. In the second series three sizes of suspended load, two depths and two bed slopes were investigated. A total of 22 runs were performed but only one (run 11) has been judged to be in near-capacity condition. The vertical mean concentration profiles were not given.

- 8) *Vanoni and Nomicos, 1960*

The flume was 12.2 [m] long and 27 [cm] wide. The velocity profile was measured with a Prandtl pitot-static tube while the concentration profile was obtained by suction. A run with uniform flow was first established with determination of depth, water discharge, sediment discharge and slope. Subsequently, the flow was stopped and the water drained off. The bed, having bed forms, was then solidified by spraying with chemicals. After the chemical had set, experiments with the stable bed were made, first using clear water and then varying small amounts of sediment added to the system. The four runs, on a total of 25, considered here had a bed of loose sand covering the fixed bed. These runs, were classed in category a-2.

Both authors, *Vanoni* (1946) and *Vanoni and Nomicos* (1960) evaluated their measured vertical concentration profiles (not given in the publications) and obtained the modified Rouse number,  $z'$ , being a best fitting to the modified Rouse equation. One can write:  $z' = \frac{v_{ss}}{\kappa \cdot u_*} \cdot \frac{1}{\bar{\beta}}$

The settling velocity,  $v_{ss}$ , and the shear velocity,  $u_*$ , were taken from the authors, while the Karman constant was posed equal to  $\kappa = 0.4$ . Thus, the  $\beta$ -value could be evaluated.

### 9) *Coleman, 1970*

The recirculating flume was a rectangular Plexiglas channel 35.6 [mm] wide and 15 [m] long. A combination probe measured both the velocity profile –by a pressure transducer – and the concentration by suction. A total of 16 runs were performed with two particle diameters and 8 flow conditions. In the experiments a flow depth and a discharge were selected, and the flume slope was adjusted until flow was uniform in the vicinity of the measuring section. Sand was then added to the flow in small amounts until the flow was carrying sand in suspension at capacity without forming a sand bed.

*Coleman* (1970), does not present the vertical suspended concentration profile but gives the vertical distribution of the sediment diffusion coefficient calculated according to:

$$\varepsilon_s = \frac{\overline{c'_s v'}}{\partial c_s / \partial y} \quad \text{where: } \overline{c'_s v'} = \bar{c}_s \cdot v_{ss}$$

The sediment flux,  $\overline{c'_s v'}$ , was computed by *Coleman*, knowing the vertical mean concentration profile,  $\bar{c}_s(y)$ , and the settling velocity,  $v_{ss}$ . Dimensionless sediment diffusion coefficient profiles, as presented by *Coleman*, are plotted in Fig. B3.

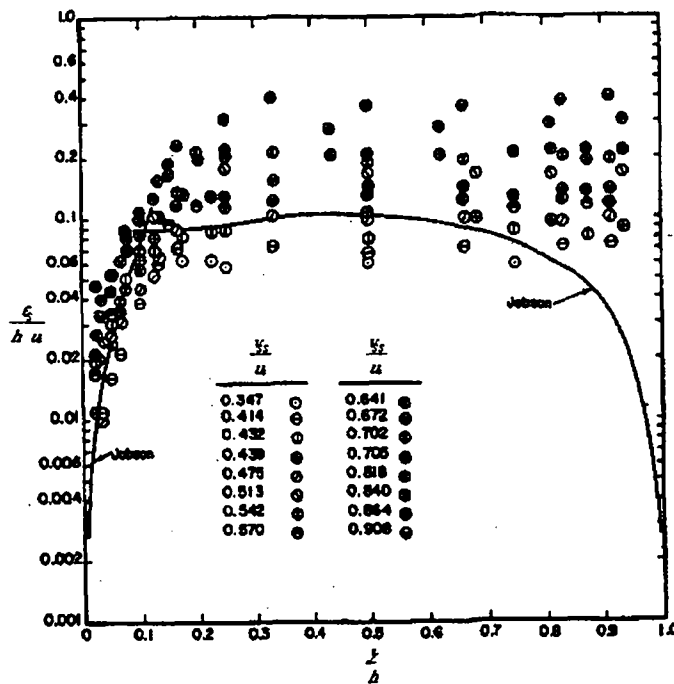


Fig. B3: Sediment diffusion coefficient as presented by *Coleman*, 1970.

The depth-averaged  $\bar{\beta}$ -value can be calculated as being the ratio of the depth-averaged value of the sediment and the momentum diffusion coefficient:

$$\bar{\beta} = \frac{\frac{1}{h-a} \int_a^h \varepsilon_s \cdot dy}{\frac{1}{h} \int_0^h \varepsilon_m \cdot dy} = \frac{\bar{\varepsilon}_s}{\bar{\varepsilon}_m} \quad (B1)$$

The depth-averaged value of the sediment diffusion coefficient,  $\bar{\varepsilon}_s$ , has been obtained by numerical integration of the profiles in Fig B3, while the depth-averaged value of the momentum diffusion coefficient,  $\bar{\varepsilon}_m$ , can be easily obtained by its theoretical value:

$$\varepsilon_m = \kappa u_* \frac{y}{h} (h-y) \quad \Rightarrow \quad \bar{\varepsilon}_m = \frac{1}{h} \int_{y=0}^{y=h} \varepsilon_m \cdot dy = \frac{\kappa \cdot u_* \cdot h}{6} \quad (B2)$$

#### 10) Nordin and Dempster, 1963

Samples of suspended sediment and measurements of velocity in a vertical were used to define vertical concentration distribution and velocity profiles for cross sections in reaches of the Rio Grande near Bernalillo and Socorro, N. Mex., USA. The Bernalillo and Socorro data series were considered because the river bed was in equilibrium. The 23 observations presented were grouped in category a-2 due to the presence of bed forms. Limited data for the Rio Puerco, a tributary of the Rio Grande, also are included but they have not been considered here because the river bed was clay-armored.

Velocities were measured with a Price current meter and samples of suspended sediment were collected at points in the vertical with a US P-46 sampler or a modified DH-48 hand sampler. The number of measurement points in a vertical varied from 3 to 5. Obtained concurrently with velocity and suspended-sediment samples were water discharge, width, mean depth, mean velocity, water temperature, water-surface slope, and bed-material samples. The vertical distribution of suspended-sediment concentration for several size ranges was determined from particle-size analysis of point-integrated samples. The size ranges investigated were: 0.062-0.125 [mm], 0.125-0.250 [mm], and 0.250-0.500 [mm].

The authors do not present the vertical mean concentration profiles. They obtained, for each size range, the modified Rouse number,  $z'$ , fitting the river concentration distribution to the modified Rouse equation. Thus, it has been possible to compute the  $\bar{\beta}$ -value of each size ranges for all the observations on the Rio Grande.

## B 5 Discussion

The data from the literature – 9 publications are retained for our study – have been evaluated to obtain the  $\bar{\beta}$ -values; they are supplemented with the results of this thesis. In 5 publications referring to channel data (n.<sup>o</sup> 1-5) the measured concentration profiles are given; thus it was possible to obtain the  $\bar{\beta}$ -values by best-fitting the Rouse or Hunt equation to the vertical mean concentration profiles (using the least-square method). The results are summarized in Table B1.

In 2 publications referring to channel data (n.<sup>o</sup> 7, 8) and 1 publication referring to river data (no<sup>o</sup> 10) the modified Rouse number,  $z'$ , best-fitting the measured vertical mean concentration profiles (not given in the publications) was presented. Using the values of  $z'$ , the  $\bar{\beta}$ -values have been computed. The channel data are summarized in Table B2a, while the river data are summarized in Table B2b.

In 1 publication referring to channel data (no<sup>o</sup> 9) the sediment-diffusion coefficient profiles were given. The  $\bar{\beta}$ -values were obtained dividing the depth-averaged value of the sediment diffusion coefficient profile by the depth-averaged value of the theoretical momentum diffusion coefficient profile, see eqs. B1 and B2. The results of this computation are presented in Table B2a.

An important parameter involved in the diffusion of sediments is the settling velocity,  $v_{ss}$ . On the other hand, another important parameter involved in the momentum diffusion is the shear velocity,  $u_*$ . Thus, it seems reasonable to scale the  $\bar{\beta}$ -values with the parameter  $v_{ss}/u_*$ . The plot of  $\bar{\beta} = f(v_{ss}/u_*)$  is presented in Fig. B4 for channel and river data plotted separately and together.

In a second approximation also the suspended concentration affects the diffusion of fluid and sediment particles (see the effects of the increasing concentration on the  $\bar{\beta}$ -values, Fig. B1). The effect of the suspended concentration can be summarized by the ratio of depth-averaged concentration,  $C_s^m$ , and the reference concentration,  $\bar{c}_{sa}^m$ . The parameter thus-obtained is:  $v_{ss}/u_* \cdot C_s^m / \bar{c}_{sa}^m$ . The plot of  $\bar{\beta} = f(v_{ss}/u_* \cdot C_s^m / \bar{c}_{sa}^m)$  is presented in Fig. B4 for channel and river data.

The dimensionless parameter,  $v_{ss}/u_*$ , does not scale well – especially for river data (see Fig. B4) – the  $\bar{\beta}$  -values. A proportionality of the  $\bar{\beta}$  -values to the parameter  $v_{ss}/u_*$  is however somehow evident in channel data.

By using channel data, the proportionality of the  $\bar{\beta}$  -values to the parameter  $v_{ss}/u_* \cdot C_s/c_{sa}$  is more evident.

Fig. B4 can be used to obtain an approximated  $\bar{\beta}$ -value to establish the vertical concentration profile using the Rouse or Hunt equations. In Fig. B4 the black points (group a) represent  $\bar{\beta}$ -values referring to suspension flows in capacity condition without bed forms. The gray points (group b) refer to flow in near-capacity condition or to flow in capacity condition but in presence of

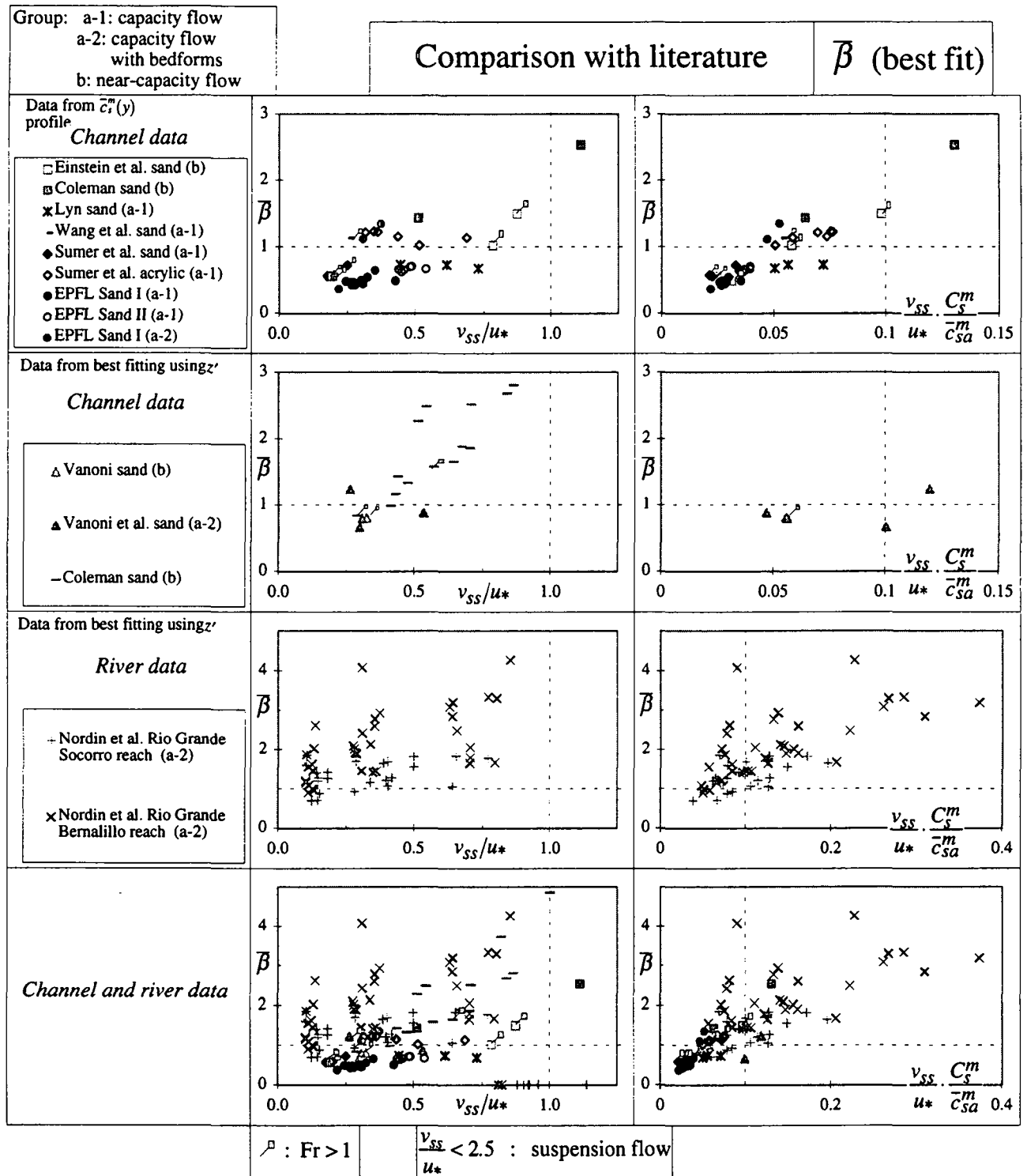


Fig. B4: Resume of the data taken from the literature

bed forms. It seems that the scatter of the gray points (near-capacity or bed forms) in all plots is larger than the black points one (capacity condition).

The  $\bar{\beta}$ -values obtained from the Rio Grande river (*Nordin and Dempster, 1963*), show large  $\bar{\beta}$ -values,  $1 < \bar{\beta} < 4$ . It seems reasonable to think that the bed forms – usually present in river flows – are at least partially responsible for these large  $\bar{\beta}$ -values. In Appendix D, where the results of the experimental investigation of suspension flow over bed forms are presented, this discrepancy is studied.

In Fig. B4 the  $\bar{\beta}$ -values referring to supercritical flow are distinguished using a special symbol (gray flag). No special difference on the  $\bar{\beta}$ -values tendency can be observed for sub- and supercritical flows.

## B 6 Conclusions

This Appendix evaluates and summarizes the results of this thesis and the available data on suspension flows – investigated in laboratory channels and in natural river – as found in the literature. Only data which are considered to be capacity or near-capacity flow data were analyzed. These data are compared with the ones obtained in this thesis investigating suspension flows in capacity condition. The following conclusions can be drawn:

- i) The  $\bar{\beta}$ -values can be scaled using dimensionless parameters,  $v_{ss}/u_*$  or  $v_{ss}/u_* \cdot C_s^m / \bar{c}_{sa}^m$ . The resulting plots (see Fig. B4) can be used to obtain an approximated  $\bar{\beta}$ -value to establish the vertical concentration profile using the Rouse or Hunt equations.
- ii) The proposed scaling parameters seem to correlate acceptably the  $\bar{\beta}$ -values only in case of capacity flow. The  $\bar{\beta}$ -values are usually  $\bar{\beta} \leq 1$ . If the flow is in non-capacity flow or if bed forms are present, the  $\bar{\beta}$ -values are usually  $\bar{\beta} > 1$  (see Fig. B4).
- iii) Sub- and supercritical flow conditions seem not to influence the  $\bar{\beta}$ -values (see Fig. B4).
- iv) According to the value of  $v_{ss}/u_*$  or  $v_{ss}/u_* \cdot C_s^m / \bar{c}_{sa}^m$ , the  $\bar{\beta}$ -values can be smaller (suspension flow over plane bed), equal, but also larger (suspension flows over bed with bed forms) than unity.

Author	run	Group	$Q$	$h$	$B/h$	$U$	$S_b$	$Re \cdot 10^3$	$Fr$	$u_*$	$f$	$k_r$	$\frac{u_* k_r}{v_m}$	$\rho_s$	$v_u/v_u$	$C_{fr}$	$\bar{C}_{sa}^m$	$\bar{\rho}_m$	$Ri$	$z = \frac{v_u}{k \cdot u_*}$ (best fit)	$\beta'$	
Einstein et al.	5.4	b	0.0735	0.175	2.7	2.01	2.50	5.510	1.98	0.143	0.037	0.063	9.0	7.300	2650	123.0	0.87	21.78	194.00	1013.36	6.310	2.185
Einstein et al.	5.70	b	0.081	0.170	2.4	2.010	2.840	5.657	1.94	0.126	0.031	0.242	153.9	0.940	2650	99.0	0.79	13.86	187.80	1008.63	9.020	1.963
Einstein et al.	5.75	b	0.0778	0.174	2.5	2.025	2.500	5.497	1.83	0.120	0.028	0.833	97.0	0.274	2650	36.6	0.31	55.00	537.50	1034.52	27.186	0.763
Coleman	20	b	0.0664	0.170	2.1	1.058	2.000	3.671	0.82	0.041	0.012	0.028	1.1	0.105	2650	8.0	0.20	7.89	60.95	104.91	37.286	0.763
Coleman	31	b	0.0664	0.172	2.1	1.051	2.000	3.655	0.80	0.041	0.012	0.032	1.3	0.210	2650	21.0	0.51	3.98	31.80	1002.38	19.577	1.280
Coleman	40	b	0.0664	0.171	2.1	1.051	0.220	3.655	0.81	0.041	0.015	0.035	3.4	0.120	2650	30.0	0.11	0.81	6.89	1000.30	3.458	2.339
Lyn	1563EO	a-1	0.0711	0.0655	4.1	0.628	0.244	1.092	0.79	0.036	0.026	0.398	14.2	0.130	2650	16.0	0.45	1.26	16.00	1000.78	3.056	1.117
Lyn	1963EO	a-1	0.0711	0.0655	4.1	0.636	0.251	1.113	0.80	0.038	0.028	0.508	19.0	0.190	2650	23.0	0.61	6.22	1000.45	1.750	1.533	2.035
Wang et al.	SO3	b	0.0435	0.080	3.8	1.880	0.000	3.868	2.12	0.043	0.012	0.019	1.4	0.137	2650	0.99	14.30	1000.62	3.160	1.824	2.667	0.684
Sumar et al.	J12	a-1	0.013	0.112	2.7	0.402	0.145	1.009	0.38	0.029	0.042	0.318	9.1	0.600	1130	20.0	0.69	9.31	109.61	1001.07	16.100	1.718
Sumar et al.	J20	a-1	0.023	0.118	2.6	0.537	0.246	1.326	0.51	0.039	0.041	0.322	11.9	0.800	1130	20.0	0.52	22.63	230.52	1002.60	19.470	1.261
Sumar et al.	J33	a-1	0.027	0.124	2.4	0.721	0.426	1.741	0.65	0.035	0.046	0.514	25.1	0.680	1130	20.0	0.36	60.69	289.28	1006.38	12.800	0.911
Sumar et al.	J34	a-1	0.029	0.129	2.3	0.749	0.447	1.811	0.67	0.037	0.047	0.567	27.8	0.660	1130	20.0	0.35	62.05	322.05	1008.03	14.080	1.709
Sumar et al.	J37	a-1	0.031	0.132	2.3	0.773	0.500	1.892	0.68	0.033	0.053	0.603	44.1	0.680	1130	20.0	0.32	71.06	324.31	1008.17	11.930	0.794
Sumar et al.	J42	a-1	0.026	0.103	2.9	0.833	0.479	2.030	0.83	0.048	0.027	0.063	3.0	0.130	2650	12.0	0.25	12.92	96.46	1008.05	26.070	0.624
Sumar et al.	J50	a-1	0.031	0.101	3.0	0.244	0.132	1.326	0.51	0.039	0.041	0.344	14.3	0.600	1130	20.0	0.44	43.87	261.03	1005.05	15.410	1.094
Sumar et al.	J55	a-1	0.036	0.105	2.9	1.138	0.383	2.767	1.12	0.068	0.028	0.085	5.7	0.130	2650	12.0	0.18	43.43	339.73	1027.94	46.110	0.952
EPFL 1997	Q4659003	a-1	0.049	0.120	5.0	0.680	0.030	3.30	0.65	0.028	0.016	0.050	1.4	0.135	2650	12.0	0.43	2.05	24.62	101.28	21.364	1.071
EPFL 1997	Q4530005	a-1	0.058	0.120	5.0	0.806	0.035	2.761	0.74	0.034	0.014	0.063	2.2	0.600	1130	12.0	0.35	28.62	1001.75	15.633	0.882	1.333
EPFL 1997	Q48590075	a-1	0.060	0.120	5.0	0.829	0.035	2.840	0.76	0.037	0.015	0.08	4.0	0.135	2650	12.0	0.32	21.96	308.33	16.872	0.811	1.489
EPFL 1997	Q5059010	a-1	0.057	0.120	5.0	0.792	0.100	2.030	0.83	0.048	0.027	0.063	3.0	0.130	2650	12.0	0.31	36.04	102.97	164.50	1.504	0.872
EPFL 1997	Q5359015	a-1	0.062	0.120	5.0	0.838	0.150	2.822	0.76	0.040	0.019	0.148	5.9	0.133	2650	12.0	0.30	4.41	46.05	1002.75	18.120	0.784
EPFL 1997	Q57590175	a-1	0.062	0.120	5.0	0.855	0.175	2.922	0.79	0.044	0.021	0.292	12.8	0.135	2650	12.0	0.27	4.73	49.47	1002.95	18.610	0.682
EPFL 1997	Q6059020	a-1	0.063	0.120	5.0	0.905	0.200	3.098	0.84	0.045	0.021	0.337	9.3	0.133	2650	12.0	0.27	12.92	1003.06	17.380	0.667	1.550
EPFL 1997	Q65590225	a-1	0.066	0.120	5.0	0.916	0.225	3.135	0.85	0.046	0.020	0.337	10.6	0.133	2650	12.0	0.26	5.08	51.82	1003.33	16.872	0.548
EPFL 1997	Q7559025	a-1	0.059	0.120	5.0	0.897	0.23	2.822	0.76	0.040	0.019	0.348	17.3	0.135	2650	12.0	0.31	3.61	39.33	1002.25	18.830	0.769
EPFL 1997	Q755903	a-1	0.058	0.120	5.0	0.801	0.100	2.743	0.74	0.043	0.020	0.222	9.5	0.133	2650	12.0	0.28	4.41	44.05	1002.97	16.450	1.506
EPFL 1998	Q5059010/II	a-1	0.060	0.120	5.0	0.833	0.150	2.855	0.77	0.044	0.022	0.334	14.5	0.210	2650	21.0	0.54	1.57	21.31	1000.98	102.75	1.346
EPFL 1998	Q55590175/II	a-1	0.060	0.120	5.0	0.836	0.175	2.864	0.77	0.045	0.023	0.425	19.3	0.210	2650	21.0	0.49	2.01	24.77	1001.43	10.870	1.207
EPFL 1998	Q6059020/II	a-1	0.061	0.120	5.0	0.850	0.200	2.911	0.78	0.045	0.023	0.425	19.3	0.210	2650	21.0	0.46	1.90	23.29	1001.18	8.260	1.154
EPFL 1998	Q65590225/II	a-1	0.062	0.120	5.0	0.865	0.225	2.964	0.80	0.047	0.023	0.444	20.6	0.210	2650	21.0	0.45	2.78	34.36	1001.73	11.370	1.128
EPFL 1998	Q7059025/II	a-1	0.063	0.120	5.0	0.868	0.250	2.974	0.80	0.048	0.024	0.444	24.9	0.210	2650	21.0	0.44	2.84	33.83	1001.77	10.910	1.103
EPFL 1998	BF_S013	a-2	0.038	0.110	5.5	0.575	0.150	6.322	0.55	0.032	0.025	0.593	18.9	0.135	2650	12.0	0.38	3.01	21.47	1001.87	13.980	0.696
EPFL 1998	BF_S02	a-2	0.043	0.118	5.1	0.609	0.200	2.189	0.57	0.039	0.033	0.671	65.1	0.135	2650	12.0	0.31	1.94	12.69	1001.21	4.020	0.769

Author : Name of the experimenter  
run : Name of the run  
Group : Category of the run  
 $Q [m^3/s]$ : Flow discharge  
 $h [m]$ : Flow depth  
 $U [m/s]$ : Depth averaged velocity  
 $\zeta [\%]$ : Bed slope

$F_F [-]$  : Froude number  $F_F = U/\sqrt{gh}$   
 $u_* [m/s]$ : Shear velocity, usually taken as:  $u_* = \sqrt{g R_h S_b}$   
 $f [-]$ : friction factor,  $f = 8(u_*/U)^2$   
 $k_s [\text{mm}]$ : Equivalent roughness evaluated with Colebrook and White eq.  $R_i [-]$ : Richardson number,  $R_i = \frac{u_* k_s}{\nu_m}$

$C_s^m [\text{kg/m}^3]$ : Depth - averaged concentration  
 $\bar{C}_{sa}^m [\text{kg/m}^3]$ : Reference concentration measured at  $y = a \equiv 0.05h$   
 $\bar{\rho}_m [\text{kg/m}^3]$  : Depth - averaged mixture density,  $\bar{\rho}_m = \rho_w + (\rho_s - \rho_w) \mathcal{C}_s$ ,  $\bar{\rho}_m = \frac{\rho_w + (\rho_s - \rho_w) \mathcal{C}_s}{1 + (\rho_s - \rho_w) \mathcal{C}_s}$   
 $R_i$  : Richardson number,  $R_i = \frac{g h \rho_m (y-a)}{\bar{\rho}_m U^2}$   
 $h [m]$ : Flow depth  
 $U [m/s]$ : Depth averaged velocity  
 $\zeta [\%]$ : Bed slope

$Re [-]$  : Reynolds number  $Re = \frac{4 \cdot U \cdot R_k}{\nu_m}$   
 $v_s [\text{mm/s}]$ : Settling velocity, taken in still clear water  
 $\rho_s [\text{kg/m}^3]$ : Sediment density  
 $\beta [-]$  :  $\bar{\beta}$  - value (of best fit)

Table B1: Summary of data using the concentration distribution. – Channel data

Author	run	Group	$Q$	$h$	$B/h$	$U$	$S_b$	$Re \cdot 10^4$	$Fr$	$u$	$f$	$k_s$	$\frac{u_s k_s}{v_s}$	$d_{so}$	$\rho_s$	$v_u$	$\frac{v_u}{u_s}$	$C_t^*$	$\bar{C}_{so}^*$	$\bar{\rho}_m$	$Ri$	$z = \frac{v_u}{k_s u_s}$	$z'$	$\beta$
			[ $m^3/s$ ]	[ $m$ ]	[ $-$ ]	[ $m/s$ ]	[ $\%$ ]	[ $-$ ]	[ $m/s$ ]	[ $-$ ]	[ $m$ ]	[ $-$ ]	[ $mm$ ]	[ $kg/m^3$ ]	[ $mm/s$ ]	[ $-$ ]	[ $kg/m^3$ ]	[ $kg/m^3$ ]	[ $-$ ]	[ $kg/m^3$ ]	[ $-$ ]	[ $-$ ]	[ $-$ ]	[ $-$ ]
<i>Vanoni</i>	<i>II</i>	<i>b</i>	0.148	0.145	5.79	1.211	0.25	5.22	1.02	0.059	0.019	0.293	17.3	0.76	2650	19.2	0.33	3.36	19.60	1002.09	---	0.81	1.01	0.81
<i>Vanoni et al.</i>	<i>I</i>	<i>a-2</i>	0.009	0.087	3.07	0.375	0.25	0.79	0.41	0.036	0.074	8.824	317.2	0.091	2650	9.5	0.26	3.64	8.00	1002.27	---	0.66	0.53	1.24
<i>Vanoni et al.</i>	<i>3</i>	<i>a-2</i>	0.012	0.074	3.6	0.616	0.2	1.17	0.72	0.037	0.020	0.154	4.7	0.091	2650	9.5	0.31	4.60	25.00	1002.86	---	0.77	0.97	0.79
<i>Vanoni et al.</i>	<i>5</i>	<i>a-2</i>	0.014	0.078	3.42	0.689	0.206	1.35	0.79	0.032	0.017	0.081	2.6	0.091	2650	9.5	0.30	8.08	24.00	1005.03	---	0.75	1.13	0.66
<i>Vanoni et al.</i>	<i>7</i>	<i>a-2</i>	0.014	0.078	3.42	0.695	0.238	1.37	0.79	0.035	0.021	0.190	6.7	0.148	2650	18.9	0.53	3.61	41.00	1002.25	---	1.34	1.53	0.87
<i>Coleman</i>	<i>vsd/u_s = 0.287</i>	<i>b</i>	0.054	0.122	2.92	1.235	0.417	3.58	1.13	0.062	0.020	0.239	14.7	0.149	2650	17.7	0.29	---	---	---	---	0.72	0.86	0.84
<i>Coleman</i>	<i>vsd/u_s = 0.414</i>	<i>b</i>	0.057	0.183	1.95	0.872	0.18	3.15	0.65	0.063	0.019	0.255	10.9	0.149	2650	17.7	0.41	---	---	---	---	1.04	1.06	0.98
<i>Coleman</i>	<i>vsd/u_s = 0.332</i>	<i>b</i>	0.044	0.122	2.92	1.007	0.308	2.91	0.92	0.044	0.013	0.037	1.5	0.149	2650	17.7	0.43	---	---	---	---	1.08	0.93	1.16
<i>Coleman</i>	<i>vsd/u_s = 0.359</i>	<i>b</i>	0.065	0.244	1.46	0.747	0.085	3.08	0.48	0.040	0.023	0.622	25.1	0.149	2650	17.7	0.44	---	---	---	---	1.10	0.77	1.43
<i>Coleman</i>	<i>vsd/u_s = 0.475</i>	<i>b</i>	0.046	0.183	1.95	0.698	0.12	2.52	0.52	0.037	0.023	0.501	18.6	0.149	2650	17.7	0.48	---	---	---	---	1.19	0.89	1.53
<i>Coleman</i>	<i>vsd/u_s = 0.513</i>	<i>b</i>	0.034	0.244	1.46	0.619	0.067	2.55	0.49	0.034	0.025	0.93	27.3	0.149	2650	17.7	0.51	---	---	---	---	1.28	0.57	2.27
<i>Coleman</i>	<i>vsd/u_s = 0.542</i>	<i>b</i>	0.037	0.183	1.95	0.567	0.085	2.05	0.42	0.033	0.026	0.880	28.7	0.149	2650	17.7	0.54	---	---	---	---	1.36	0.54	2.49
<i>Coleman</i>	<i>vsd/u_s = 0.570</i>	<i>b</i>	0.048	0.122	2.92	1.104	0.422	3.20	1.01	0.048	0.015	0.074	3.6	0.21	2650	27.5	0.57	---	---	---	---	1.42	0.90	1.58
<i>Coleman</i>	<i>vsd/u_s = 0.641</i>	<i>b</i>	0.058	0.183	1.95	0.888	0.156	3.20	0.66	0.043	0.019	0.248	10.8	0.21	2650	27.8	0.64	---	---	---	---	1.60	0.97	1.65
<i>Coleman</i>	<i>vsd/u_s = 0.72</i>	<i>b</i>	0.048	0.183	1.95	0.735	0.135	2.65	0.55	0.041	0.025	0.639	28.2	0.21	2650	27.5	0.67	---	---	---	---	1.68	0.89	1.89
<i>Coleman</i>	<i>vsd/u_s = 0.702</i>	<i>b</i>	0.032	0.122	2.92	0.726	0.16	2.10	0.66	0.026	0.010	0.008	0.2	0.149	2650	18.0	0.70	---	---	---	---	1.76	0.94	1.87
<i>Coleman</i>	<i>vsd/u_s = 0.705</i>	<i>b</i>	0.068	0.244	1.46	0.781	0.082	3.21	0.50	0.039	0.020	0.369	14.5	0.21	2650	27.8	0.71	---	---	---	---	1.76	0.70	2.52
<i>Coleman</i>	<i>vsd/u_s = 0.818</i>	<i>b</i>	0.053	0.244	1.46	0.610	0.065	2.51	0.39	0.034	0.024	0.726	24.3	0.21	2650	27.5	0.82	---	---	---	---	2.05	0.55	3.74
<i>Coleman</i>	<i>vsd/u_s = 0.840</i>	<i>b</i>	0.036	0.122	2.92	0.870	0.348	2.38	0.75	0.032	0.012	0.027	0.9	0.21	2650	27.1	0.84	---	---	---	---	2.10	0.78	2.68
<i>Coleman</i>	<i>vsd/u_s = 0.864</i>	<i>b</i>	0.032	0.122	2.92	0.738	0.144	2.14	0.67	0.037	0.014	0.059	1.8	0.21	2650	27.1	0.86	---	---	---	---	2.16	0.77	2.81
<i>Coleman</i>	<i>vsd/u_s = 0.908</i>	<i>b</i>	0.039	0.183	1.95	0.595	0.075	2.15	0.44	0.030	0.020	0.317	9.5	0.21	2650	29.9	1.00	---	---	---	---	2.50	0.51	4.85

Obtained from the sediment coefficient  
diffusion coefficient

Author : Name of the experimenter

$Fr [-]$  : Froude number  $Fr = U/\sqrt{gh}$

$u_*$  [m/s] : Shear velocity, usually taken as :  $u_* = \sqrt{gR_h S_b}$

$f [-]$ : friction factor,  $f = 8(u_*/U)^2$

$k_s$  [mm] : Equivalent roughness evaluated with Colebrook and White eq.

$Ri [-]$  : Richardson number,  $Ri = \frac{gh[\rho_m(y=a) - \rho_m(y=h)]}{\rho_m u_*^2}$

$R$  [-] : Reynolds number  $Re = \frac{4 \cdot U \cdot R_h}{V_m}$

$z$  [-] : Rouse number,  $z = \frac{v_u}{k_s u_*}$

$z'$  [-] : modified Rouse number,  $z' = \frac{v_u}{\kappa \cdot u_*}$

$\beta$  [-] :  $\bar{\beta}$  - value (of best fit)

Table B2a: Summary of data using modified Rouse number,  $z'$  - Channel data



## B 7 References

- COLEMAN, N. L. (1970). "Flume Studies of the Sediment Transfer Coefficient." *Water Res. Res.*, Vol. 6, N°. 3, pp. 801-809.
- COLEMAN, N. L. (1986). "Effects of Suspended Sediment on the Open-Channel Velocity Distribution.", *Water Res. Res.*, vol. 22, N°. 10, pp. 1377-1384.
- EINSTEIN, H. A. and CHIEN, N. (1955). "Effects of Heavy Sediment Concentration Near the Bed on the Velocity and Sediment Distribution.", Uni. of Cal., Berkeley, US Army Corps of Engr., Missouri River Div.
- LYN, D. A. (1988). "A similarity approach to turbulent sediment-laden flows in open channels." *J. Fluid Mech.*, Vol. 193, pp. 1-26.
- NORDIN, C. F. and DEMPSTER, G. R. (1963). "Vertical Distribution of Velocity and Suspended Sediment Middle Rio Grande New Mexico.", U.S. Geol. Survey; Professional Paper 462-B.
- SUMER, B. M. et al. (1996). "Velocity and Concentration Profiles in Sheet-Flow Layer of Movable Bed." *J. Hydr. Engr.*, vol. 122, N°. 10, pp. 549-558.
- VANONI, V. A. (1946). "Transportation of Suspended Sediment by Water.", *Trans. ASCE*, vol. 111, pp. 67-133.
- VANONI, V. A. and NOMICOS, G. N. (1960). "Resistance Properties of Sediment-Laden Streams.", *Trans. Am. Soc. Civil Engrs.*, vol. 125/I, pp. 1140-1175.
- WANG, X. and QIAN, N. (1989). "Turbulence Characteristics of Sediment-Laden Flow.", *J. Hydr. Engr.*, vol. 115, N° 6, pp. 781-799.

## Data from $\bar{c}_s^m$ -profile

- |  |                   |
|--|-------------------|
| 1) <i>Einstein and Chien, 1955</i>                       | (pp. B-20 - B-22) |
| 2) <i>Coleman, 1986</i>                                  | (pp. B-23 - B-25) |
| 3) <i>Lyn, 1988</i>                                      | (pp. B-26 - B-28) |
| 4) <i>Wang and Qian, 1989</i>                            | (p. B-29)         |
| 5) <i>Sumer, Kozakiewicz, Fredsøe and Deigaard, 1996</i> | (pp. B-30 - B-38) |
| 6a) <i>EPFL, 1997</i>                                    | (pp. B-39 - B-49) |
| 6b) <i>EPFL, 1998</i>                                    | (pp. B-50 - B-57) |

The data of each run are found on individual worksheets which are put at the end of this Appendix.

On the next page is presented such a worksheet for a typical run (example: run 155 made by *Sumer et al., 1996*). All the numbers written in italic were given by the experimenter, the others were calculated by the author of this thesis.

The presence of a flat sediment layer on the bed, as described by *Sumer et al.*, suggests to class this run in group a-1.

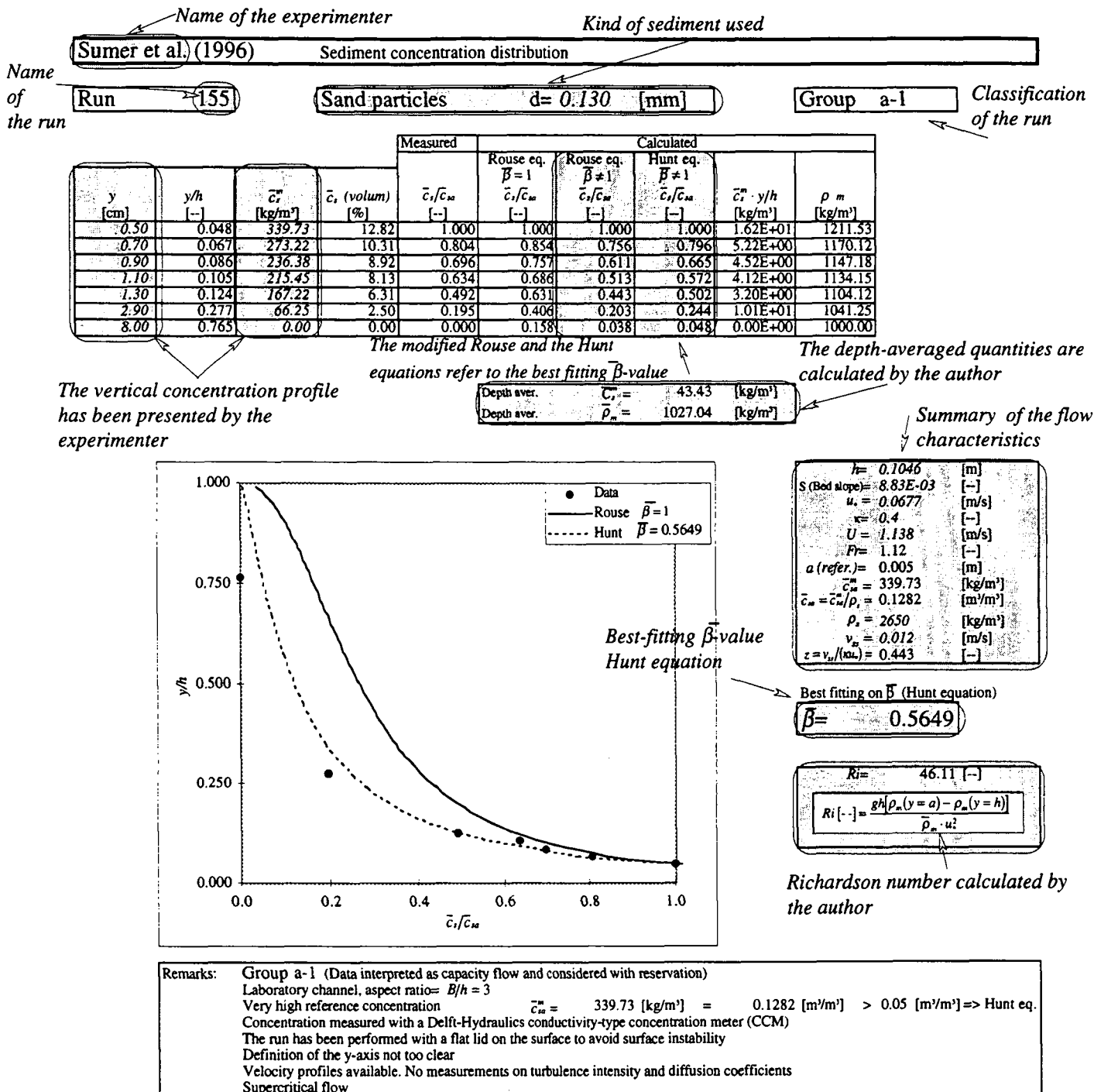
The reference concentration has been taken equal to the one measured closest to  $a = 0.05 \cdot h$ , such as:

$$\bar{c}_{sa}^m = \bar{c}_s^m (y = 0.048 \cdot h) = 339.73 \text{ [kg/m}^3\text{]} \text{ or } \bar{c}_{sa} = 0.1282 \text{ [m}^3\text{/m}^3\text{]}$$

The volumetric reference concentration,  $\bar{c}_{sa} = 0.1282 \text{ [m}^3\text{/m}^3\text{]}$ , is larger than 0.05, therefore the best fitting has been made to the Hunt equation leading to a  $\bar{\beta}$ -value of 0.5649.

In the graph are presented the dimensionless concentration profile given by the experimenter, the Rouse equation ( $\bar{\beta} = 1$ ) and the Hunt equation in which  $\bar{\beta} = 0.5649$ . The Rouse equation with  $\bar{\beta} = 0.5649$ , has been calculated (seventh column) but has not been plotted. The agreement between the Hunt equation and data points is much better than the one obtained with the Rouse equation ( $\bar{\beta} = 1$ ).

It is important to note, that this run has been performed under a very special condition. On the surface a flat lid was present to avoid perturbation of the surface. Observations on the characteristic of the instrument or on the condition of the flow are written in the remarks below the graph.



Typical example of a worksheet

Run S-4

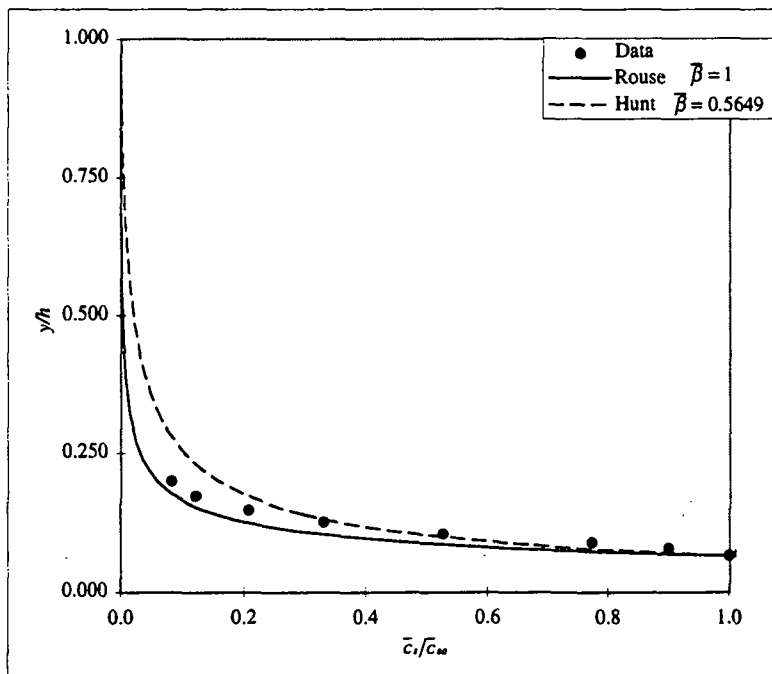
Sand particles

d = 1.300 [mm]

Group b

y [cm]	y/h [--]	$\bar{c}_s$ [kg/m³]	$\bar{c}_s$ (volum) [%]	Measured		Calculated							
				$\bar{c}_s/\bar{c}_{sa}$	[--]	Rouse eq. $\beta = 1$ $\bar{c}_s/\bar{c}_{sa}$	[--]	Rouse eq. $\beta \neq 1$ $\bar{c}_s/\bar{c}_{sa}$	[--]	Hunt eq. $\beta \neq 1$ $\bar{c}_s/\bar{c}_{sa}$	[--]	$\bar{c}_s \cdot y/h$ [kg/m³]	$\rho_m$ [kg/m³]
0.75	0.065	194.00	7.32	1.000		1.000		1.000		1.000		1.26E+01	1120.79
0.81	0.070	197.50	7.45	1.018		0.833		0.885		0.890		1.03E+00	1122.97
0.90	0.078	174.50	6.58	0.899		0.647		0.747		0.757		1.39E+00	1108.65
1.02	0.089	150.00	5.66	0.773		0.478		0.610		0.622		1.58E+00	1093.40
1.20	0.104	102.40	3.86	0.528		0.321		0.467		0.480		1.62E+00	1063.76
1.45	0.126	64.25	2.42	0.331		0.203		0.345		0.356		1.36E+00	1040.00
1.69	0.147	40.50	1.53	0.209		0.138		0.265		0.275		8.50E-01	1025.22
1.99	0.173	23.65	0.89	0.122		0.089		0.199		0.207		6.24E-01	1014.73
2.30	0.200	16.08	0.61	0.083		0.061		0.154		0.160		4.28E-01	1010.01
2.69	0.234	8.78	0.33	0.045		0.039		0.114		0.120		2.99E-01	1005.47

$$\begin{aligned} \text{Depth aver. } \bar{c}_s &= 21.78 \text{ [kg/m³]} \\ \text{Depth aver. } \bar{\rho}_m &= 1013.56 \text{ [kg/m³]} \end{aligned}$$



$$\begin{aligned} h &= 0.115 \text{ [m]} \\ S (\text{Bed slope}) &= 2.50E-02 \text{ [--]} \\ u_* &= 0.143 \text{ [m/s]} \\ \kappa &= 0.4 \text{ [--]} \\ U &= 2.101 \text{ [m/s]} \\ Fr &= 1.98 \text{ [--]} \\ a (\text{refer.}) &= 0.0075 \text{ [m]} \\ \bar{c}_{sa} &= 194.00 \text{ [kg/m³]} \\ \bar{c}_{sa} &= \bar{c}_s / \rho_i = 0.073 \text{ [m³/m³]} \\ \rho_i &= 2650 \text{ [kg/m³]} \\ v_{u_*} &= 0.125 \text{ [m/s]} \\ z &= v_{u_*} / (a \bar{c}_s) = 2.190 \text{ [--]} \end{aligned}$$

Best fitting on  $\beta$  (Hunt equation)

$$\bar{\beta} = 1.4946$$

$$Ri = 6.31 \text{ [--]}$$

$$Ri [-] = \frac{gh[\rho_m(y=a) - \rho_m(y=h)]}{\bar{\rho}_m \cdot u_*^2}$$

Remarks: Group b (Data interpreted as capacity-flow)  
 Laboratory channel, aspect ratio =  $B/h = 2.7$   
 High reference concentration  $\bar{c}_s = 194.00 \text{ [kg/m³]} = 0.07 \text{ [m³/m³]} > 0.05 \text{ [m³/m³]} \Rightarrow$  Hunt eq.  
 Concentration measured with a suction method  
 The concentration distribution has not been measured in the upper part of the flow  
 Bed roughness composed by glued sand of the same kind of the suspended load  
 Velocity profiles available. No measurements on turbulence intensity and diffusion coefficients  
 Supercritical flow

Einstein and Chien, (1955)

Sediment concentration distribution

Run S-10

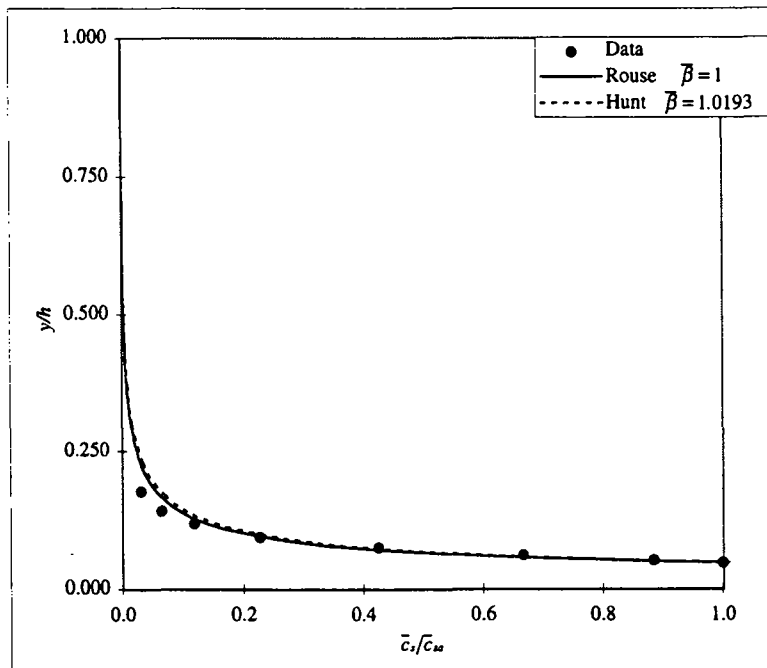
Sand particles

d= 0.940 [mm]

Group b

y [cm]	y/h [-]	$\bar{c}_s$ [kg/m³]	$\bar{c}_s$ (volum) [%]	Calculated					
				$\bar{c}_s/\bar{c}_{s0}$	Rouse eq. $\beta = 1$	Rouse eq. $\beta \neq 1$	Hunt eq. $\beta \neq 1$	$\bar{c}_s \cdot y/h$ [kg/m³]	$\rho_m$ [kg/m³]
0.62	0.048	187.80	7.09	1.000	1.000	1.000	1.000	8.92E+00	1116.93
0.68	0.052	166.00	6.26	0.884	0.822	0.825	0.835	7.82E-01	1103.36
0.80	0.062	125.20	4.72	0.667	0.580	0.586	0.604	1.19E+00	1077.95
0.99	0.076	79.80	3.01	0.425	0.375	0.382	0.399	1.13E+00	1049.69
1.23	0.095	42.50	1.60	0.226	0.232	0.238	0.252	8.09E-01	1026.46
1.54	0.119	22.35	0.84	0.119	0.142	0.147	0.156	5.32E-01	1013.92
1.85	0.142	12.10	0.46	0.064	0.094	0.098	0.105	2.87E-01	1007.53
2.31	0.178	5.66	0.21	0.030	0.056	0.059	0.063	2.01E-01	1003.52

$$\begin{aligned} \text{Depth aver. } \bar{c}_s &= 13.86 \text{ [kg/m}^3\text{]} \\ \text{Depth aver. } \bar{\rho}_m &= 1008.63 \text{ [kg/m}^3\text{]} \end{aligned}$$



$$\begin{aligned} h &= 0.12993 \text{ [m]} \\ S (\text{Bed slope}) &\approx 1.84E-02 \text{ [-]} \\ u_* &= 0.126 \text{ [m/s]} \\ \kappa &= 0.4 \text{ [-]} \\ U &= 2.01 \text{ [m/s]} \\ Fr &= 1.78 \text{ [-]} \\ a (\text{refer.}) &= 0.00617245 \text{ [m]} \\ \bar{c}_{s0} &= 187.80 \text{ [kg/m}^3\text{]} \\ \bar{c}_{s0} &= \bar{c}_s / \rho_m = 0.071 \text{ [m}^3/\text{m}^3\text{]} \\ \rho_s &= 2650 \text{ [kg/m}^3\text{]} \\ v_n &= 0.099 \text{ [m/s]} \\ z &= v_n / (\kappa u_*) = 1.966 \text{ [-]} \end{aligned}$$

Best fitting on  $\beta$  (Hunt equation)

$$\beta = 1.0193$$

$$Ri = 9.02 \text{ [-]}$$

$$Ri [-] = \frac{gh[\rho_m(y=a) - \rho_m(y=h)]}{\bar{\rho}_m \cdot u_*^2}$$

Remarks: Group b (Data interpreted as capacity-flow)  
Laboratory channel, aspect ratio=B/h = 2.8  
High reference concentration  $\bar{c}_s = 188 \text{ [kg/m}^3\text{]} = 0.07 \text{ [m}^3/\text{m}^3\text{]} > 0.05 \text{ [m}^3/\text{m}^3\text{]} \Rightarrow \text{Hunt eq.}$   
Concentration measured with a suction method  
The concentration distribution has not been measured in the upper part of the flow  
Bed roughness composed by glued sand of the same kind of the suspended load  
Velocity profiles available. No measurements on turbulence intensity and diffusion coefficients  
Supercritical flow

Einstein and Chien, (1955)

Sediment concentration distribution

Run S-15

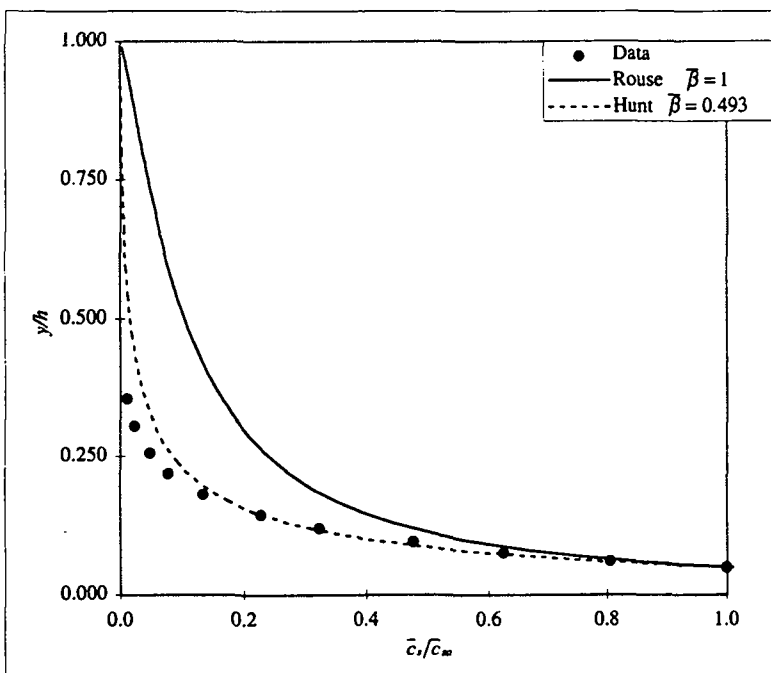
Sand particles

d = 0.274 [mm]

Group b

y [cm]	y/h [-]	$\bar{c}_s^m$ [kg/m³]	$\bar{c}_s$ (volum) [%]	$\bar{c}_s/\bar{c}_{ss}$ [-]	Calculated				
					Rouse eq. $\beta = 1$	Rouse eq. $\beta \neq 1$	Hunt eq. $\beta \neq 1$	$\bar{c}_s \cdot y/h$ [kg/m³]	$\rho_m$ [kg/m³]
0.61	0.049	537.50	20.28	1.000	1.000	0.695	0.777	2.64E+01	1334.67
0.76	0.061	433.00	16.34	0.806	0.836	0.701	0.486	5.29E+00	1269.60
0.95	0.076	336.00	12.68	0.625	0.701	0.486	0.593	4.96E+00	1209.21
1.19	0.096	256.00	9.66	0.476	0.578	0.329	0.433	5.04E+00	1159.40
1.50	0.120	173.40	6.54	0.323	0.476	0.222	0.308	4.26E+00	1107.97
1.80	0.145	122.00	4.60	0.227	0.404	0.159	0.229	3.00E+00	1075.96
2.26	0.182	72.20	2.72	0.134	0.329	0.105	0.155	2.66E+00	1044.95
2.72	0.218	42.20	1.59	0.079	0.276	0.073	0.111	1.54E+00	1026.28
3.18	0.256	25.45	0.96	0.047	0.236	0.053	0.082	9.52E-01	1015.85
3.79	0.305	12.22	0.46	0.023	0.196	0.037	0.056	6.00E-01	1007.61
4.41	0.355	5.9	0.22	0.011	0.165	0.026	0.040	2.93E-01	1003.67

$$\begin{aligned} \text{Depth aver. } \bar{c}_s^m &= 55.00 \text{ [kg/m}^3\text{]} \\ \text{Depth aver. } \bar{\rho}_m &= 1034.25 \text{ [kg/m}^3\text{]} \end{aligned}$$



$$\begin{aligned} h &= 0.124 \text{ [m]} \\ S (\text{Bed slope}) &= 2.50E-02 \text{ [-]} \\ u_* &= 0.120 \text{ [m/s]} \\ x &= 0.4 \text{ [-]} \\ U &= 2.025 \text{ [m/s]} \\ Fr &= 1.83 \text{ [-]} \\ a (\text{refer.}) &= 0.0061 \text{ [m]} \\ \bar{c}_{ss} &= 537.50 \text{ [kg/m}^3\text{]} \\ \bar{c}_m &= \bar{c}_{ss}/\rho_m = 0.203 \text{ [m}^3\text{/m}^3\text{]} \\ \rho_m &= 2650 \text{ [kg/m}^3\text{]} \\ v_n &= 0.037 \text{ [m/s]} \\ z &= v_n/(aU) = 0.763 \text{ [-]} \end{aligned}$$

Best fitting on  $\beta$  (Hunt equation)

$$\beta = 0.493$$

$$Ri = 27.18 \text{ [-]}$$

$$Ri [-] = \frac{gh[\rho_m(y=a) - \rho_m(y=h)]}{\bar{\rho}_m \cdot u_*^2}$$

Remarks: Group b (Data interpreted as capacity-flow)  
Laboratory channel, aspect ratio =  $B/h = 2.8$   
Very high reference concentration  $\bar{c}_{ss} = 538 \text{ [kg/m}^3\text{]} = 0.20 \text{ [m}^3\text{/m}^3\text{]} > 0.05 \text{ [m}^3\text{/m}^3\text{]} \Rightarrow \text{Hunt eq.}$   
Concentration measured with a suction method  
The concentration distribution has not been measured in the upper part of the flow  
Bed roughness composed by glued sand of the same kind of the suspended load  
Velocity profiles available. No measurements on turbulence intensity and diffusion coefficients  
Supercritical flow

Coleman (1986):

Sediment concentration distribution

Run 20

Sand particles

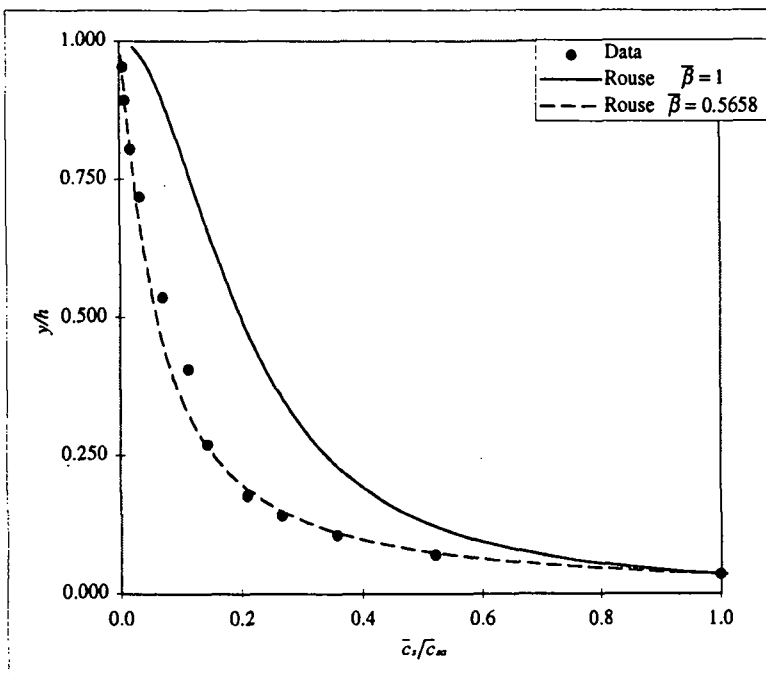
d= 0.105 [mm]

Group b

y [cm]	y/h [-]	$\bar{c}_s^m$ [kg/m³]	$\bar{c}_s$ (volum) [%]	Measured		Calculated			$\rho_m$ [kg/m³]
				$\bar{c}_s/\bar{c}_{s0}$ [-]	Rouse eq. $\beta = 1$ $\bar{c}_s/\bar{c}_{s0}$ [-]	Rouse eq. $\beta \neq 1$ $\bar{c}_s/\bar{c}_{s0}$ [-]	Hunt eq. $\beta \neq 1$ $\bar{c}_s/\bar{c}_{s0}$ [-]		
0.60	0.035	60.95	2.30	1.000	1.000	1.000	1.000	2.15E+00	1037.95
1.20	0.071	31.80	1.20	0.522	0.700	0.533	0.543	1.12E+00	1019.80
1.80	0.106	21.73	0.82	0.357	0.564	0.363	0.373	7.67E-01	1013.53
2.40	0.141	16.17	0.61	0.265	0.480	0.274	0.282	5.71E-01	1010.07
3.00	0.176	12.72	0.48	0.209	0.422	0.218	0.225	4.49E-01	1007.92
4.60	0.271	8.75	0.33	0.143	0.323	0.136	0.141	8.23E-01	1005.45
6.90	0.406	6.89	0.26	0.113	0.240	0.080	0.083	9.32E-01	1004.29
9.10	0.535	4.24	0.16	0.070	0.186	0.051	0.053	5.49E-01	1002.64
12.20	0.718	2.014	0.08	0.033	0.126	0.026	0.027	3.67E-01	1001.25
13.70	0.806	1.06	0.04	0.017	0.099	0.017	0.018	9.35E-02	1000.66
15.20	0.894	0.53	0.02	0.009	0.070	0.009	0.010	4.68E-02	1000.33
16.20	0.953	0.2915	0.01	0.005	0.046	0.004	0.004	1.71E-02	1000.18

$$\text{Depth aver. } \bar{c}_s^m = 7.89 \text{ [kg/m}^3\text{]}$$

$$\text{Depth aver. } \bar{\rho}_m = 1004.91 \text{ [kg/m}^3\text{]}$$



$$\begin{aligned}
 h &= 0.170 & [\text{m}] \\
 S (\text{Bed slope}) &= 2.00E-03 & [-] \\
 u_* &= 0.041 & [\text{m/s}] \\
 \kappa &= 0.4 & [-] \\
 U &= 1.058 & [\text{m/s}] \\
 Fr &= 0.82 & [-] \\
 a (\text{refer.}) &= 0.0060 & [\text{m}] \\
 \bar{c}_{s0} &= 60.95 & [\text{kg/m}^3] \\
 \bar{c}_{s0} = \bar{c}_s^m / \rho_m &= 0.023 & [\text{m}^3/\text{m}^3] \\
 \rho_m &= 2650 & [\text{kg/m}^3] \\
 v_u &= 0.008 & [\text{m/s}] \\
 z = v_u / (\kappa u_*) &= 0.488 & [-]
 \end{aligned}$$

Best fitting on  $\beta$  (Rouse equation)

$$\beta = 0.5658$$

$$Ri = 37.29 [-]$$

$$Ri [-] = \frac{gh[\rho_m(y=a) - \rho_m(y=h)]}{\bar{\rho}_m \cdot u_*^2}$$

Remarks: Group b (Data defined by the author as "near-capacity flow")  
 Laboratory channel, aspect ratio=  $B/h = 2.11$   
 Small reference concentration  $\bar{c}_{s0} = 60.95 \text{ [kg/m}^3\text{]} = 0.023 \text{ [m}^3/\text{m}^3\text{]} < 0.05 \text{ [m}^3/\text{m}^3\text{]} \Rightarrow \text{Rouse eq.}$   
 Concentration measured with a suction method  
 Bottom hydraulically smooth  
 Velocity profiles available. No measurements on turbulence intensity and diffusion coefficients

Coleman (1986): Sediment concentration distribution

Run 31

Sand particles

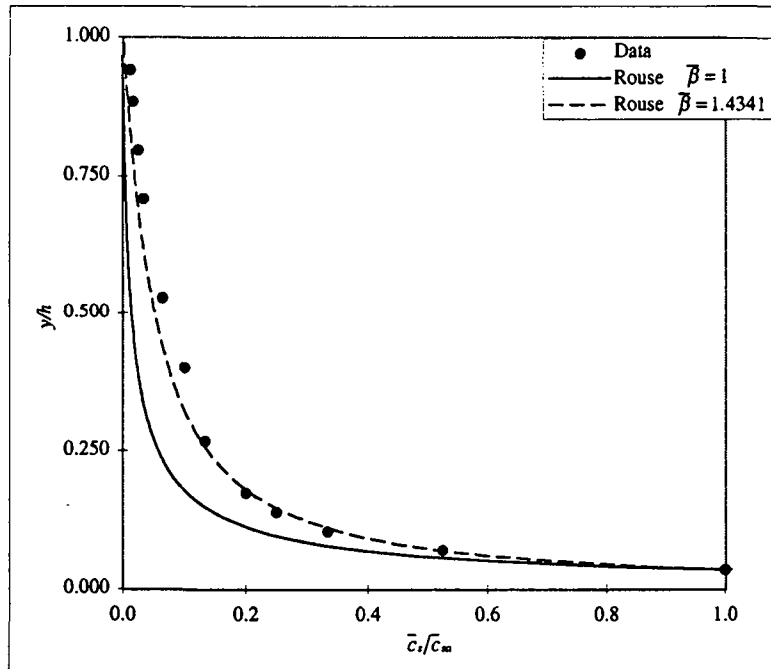
$d = 0.210$  [mm]

Group b

y [cm]	$y/h$ [-]	$\bar{c}_s^*$ [kg/m³]	$\bar{c}_s$ (volum) [%]	$\bar{c}_s/\bar{c}_{s0}$ [-]	Calculated				
					Rouse eq. $\beta = 1$	Rouse eq. $\beta \neq 1$	Hunt eq. $\beta \neq 1$	$\bar{c}_s^* \cdot y/h$ [kg/m³]	$\rho_m$ [kg/m³]
0.60	0.035	31.80	1.20	1.000	1.000	1.000	1.000	1.11E+00	1019.80
1.20	0.070	16.70	0.63	0.525	0.393	0.521	0.523	5.82E-01	1010.40
1.80	0.105	10.60	0.40	0.333	0.222	0.351	0.353	3.70E-01	1006.60
2.40	0.140	7.95	0.30	0.250	0.146	0.262	0.263	2.77E-01	1004.95
3.00	0.174	6.36	0.24	0.200	0.104	0.207	0.208	2.22E-01	1003.96
4.60	0.267	4.24	0.16	0.133	0.052	0.127	0.128	3.94E-01	1002.64
6.90	0.401	3.18	0.12	0.100	0.024	0.074	0.074	4.25E-01	1001.98
9.10	0.529	2.04	0.08	0.064	0.012	0.046	0.047	2.61E-01	1001.27
12.20	0.709	1.09	0.04	0.034	0.005	0.023	0.023	1.96E-01	1000.68
13.70	0.797	0.80	0.03	0.025	0.002	0.015	0.015	6.93E-02	1000.50
15.20	0.884	0.53	0.02	0.017	0.001	0.008	0.009	4.62E-02	1000.33
16.20	0.942	0.40	0.02	0.013	0.000	0.004	0.004	2.31E-02	1000.25

$$\text{Depth aver. } \bar{c}_s^* = 3.98 \text{ [kg/m}^3\text{]}$$

$$\text{Depth aver. } \bar{\rho}_m = 1002.48 \text{ [kg/m}^3\text{]}$$



$$\begin{aligned}
 h &= 0.172 \text{ [m]} \\
 S (\text{Bed slope}) &\approx 2.00E-03 \text{ [-]} \\
 u_* &= 0.041 \text{ [m/s]} \\
 \kappa &= 0.4 \text{ [-]} \\
 U &= 1.045 \text{ [m/s]} \\
 Fr &= 0.80 \text{ [-]} \\
 a (\text{refer.}) &= 0.0060 \text{ [m]} \\
 \bar{c}_{s0} &= 31.80 \text{ [kg/m}^3\text{]} \\
 \bar{c}_{s0} = \bar{c}_s^*/\rho_m &= 0.012 \text{ [m}^3/\text{m}^3\text{]} \\
 \rho_s &= 2650 \text{ [kg/m}^3\text{]} \\
 v_B &= 0.021 \text{ [m/s]} \\
 z = v_B/(\kappa u) &= 1.280 \text{ [-]}
 \end{aligned}$$

Best fitting on  $\beta$  (Rouse equation)

$$\bar{\beta} = 1.4341$$

$$\begin{aligned}
 Ri &= 19.58 \text{ [-]} \\
 Ri [-] &= \frac{gh[\rho_m(y=a) - \rho_m(y=h)]}{\bar{\rho}_m \cdot u_*^2}
 \end{aligned}$$

Remarks: Group b (Data defined by the author as "near-capacity flow")  
Laboratory channel, aspect ratio =  $B/h = 2.11$   
Very small reference concentration  $\bar{c}_{s0} = 31.80 \text{ [kg/m}^3\text{]} = 0.012 \text{ [m}^3/\text{m}^3\text{]} < 0.05 \text{ [m}^3/\text{m}^3\text{]} \Rightarrow \text{Rouse eq.}$   
Concentration measured with a suction method  
Bottom hydraulically smooth  
Velocity profiles available. No measurements on turbulence intensity and diffusion coefficients

Coleman (1986):

Sediment concentration distribution

Run 40

Sand particles

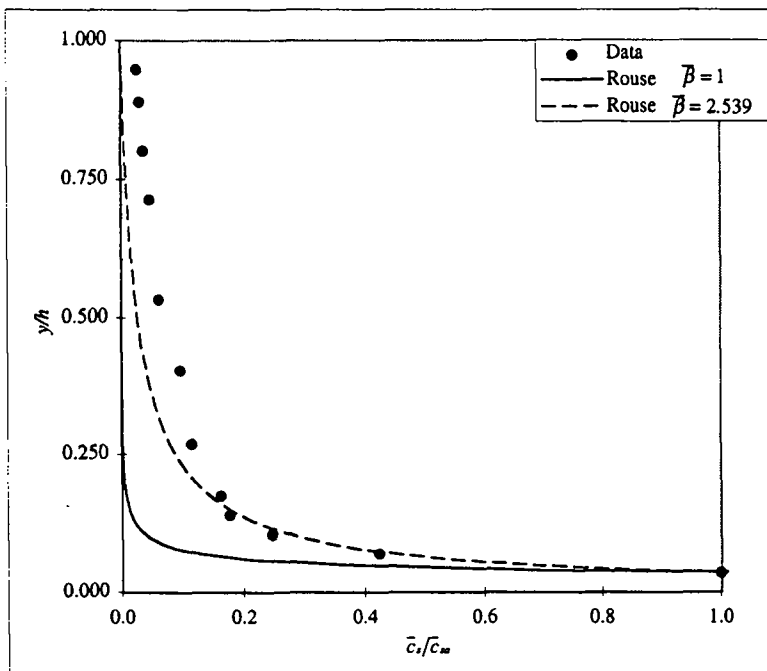
d = 0.420 [mm]

Group b

y [cm]	y/h [-]	$\bar{c}_s^m$ [kg/m³]	$\bar{c}_s$ (volum) [%]	$\bar{c}_s/\bar{c}_{sa}$ [-]	Calculated				
					Rouse eq. $\beta = 1$ $\bar{c}_s/\bar{c}_{sa}$ [-]	Rouse eq. $\beta \neq 1$ $\bar{c}_s/\bar{c}_{sa}$ [-]	Hunt eq. $\beta \neq 1$ $\bar{c}_s/\bar{c}_{sa}$ [-]	$\bar{c}_s^m \cdot y/h$ [kg/m³]	$\rho_m$ [kg/m³]
0.60	0.035	6.89	0.26	1.000	1.000	1.000	1.000	2.42E-01	1004.29
1.20	0.070	2.92	0.11	0.423	0.132	0.450	0.450	1.02E-01	1001.82
1.80	0.105	1.70	0.06	0.246	0.038	0.277	0.277	5.95E-02	1001.06
2.40	0.140	1.22	0.05	0.177	0.015	0.193	0.194	4.28E-02	1000.76
3.00	0.175	1.11	0.04	0.162	0.007	0.145	0.145	3.91E-02	1000.69
4.60	0.269	0.80	0.03	0.115	0.002	0.079	0.080	7.44E-02	1000.50
6.90	0.404	0.66	0.03	0.096	0.000	0.041	0.041	8.91E-02	1000.41
9.10	0.532	0.42	0.02	0.062	0.000	0.023	0.023	5.45E-02	1000.26
12.20	0.713	0.32	0.01	0.046	0.000	0.010	0.010	5.76E-02	1000.20
13.70	0.801	0.26	0.01	0.037	0.000	0.006	0.006	2.25E-02	1000.16
15.20	0.889	0.21	0.01	0.031	0.000	0.003	0.003	1.86E-02	1000.13
16.20	0.947	0.18	0.01	0.027	0.000	0.001	0.001	1.07E-02	1000.11

$$\text{Depth aver. } \bar{C}_s^m = 0.81 \text{ [kg/m}^3\text{]}$$

$$\text{Depth aver. } \bar{\rho}_m = 1000.51 \text{ [kg/m}^3\text{]}$$



$$\begin{aligned}
 h &= 0.171 \text{ [m]} \\
 S (\text{Bed slope}) &= 2.20E-03 \text{ [-]} \\
 u_* &= 0.045 \text{ [m/s]} \\
 \kappa &= 0.4 \text{ [-]} \\
 U &= 1.051 \text{ [m/s]} \\
 Fr &= 0.81 \text{ [-]} \\
 a (\text{refer.}) &= 0.0060 \text{ [m]} \\
 \bar{C}_{sa} &= 6.89 \text{ [kg/m}^3\text{]} \\
 \bar{c}_{sa} &= \bar{C}_{sa}/\rho_m = 0.003 \text{ [m}^3/\text{m}^3\text{]} \\
 \rho_m &= 2650 \text{ [kg/m}^3\text{]} \\
 v_u &= 0.050 \text{ [m/s]} \\
 z &= v_u/(\alpha c) = 2.778 \text{ [-]}
 \end{aligned}$$

Best fitting on  $\beta$  (Rouse equation)

$$\bar{\beta} = 2.539$$

$$Ri = 3.46 \text{ [-]}$$

$$Ri [-] = \frac{gh[\rho_m(y=a) - \rho_m(y=h)]}{\bar{\rho}_m \cdot u_*^2}$$

Remarks: Group b (Data defined by the author as "near-capacity flow")  
Laboratory channel, aspect ratio =  $B/h = 2.11$   
Very small reference concentration  $\bar{c}_{sa} = 6.89 \text{ [kg/m}^3\text{]} = 0.003 \text{ [m}^3/\text{m}^3\text{]}$   $< 0.05 \text{ [m}^3/\text{m}^3\text{]}$  => Rouse eq.  
Concentration measured with a suction method  
Bottom hydraulically smooth  
Velocity profiles available. No measurements on turbulence intensity and diffusion coefficients

Lyn (1988):

Sediment concentration distribution

Run 1565EQ

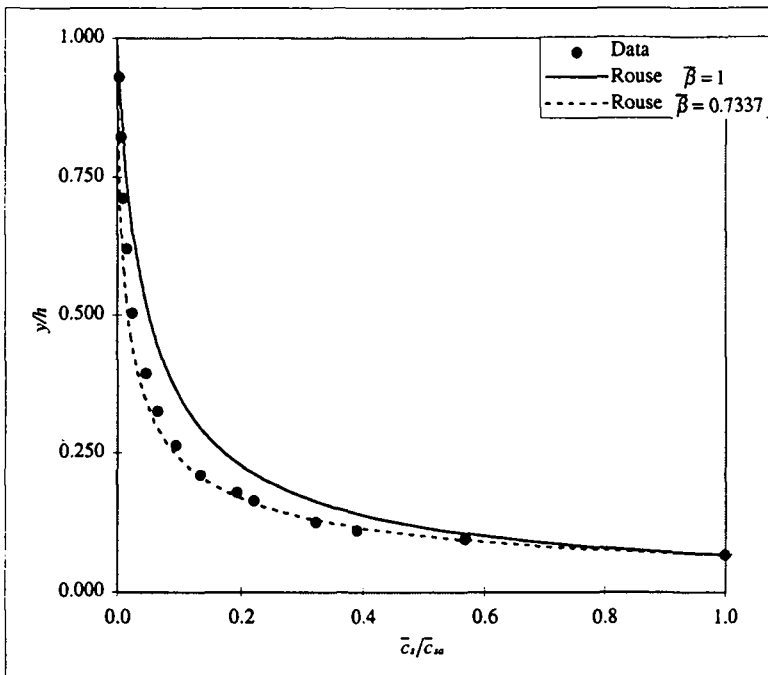
Sand particles

d = 0.150 [mm]

Group a-1

y [cm]	y/h [-]	$\bar{c}_s^m$ [kg/m³]	$\bar{c}_s$ (volum) [%]	$\bar{c}_s/\bar{c}_{sa}$ [-]	Calculated				
					Rouse eq. $\beta = 1$ $\bar{c}_s/\bar{c}_{sa}$ [-]	Rouse eq. $\beta \neq 1$ $\bar{c}_s/\bar{c}_{sa}$ [-]	Hunt eq. $\beta \neq 1$ $\bar{c}_s/\bar{c}_{sa}$ [-]	$\bar{c}_s^m \cdot y/h$ [kg/m³]	$\rho_m$ [kg/m³]
0.00	0.065	10.00	0.38	1.000	1.000	1.000	1.000	6.50E-01	1006.23
0.01	0.093	5.69	0.21	0.569	0.648	0.553	0.555	1.59E-01	1003.54
0.01	0.109	3.90	0.15	0.390	0.532	0.423	0.424	6.23E-02	1002.43
0.01	0.124	3.21	0.12	0.321	0.452	0.339	0.340	4.82E-02	1002.00
0.01	0.162	2.20	0.08	0.220	0.319	0.211	0.212	8.36E-02	1001.37
0.01	0.178	1.93	0.07	0.193	0.281	0.177	0.178	3.09E-02	1001.20
0.01	0.209	1.36	0.05	0.136	0.225	0.131	0.131	4.20E-02	1000.84
0.02	0.264	0.94	0.04	0.094	0.160	0.082	0.083	5.15E-02	1000.58
0.02	0.326	0.641	0.02	0.064	0.114	0.052	0.052	3.97E-02	1000.40
0.03	0.395	0.458	0.02	0.046	0.082	0.033	0.033	3.16E-02	1000.29
0.03	0.504	0.245	0.01	0.025	0.050	0.017	0.017	2.67E-02	1000.15
0.04	0.620	0.144	0.01	0.014	0.029	0.008	0.008	1.67E-02	1000.09
0.05	0.713	0.091	0.00	0.009	0.018	0.004	0.004	8.46E-03	1000.06
0.05	0.822	0.053	0.00	0.005	0.009	0.002	0.002	5.78E-03	1000.03
0.06	0.930	0.0315	0.00	0.003	0.003	0.000	0.000	3.40E-03	1000.02

$$\begin{aligned} \text{Depth aver. } \bar{c}_s^m &= 1.26 \text{ [kg/m}^3\text{]} \\ \text{Depth aver. } \bar{\rho}_m &= 1000.78 \text{ [kg/m}^3\text{]} \end{aligned}$$



$$\begin{aligned} h &= 0.0645 \text{ [m]} \\ S (\text{Bed slope}) &\approx 2.44E-03 \text{ [-]} \\ u_* &= 0.0358 \text{ [m/s]} \\ \kappa &= 0.4 \text{ [-]} \\ U &= 0.628 \text{ [m/s]} \\ Fr &= 0.79 \text{ [-]} \\ a (\text{refer.}) &= 0.0041925 \text{ [m]} \\ \bar{c}_m &= \bar{c}_s^m / \bar{\rho}_m = 10.00 \text{ [kg/m}^3\text{]} \\ \bar{c}_s &= \bar{c}_m / \rho_m = 0.004 \text{ [m}^3/\text{m}^3\text{]} \\ \rho_s &= 2650 \text{ [kg/m}^3\text{]} \\ v_u &= 0.016 \text{ [m/s]} \\ z &= v_u / (\kappa U) = 1.117 \text{ [-]} \end{aligned}$$

Best fitting on  $\beta$  (Rouse equation)

$$\beta = 0.7337$$

$$\begin{aligned} Ri &= 3.06 \text{ [-]} \\ Ri [-] &= \frac{gh[\rho_m(y=a) - \rho_m(y=h)]}{\bar{\rho}_m \cdot u_*^2} \end{aligned}$$

Remarks: Group a-1 (Data made available by Lyn (1997) confirming capacity condition)  
Laboratory channel, aspect ratio=  $B/h = 4$   
Small reference concentration  $\bar{c}_s^m = 10.000 \text{ [kg/m}^3\text{]} = 0.004 \text{ [m}^3/\text{m}^3\text{]}$   $< 0.05 \text{ [m}^3/\text{m}^3\text{]}$  => Rouse eq.  
Bed covered by a layer of fine sand, estimated to be of diameter, 0.15 [mm] or less  
Concentration measured by suction  
The origin of y is the top of the sediment bed found after the cessation of flow  
Subcritical flow  
Velocity and turbulence intensity profiles available. No measurements on diffusion coefficients

Lyn (1988):

Sediment concentration distribution

Run 1965EQ

Sand particles

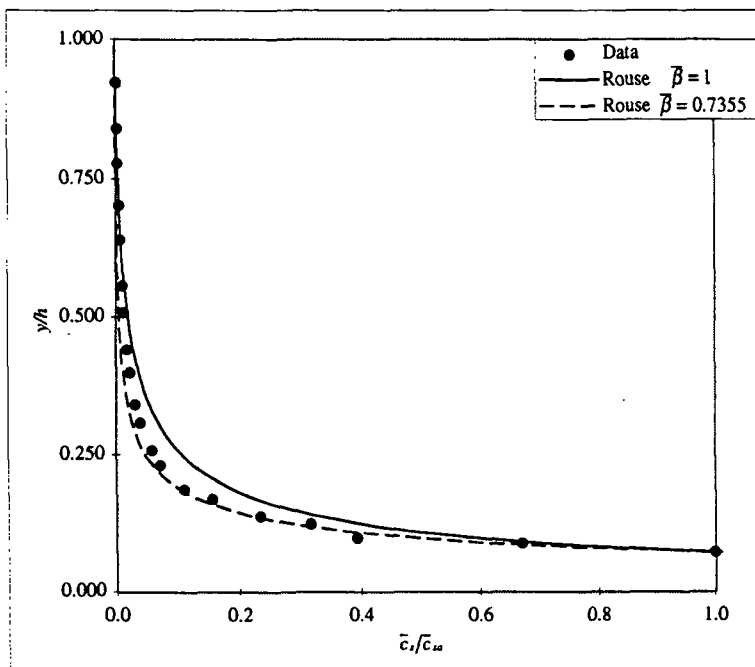
$d = 0.190$  [mm]

Group a-1

y [cm]	y/h [-]	$\bar{c}_s''$ [kg/m³]	$\bar{c}_s$ (volum) [%]	Measured		Calculated		
				$\bar{c}_s/\bar{c}_{\infty}$	Rouse eq. $\beta = 1$ $\bar{c}_s/\bar{c}_{\infty}$	Rouse eq. $\beta \neq 1$ $\bar{c}_s/\bar{c}_{\infty}$	Hunt eq. $\beta \neq 1$ $\bar{c}_s/\bar{c}_{\infty}$	$\bar{c}_s'' \cdot y/h$ [kg/m³]
0.00	0.072	6.22	0.23	1.000	1.000	0.635	1.000	4.48E-01 1003.87
0.01	0.088	4.16	0.16	0.669	0.716	0.496	0.496	6.66E-02 1002.59
0.01	0.098	2.45	0.09	0.394	0.597	0.225	0.225	2.45E-02 1001.53
0.01	0.123	1.97	0.07	0.317	0.403	0.134	0.134	4.93E-02 1001.23
0.01	0.137	1.45	0.05	0.233	0.334	0.091	0.091	2.03E-02 1000.90
0.01	0.169	0.96	0.04	0.155	0.228	0.055	0.055	3.08E-02 1000.60
0.01	0.187	0.69	0.03	0.111	0.189	0.041	0.041	1.24E-02 1000.43
0.02	0.231	0.45	0.02	0.072	0.125	0.029	0.029	1.96E-02 1000.28
0.02	0.257	0.36	0.01	0.058	0.101	0.026	0.026	9.36E-03 1000.22
0.02	0.308	0.245	0.01	0.039	0.069	0.019	0.019	1.25E-02 1000.15
0.02	0.341	0.193	0.01	0.031	0.055	0.011	0.011	6.37E-03 1000.12
0.03	0.400	0.136	0.01	0.022	0.037	0.008	0.008	8.02E-03 1000.08
0.03	0.441	0.115	0.00	0.018	0.029	0.005	0.005	4.72E-03 1000.07
0.03	0.508	0.076	0.00	0.012	0.019	0.005	0.005	5.09E-03 1000.05
0.04	0.556	0.066	0.00	0.011	0.014	0.003	0.003	3.17E-03 1000.04
0.04	0.639	0.045	0.00	0.007	0.008	0.001	0.001	3.74E-03 1000.03
0.05	0.702	0.032	0.00	0.005	0.005	0.001	0.001	2.02E-03 1000.02
0.05	0.777	0.022	0.00	0.004	0.003	0.000	0.000	1.65E-03 1000.01
0.05	0.840	0.017	0.00	0.003	0.002	0.000	0.000	1.07E-03 1000.01
0.06	0.923	0.011	0.00	0.002	0.000	0.000	0.000	9.21E-04 1000.01

$$\text{Depth aver. } \bar{C}_s'' = 0.73 \text{ [kg/m}^3]$$

$$\text{Depth aver. } \bar{\rho}_m = 1000.45 \text{ [kg/m}^3]$$



$$\begin{aligned}
 h &= 0.0651 \text{ [m]} \\
 S(\text{Bed slope}) &= 2.51E-03 \text{ [-]} \\
 u_* &= 0.0375 \text{ [m/s]} \\
 \kappa &= 0.4 \text{ [-]} \\
 U &= 0.636 \text{ [m/s]} \\
 Fr &= 0.80 \text{ [-]} \\
 a(\text{refer.}) &= 0.0046872 \text{ [m]} \\
 \bar{c}_{\infty}'' &= 6.22 \text{ [kg/m}^3] \\
 \bar{c}_s = \bar{c}_{\infty}'' / \bar{\rho}_m &= 0.002 \text{ [m}^3/\text{m}^3] \\
 \rho_m &= 2650 \text{ [kg/m}^3] \\
 v_u &= 0.023 \text{ [m/s]} \\
 z = v_{u,0} / (\alpha u_*) &= 1.533 \text{ [-]}
 \end{aligned}$$

Best fitting on  $\beta$  (Rouse equation)

$$\beta = 0.7355$$

$$\begin{aligned}
 Ri &= 1.75 \text{ [-]} \\
 Ri [-] &= \frac{gh[\rho_m(y=a) - \rho_m(y=h)]}{\bar{\rho}_m \cdot u_*^2}
 \end{aligned}$$

Remarks: Group a-1 (Data made available by Lyn (1997) confirming capacity condition)  
Laboratory channel, aspect ratio=  $B/h = 4$   
Small reference concentration  $\bar{c}_{\infty}'' = 6.22 \text{ [kg/m}^3] = 0.002 \text{ [m}^3/\text{m}^3] < 0.05 \text{ [m}^3/\text{m}^3]$  =>Rouse eq.  
Bed covered by a layer of fine sand, estimated to be of diameter, 0.15 [mm] or less  
Concentration measured by suction  
The origin of y is the top of the sediment bed found after the cessation of flow  
Subcritical flow  
Velocity and turbulence intensity profiles available. No measurements on diffusion coefficients

Lyn (1988):

## Sediment concentration distribution

Run 2565EQ

Sand particles

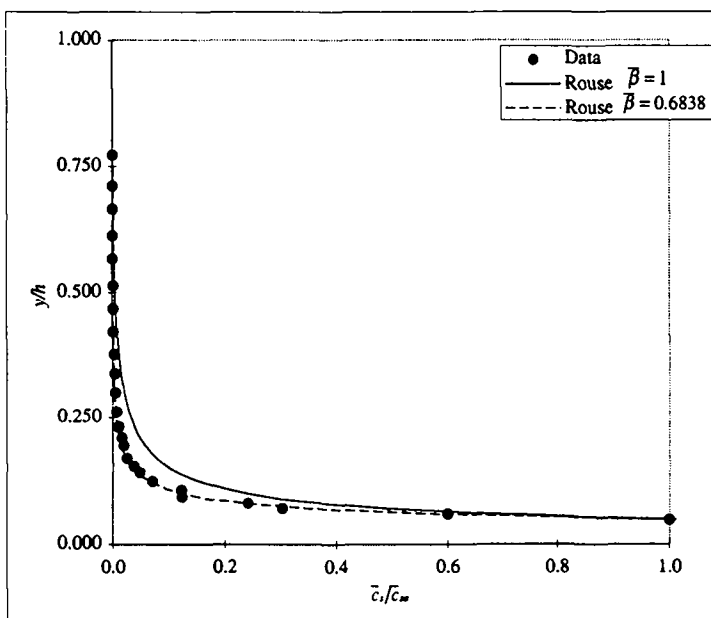
d= 0.240 [mm]

Group a-1

y [cm]	y/h [-]	$\bar{c}_s^*$ [kg/m³]	$\bar{c}_s$ (volum) [%]	Measured		Calculated			$\bar{c}_s \cdot y/h$ [kg/m³]	$\rho_m$ [kg/m³]
				$\bar{c}_s/\bar{c}_{\infty}$ [-]	Rouse eq. $\beta = 1$	$\bar{c}_s/\bar{c}_{\infty}$ [-]	Rouse eq. $\beta \neq 1$	Hunt eq. $\beta \neq 1$		
0.00	0.049	14.30	0.54	1.000	1.000	1.000	1.000	1.000	6.98E-01	1008.90
0.00	0.060	8.57	0.32	0.599	0.682	0.572	0.574	0.574	9.17E-02	1005.34
0.00	0.072	4.34	0.16	0.303	0.474	0.336	0.338	0.338	5.29E-02	1002.70
0.01	0.082	3.46	0.13	0.242	0.361	0.225	0.227	0.227	3.67E-02	1002.15
0.01	0.095	1.79	0.07	0.125	0.274	0.150	0.152	0.152	2.18E-02	1001.11
0.01	0.107	1.76	0.07	0.123	0.213	0.104	0.105	0.105	2.20E-02	1001.10
0.01	0.125	1.01	0.04	0.071	0.155	0.065	0.066	0.066	1.82E-02	1000.63
0.01	0.143	0.68	0.03	0.048	0.116	0.043	0.043	0.043	1.22E-02	1000.42
0.01	0.156	0.524	0.02	0.037	0.097	0.033	0.033	0.033	6.81E-03	1000.33
0.01	0.171	0.368	0.01	0.026	0.079	0.024	0.025	0.025	5.52E-03	1000.23
0.01	0.197	0.27	0.01	0.019	0.058	0.015	0.016	0.016	7.02E-03	1000.17
0.01	0.212	0.229	0.01	0.016	0.049	0.012	0.012	0.012	3.44E-03	1000.14
0.02	0.232	0.151	0.01	0.011	0.039	0.009	0.009	0.009	3.02E-03	1000.09
0.02	0.262	0.0933	0.00	0.007	0.029	0.006	0.006	0.006	2.80E-03	1000.06
0.02	0.300	0.059	0.00	0.004	0.021	0.003	0.004	0.004	2.24E-03	1000.04
0.02	0.338	0.05	0.00	0.003	0.015	0.002	0.002	0.002	1.90E-03	1000.03
0.02	0.377	0.03	0.00	0.002	0.011	0.001	0.001	0.001	1.17E-03	1000.02
0.03	0.422	0.02	0.00	0.001	0.008	0.001	0.001	0.001	9.00E-04	1000.01
0.03	0.468	0.0145	0.00	0.001	0.006	0.001	0.001	0.001	6.67E-04	1000.01
0.03	0.514	0.0088	0.00	0.001	0.004	0.000	0.000	0.000	4.05E-04	1000.01
0.04	0.567	0.0051	0.00	0.000	0.003	0.000	0.000	0.000	2.70E-04	1000.00
0.04	0.613	0.0048	0.00	0.000	0.002	0.000	0.000	0.000	2.21E-04	1000.00
0.04	0.666	0.00245	0.00	0.000	0.001	0.000	0.000	0.000	1.30E-04	1000.00
0.05	0.712	0.0017	0.00	0.000	0.001	0.000	0.000	0.000	7.82E-05	1000.00
0.05	0.773	0.0011	0.00	0.000	0.000	0.000	0.000	0.000	6.71E-05	1000.00

$$\text{Depth aver. } \bar{c}_s^* = 0.99 \text{ [kg/m}^3\text{]}$$

$$\text{Depth aver. } \bar{\rho}_m = 1000.62 \text{ [kg/m}^3\text{]}$$



$$h = 0.0654 \text{ [m]}$$

$$S(\text{Bed slope}) = 2.96E-03 \text{ [-]}$$

$$u_* = 0.0425 \text{ [m/s]}$$

$$\kappa = 0.4 \text{ [-]}$$

$$U = 0.692 \text{ [m/s]}$$

$$Fr = 0.86 \text{ [-]}$$

$$a(\text{refer.}) = 0.0031915 \text{ [m]}$$

$$\bar{c}_{\infty} = \bar{c}_s / \rho_m = 0.005 \text{ [m}^3\text{/m}^3\text{]}$$

$$\rho_s = 2650 \text{ [kg/m}^3\text{]}$$

$$v_s = 0.031 \text{ [m/s]}$$

$$z = v_s / (\kappa u_*) = 1.824 \text{ [-]}$$

Best fitting on  $\beta$  (Rouse equation)

$$\beta = 0.6838$$

$$Ri = 3.16 \text{ [-]}$$

$$Ri [-] = \frac{gh[\rho_m(y=a) - \rho_m(y=h)]}{\bar{\rho}_m \cdot u_*^2}$$

Remarks: Group a-1 (Data made available by Lyn (1997) confirming capacity condition)  
 Laboratory channel, aspect ratio=  $B/h = 4$   
 Small reference concentration  $\bar{c}_{\infty} = 14.30 \text{ [kg/m}^3\text{]} = 0.005 \text{ [m}^3\text{/m}^3\text{]}$   $< 0.05 \text{ [m}^3\text{/m}^3\text{]}$  => Rouse eq.  
 Bed covered by a layer of fine sand, estimated to be of diameter, 0.15 [mm] or less  
 Concentration measured by suction  
 The origin of y is the top of the sediment bed found after the cessation of flow  
 Subcritical flow  
 Velocity and turbulence intensity profiles available. No measurements on diffusion coefficients

Wang and Qian (1989): Sediment concentration distribution

Run SQ3

Sand particles

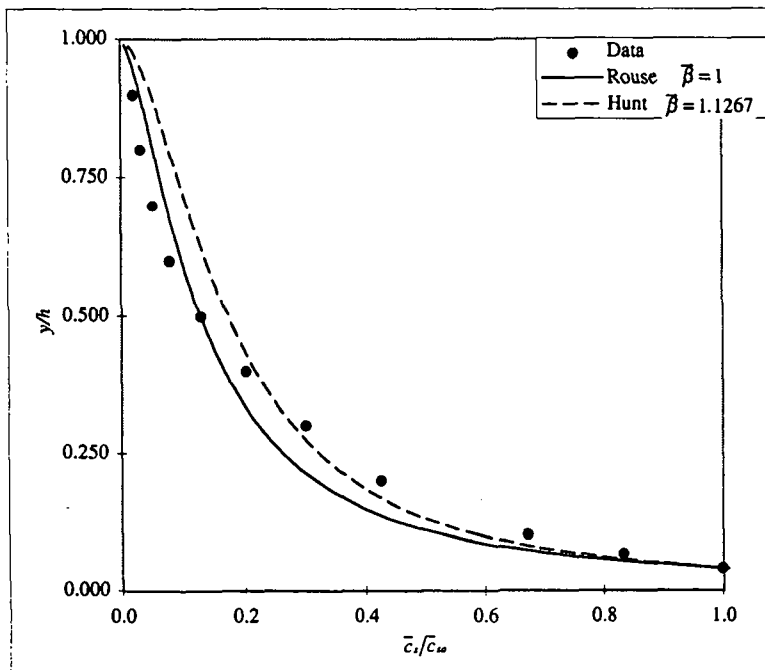
$d = 0.137$  [mm]

Group b

$y$ [cm]	$y/h$ [-]	$\bar{c}_s^*$ [kg/m³]	$\bar{c}_s$ (volum) [%]	Measured		Calculated			
				$\bar{c}_s/\bar{c}_{s0}$ [-]	Rouse eq. $\beta = 1$ $\bar{c}_s/\bar{c}_{s0}$ [-]	Rouse eq. $\beta \neq 1$ $\bar{c}_s/\bar{c}_{s0}$ [-]	Hunt eq. $\beta \neq 1$ $\bar{c}_s/\bar{c}_{s0}$ [-]	$\bar{c}_s^* \cdot y/h$ [kg/m³]	$\rho_m$ [kg/m³]
0.32	0.040	219.65	8.32	1.000	1.000	1.000	1.000	8.79E+00	1136.45
0.52	0.065	182.95	6.93	0.833	0.720	0.747	0.762	4.57E+00	1113.65
0.80	0.100	147.58	5.59	0.672	0.533	0.572	0.591	5.17E+00	1091.68
1.60	0.200	93.72	3.55	0.427	0.317	0.361	0.379	9.37E+00	1058.22
2.40	0.300	66.00	2.50	0.300	0.224	0.265	0.281	6.60E+00	1041.00
3.20	0.400	44.62	1.69	0.203	0.169	0.206	0.219	4.46E+00	1027.72
4.00	0.500	28.51	1.08	0.130	0.130	0.164	0.175	2.85E+00	1017.71
4.80	0.600	17.69	0.67	0.081	0.101	0.130	0.139	1.77E+00	1010.99
5.60	0.700	11.62	0.44	0.053	0.076	0.101	0.108	1.16E+00	1007.22
6.40	0.800	7.13	0.27	0.032	0.054	0.074	0.080	7.13E-01	1004.43
7.20	0.900	4.49	0.17	0.020	0.032	0.047	0.051	4.49E-01	1002.79

$$\text{Depth aver. } \bar{c}_s^* = 45.90 \text{ [kg/m}^3\text{]}$$

$$\text{Depth aver. } \bar{\rho}_m = 1028.51 \text{ [kg/m}^3\text{]}$$



$$\begin{aligned}
 h &= 0.080 & [\text{m}] \\
 S(\text{Bed slope}) &= 1.00E-02 & [-] \\
 u_* &= 0.074 & [\text{m/s}] \\
 \kappa &= 0.4 & [-] \\
 U &= 1.88 & [\text{m/s}] \\
 Fr &= 2.12 & [-] \\
 a(\text{refer.}) &= 0.0032 & [\text{m}] \\
 \bar{c}_s^* &= 219.65 & [\text{kg/m}^3] \\
 \bar{c}_{s0} &= \bar{c}_s^*/\rho_s = 0.083 & [\text{m}^3/\text{m}^3] \\
 \rho_s &= 2640 & [\text{kg/m}^3] \\
 v_s &= 0.019 & [\text{m/s}] \\
 z &= v_s/(u_*\kappa) = 0.641 & [-]
 \end{aligned}$$

Best fitting on  $\beta$  (Hunt equation)

$$\beta = 1.1267$$

$$Ri = 18.78 [-]$$

$$Ri [-] = \frac{gh[\rho_m(y=a) - \rho_m(y=h)]}{\bar{\rho}_m u_*^2}$$

Remarks: Group b (Data interpreted as near-capacity flow)  
 Laboratory channel, aspect ratio =  $B/h = 3.75$   
 High reference concentration  $\bar{c}_{s0} = 219.65 \text{ [kg/m}^3\text{]} = 0.083 \text{ [m}^3/\text{m}^3\text{]} > 0.05 \text{ [m}^3/\text{m}^3\text{]} \Rightarrow \text{Hunt eq.}$   
 Concentration measured with a suction method  
 Bottom hydraulically smooth  
 Supercritical flow  
 Velocity profiles available  
 The measured turbulence intensity profiles show a turbulence reduction due to the suspended particles

Run 112

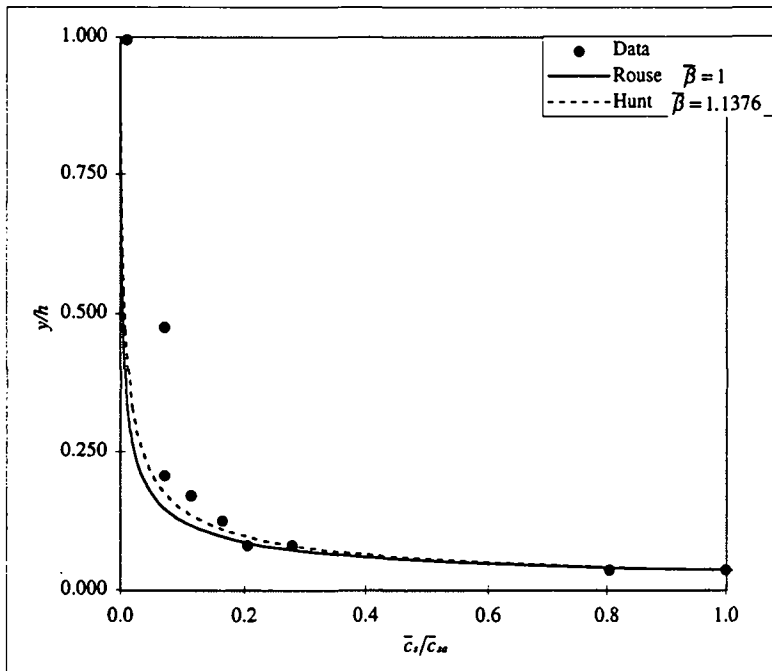
Acrylic particles

d= 0.600 [mm]

Group a-1

y [cm]	y/h [--]	$\bar{c}_s^m$ [kg/m³]	$\bar{c}_s$ (volum) [%]	$\bar{c}_s/\bar{c}_{sa}$ [--]	Calculated				
					Rouse eq. $\beta = 1$ $\bar{c}_s/\bar{c}_{sa}$ [--]	Rouse eq. $\beta \neq 1$ $\bar{c}_s/\bar{c}_{sa}$ [--]	Hunt eq. $\beta \neq 1$ $\bar{c}_s/\bar{c}_{sa}$ [--]	$\bar{c}_s^m \cdot y/h$ [kg/m³]	$\rho_m$ [kg/m³]
0.40	0.036	109.61	9.70	1.000	1.000	1.000	1.000	3.93E+00	1012.61
0.40	0.036	88.14	7.80	0.804	1.000	1.000	1.000	0.00E+00	1010.14
0.90	0.081	22.60	2.00	0.206	0.229	0.273	0.292	1.01E+00	1002.60
0.90	0.081	30.51	2.70	0.278	0.229	0.273	0.292	0.00E+00	1003.51
1.40	0.126	18.08	1.60	0.165	0.098	0.130	0.141	8.11E-01	1002.08
1.90	0.170	12.43	1.10	0.113	0.053	0.076	0.082	5.57E-01	1001.43
2.30	0.206	7.91	0.70	0.072	0.035	0.053	0.058	2.84E-01	1000.91
5.30	0.475	7.91	0.70	0.072	0.004	0.008	0.009	2.13E+00	1000.91
11.10	0.996	1.13	0.10	0.010	0.000	0.000	0.000	5.88E-01	1000.13

$$\begin{aligned} \text{Depth aver. } \bar{c}_s^m &= 9.31 \text{ [kg/m}^3\text{]} \\ \text{Depth aver. } \rho_m &= 1001.07 \text{ [kg/m}^3\text{]} \end{aligned}$$



$$\begin{aligned} h &= 0.1115 \text{ [m]} \\ S(\text{Bed slope}) &= 1.45E-03 \text{ [--]} \\ u_* &= 0.0291 \text{ [m/s]} \\ \kappa &= 0.4 \text{ [--]} \\ U &= 0.402 \text{ [m/s]} \\ Fr &= 0.38 \text{ [--]} \\ a(\text{refer.}) &= 0.004 \text{ [m]} \\ \bar{c}_{sa} &= 109.61 \text{ [kg/m}^3\text{]} \\ \bar{c}_s &= \bar{c}_{sa}/\rho_s = 0.097 \text{ [m}^3/\text{m}^3\text{]} \\ \rho_s &= 1130 \text{ [kg/m}^3\text{]} \\ v_u &= 0.02 \text{ [m/s]} \\ z &= v_u/(\kappa u) = 1.718 \text{ [--]} \end{aligned}$$

Best fitting on  $\beta$  (Hunt equation)

$$\beta = 1.1376$$

$$Ri = 16.10 \text{ [--]}$$

$$Ri [-] = \frac{gh[\rho_m(y=a) - \rho_m(y=h)]}{\bar{\rho}_m \cdot u_*^2}$$

Remarks: Group a-1 (Data interpreted as capacity flow and considered with reservation)  
 Laboratory channel, aspect ratio= $B/h = 3$        $\bar{c}_s^m = 109.61 \text{ [kg/m}^3\text{]} = 0.097 \text{ [m}^3/\text{m}^3\text{]}$        $> 0.05 \text{ [m}^3/\text{m}^3\text{]} \Rightarrow$  Hunt eq.  
 High reference concentration  
 Concentration measured with a Delft-Hydraulics conductivity-type concentration meter (CCM)  
 The run has been performed with a flat lid on the surface to avoid surface instability  
 Definition of the y-axis not too clear  
 Velocity profiles available. No measurements on turbulence intensity and diffusion coefficients  
 Subcritical flow

Sumer et al. (1996)

Sediment concentration distribution

Run 120

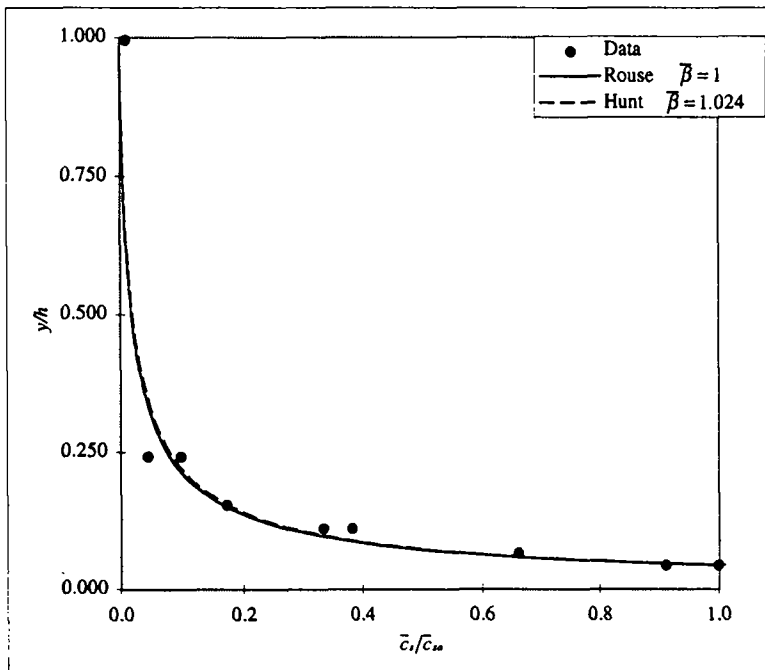
Acrylic particles

d= 0.600 [mm]

Group a-1

y [cm]	y/h [-]	$\bar{c}_s^*$ [kg/m³]	$\bar{c}_s$ (volum) [%]	$\bar{c}_s/\bar{c}_{s0}$ [-]	Calculated				
					Rouse eq. $\beta = 1$	Rouse eq. $\beta \neq 1$	Hunt eq. $\beta \neq 1$	$\bar{c}_s \cdot y/h$ [kg/m³]	$\rho_m$ [kg/m³]
0.49	0.043	230.52	20.40	1.000	1.000	1.000	1.000	9.95E+00	1026.52
0.49	0.043	210.18	18.60	0.912	1.000	1.000	1.000	0.00E+00	1024.18
0.74	0.065	152.55	13.50	0.662	0.570	0.577	0.631	3.36E+00	1017.55
1.24	0.109	88.14	7.80	0.382	0.275	0.283	0.331	3.88E+00	1010.14
1.24	0.109	76.84	6.80	0.333	0.275	0.283	0.331	0.00E+00	1008.84
1.74	0.153	39.55	3.50	0.172	0.166	0.173	0.208	1.74E+00	1004.55
2.74	0.241	22.60	2.00	0.098	0.080	0.085	0.104	1.99E+00	1002.60
2.74	0.241	10.17	0.90	0.044	0.080	0.085	0.104	0.00E+00	1001.17
11.30	0.996	2.26	0.20	0.010	0.000	0.000	0.000	1.70E+00	1000.26

Depth aver.	$\bar{c}_s^* = 22.63$ [kg/m³]
Depth aver.	$\bar{\rho}_m = 1002.60$ [kg/m³]



$h = 0.1135$ [m]
$S$ (Bed slope) $\approx 2.46E-03$ [-]
$u_* = 0.0387$ [m/s]
$\kappa = 0.4$ [-]
$U = 0.537$ [m/s]
$Fr = 0.51$ [-]
$a$ (refer.) $= 0.0049$ [m]
$\bar{c}_{s0}^* = 230.52$ [kg/m³]
$\bar{c}_{s0} = \bar{c}_{s0}^*/\rho_m = 0.204$ [m³/m³]
$\rho_s = 1130$ [kg/m³]
$v_u = 0.02$ [m/s]
$z = v_u/(\kappa u) = 1.292$ [-]

Best fitting on  $\beta$  (Hunt equation)

$$\beta = 1.024$$

$Ri = 19.47$ [-]
$Ri [-] = \frac{gh[\rho_m(y=a) - \rho_m(y=h)]}{\bar{\rho}_m \cdot u^2}$

Remarks: Group a-1 (Data interpreted as capacity flow and considered with reservation)  
Laboratory channel, aspect ratio=  $B/h = 3$        $\bar{c}_{s0}^* = 230.52$  [kg/m³]       $= 0.204$  [m³/m³]       $> 0.05$  [m³/m³]  $\Rightarrow$  Hunt eq.  
Very high reference concentration  
Concentration measured with a Delft-Hydraulics conductivity-type concentration meter (CCM)  
The run has been performed with a flat lid on the surface to avoid surface instability  
Definition of the y-axis not too clear  
Velocity profiles available. No measurements on turbulence intensity and diffusion coefficients  
Subcritical flow

Run 126

Acrylic particles

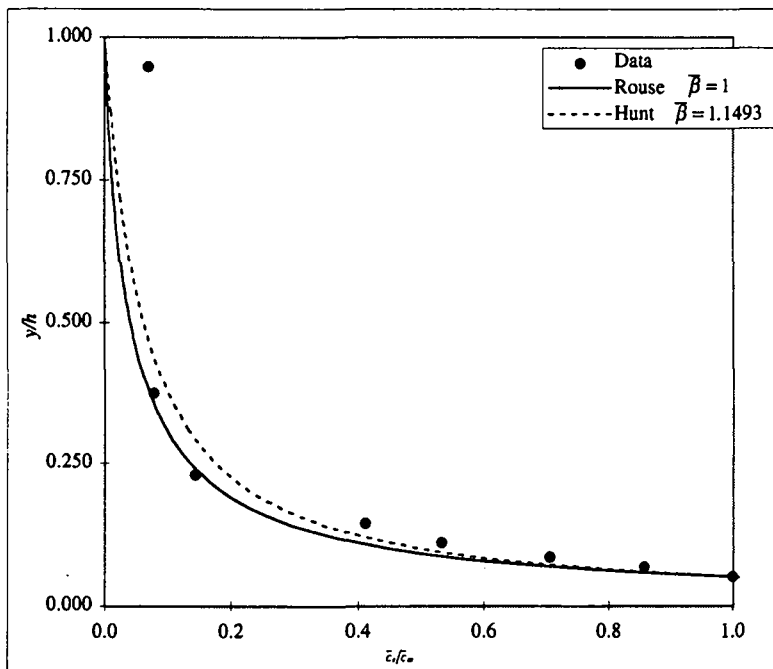
d= 0.600 [mm]

Group a-1

y [cm]	y/h [-]	$\bar{c}_s^*$ [kg/m³]	$\bar{c}_s$ (volum) [%]	$\bar{c}_s/\bar{c}_{ss}$ [-]	Calculated				
					Rouse eq. $\beta = 1$ $\bar{c}_s/\bar{c}_{ss}$ [-]	Rouse eq. $\beta \neq 1$ $\bar{c}_s/\bar{c}_{ss}$ [-]	Hunt eq. $\beta \neq 1$ $\bar{c}_s/\bar{c}_{ss}$ [-]	$\bar{c}_s^* \cdot y/h$ [kg/m³]	$\rho_m$ [kg/m³]
0.60	0.051	261.03	23.10	1.000	1.000	1.000	1.000	1.33E+01	1030.03
0.80	0.068	223.74	19.80	0.857	0.716	0.748	0.789	3.79E+00	1025.74
1.00	0.085	184.19	16.30	0.706	0.550	0.594	0.648	3.12E+00	1021.19
1.30	0.110	138.99	12.30	0.532	0.400	0.450	0.508	3.53E+00	1015.99
1.70	0.144	107.35	9.50	0.411	0.286	0.336	0.389	3.64E+00	1012.35
2.70	0.229	37.29	3.30	0.143	0.154	0.196	0.235	3.16E+00	1004.29
4.40	0.373	20.34	1.80	0.078	0.072	0.101	0.124	2.93E+00	1002.34
11.20	0.949	18.08	1.60	0.069	0.002	0.004	0.005	1.04E+01	1002.08

$$\text{Depth aver. } \bar{C}_s^* = 43.87 \text{ [kg/m}^3\text{]}$$

$$\text{Depth aver. } \bar{\rho}_m = 1005.05 \text{ [kg/m}^3\text{]}$$



$$\begin{aligned}
 h &= 0.118 \text{ [m]} \\
 S (\text{Bed slope}) &= 3.24E-03 \text{ [-]} \\
 u_* &= 0.0457 \text{ [m/s]} \\
 \kappa &= 0.4 \text{ [-]} \\
 U &= 0.636 \text{ [m/s]} \\
 Fr &= 0.59 \text{ [-]} \\
 a (\text{refer.}) &= 0.006 \text{ [m]} \\
 \bar{c}_s^* &= 261.03 \text{ [kg/m}^3\text{]} \\
 \bar{c}_{ss} &= \bar{c}_s^*/\rho_* = 0.231 \text{ [m}^3\text{/m}^3\text{]} \\
 \rho_* &= 1130 \text{ [kg/m}^3\text{]} \\
 v_u &= 0.02 \text{ [m/s]} \\
 z &= v_u/(\kappa U) = 1.094 \text{ [-]}
 \end{aligned}$$

Best fitting on  $\beta$  (Hunt equation)

$$\beta = 1.1493$$

$$Ri = 15.41 \text{ [-]}$$

$$Ri [-] = \frac{gh[\rho_m(y=a) - \rho_m(y=h)]}{\bar{\rho}_m \cdot u_*^2}$$

Remarks: Group a-1 (Data interpreted as capacity flow and considered with reservation)  
 Laboratory channel, aspect ratio=  $B/h = 3$        $\bar{c}_s^* = 261.03 \text{ [kg/m}^3\text{]} = 0.231 \text{ [m}^3\text{/m}^3\text{]} > 0.05 \text{ [m}^3\text{/m}^3\text{]} \Rightarrow \text{Hunt eq.}$   
 Very high reference concentration  
 Concentration measured with a Delft-Hydraulics conductivity-type concentration meter (CCM)  
 The run has been performed with a flat lid on the surface to avoid surface instability  
 Definition of the y-axis not too clear  
 Velocity profiles available. No measurements on turbulence intensity and diffusion coefficients  
 Subcritical flow

Sumer et al. (1996)

Sediment concentration distribution

Run 133

Acrylic particles

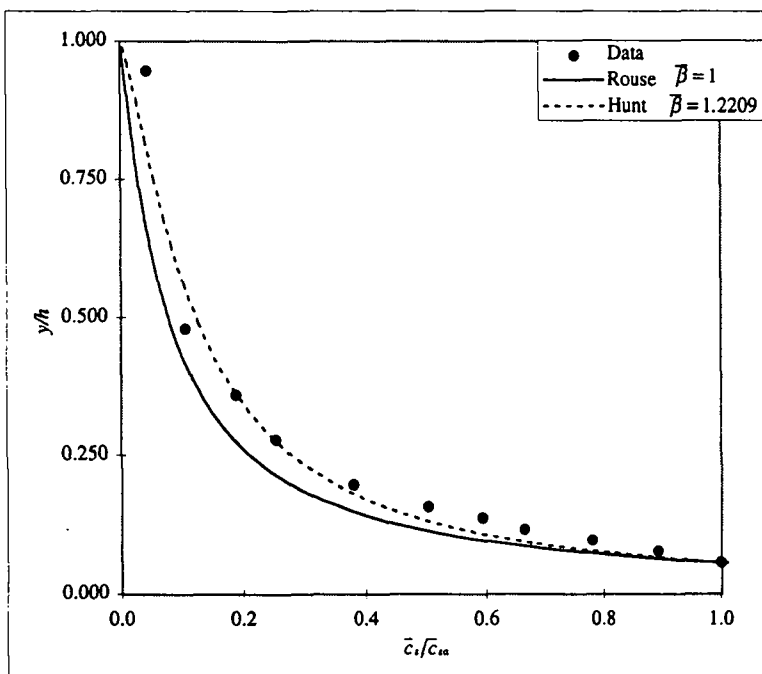
d = 0.600 [mm]

Group a-1

y [cm]	y/h [-]	$\bar{c}_s^m$ [kg/m³]	$\bar{c}_s$ (volum) [%]	$\bar{c}_s/\bar{c}_{sa}$ [-]	Calculated				$\rho_m$ [kg/m³]
					Rouse eq. $\beta=1$	Rouse eq. $\beta \neq 1$	Hunt eq. $\beta \neq 1$	$\bar{c}_s \cdot y/h$ [kg/m³]	
0.71	0.057	289.28	25.60	1.000	1.000	1.000	1.000	1.65E+01	1033.28
0.96	0.077	258.77	22.90	0.895	0.745	0.786	0.824	5.20E+00	1029.77
1.21	0.097	226.00	20.00	0.781	0.591	0.650	0.704	4.55E+00	1026.00
1.46	0.117	192.10	17.00	0.664	0.488	0.556	0.615	3.86E+00	1022.10
1.71	0.138	171.76	15.20	0.594	0.414	0.486	0.547	3.45E+00	1019.76
1.96	0.158	145.77	12.90	0.504	0.358	0.431	0.492	2.93E+00	1016.77
2.46	0.198	109.61	9.70	0.379	0.278	0.351	0.408	4.41E+00	1012.61
3.46	0.278	73.45	6.50	0.254	0.185	0.251	0.300	5.91E+00	1008.45
4.46	0.359	54.24	4.80	0.188	0.132	0.190	0.231	4.36E+00	1006.24
5.96	0.479	30.51	2.70	0.105	0.084	0.131	0.000	3.68E+00	1003.51
11.76	0.946	12.43	1.10	0.043	0.006	0.015	0.000	5.80E+00	1001.43

$$\text{Depth aver. } \bar{c}_s^m = 60.69 \text{ [kg/m}^3\text{]}$$

$$\text{Depth aver. } \bar{\rho}_m = 1006.98 \text{ [kg/m}^3\text{]}$$



$$\begin{aligned}
 h &= 0.1243 \text{ [m]} \\
 S (\text{Bed slope}) &= 4.26E-03 \text{ [-]} \\
 u_* &= 0.0549 \text{ [m/s]} \\
 x &= 0.4 \text{ [-]} \\
 U &= 0.721 \text{ [m/s]} \\
 Fr &= 0.65 \text{ [-]} \\
 a (\text{refer.}) &= 0.0071 \text{ [m]} \\
 \bar{c}_s^m &= 289.28 \text{ [kg/m}^3\text{]} \\
 \bar{c}_s &= \bar{c}_s^m / \rho_i = 0.256 \text{ [m}^3/\text{m}^3\text{]} \\
 \rho_i &= 1130 \text{ [kg/m}^3\text{]} \\
 v_u &= 0.02 \text{ [m/s]} \\
 z &= v_u / (\rho_i g) = 0.911 \text{ [-]}
 \end{aligned}$$

Best fitting on  $\beta$  (Hunt equation)

$$\beta = 1.2209$$

$$Ri = 12.80 \text{ [-]}$$

$$Ri = \frac{gh[\rho_m(y=a) - \rho_m(y=h)]}{\bar{\rho}_m u_*^2}$$

Remarks: Group a-1 (Data interpreted as capacity flow and considered with reservation)  
Laboratory channel, aspect ratio =  $B/h = 3$        $\bar{c}_s^m = 289.28 \text{ [kg/m}^3\text{]} = 0.256 \text{ [m}^3/\text{m}^3\text{]} > 0.05 \text{ [m}^3/\text{m}^3\text{]} \Rightarrow \text{Hunt eq.}$   
Very high reference concentration  
Concentration measured with a Delft-Hydraulics conductivity-type concentration meter (CCM)  
The run has been performed with a flat lid on the surface to avoid surface instability  
Definition of the y-axis not too clear  
Velocity profiles available. No measurements on turbulence intensity and diffusion coefficients  
Subcritical flow

Run 134

Acrylic particles

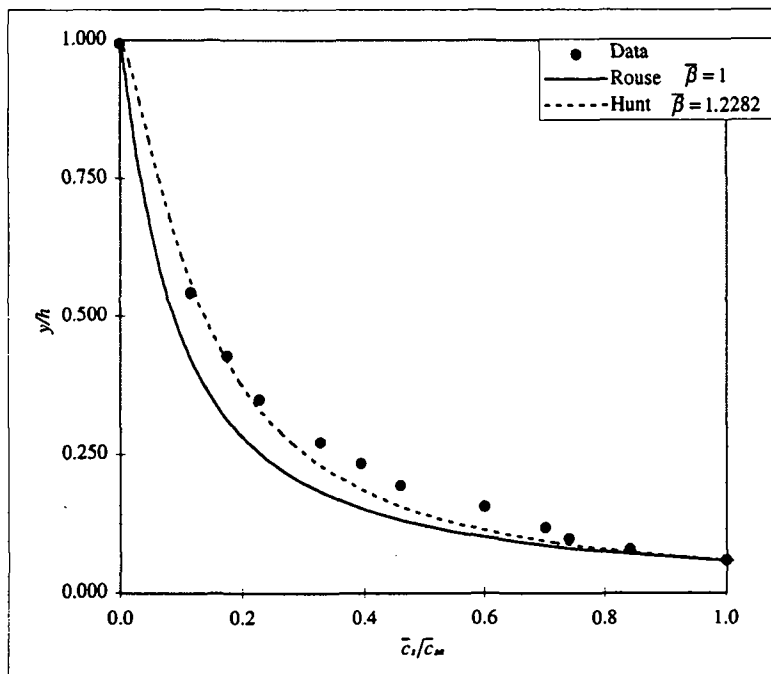
d= 0.600 [mm]

Group a-1

y [cm]	y/h [-]	$\bar{c}_m$ [kg/m³]	$\bar{c}_s$ (volum) [%]	$\bar{c}_s/\bar{c}_{sa}$ [-]	Calculated				
					Rouse eq. $\beta = 1$	Rouse eq. $\beta \neq 1$	Hunt eq. $\beta \neq 1$	$\bar{c}_s \cdot y/h$ [kg/m³]	$\rho_m$ [kg/m³]
0.75	0.058	322.05	28.50	1.000	1.000	0.842	0.764	1.000	1.88E+01
1.00	0.078	271.20	24.00	0.842	0.803	0.764	0.803	5.27E+00	1031.20
1.25	0.097	238.43	21.10	0.740	0.618	0.676	0.733	4.63E+00	1027.43
1.50	0.117	226.00	20.00	0.702	0.517	0.585	0.650	4.39E+00	1026.00
2.00	0.155	193.23	17.10	0.600	0.387	0.462	0.531	7.51E+00	1022.23
2.50	0.194	148.03	13.10	0.460	0.306	0.381	0.448	5.75E+00	1017.03
3.00	0.233	126.56	11.20	0.393	0.250	0.323	0.386	4.92E+00	1014.56
3.50	0.272	105.09	9.30	0.326	0.209	0.279	0.338	4.08E+00	1012.09
4.50	0.350	73.45	6.50	0.228	0.152	0.216	0.266	5.71E+00	1008.45
5.50	0.427	56.5	5.00	0.175	0.114	0.171	0.000	4.39E+00	1006.50
7.00	0.544	37.29	3.30	0.116	0.076	0.123	0.000	4.35E+00	1004.29
12.8	0.995	0	0.00	0.000	0.001	0.003	0.000	0.00E+00	1000.00

$$\text{Depth aver. } \bar{c}_m = 69.76 \text{ [kg/m}^3\text{]}$$

$$\text{Depth aver. } \bar{\rho}_m = 1008.03 \text{ [kg/m}^3\text{]}$$



$$\begin{aligned}
 h &= 0.1287 \text{ [m]} \\
 S (\text{Bed slope}) &= 4.47E-03 \text{ [-]} \\
 u_* &= 0.0574 \text{ [m/s]} \\
 \kappa &= 0.4 \text{ [-]} \\
 U &= 0.749 \text{ [m/s]} \\
 Fr &= 0.67 \text{ [-]} \\
 a (\text{refer.}) &= 0.0075 \text{ [m]} \\
 \bar{c}_m &= 322.05 \text{ [kg/m}^3\text{]} \\
 \bar{c}_{sa} &= \bar{c}_m / \rho_m = 0.285 \text{ [m}^3\text{/m}^3\text{]} \\
 \rho_m &= 1130 \text{ [kg/m}^3\text{]} \\
 v_u &= 0.02 \text{ [m/s]} \\
 z &= v_u / (\kappa U) = 0.871 \text{ [-]}
 \end{aligned}$$

Best fitting on  $\beta$  (Hunt equation)

$$\bar{\beta} = 1.2282$$

$$\begin{aligned}
 Ri &= 14.08 \text{ [-]} \\
 Ri [-] &= \frac{gh[\rho_m(y=a) - \rho_m(y=h)]}{\bar{\rho}_m \cdot u_*^2}
 \end{aligned}$$

Remarks: Group a-1 (Data interpreted as capacity flow and considered with reservation)  
 Laboratory channel, aspect ratio=  $B/h = 3$        $\bar{c}_{sa} = 322.05 \text{ [kg/m}^3\text{]} = 0.285 \text{ [m}^3\text{/m}^3\text{]} > 0.05 \text{ [m}^3\text{/m}^3\text{]} \Rightarrow \text{Hunt eq.}$   
 Very high reference concentration  
 Concentration measured with a Delft-Hydraulics conductivity-type concentration meter (CCM)  
 The run has been performed with a flat lid on the surface to avoid surface instability  
 Definition of the y-axis not too clear  
 Velocity profiles available. No measurements on turbulence intensity and diffusion coefficients  
 Subcritical flow

Sumer et al. (1996)

Sediment concentration distribution

Run 137

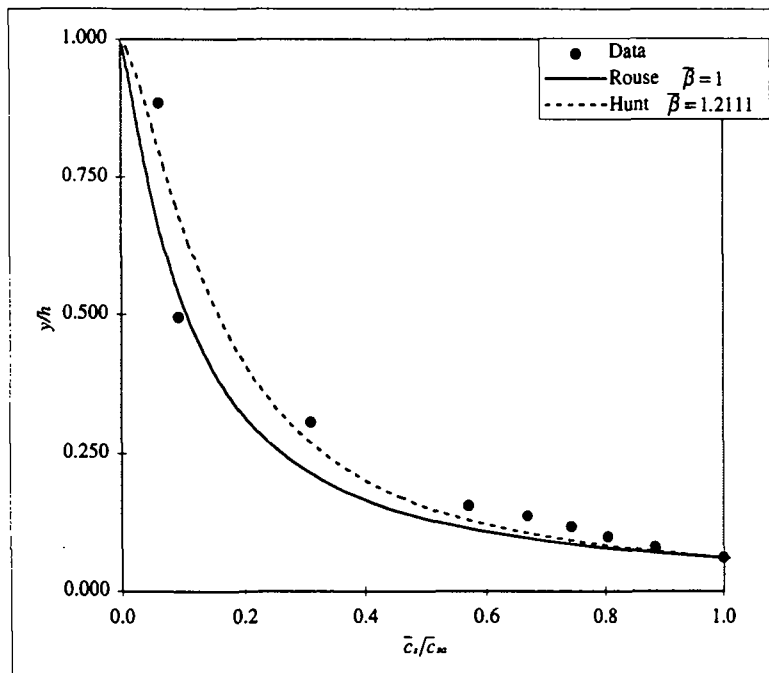
Acrylic particles

d= 0.600 [mm]

Group a-1

y [cm]	y/h [-]	$\bar{c}_s^m$ [kg/m³]	$\bar{c}_s$ (volum) [%]	$\bar{c}_s/\bar{c}_{\infty}$ [-]	Calculated				
					Rouse eq. $\beta = 1$ $\bar{c}_s/\bar{c}_{\infty}$ [-]	Rouse eq. $\beta \neq 1$ $\bar{c}_s/\bar{c}_{\infty}$ [-]	Hunt eq. $\beta \neq 1$ $\bar{c}_s/\bar{c}_{\infty}$ [-]	$\bar{c}_s^m \cdot y/h$ [kg/m³]	$\rho_m$ [kg/m³]
0.80	0.061	324.31	28.70	1.000	1.000	1.000	1.000	1.96E+01	1037.31
1.05	0.079	287.02	25.40	0.885	0.788	0.822	0.860	5.43E+00	1033.02
1.30	0.098	261.03	23.10	0.805	0.651	0.702	0.758	4.94E+00	1030.03
1.55	0.117	240.69	21.30	0.742	0.555	0.615	0.679	4.55E+00	1027.69
1.80	0.136	216.96	19.20	0.669	0.483	0.548	0.617	4.10E+00	1024.96
2.05	0.155	185.32	16.40	0.571	0.426	0.495	0.565	3.50E+00	1021.32
4.05	0.306	100.57	8.90	0.310	0.209	0.274	0.333	1.52E+01	1011.57
6.55	0.495	30.51	2.70	0.094	0.109	0.160	0.202	5.77E+00	1003.51
11.70	0.885	20.34	1.80	0.063	0.020	0.040	0.052	7.92E+00	1002.34

$$\begin{aligned} \text{Depth aver. } \bar{c}_s^m &= 71.06 \text{ [kg/m}^3\text{]} \\ \text{Depth aver. } \bar{\rho}_m &= 1008.17 \text{ [kg/m}^3\text{]} \end{aligned}$$



$$\begin{aligned} h &= 0.1322 \text{ [m]} \\ S (\text{Bed slope}) &= 5.00E-03 \text{ [-]} \\ u &= 0.0614 \text{ [m/s]} \\ \kappa &= 0.4 \text{ [-]} \\ U &= 0.773 \text{ [m/s]} \\ Fr &= 0.68 \text{ [-]} \\ a (\text{refer.}) &= 0.008 \text{ [m]} \\ \bar{c}_s^m &= 324.31 \text{ [kg/m}^3\text{]} \\ \bar{c}_{\infty} &= \bar{c}_s^m / \rho_m = 0.287 \text{ [m}^3/\text{m}^3\text{]} \\ \rho_s &= 1130 \text{ [kg/m}^3\text{]} \\ v_u &= 0.02 \text{ [m/s]} \\ z &= v_u / (\alpha g) = 0.814 \text{ [-]} \end{aligned}$$

Best fitting on  $\beta$  (Hunt equation)

$$\beta = 1.2111$$

$$Ri = 11.93 \text{ [-]}$$

$$Ri [-] = \frac{gh[\rho_m(y=a) - \rho_m(y=h)]}{\bar{\rho}_m \cdot u^2}$$

Remarks: Group a-1 (Data interpreted as capacity flow and considered with reservation)  
 Laboratory channel, aspect ratio=  $B/h = 3$        $\bar{c}_s^m = 324.31 \text{ [kg/m}^3\text{]} = 0.287 \text{ [m}^3/\text{m}^3\text{]} > 0.05 \text{ [m}^3/\text{m}^3\text{]} \Rightarrow$  Hunt eq.  
 Very high reference concentration  
 Concentration measured with a Delft-Hydraulics conductivity-type concentration meter (CCM)  
 The run has been performed with a flat lid on the surface to avoid surface instability  
 Definition of the y-axis not too clear  
 Velocity profiles available. No measurements on turbulence intensity and diffusion coefficients  
 Subcritical flow

Run 142

Sand particles

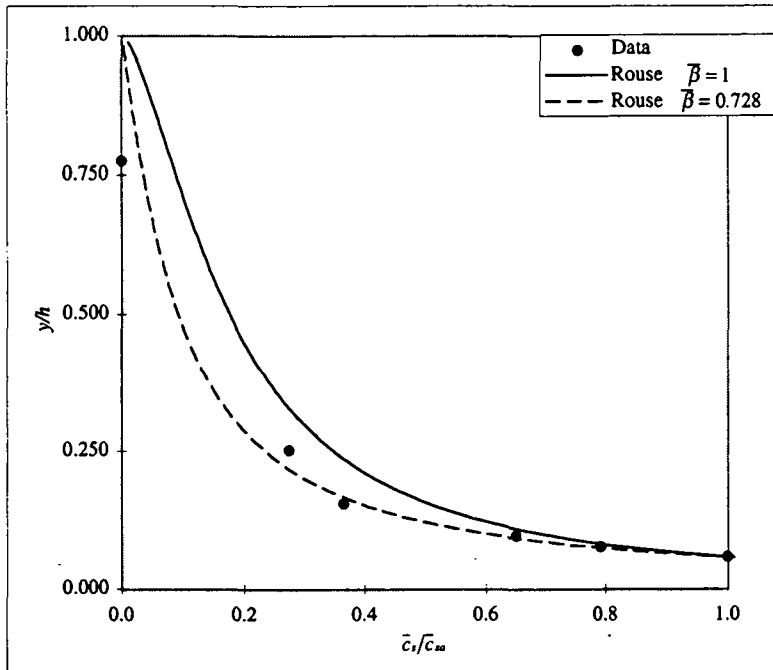
d= 0.130 [mm]

Group a-1

y [cm]	y/h [-]	$\bar{c}_s^*$ [kg/m³]	$\bar{c}_s$ (volum) [%]	$\bar{c}_s/\bar{c}_{s0}$ [-]	Calculated				$\rho_m$ [kg/m³]
					Rouse eq. $\beta = 1$ $\bar{c}_s/\bar{c}_{s0}$ [-]	Rouse eq. $\beta \neq 1$ $\bar{c}_s/\bar{c}_{s0}$ [-]	Hunt eq. $\beta \neq 1$ $\bar{c}_s/\bar{c}_{s0}$ [-]	$\bar{c}_s^* \cdot y/h$ [kg/m³]	
0.60	0.058	96.46	3.64	1.000	1.000	1.000	1.000	5.61E+00	1060.06
0.80	0.078	76.32	2.88	0.791	0.825	0.768	0.777	1.48E+00	1047.52
1.00	0.097	62.81	2.37	0.651	0.708	0.623	0.635	1.22E+00	1039.11
1.60	0.155	35.25	1.33	0.365	0.507	0.393	0.405	2.05E+00	1021.95
2.60	0.252	26.50	1.00	0.275	0.347	0.234	0.243	2.57E+00	1016.50
8.00	0.775	0.00	0.00	0.000	0.081	0.032	0.033	0.00E+00	1000.00

$$\text{Depth aver. } \bar{c}_s^* = 12.92 \text{ [kg/m}^3\text{]}$$

$$\text{Depth aver. } \bar{\rho}_m = 1008.05 \text{ [kg/m}^3\text{]}$$



$$\begin{aligned}
 h &= 0.1032 \text{ [m]} \\
 S(\text{Bed slope}) &= 4.79E-03 \text{ [-]} \\
 u_* &= 0.0481 \text{ [m/s]} \\
 \kappa &= 0.4 \text{ [-]} \\
 U &= 0.833 \text{ [m/s]} \\
 Fr &= 0.83 \text{ [-]} \\
 a(\text{refer.}) &= 0.006 \text{ [m]} \\
 \bar{c}_{s0} &= 96.46 \text{ [kg/m}^3\text{]} \\
 \bar{c}_{s0} = \bar{c}_s^*/\bar{\rho}_m &= 0.0364 \text{ [m}^3/\text{m}^3\text{]} \\
 \bar{\rho}_m &= 2650 \text{ [kg/m}^3\text{]} \\
 v_* &= 0.012 \text{ [m/s]} \\
 z = v_u / (\bar{\rho}_m) &= 0.624 \text{ [-]}
 \end{aligned}$$

Best fitting on  $\beta$  (Rouse equation)

$$\beta = 0.728$$

$$Ri = 26.07 \text{ [-]}$$

$$Ri [-] = \frac{gh[\rho_m(y=a) - \rho_m(y=h)]}{\bar{\rho}_m \cdot u_*^2}$$

Remarks: Group a-1 (Data interpreted as capacity flow and considered with reservation)  
Laboratory channel, aspect ratio=  $B/h = 3$        $\bar{c}_s^* = 96.46 \text{ [kg/m}^3\text{]} = 0.0364 \text{ [m}^3/\text{m}^3\text{]} < 0.05 \text{ [m}^3/\text{m}^3\text{]} \Rightarrow \text{Rouse eq.}$   
Small reference concentration  
Concentration measured with a Delft-Hydraulics conductivity-type concentration meter (CCM)  
The run has been performed with a flat lid on the surface to avoid surface instability  
Definition of the y-axis not too clear  
Velocity profiles available. No measurements on turbulence intensity and diffusion coefficients  
Subcritical flow

Run 150

Sand particles

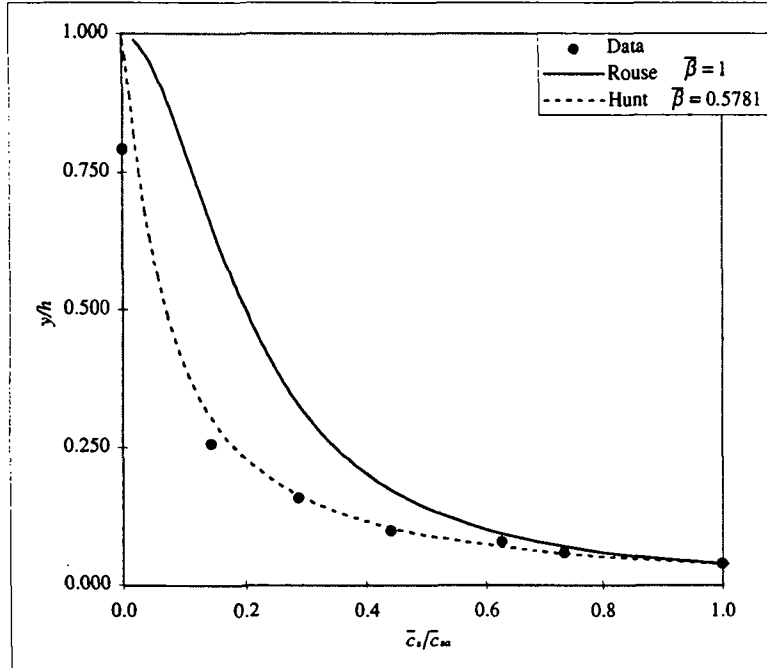
d = 0.130 [mm]

Group a-1

y [cm]	y/h [-]	$\bar{c}_s^m$ [kg/m³]	$\bar{c}_s$ (volum) [%]	$\bar{c}_s/\bar{c}_{so}$ [-]	Calculated				
					Rouse eq. $\beta = 1$	Rouse eq. $\beta \neq 1$	Hunt eq. $\beta \neq 1$	$\bar{c}_s \cdot y/h$ [kg/m³]	$\rho_m$ [kg/m³]
0.40	0.040	219.42	8.28	1.000	1.000	1.000	1.000	8.70E+00	1136.62
0.60	0.059	161.12	6.08	0.734	0.807	0.689	0.720	3.19E+00	1100.32
0.80	0.079	137.54	5.19	0.627	0.690	0.527	0.563	2.73E+00	1085.64
1.00	0.099	96.46	3.64	0.440	0.610	0.425	0.462	1.91E+00	1060.06
1.60	0.159	62.81	2.37	0.286	0.465	0.266	0.296	3.73E+00	1039.11
2.60	0.258	31.80	1.20	0.145	0.342	0.156	0.177	3.15E+00	1019.80
8.00	0.793	0.00	0.00	0.000	0.102	0.019	0.022	0.00E+00	1000.00

$$\text{Depth aver. } \bar{C}_s^m = 23.42 \text{ [kg/m}^3\text{]}$$

$$\text{Depth aver. } \bar{\rho}_m = 1014.58 \text{ [kg/m}^3\text{]}$$



$$\begin{aligned}
 h &= 0.1009 \text{ [m]} \\
 S (\text{Bed slope}) &= 7.26E-03 \text{ [-]} \\
 u_* &= 0.0595 \text{ [m/s]} \\
 \kappa &= 0.4 \text{ [-]} \\
 U &= 1.024 \text{ [m/s]} \\
 Fr &= 1.03 \text{ [-]} \\
 a (\text{refer.}) &= 0.004 \text{ [m]} \\
 \bar{c}_s^m &= 219.42 \text{ [kg/m}^3\text{]} \\
 \bar{c}_{so} &= \bar{c}_s^m / \rho_i = 0.0828 \text{ [m}^3/\text{m}^3\text{]} \\
 \rho_i &= 2650 \text{ [kg/m}^3\text{]} \\
 v_{u_*} &= 0.012 \text{ [m/s]} \\
 z &= v_{u_*} / (\alpha u_*) = 0.504 \text{ [-]}
 \end{aligned}$$

Best fitting on  $\beta$  (Hunt equation)

$$\beta = 0.5781$$

$$\begin{aligned}
 Ri &= 37.65 \text{ [-]} \\
 Ri [-] &= \frac{gh[\rho_m(y=a) - \rho_m(y=h)]}{\bar{\rho}_m \cdot u_*^2}
 \end{aligned}$$

Remarks: Group a-1 (Data interpreted as capacity flow and considered with reservation)  
Laboratory channel, aspect ratio =  $B/h = 3$        $\bar{c}_s^m = 219.42 \text{ [kg/m}^3\text{]} = 0.0828 \text{ [m}^3/\text{m}^3\text{]} > 0.05 \text{ [m}^3/\text{m}^3\text{]} \Rightarrow \text{Hunt eq.}$   
High reference concentration  
Concentration measured with a Delft-Hydraulics conductivity-type concentration meter (CCM)  
The run has been performed with a flat lid on the surface to avoid surface instability  
Definition of the y-axis not too clear  
Velocity profiles available. No measurements on turbulence intensity and diffusion coefficients  
Supercritical flow

Run 155

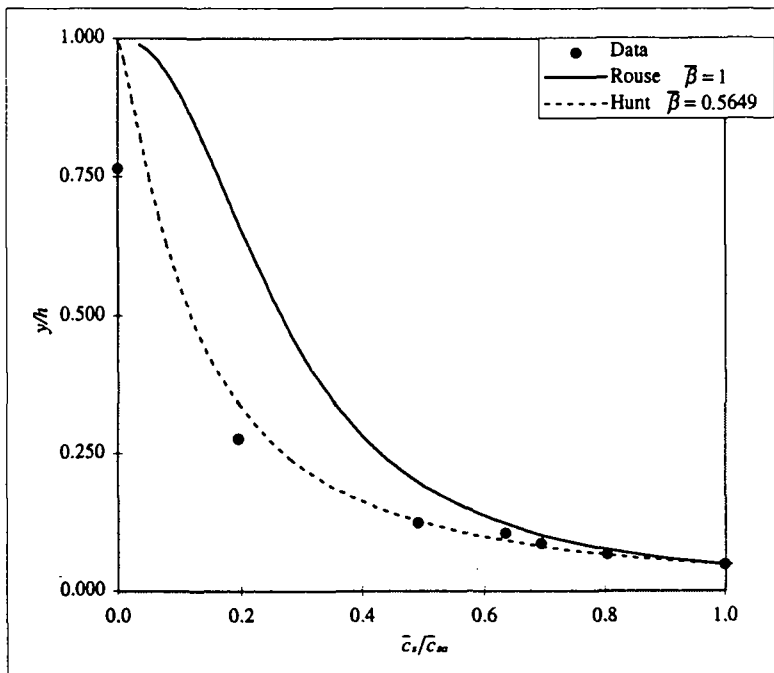
Sand particles

d= 0.130 [mm]

Group a-1

y [cm]	y/h [-]	$\bar{c}_s^m$ [kg/m³]	$\bar{c}_s$ (volum) [%]	$\bar{c}_s/\bar{c}_{so}$ [-]	Calculated				
					Rouse eq. $\beta = 1$ $\bar{c}_s/\bar{c}_{so}$ [-]	Rouse eq. $\beta \neq 1$ $\bar{c}_s/\bar{c}_{so}$ [-]	Hunt eq. $\beta \neq 1$ $\bar{c}_s/\bar{c}_{so}$ [-]	$\bar{c}_s^m \cdot y/h$ [kg/m³]	$\rho_m$ [kg/m³]
0.50	0.048	339.73	12.82	1.000	1.000	1.000	1.000	1.62E+01	1211.53
0.70	0.067	273.22	10.31	0.804	0.854	0.756	0.796	5.22E+00	1170.12
0.90	0.086	236.38	8.92	0.696	0.757	0.611	0.665	4.52E+00	1147.18
1.10	0.105	215.45	8.13	0.634	0.686	0.513	0.572	4.12E+00	1134.15
1.30	0.124	167.22	6.31	0.492	0.631	0.443	0.502	3.20E+00	1104.12
2.90	0.277	66.25	2.50	0.195	0.406	0.203	0.244	1.01E+01	1041.25
8.00	0.765	0.00	0.00	0.000	0.158	0.038	0.048	0.00E+00	1000.00

Depth aver.	$\bar{c}_s^m = 43.43$ [kg/m³]
Depth aver.	$\bar{\rho}_m = 1027.04$ [kg/m³]



$h = 0.1046$ [m]
S (Bed slope) = $8.83E-03$ [-]
$u_* = 0.0677$ [m/s]
$\kappa = 0.4$ [-]
$U = 1.138$ [m/s]
$Fr = 1.12$ [-]
$a (\text{refer.}) = 0.005$ [m]
$\bar{c}_{so}^m = 339.73$ [kg/m³]
$\bar{c}_{so} = \bar{c}_{so}^m / \rho_m = 0.1282$ [m³/m³]
$\rho_m = 2650$ [kg/m³]
$v_* = 0.012$ [m/s]
$z = v_*/(\kappa u_*) = 0.443$ [-]

Best fitting on  $\beta$  (Hunt equation)

$$\bar{\beta} = 0.5649$$

$Ri = 46.11$ [-]
$Ri [-] = \frac{gh[\rho_m(y=a) - \rho_m(y=h)]}{\bar{\rho}_m \cdot U^2}$

Remarks: Group a-1 (Data interpreted as capacity flow and considered with reservation)  
Laboratory channel, aspect ratio =  $B/h = 3$   
Very high reference concentration  $\bar{c}_{so}^m = 339.73$  [kg/m³] =  $0.1282$  [m³/m³] >  $0.05$  [m³/m³] => Hunt eq.  
Concentration measured with a Delft-Hydraulics conductivity-type concentration meter (CCM)  
The run has been performed with a flat lid on the surface to avoid surface instability  
Definition of the y-axis not too clear  
Velocity profiles available. No measurements on turbulence intensity and diffusion coefficients  
Supercritical flow

EPFL, (1997)

## Sediment concentration distribution

Run Q40S003

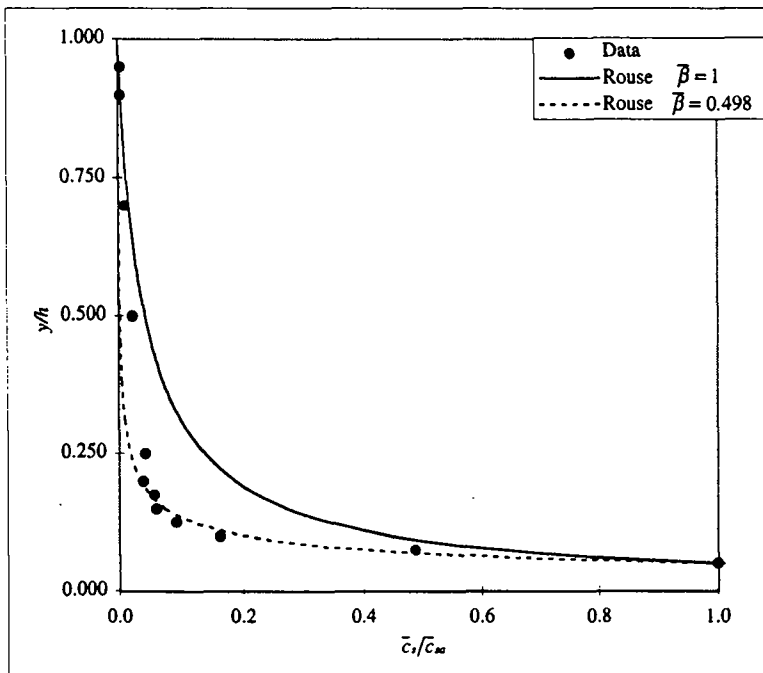
Sand particles

d= 0.135 [mm]

Group a-1

y [cm]	y/h [--]	$\bar{c}_s^m$ [kg/m³]	$\bar{c}_s$ (volum.) [%]	Measured		Calculated			
				$\bar{c}_s/\bar{c}_{sa}$ [--]	Rouse eq. $\beta = 1$	Rouse eq. $\beta \neq 1$	Hunt eq. $\beta \neq 1$	$\bar{c}_s \cdot y/h$ [kg/m³]	$\rho_m$ [kg/m³]
0.60	0.050	24.62	0.93	1.000	1.000	1.000	1.000	1.23E+00	1015.33
0.90	0.075	12.04	0.45	0.489	0.629	0.395	0.399	3.01E-01	1007.49
1.20	0.100	4.01	0.15	0.163	0.449	0.200	0.203	1.00E-01	1002.50
1.50	0.125	2.26	0.09	0.092	0.343	0.117	0.119	5.65E-02	1001.41
1.80	0.150	1.48	0.06	0.060	0.274	0.074	0.075	3.70E-02	1000.92
2.10	0.175	1.41	0.05	0.057	0.225	0.050	0.051	3.53E-02	1000.88
2.40	0.200	0.97	0.04	0.039	0.188	0.035	0.036	2.41E-02	1000.60
3.00	0.250	1.04	0.04	0.042	0.138	0.019	0.019	5.20E-02	1000.65
6.00	0.500	0.56	0.02	0.023	0.043	0.002	0.000	1.39E-01	1000.35
8.40	0.700	0.23	0.01	0.009	0.017	0.000	0.000	4.56E-02	1000.14
10.80	0.900	0.09	0.00	0.004	0.004	0.000	0.000	1.73E-02	1000.05
11.40	0.950	0.08	0.00	0.003	0.002	0.000	0.000	3.80E-03	1000.05

$$\begin{aligned} \text{Depth aver. } \bar{C}_s^m &= 2.04 \text{ [kg/m}^3\text{]} \\ \text{Depth aver. } \bar{\rho}_m &= 1001.27 \text{ [kg/m}^3\text{]} \end{aligned}$$



$$\begin{aligned} h &= 0.12 \text{ [m]} \\ S (\text{Bed slope}) &= 3.00E-04 \text{ [--]} \\ u_* &= 0.028 \text{ [m/s]} \\ \kappa &= 0.4 \text{ [--]} \\ U &= 0.68 \text{ [m/s]} \\ Fr &= 0.63 \text{ [--]} \\ a (\text{refer.}) &= 0.006 \text{ [m]} \\ \bar{c}_s^m &= 24.62 \text{ [kg/m}^3\text{]} \\ \bar{c}_{sa} &= \bar{c}_s^m / \rho_s = 0.009 \text{ [m}^3\text{/m}^3\text{]} \\ \rho_s &= 2650 \text{ [kg/m}^3\text{]} \\ v_u &= 0.012 \text{ [m/s]} \\ z = v_u / (\kappa U) &= 1.071 \text{ [--]} \end{aligned}$$

Best fitting on  $\beta$  (Rouse equation)  
 $\bar{\beta} = 0.498$

$$Ri = 22.92 \text{ [--]}$$

$$Ri [-] = \frac{gH[\rho_m(y=a) - \rho_m(y=h)]}{\bar{\rho}_m \cdot U^2}$$

Remarks: Group a-1 (Erodible flat sediment layer on the bottom => capacity-flow)  
Laboratory channel, aspect ratio=  $B/h = 5.0$   
Small reference concentration  $\bar{c}_{sa} = 24.62 \text{ [kg/m}^3\text{]} = 0.009 \text{ [m}^3\text{/m}^3\text{]} < 0.05 \text{ [m}^3\text{/m}^3\text{]} \Rightarrow$  Rouse eq.  
Instantaneous velocity and concentration measured with the APFP ultrasonic instrument  
The calibration of the APFP instrument has been made measuring by suction the concentration distribution (shown here).  
Thickness of the sediment layer  $\approx 2 \text{ [mm]}$   
Subcritical flow

EPFL, (1997)

## Sediment concentration distribution

Run Q45S005

Sand particles

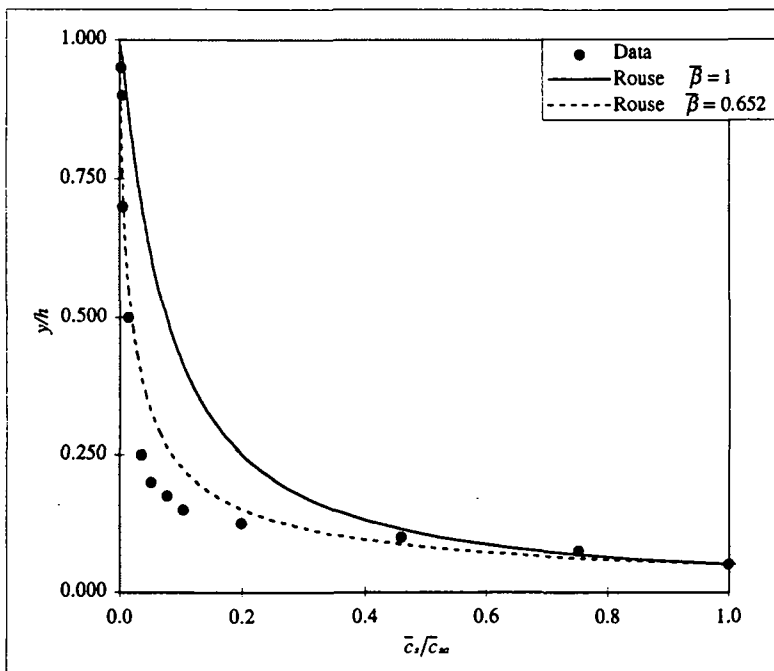
d= 0.135 [mm]

Group a-1

y [cm]	y/h [-]	$\bar{c}_s^*$ [kg/m³]	$\bar{c}_s$ (volum.) [%]	$\bar{c}_s/\bar{c}_{su}$ [-]	Calculated				$\rho_m$ [kg/m³]
					Rouse eq. $\beta = 1$ $\bar{c}_s/\bar{c}_{su}$ [-]	Rouse eq. $\beta \neq 1$ $\bar{c}_s/\bar{c}_{su}$ [-]	Hunt eq. $\beta \neq 1$ $\bar{c}_s/\bar{c}_{su}$ [-]	$\bar{c}_s^* \cdot y/h$ [kg/m³]	
0.60	0.050	28.62	1.08	1.000	1.000	1.000	1.000	1.43E+00	1017.82
0.90	0.075	21.52	0.81	0.752	0.687	0.562	0.566	5.38E-01	1013.40
1.20	0.100	13.15	0.50	0.459	0.522	0.369	0.373	3.29E-01	1008.19
1.50	0.125	5.67	0.21	0.198	0.420	0.264	0.267	1.42E-01	1003.53
1.80	0.150	2.99	0.11	0.105	0.349	0.199	0.202	7.48E-02	1001.86
2.10	0.175	2.24	0.08	0.078	0.298	0.156	0.158	5.59E-02	1001.39
2.40	0.200	1.48	0.06	0.052	0.258	0.125	0.127	3.70E-02	1000.92
3.00	0.250	1.03	0.04	0.036	0.201	0.085	0.087	5.16E-02	1000.64
6.00	0.500	0.38	0.01	0.013	0.077	0.020	0.000	9.53E-02	1000.24
8.40	0.700	0.16	0.01	0.006	0.037	0.006	0.000	3.23E-02	1000.10
10.80	0.900	0.11	0.00	0.004	0.011	0.001	0.001	2.18E-02	1000.07
11.40	0.950	0.05	0.00	0.002	0.006	0.000	0.000	2.55E-03	1000.03

$$\text{Depth aver. } \bar{c}_s^* = 2.81 \text{ [kg/m}^3\text{]}$$

$$\text{Depth aver. } \bar{\rho}_m = 1001.75 \text{ [kg/m}^3\text{]}$$



$$\begin{aligned} h &= 0.12 \text{ [m]} \\ S (\text{Bed slope}) &= 5.00E-04 \text{ [-]} \\ u_* &= 0.034 \text{ [m/s]} \\ \kappa &= 0.4 \text{ [-]} \\ U &= 0.806 \text{ [m/s]} \\ Fr &= 0.74 \text{ [-]} \\ a (\text{refer.}) &= 0.006 \text{ [m]} \\ \bar{c}_s^* &= 28.62 \text{ [kg/m}^3\text{]} \\ \bar{c}_{su} &= \bar{c}_s^*/\rho_m = 0.011 \text{ [m}^3/\text{m}^3\text{]} \\ \rho_s &= 2650 \text{ [kg/m}^3\text{]} \\ v_u &= 0.012 \text{ [m/s]} \\ z &= v_u/(\kappa u_*) = 0.870 \text{ [-]} \end{aligned}$$

Best fitting on  $\beta$  (Rouse equation)

$$\beta = 0.652$$

$$Ri = 17.56 \text{ [-]}$$

$$Ri [-] = \frac{gh[\rho_m(y=a) - \rho_m(y=h)]}{\bar{\rho}_m \cdot u_*^2}$$

Remarks: Group a-1 (Erodible flat sediment layer on the bottom => capacity-flow)  
 Laboratory channel, aspect ratio=  $B/h = 5.0$   
 Small reference concentration  $\bar{c}_{su} = 28.62 \text{ [kg/m}^3\text{]} = 0.011 \text{ [m}^3/\text{m}^3\text{]} < 0.05 \text{ [m}^3/\text{m}^3\text{]} \Rightarrow \text{Rouse eq.}$   
 Instantaneous velocity and concentration measured with the APFP ultrasonic instrument  
 The calibration of the APFP instrument has been made measuring by suction the concentration distribution (shown here).  
 Thickness of the sediment layer  $\approx 2 \text{ [mm]}$   
 Subcritical flow

EPFL, (1997)

## Sediment concentration distribution

Run Q48S0075

Sand particles

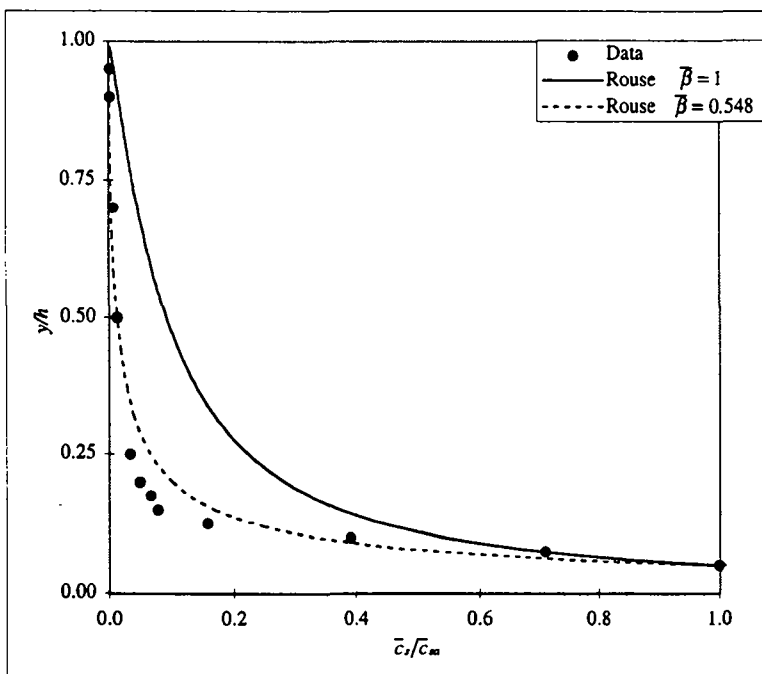
d= 0.135 [mm]

Group a-1

y [cm]	y/h [-]	$\bar{c}_s^*$ [kg/m³]	$\bar{c}_s$ (volum.) [%]	$\bar{c}_s/\bar{c}_{sa}$ [-]	Calculated				
					Rouse eq. $\beta = 1$ $\bar{c}_s/\bar{c}_{sa}$ [-]	Rouse eq. $\beta \neq 1$ $\bar{c}_s/\bar{c}_{sa}$ [-]	Hunt eq. $\beta \neq 1$ $\bar{c}_s/\bar{c}_{sa}$ [-]	$\bar{c}_s^* \cdot y/h$ [kg/m³]	$\rho_m$ [kg/m³]
0.60	0.05	31.62	1.19	1.000	1.000	1.000	1.000	1.58E+00	1019.69
0.90	0.08	22.45	0.85	0.710	0.704	0.528	0.533	5.61E-01	1013.98
1.20	0.10	12.34	0.47	0.390	0.546	0.331	0.336	3.08E-01	1007.68
1.50	0.13	5.00	0.19	0.158	0.445	0.228	0.232	1.25E-01	1003.12
1.80	0.15	2.47	0.09	0.078	0.375	0.167	0.170	6.18E-02	1001.54
2.10	0.18	2.10	0.08	0.066	0.323	0.127	0.130	5.24E-02	1001.31
2.40	0.20	1.54	0.06	0.049	0.283	0.100	0.102	3.84E-02	1000.96
3.00	0.25	1.06	0.04	0.034	0.224	0.065	0.066	5.32E-02	1000.66
6.00	0.50	0.40	0.01	0.013	0.092	0.013	0.000	9.92E-02	1000.25
8.40	0.70	0.21	0.01	0.007	0.046	0.004	0.000	4.30E-02	1000.13
10.80	0.90	0.07	0.00	0.002	0.015	0.000	0.001	1.38E-02	1000.04
11.40	0.95	0.05	0.00	0.002	0.008	0.000	0.000	2.51E-03	1000.03

$$\text{Depth aver. } \bar{C}_s^* = 2.94 \text{ [kg/m}^3\text{]}$$

$$\text{Depth aver. } \bar{\rho}_m = 1001.83 \text{ [kg/m}^3\text{]}$$



$$\begin{aligned}
 h &= 0.12 \text{ [m]} \\
 S (\text{Bed slope}) &= 7.50E-4 \text{ [-]} \\
 u_* &= 0.037 \text{ [m/s]} \\
 \kappa &= 0.4 \text{ [-]} \\
 U &= 0.829 \text{ [m/s]} \\
 Fr &= 0.76 \text{ [-]} \\
 a (\text{refer.}) &= 0.006 \text{ [m]} \\
 \bar{c}_{sa} &= 31.62 \text{ [kg/m}^3\text{]} \\
 \bar{c}_{sa} = \bar{c}_s^*/\rho_s &= 0.012 \text{ [m}^3/\text{m}^3\text{]} \\
 \rho_s &= 2650 \text{ [kg/m}^3\text{]} \\
 v_u &= 0.012 \text{ [m/s]} \\
 z = v_u / (\kappa u) &= 0.811 \text{ [-]}
 \end{aligned}$$

Best fitting on  $\beta$  (Rouse equation)

$$\bar{\beta} = 0.548$$

$$\begin{aligned}
 Ri &= 16.87 \text{ [-]} \\
 Ri [-] &= \frac{gh[\rho_m(y=a) - \rho_m(y=h)]}{\bar{\rho}_m \cdot u_*^2}
 \end{aligned}$$

Remarks: Group a-1 (Erodible flat sediment layer on the bottom => capacity-flow)  
Laboratory channel, aspect ratio=  $B/h = 5.0$   
Small reference concentration  $\bar{c}_s^* = 31.62 \text{ [kg/m}^3\text{]} = 0.012 \text{ [m}^3/\text{m}^3\text{]} < 0.05 \text{ [m}^3/\text{m}^3\text{]}$  => Rouse eq.  
Instantaneous velocity and concentration measured with the APFP ultrasonic instrument  
The calibration of the APFP instrument has been made measuring by suction the concentration distribution (shown here).  
Thickness of the sediment layer  $\approx 2 \text{ [mm]}$   
Subcritical flow

EPFL, (1997)

## Sediment concentration distribution

Run Q50S01

Sand particles

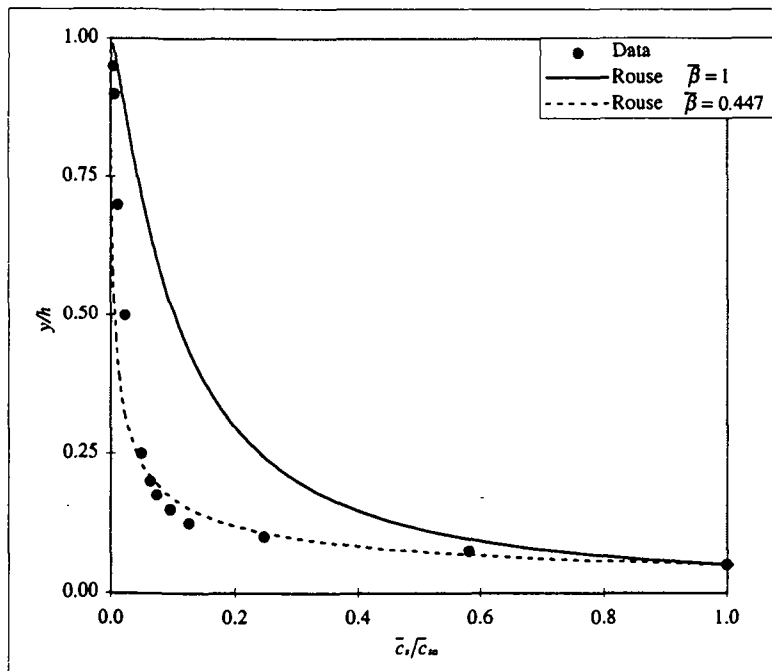
d= 0.135 [mm]

Group a-1

y [cm]	y/h [-]	$\bar{c}_s^m$ [kg/m³]	$\bar{c}_s$ (volum.) [%]	$\bar{c}_s/\bar{c}_{sa}$ [-]	Calculated				
					Rouse eq. $\beta = 1$ $\bar{c}_s/\bar{c}_{sa}$ [-]	Rouse eq. $\beta \neq 1$ $\bar{c}_s/\bar{c}_{sa}$ [-]	Hunt eq. $\beta \neq 1$ $\bar{c}_s/\bar{c}_{sa}$ [-]	$\bar{c}_s^m \cdot y/h$ [kg/m³]	$\rho_m$ [kg/m³]
0.60	0.05	39.33	1.48	1.000	1.000	1.000	1.000	1.97E+00	1024.49
0.90	0.08	22.87	0.86	0.581	0.717	0.475	0.484	5.72E-01	1014.24
1.20	0.10	9.76	0.37	0.248	0.563	0.276	0.283	2.44E-01	1006.08
1.50	0.13	4.98	0.19	0.127	0.464	0.179	0.184	1.25E-01	1003.10
1.80	0.15	3.81	0.14	0.097	0.394	0.125	0.128	9.53E-02	1002.37
2.10	0.18	2.95	0.11	0.075	0.342	0.091	0.094	7.38E-02	1001.84
2.40	0.20	2.53	0.10	0.064	0.302	0.068	0.071	6.33E-02	1001.58
3.00	0.25	1.94	0.07	0.049	0.242	0.042	0.043	9.70E-02	1001.21
6.00	0.50	0.88	0.03	0.022	0.104	0.006	0.000	2.20E-01	1000.55
8.40	0.70	0.46	0.02	0.012	0.054	0.001	0.000	9.20E-02	1000.29
10.80	0.90	0.25	0.01	0.006	0.019	0.000	0.000	5.00E-02	1000.16
11.40	0.95	0.16	0.01	0.004	0.011	0.000	0.000	8.00E-03	1000.10

$$\text{Depth aver. } \bar{c}_s^m = 3.61 \text{ [kg/m}^3\text{]}$$

$$\text{Depth aver. } \bar{\rho}_m = 1002.25 \text{ [kg/m}^3\text{]}$$



$$\begin{aligned}
 h &= 0.12 \text{ [m]} \\
 S (\text{Bed slope}) &= 1.00E-3 \text{ [-]} \\
 u_* &= 0.039 \text{ [m/s]} \\
 \kappa &= 0.4 \text{ [-]} \\
 U &= 0.792 \text{ [m/s]} \\
 Fr &= 0.73 \text{ [-]} \\
 a (\text{refer.}) &= 0.006 \text{ [m]} \\
 \bar{c}_s^m &= 39.33 \text{ [kg/m}^3\text{]} \\
 \bar{c}_{sa} &= \bar{c}_s^m / \bar{\rho}_m = 0.015 \text{ [m}^3\text{/m}^3\text{]} \\
 \rho_s &= 2650 \text{ [kg/m}^3\text{]} \\
 v_u &= 0.012 \text{ [m/s]} \\
 z &= v_u / (\kappa u) = 0.769 \text{ [-]}
 \end{aligned}$$

Best fitting on  $\beta$  (Rouse equation)

$$\beta = 0.447$$

$$Ri = 18.83 \text{ [-]}$$

$$Ri [-] = \frac{gh[\rho_m(y=a) - \rho_m(y=h)]}{\bar{\rho}_m \cdot u_*^2}$$

Remarks: Group a-1 (Erodible flat sediment layer on the bottom => capacity-flow)  
Laboratory channel, aspect ratio=  $B/h = 5.0$   
Small reference concentration  $\bar{c}_s^m = 39.33 \text{ [kg/m}^3\text{]} = 0.015 \text{ [m}^3\text{/m}^3\text{]} < 0.05 \text{ [m}^3\text{/m}^3\text{]}$  => Rouse eq.  
Instantaneous velocity and concentration measured with the APFP ultrasonic instrument  
The calibration of the APFP instrument has been made measuring by suction the concentration distribution (shown here).  
Thickness of the sediment layer  $\approx 2 \text{ [mm]}$   
Subcritical flow

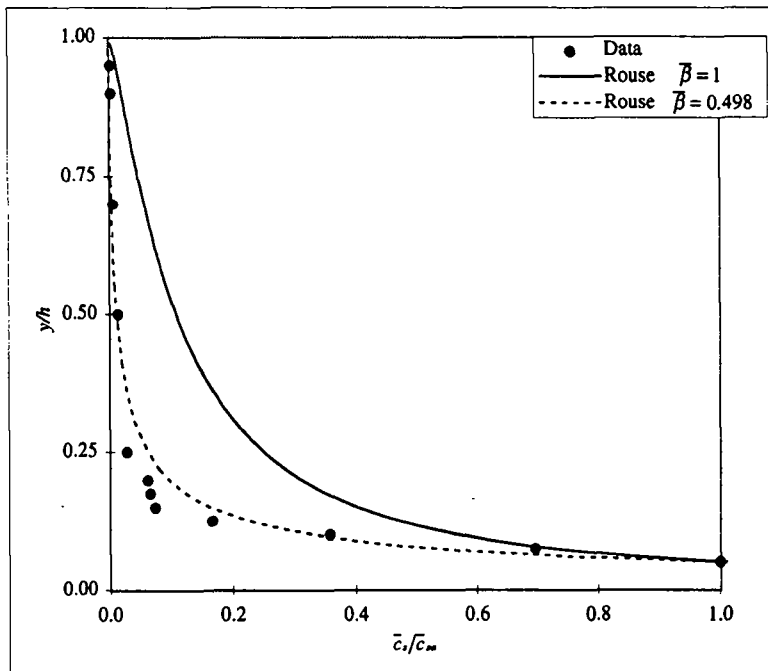
EPFL, (1997)

## Sediment concentration distribution

Run	Q53S0125	Sand particles	d= 0.135 [mm]	Group a-1
-----	----------	----------------	---------------	-----------

y [cm]	y/h [-]	$\bar{c}_s^m$ [kg/m³]	$\bar{c}_s$ (volum.) [%]	$\bar{c}_s/\bar{c}_{sa}$ [-]	Calculated				
					Rouse eq. $\beta = 1$ $\bar{c}_s/\bar{c}_{sa}$ [-]	Rouse eq. $\beta \neq 1$ $\bar{c}_s/\bar{c}_{sa}$ [-]	Hunt eq. $\beta \neq 1$ $\bar{c}_s/\bar{c}_{sa}$ [-]	$\bar{c}_s^m \cdot y/h$ [kg/m³]	$\rho_m$ [kg/m³]
0.60	0.05	36.04	1.36	1.000	1.000	1.000	1.000	1.80E+00	1022.44
0.90	0.08	25.11	0.95	0.697	0.723	0.522	0.528	6.28E-01	1015.64
1.20	0.10	12.91	0.49	0.358	0.571	0.325	0.331	3.23E-01	1008.04
1.50	0.13	6.03	0.23	0.167	0.473	0.222	0.227	1.51E-01	1003.75
1.80	0.15	2.68	0.10	0.074	0.404	0.162	0.165	6.70E-02	1001.67
2.10	0.18	2.41	0.09	0.067	0.352	0.123	0.126	6.01E-02	1001.50
2.40	0.20	2.23	0.08	0.062	0.311	0.096	0.098	5.56E-02	1001.39
3.00	0.25	1.01	0.04	0.028	0.250	0.062	0.064	5.04E-02	1000.63
6.00	0.50	0.48	0.02	0.013	0.110	0.012	0.000	1.20E-01	1000.30
8.40	0.70	0.21	0.01	0.006	0.058	0.003	0.000	4.26E-02	1000.13
10.80	0.90	0.10	0.00	0.003	0.021	0.000	0.000	1.98E-02	1000.06
11.40	0.95	0.06	0.00	0.002	0.012	0.000	0.000	2.91E-03	1000.04

Depth aver.	$\bar{c}_s^m =$	3.32 [kg/m³]
Depth aver.	$\rho_m =$	1002.07 [kg/m³]



$h = 0.12$ [m]
$S$ (Bed slope)= $1.25E-3$ [-]
$u_* = 0.040$ [m/s]
$\kappa = 0.4$ [-]
$U = 0.824$ [m/s]
$Fr = 0.76$ [-]
$a$ (refer.)= 0.006 [m]
$\bar{c}_s^m = 36.04$ [kg/m³]
$\bar{c}_{sa} = \bar{c}_s^m / \rho_s = 0.014$ [m³/m³]
$\rho_s = 2650$ [kg/m³]
$v_s = 0.012$ [m/s]
$z = v_s / (\kappa U) = 0.750$ [-]

Best fitting on  $\beta$  (Rouse equation)  
 $\beta = 0.498$

$Ri = 16.45$ [-]
$Ri [-] = \frac{gh[\rho_m(y=a) - \rho_m(y=h)]}{\bar{\rho}_m \cdot u_*^2}$

Remarks: Group a-1 (Erodible flat sediment layer on the bottom => capacity-flow)  
Laboratory channel, aspect ratio=  $B/h = 5.0$   
Small reference concentration  $\bar{c}_{sa} = 36.04$  [kg/m³] = 0.014 [m³/m³] < 0.05 [m³/m³] => Rouse eq.  
Instantaneous velocity and concentration measured with the APFP ultrasonic instrument  
The calibration of the APFP instrument has been made measuring by suction the concentration distribution (shown here).  
Thickness of the sediment layer ≈ 2 [mm]  
Subcritical flow

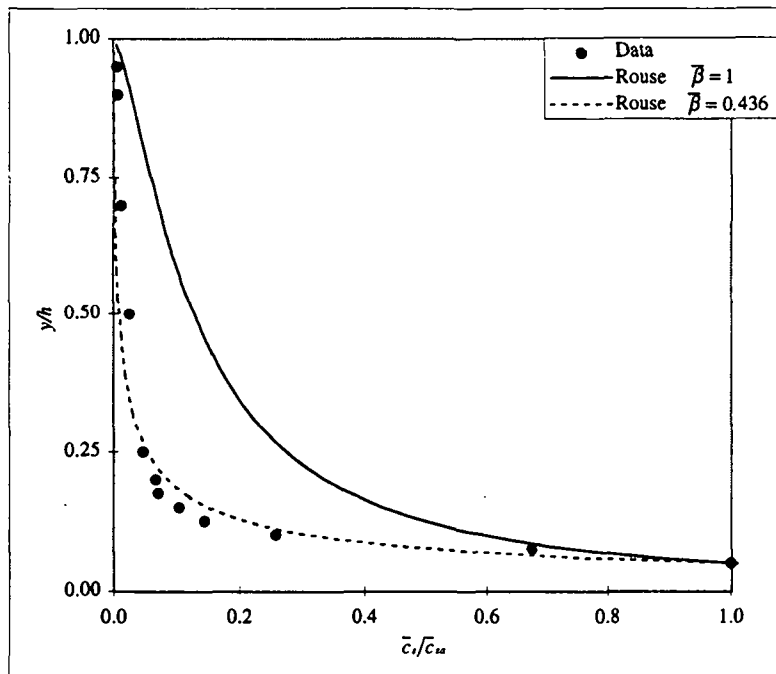
EPFL, (1997)

## Sediment concentration distribution

Run	Q55S015	Sand particles	$d = 0.135$ [mm]	Group	a-1
-----	---------	----------------	------------------	-------	-----

$y$ [cm]	$y/h$ [-]	$\bar{c}_s^m$ [kg/m³]	$\bar{c}_s$ (volum.) [%]	$\bar{c}_s/\bar{c}_{sa}$ [-]	Calculated				
					Rouse eq. $\beta = 1$ $\bar{c}_s/\bar{c}_{sa}$ [-]	Rouse eq. $\beta \neq 1$ $\bar{c}_s/\bar{c}_{sa}$ [-]	Hunt eq. $\beta \neq 1$ $\bar{c}_s/\bar{c}_{sa}$ [-]	$\bar{c}_s^m \cdot y/h$ [kg/m³]	$\rho_m$ [kg/m³]
0.60	0.05	46.06	1.74	1.000	1.000	1.000	1.000	2.30E+00	1028.68
0.90	0.08	31.07	1.17	0.675	0.740	0.501	0.511	7.77E-01	1019.34
1.20	0.10	11.89	0.45	0.258	0.594	0.303	0.311	2.97E-01	1007.41
1.50	0.13	6.65	0.25	0.144	0.498	0.202	0.209	1.66E-01	1004.14
1.80	0.15	4.79	0.18	0.104	0.430	0.144	0.149	1.20E-01	1002.98
2.10	0.18	3.24	0.12	0.070	0.378	0.107	0.111	8.10E-02	1002.02
2.40	0.20	3.06	0.12	0.066	0.337	0.083	0.086	7.66E-02	1001.91
3.00	0.25	2.13	0.08	0.046	0.276	0.052	0.054	1.06E-01	1001.32
6.00	0.50	1.17	0.04	0.025	0.128	0.009	0.000	2.93E-01	1000.73
8.40	0.70	0.55	0.02	0.012	0.071	0.002	0.000	1.10E-01	1000.34
10.80	0.90	0.30	0.01	0.006	0.028	0.000	0.000	5.93E-02	1000.18
11.40	0.95	0.23	0.01	0.005	0.016	0.000	0.000	1.13E-02	1000.14

Depth aver.  $\bar{C}_s^m = 4.40$  [kg/m³]  
 Depth aver.  $\bar{\rho}_m = 1002.74$  [kg/m³]



$h = 0.12$  [m]  
 $S$  (Bed slope) =  $1.50E-3$  [-]  
 $u_* = 0.043$  [m/s]  
 $\kappa = 0.4$  [-]  
 $U = 0.858$  [m/s]  
 $Fr = 0.79$  [-]  
 $a$  (refer.) = 0.006 [m]  
 $\bar{c}_s^m = 46.06$  [kg/m³]  
 $\bar{c}_{sa} = \bar{c}_s^m / \rho_s = 0.017$  [m³/m³]  
 $\rho_s = 2650$  [kg/m³]  
 $v_u = 0.012$  [m/s]  
 $z = v_u / (\kappa U) = 0.698$  [-]

Best fitting on  $\beta$  (Rouse equation)  
 $\beta = 0.436$

$Ri = 18.12$  [-]  
 $Ri [-] = \frac{gh[\rho_s(y=a) - \rho_s(y=h)]}{\bar{\rho}_m \cdot u_*^2}$

Remarks: Group a-1 (Erodible flat sediment layer on the bottom => capacity-flow)  
 Laboratory channel, aspect ratio =  $B/h = 5.0$   
 Small reference concentration  $\bar{c}_s^m = 46.06$  [kg/m³] = 0.017 [m³/m³] < 0.05 [m³/m³] => Rouse eq.  
 Instantaneous velocity and concentration measured with the APFP ultrasonic instrument  
 The calibration of the APFP instrument has been made measuring by suction the concentration distribution (shown here).  
 Thickness of the sediment layer ≈ 2 [mm]  
 Subcritical flow

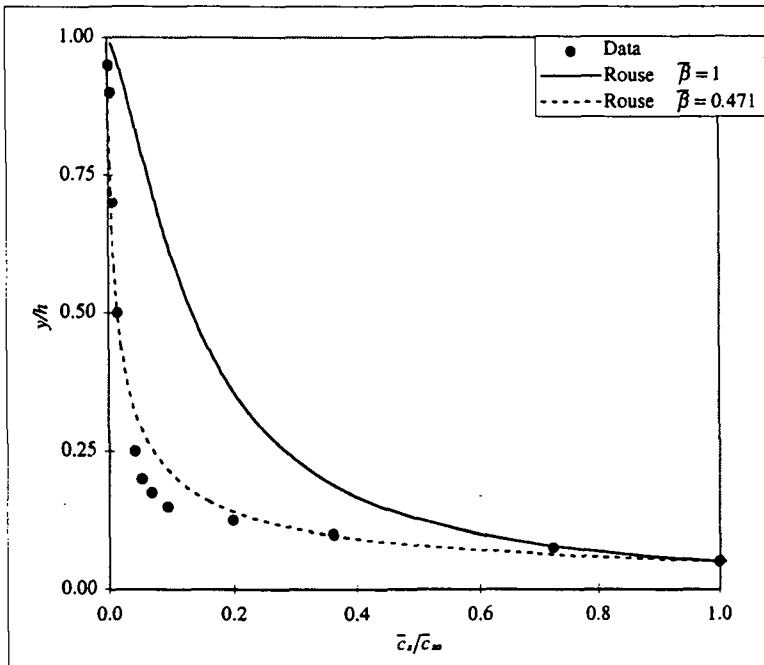
EPFL, (1997)

## Sediment concentration distribution

Run	Q57S0175	Sand particles	$d = 0.135$ [mm]	Group	a-1
-----	----------	----------------	------------------	-------	-----

$y$ [cm]	$y/h$ [-]	$\bar{c}_s^*$ [kg/m³]	$\bar{c}_s$ (volum.) [%]	$\bar{c}_s/\bar{c}_{ss}$ [-]	Calculated				
					Rouse eq. $\beta = 1$ $\bar{c}_s/\bar{c}_{ss}$ [-]	Rouse eq. $\beta \neq 1$ $\bar{c}_s/\bar{c}_{ss}$ [-]	Hunt eq. $\beta \neq 1$ $\bar{c}_s/\bar{c}_{ss}$ [-]	$\bar{c}_s^* \cdot y/h$ [kg/m³]	$\rho_m$ [kg/m³]
0.60	0.05	49.41	1.86	1.000	1.000	1.000	1.000	2.47E+00	1030.76
0.90	0.08	35.73	1.35	0.723	0.745	0.535	0.545	8.93E-01	1022.24
1.20	0.10	17.89	0.67	0.362	0.601	0.339	0.348	4.47E-01	1011.14
1.50	0.13	9.87	0.37	0.200	0.506	0.236	0.243	2.47E-01	1006.15
1.80	0.15	4.68	0.18	0.095	0.438	0.174	0.179	1.17E-01	1002.91
2.10	0.18	3.38	0.13	0.068	0.387	0.133	0.138	8.45E-02	1002.10
2.40	0.20	2.60	0.10	0.053	0.346	0.105	0.109	6.50E-02	1001.62
3.00	0.25	2.03	0.08	0.041	0.284	0.069	0.072	1.01E-01	1001.26
6.00	0.50	0.74	0.03	0.015	0.134	0.014	0.000	1.84E-01	1000.46
8.40	0.70	0.37	0.01	0.008	0.075	0.004	0.000	7.47E-02	1000.23
10.80	0.90	0.19	0.01	0.004	0.030	0.001	0.001	3.76E-02	1000.12
11.40	0.95	0.11	0.00	0.002	0.018	0.000	0.000	5.74E-03	1000.07

$$\begin{aligned} \text{Depth aver. } \bar{C}_s^* &= 4.73 \text{ [kg/m}^3\text{]} \\ \text{Depth aver. } \bar{\rho}_m &= 1002.95 \text{ [kg/m}^3\text{]} \end{aligned}$$



$$\begin{aligned} h &= 0.12 \text{ [m]} \\ S (\text{Bed slope}) &= 1.75E-3 \text{ [-]} \\ u_* &= 0.044 \text{ [m/s]} \\ \kappa &= 0.4 \text{ [-]} \\ U &= 0.855 \text{ [m/s]} \\ Fr &= 0.79 \text{ [-]} \\ a (\text{refer.}) &= 0.006 \text{ [m]} \\ \bar{c}_s^* &= 49.41 \text{ [kg/m}^3\text{]} \\ \bar{c}_{ss} &= \bar{c}_s^*/\rho_m = 0.019 \text{ [m}^3/\text{m}^3\text{]} \\ \rho_m &= 2650 \text{ [kg/m}^3\text{]} \\ v_u &= 0.012 \text{ [m/s]} \\ z &= v_u/(u_* \kappa) = 0.682 \text{ [-]} \end{aligned}$$

Best fitting on  $\beta$  (Rouse equation)  
 $\bar{\beta} = 0.471$

$$Ri = 18.61 \text{ [-]}$$

$$Ri [-] = \frac{gh[\rho_m(y=a) - \rho_m(y=h)]}{\bar{\rho}_m \cdot u_*^2}$$

Remarks: Group a-1 (Erodible flat sediment layer on the bottom => capacity-flow)  
Laboratory channel, aspect ratio =  $B/h = 5.0$   
Small reference concentration  $\bar{c}_s^* = 49.41 \text{ [kg/m}^3\text{]} = 0.019 \text{ [m}^3/\text{m}^3\text{]} < 0.05 \text{ [m}^3/\text{m}^3\text{]} =>$  Rouse eq.  
Instantaneous velocity and concentration measured with the APFP ultrasonic instrument  
The calibration of the APFP instrument has been made measuring by suction the concentration distribution (shown here).  
Thickness of the sediment layer  $\approx 2 \text{ [mm]}$   
Subcritical flow

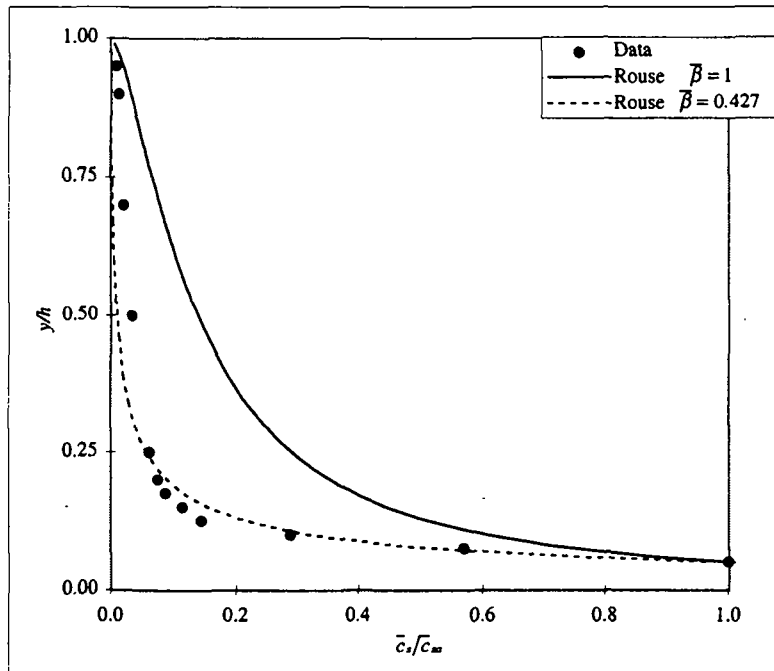
EPFL, (1997)

## Sediment concentration distribution

Run	Q60S02	Sand particles	$d = 0.135$ [mm]	Group	a-1
-----	--------	----------------	------------------	-------	-----

$y$ [cm]	$y/h$ [-]	$\bar{c}_s^m$ [kg/m³]	$\bar{c}_s$ (volum.) [%]	$\bar{c}_s/\bar{c}_{so}$ [-]	Calculated				
					Rouse eq. $\beta = 1$	Rouse eq. $\beta \neq 1$	Hunt eq. $\beta \neq 1$	$\bar{c}_s \cdot y/h$ [kg/m³]	$\rho_m$ [kg/m³]
0.60	0.05	48.58	1.83	1.000	1.000	1.000	1.000	2.43E+00	1030.25
0.90	0.08	27.68	1.04	0.570	0.750	0.509	0.520	6.92E-01	1017.23
1.20	0.10	14.02	0.53	0.289	0.608	0.311	0.321	3.51E-01	1008.73
1.50	0.13	7.04	0.27	0.145	0.514	0.210	0.218	1.76E-01	1004.38
1.80	0.15	5.62	0.21	0.116	0.446	0.151	0.157	1.41E-01	1003.50
2.10	0.18	4.27	0.16	0.088	0.395	0.113	0.118	1.07E-01	1002.66
2.40	0.20	3.70	0.14	0.076	0.354	0.088	0.091	9.25E-02	1002.30
3.00	0.25	3.02	0.11	0.062	0.292	0.056	0.058	1.51E-01	1001.88
6.00	0.50	1.64	0.06	0.034	0.140	0.010	0.000	4.10E-01	1001.02
8.40	0.70	1.01	0.04	0.021	0.080	0.003	0.000	2.02E-01	1000.63
10.80	0.90	0.59	0.02	0.012	0.032	0.000	0.000	1.18E-01	1000.37
11.40	0.95	0.42	0.02	0.009	0.020	0.000	0.000	2.10E-02	1000.26

Depth aver.	$\bar{c}_s^m =$	4.89 [kg/m³]
Depth aver.	$\bar{\rho}_m =$	1003.04 [kg/m³]



$h = 0.12$ [m]
$S$ (Bed slope) = $2.00E-3$ [-]
$u_* = 0.045$ [m/s]
$\kappa = 0.4$ [-]
$U = 0.905$ [m/s]
$Fr = 0.83$ [-]
$a$ (refer.) = 0.006 [m]
$\bar{c}_{so} = 48.58$ [kg/m³]
$\bar{c}_s = \bar{c}_{so}/\rho_s = 0.018$ [ $m^3/m^3$ ]
$\rho_s = 2650$ [kg/m³]
$v_u = 0.012$ [m/s]
$z = v_u/(\kappa U) = 0.667$ [-]

Best fitting on  $\beta$  (Rouse equation)

$$\bar{\beta} = 0.427$$

$Ri = 17.38$ [-]
$Ri [-] = \frac{gh[\rho_m(y=a) - \rho_m(y=h)]}{\bar{\rho}_m \cdot u_*^2}$

Remarks: Group a-1 (Erodible flat sediment layer on the bottom => capacity-flow)  
Laboratory channel, aspect ratio =  $B/h = 5.0$   
Small reference concentration  $\bar{c}_{so} = 48.58$  [kg/m³] =  $0.018$  [ $m^3/m^3$ ] <  $0.05$  [ $m^3/m^3$ ] => Rouse eq.  
Instantaneous velocity and concentration measured with the APFP ultrasonic instrument  
The calibration of the APFP instrument has been made measuring by suction the concentration distribution (shown here).  
Thickness of the sediment layer  $\geq 2$  [mm]  
Subcritical flow

EPFL, (1997)

## Sediment concentration distribution

Run Q65S0225

Sand particles

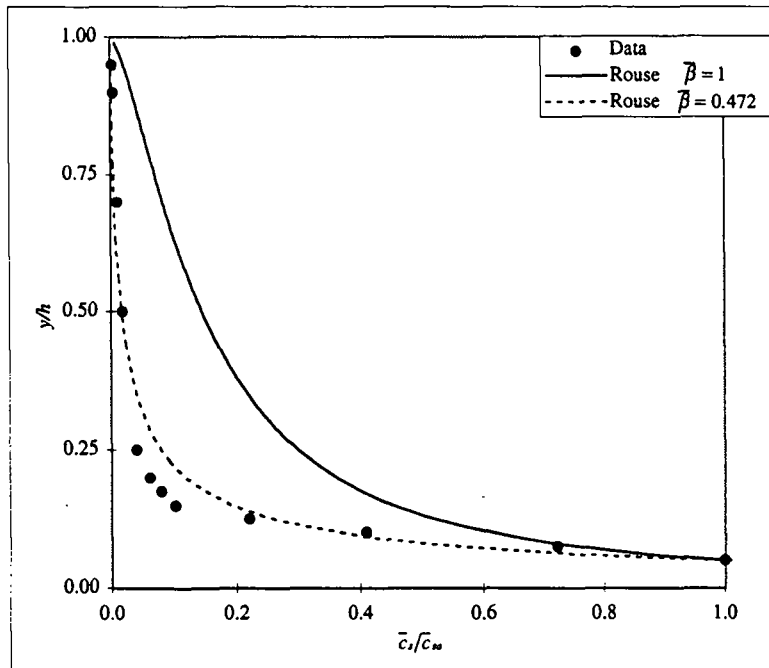
d = 0.135 [mm]

Group a-1

y [cm]	y/h [-]	$\bar{c}_s^m$ [kg/m³]	$\bar{c}_s$ (volum.) [%]	$\bar{c}_s/\bar{c}_{so}$ [-]	Calculated				
					Rouse eq. $\beta = 1$ $\bar{c}_s/\bar{c}_{so}$ [-]	Rouse eq. $\beta \neq 1$ $\bar{c}_s/\bar{c}_{so}$ [-]	Hunt eq. $\beta \neq 1$ $\bar{c}_s/\bar{c}_{so}$ [-]	$\bar{c}_s^m \cdot y/h$ [kg/m³]	$\rho_m$ [kg/m³]
0.60	0.05	50.82	1.92	1.000	1.000	1.000	1.000	2.54E+00	1031.64
0.90	0.08	36.67	1.38	0.722	0.754	0.550	0.560	9.17E-01	1022.84
1.20	0.10	20.89	0.79	0.411	0.614	0.356	0.366	5.22E-01	1013.01
1.50	0.13	11.22	0.42	0.221	0.521	0.252	0.259	2.80E-01	1006.98
1.80	0.15	5.26	0.20	0.104	0.454	0.188	0.194	1.32E-01	1003.28
2.10	0.18	4.14	0.16	0.081	0.403	0.146	0.151	1.03E-01	1002.58
2.40	0.20	3.19	0.12	0.063	0.362	0.116	0.120	7.97E-02	1001.98
3.00	0.25	2.08	0.08	0.041	0.300	0.078	0.081	1.04E-01	1001.30
6.00	0.50	0.96	0.04	0.019	0.147	0.017	0.000	2.39E-01	1000.60
8.40	0.70	0.52	0.02	0.010	0.084	0.005	0.000	1.04E-01	1000.33
10.80	0.90	0.21	0.01	0.004	0.035	0.001	0.001	4.15E-02	1000.13
11.40	0.95	0.17	0.01	0.003	0.021	0.000	0.000	8.31E-03	1000.10

$$\text{Depth aver. } \bar{c}_s^m = 5.07 \text{ [kg/m}^3\text{]}$$

$$\text{Depth aver. } \rho_m = 1003.16 \text{ [kg/m}^3\text{]}$$



$$\begin{aligned}
 h &= 0.12 \text{ [m]} \\
 S (\text{Bed slope}) &= 2.25E-3 \text{ [-]} \\
 u_* &= 0.046 \text{ [m/s]} \\
 \kappa &= 0.4 \text{ [-]} \\
 U &= 0.916 \text{ [m/s]} \\
 Fr &= 0.84 \text{ [-]} \\
 a (\text{refer.}) &= 0.006 \text{ [m]} \\
 \bar{c}_s^m &= 50.82 \text{ [kg/m}^3\text{]} \\
 \bar{c}_{so} &= \bar{c}_s^m / \rho_m = 0.019 \text{ [m}^3\text{/m}^3\text{]} \\
 \rho_m &= 2650 \text{ [kg/m}^3\text{]} \\
 v_u &= 0.012 \text{ [m/s]} \\
 z = v_u / (\kappa u) &= 0.652 \text{ [-]}
 \end{aligned}$$

Best fitting on  $\beta$  (Rouse equation)

$$\bar{\beta} = 0.472$$

$$\begin{aligned}
 Ri &= 17.49 \text{ [-]} \\
 Ri [-] &= \frac{g h [\rho_m(y=a) - \rho_m(y=h)]}{\bar{\rho}_m \cdot u_*^2}
 \end{aligned}$$

Remarks: Group a-1 (Erodible flat sediment layer on the bottom => capacity-flow)  
Laboratory channel, aspect ratio=  $B/h = 5.0$   
Small reference concentration  $\bar{c}_{so} = 50.82 \text{ [kg/m}^3\text{]} = 0.019 \text{ [m}^3\text{/m}^3\text{]} < 0.05 \text{ [m}^3\text{/m}^3\text{]}$  => Rouse eq.  
Instantaneous velocity and concentration measured with the APFP ultrasonic instrument  
The calibration of the APFP instrument has been made measuring by suction the concentration distribution (shown here).  
Thickness of the sediment layer  $\approx 2 \text{ [mm]}$   
Subcritical flow

EPFL, (1997)

## Sediment concentration distribution

Run Q70S025

Sand particles

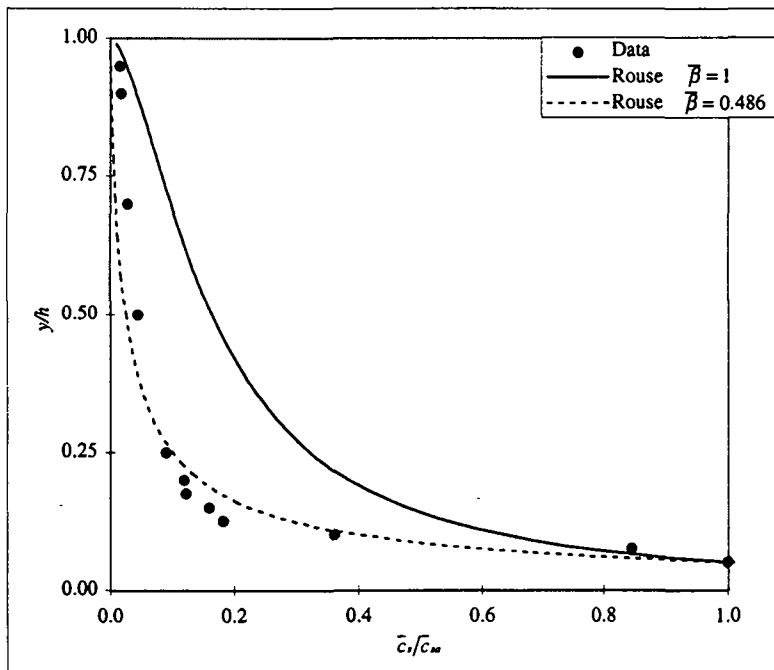
d= 0.135 [mm]

Group a-1

y [cm]	y/h [-]	$\bar{c}_r^*$ [kg/m³]	$\bar{c}_s$ (volum.) [%]	$\bar{c}_s/\bar{c}_{ss}$ [-]	Calculated				
					Rouse eq. $\beta = 1$ $\bar{c}_s/\bar{c}_{ss}$ [-]	Rouse eq. $\beta \neq 1$ $\bar{c}_s/\bar{c}_{ss}$ [-]	Hunt eq. $\beta \neq 1$ $\bar{c}_s/\bar{c}_{ss}$ [-]	$\bar{c}_r^* \cdot y/h$ [kg/m³]	$\rho_m$ [kg/m³]
0.60	0.05	50.04	1.89	1.000	1.000	1.000	1.000	2.50E+00	1031.16
0.90	0.08	42.33	1.60	0.846	0.768	0.580	0.590	1.06E+00	1026.36
1.20	0.10	18.09	0.68	0.362	0.633	0.390	0.399	4.52E-01	1011.26
1.50	0.13	9.16	0.35	0.183	0.543	0.284	0.292	2.29E-01	1005.70
1.80	0.15	7.99	0.30	0.160	0.477	0.218	0.225	2.00E-01	1004.97
2.10	0.18	6.11	0.23	0.122	0.426	0.173	0.178	1.53E-01	1003.80
2.40	0.20	5.98	0.23	0.119	0.385	0.140	0.145	1.49E-01	1003.72
3.00	0.25	4.51	0.17	0.090	0.323	0.098	0.101	2.25E-01	1002.81
6.00	0.50	2.21	0.08	0.044	0.165	0.024	0.000	5.54E-01	1001.38
8.40	0.70	1.41	0.05	0.028	0.098	0.008	0.000	2.82E-01	1000.88
10.80	0.90	0.89	0.03	0.018	0.043	0.002	0.002	1.78E-01	1000.55
11.40	0.95	0.76	0.03	0.015	0.027	0.001	0.001	3.80E-02	1000.47

$$\text{Depth aver. } \bar{C}_r^* = 6.02 \text{ [kg/m}^3\text{]}$$

$$\text{Depth aver. } \bar{\rho}_m = 1003.75 \text{ [kg/m}^3\text{]}$$



$h = 0.12 \text{ [m]}$   
 $S (\text{Bed slope}) = 2.50E-3 \text{ [-]}$   
 $u_* = 0.049 \text{ [m/s]}$   
 $\kappa = 0.4 \text{ [-]}$   
 $U = 0.917 \text{ [m/s]}$   
 $Fr = 0.85 \text{ [-]}$   
 $a (\text{refer.}) = 0.006 \text{ [m]}$   
 $\bar{c}_{ss} = 50.04 \text{ [kg/m}^3\text{]}$   
 $\bar{c}_s = \bar{c}_{ss}/\rho_m = 0.019 \text{ [m}^3/\text{m}^3\text{]}$   
 $\rho_m = 2650 \text{ [kg/m}^3\text{]}$   
 $v_{ss} = 0.012 \text{ [m/s]}$   
 $z = v_{ss}/(\kappa u_*) = 0.612 \text{ [-]}$

Best fitting on  $\beta$  (Rouse equation)

$$\beta = 0.486$$

$Ri = 14.99 \text{ [-]}$   
 $Ri [-] = \frac{gh[\rho_m(y=a) - \rho_m(y=h)]}{\bar{\rho}_m \cdot u_*^2}$

Remarks: Group a-1 (Erodible flat sediment layer on the bottom => capacity-flow)  
 Laboratory channel, aspect ratio=  $B/h = 5.0$   
 Small reference concentration  $\bar{c}_{ss} = 50.04 \text{ [kg/m}^3\text{]} = 0.019 \text{ [m}^3/\text{m}^3\text{]} < 0.05 \text{ [m}^3/\text{m}^3\text{]} =>$  Rouse eq.  
 Instantaneous velocity and concentration measured with the APFP ultrasonic instrument  
 The calibration of the APFP instrument has been made measuring by suction the concentration distribution (shown here).  
 Thickness of the sediment layer  $\approx 2 \text{ [mm]}$   
 Subcritical flow

EPFL, (1997)

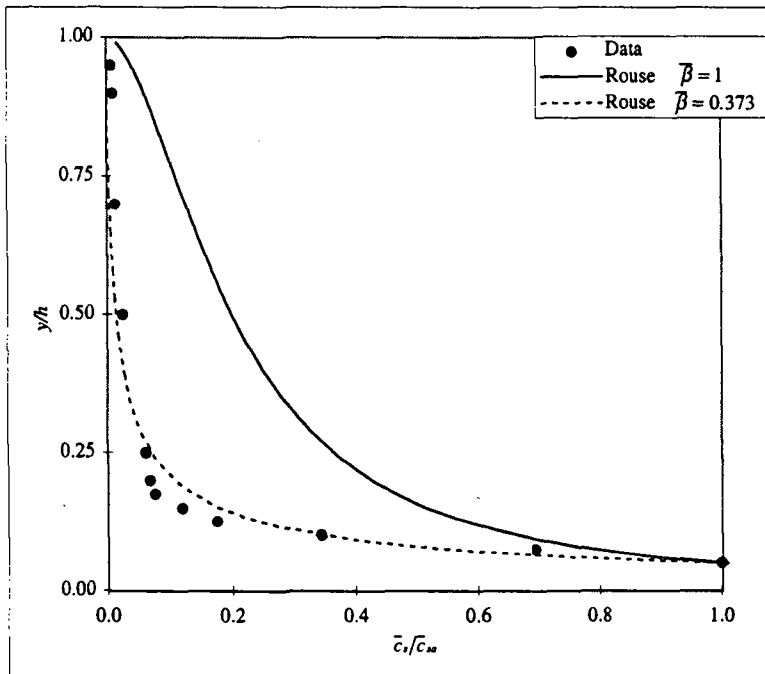
## Sediment concentration distribution

Run Q75S03 | Sand particles |  $d = 0.135$  [mm] | Group a-1

$y$ [cm]	$y/h$ [--]	$\bar{c}_s$ [kg/m³]	$\bar{c}_s$ (volum.) [%]	$\bar{c}_s/\bar{c}_{ss}$ [--]	Calculated				
					Rouse eq. $\beta = 1$ $\bar{c}_s/\bar{c}_{ss}$ [--]	Rouse eq. $\beta \neq 1$ $\bar{c}_s/\bar{c}_{ss}$ [--]	Hunt eq. $\beta \neq 1$ $\bar{c}_s/\bar{c}_{ss}$ [--]	$\bar{c}_s \cdot y/h$ [kg/m³]	$\rho_m$ [kg/m³]
0.60	0.05	62.47	2.36	1.000	1.000	1.000	1.000	3.12E+00	1038.90
0.90	0.08	43.34	1.64	0.694	0.790	0.532	0.547	1.08E+00	1026.99
1.20	0.10	21.47	0.81	0.344	0.665	0.335	0.350	5.37E-01	1013.37
1.50	0.13	10.94	0.41	0.175	0.580	0.232	0.244	2.73E-01	1006.81
1.80	0.15	7.48	0.28	0.120	0.517	0.170	0.180	1.87E-01	1004.66
2.10	0.18	4.70	0.18	0.075	0.468	0.130	0.138	1.18E-01	1002.93
2.40	0.20	4.21	0.16	0.067	0.427	0.102	0.108	1.05E-01	1002.62
3.00	0.25	3.85	0.15	0.062	0.365	0.067	0.071	1.93E-01	1002.40
6.00	0.50	1.52	0.06	0.024	0.201	0.013	0.000	3.81E-01	1000.95
8.40	0.70	0.87	0.03	0.014	0.126	0.004	0.000	1.74E-01	1000.54
10.80	0.90	0.57	0.02	0.009	0.061	0.001	0.001	1.14E-01	1000.36
11.40	0.95	0.47	0.02	0.008	0.040	0.000	0.000	2.36E-02	1000.29

$$\text{Depth aver. } \bar{c}_s = 6.31 \text{ [kg/m}^3\text{]}$$

$$\text{Depth aver. } \bar{\rho}_m = 1003.93 \text{ [kg/m}^3\text{]}$$



$h = 0.12$  [m]  
 $S(\text{Bed slope}) = 3.00E-3$  [--]  
 $u_* = 0.055$  [m/s]  
 $\kappa = 0.4$  [--]  
 $U = 0.897$  [m/s]  
 $Fr = 0.83$  [--]  
 $a(\text{refer.}) = 0.006$  [m]  
 $\bar{c}_{ss} = 62.47$  [kg/m³]  
 $\bar{c}_{ss} = \bar{c}_s / \rho_m = 0.024$  [m³/m³]  
 $\rho_s = 2650$  [kg/m³]  
 $v_n = 0.012$  [m/s]  
 $z = v_n / (\kappa u_*) = 0.545$  [--]

Best fitting on  $\beta$  (Rouse equation)

$$\bar{\beta} = 0.373$$

$$Ri = 14.96 \text{ [--]}$$

$$Ri [-] = \frac{gh[\rho_m(y=a) - \rho_m(y=h)]}{\bar{\rho}_m \cdot u_*^2}$$

Remarks: Group a-1 (Erodible flat sediment layer on the bottom => capacity-flow)  
 Laboratory channel, aspect ratio=  $B/h = 5.0$   
 Small reference concentration  $\bar{c}_s = 62.47$  [kg/m³] = 0.024 [m³/m³] < 0.05 [m³/m³] => Rouse eq.  
 Instantaneous velocity and concentration measured with the APFP ultrasonic instrument  
 The calibration of the APFP instrument has been made measuring by suction the concentration distribution (shown here).  
 Thickness of the sediment layer  $\approx 2$  [mm]  
 Subcritical flow

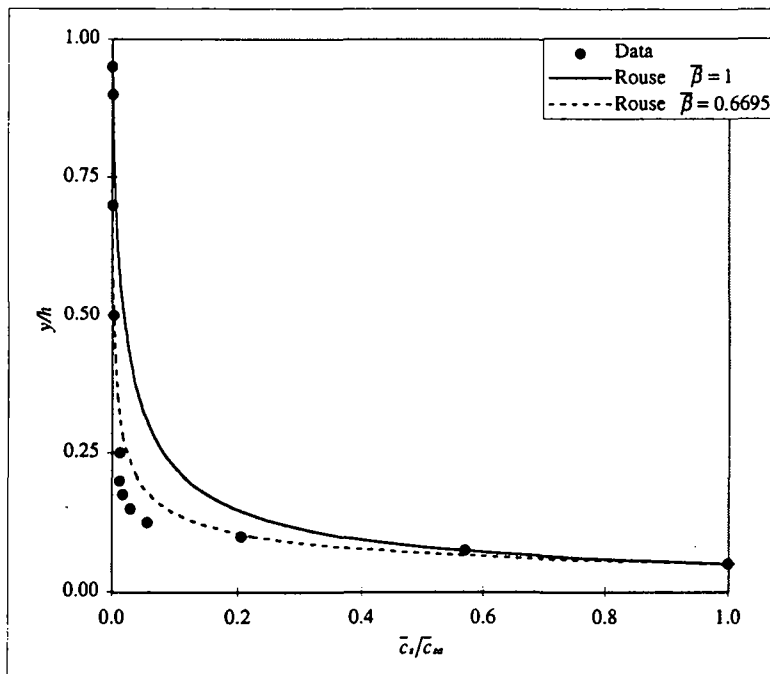
EPFL, (1998)

## Sediment concentration distribution

Run	Q50S01_II	Sand particles	$d = 0.230$ [mm]	Group a-1
-----	-----------	----------------	------------------	-----------

$y$ [cm]	$y/h$ [-]	$\bar{c}_s$ [kg/m³]	$\bar{c}_s$ (volum.) [%]	$\bar{c}_s/\bar{c}_{s0}$ [-]	Calculated				
					Rouse eq. $\beta = 1$ $\bar{c}_s/\bar{c}_{s0}$ [-]	Rouse eq. $\beta \neq 1$ $\bar{c}_s/\bar{c}_{s0}$ [-]	Hunt eq. $\beta \neq 1$ $\bar{c}_s/\bar{c}_{s0}$ [-]	$\bar{c}_s \cdot y/h$ [kg/m³]	$\rho_m$ [kg/m³]
0.60	0.05	21.31	0.80	1.000	1.000	1.000	1.000	1.07E+00	1013.27
0.90	0.08	12.14	0.46	0.570	0.559	0.419	0.422	3.04E-01	1007.56
1.20	0.10	4.37	0.16	0.205	0.366	0.223	0.225	1.09E-01	1002.72
1.50	0.13	1.21	0.05	0.057	0.261	0.134	0.136	3.03E-02	1000.76
1.80	0.15	0.63	0.02	0.030	0.196	0.088	0.089	1.58E-02	1000.39
2.10	0.18	0.38	0.01	0.018	0.153	0.061	0.061	9.53E-03	1000.24
2.40	0.20	0.28	0.01	0.013	0.123	0.044	0.044	6.91E-03	1000.17
3.00	0.25	0.26	0.01	0.012	0.083	0.024	0.025	1.32E-02	1000.16
6.00	0.50	0.05	0.00	0.002	0.019	0.003	0.003	1.15E-02	1000.03
8.40	0.70	0.03	0.00	0.001	0.006	0.000	0.000	5.02E-03	1000.02
10.80	0.90	0.02	0.00	0.001	0.001	0.000	0.000	3.18E-03	1000.01
11.40	0.95	0.01	0.00	0.000	0.000	0.000	0.000	5.10E-04	1000.01

Depth aver.  $\bar{C}_s = 1.57$  [kg/m³]  
 Depth aver.  $\rho_m = 1000.98$  [kg/m³]



$h = 0.12$  [m]  
 $S$  (Bed slope) =  $1.00E-3$  [-]  
 $u_* = 0.039$  [m/s]  
 $\kappa = 0.4$  [-]  
 $U = 0.801$  [m/s]  
 $Fr = 0.74$  [-]  
 $a$  (refer.) = 0.006 [m]  
 $\bar{c}_{s0} = 21.31$  [kg/m³]  
 $\bar{c}_{s0} = \bar{c}_s / \rho_s = 0.008$  [m³/m³]  
 $\rho_s = 2650$  [kg/m³]  
 $v_u = 0.021$  [m/s]  
 $z = v_u / (\kappa U) = 1.346$  [-]

Best fitting on  $\beta$  (Rouse equation)

$$\bar{\beta} = 0.6695$$

$Ri = 10.25$  [-]

$$Ri [-] = \frac{gh[\rho_m(y=a) - \rho_m(y=h)]}{\bar{\rho}_m \cdot u_*^2}$$

Remarks: Group a-1 (Erodible flat sediment layer on the bottom => capacity-flow)  
 Laboratory channel, aspect ratio =  $B/h = 5.0$   
 Small reference concentration  $\bar{c}_{s0} = 21.31$  [kg/m³] = 0.008 [m³/m³] < 0.05 [m³/m³] => Rouse eq.  
 Instantaneous velocity and concentration measured with the APFP ultrasonic instrument  
 The calibration of the APFP instrument has been made measuring by suction the concentration distribution (shown here).  
 Thickness of the sediment layer  $\approx 2$  [mm]  
 Subcritical flow

EPFL, (1998)

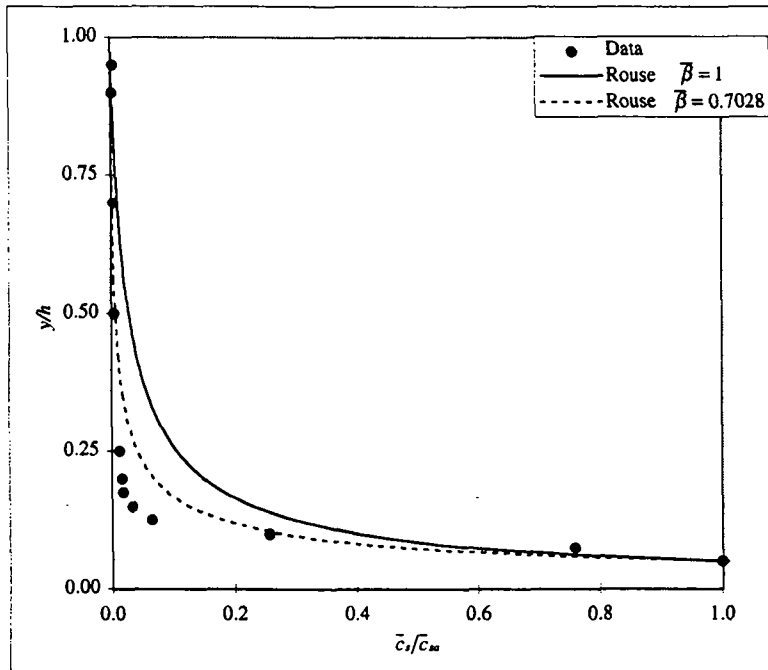
## Sediment concentration distribution

Run	Q55S015_II	Sand particles	$d = 0.230$ [mm]	Group a-1
-----	------------	----------------	------------------	-----------

$y$ [cm]	$y/h$ [-]	$\bar{c}_s^m$ [kg/m³]	$\bar{c}_s$ (volum.) [%]	Measured		Calculated			
				$\bar{c}_s/\bar{c}_{sa}$ [-]	Rouse eq. $\beta = 1$ $\bar{c}_s/\bar{c}_{sa}$ [-]	Rouse eq. $\beta \neq 1$ $\bar{c}_s/\bar{c}_{sa}$ [-]	Hunt eq. $\beta \neq 1$ $\bar{c}_s/\bar{c}_{sa}$ [-]	$\bar{c}_s^m \cdot y/h$ [kg/m³]	$\rho_m$ [kg/m³]
0.60	0.05	28.07	1.06	1.000	1.000	1.000	1.000	1.40E+00	1017.48
0.90	0.08	21.30	0.80	0.759	0.593	0.475	0.479	5.32E-01	1013.26
1.20	0.10	7.21	0.27	0.257	0.405	0.276	0.279	1.80E-01	1004.49
1.50	0.13	1.84	0.07	0.065	0.299	0.179	0.182	4.59E-02	1001.14
1.80	0.15	0.95	0.04	0.034	0.231	0.125	0.126	2.37E-02	1000.59
2.10	0.18	0.54	0.02	0.019	0.185	0.091	0.092	1.34E-02	1000.33
2.40	0.20	0.46	0.02	0.017	0.152	0.068	0.069	1.16E-02	1000.29
3.00	0.25	0.34	0.01	0.012	0.107	0.042	0.042	1.69E-02	1000.21
6.00	0.50	0.13	0.00	0.005	0.028	0.006	0.006	3.27E-02	1000.08
8.40	0.70	0.09	0.00	0.003	0.010	0.001	0.001	1.85E-02	1000.06
10.80	0.90	0.07	0.00	0.003	0.002	0.000	0.000	1.45E-02	1000.05
11.40	0.95	0.08	0.00	0.003	0.001	0.000	0.000	4.21E-03	1000.05

$$\text{Depth aver. } \bar{c}_s^m = 2.30 \text{ [kg/m}^3\text{]}$$

$$\text{Depth aver. } \bar{\rho}_m = 1001.43 \text{ [kg/m}^3\text{]}$$



$h = 0.12$  [m]  
 $S (\text{Bed slope}) = 1.50E-3$  [-]  
 $u_* = 0.043$  [m/s]  
 $\kappa = 0.4$  [-]  
 $U = 0.8333021$  [m/s]  
 $Fr = 0.77$  [-]  
 $a (\text{refer.}) = 0.006$  [m]  
 $\bar{c}_s^m = 28.07$  [kg/m³]  
 $\bar{c}_{sa} = \bar{c}_s^m / \rho_m = 0.011$  [m³/m³]  
 $\rho_m = 2650$  [kg/m³]  
 $v_u = 0.021$  [m/s]  
 $z = v_u / (\kappa U) = 1.210$  [-]

Best fitting on  $\beta$  (Rouse equation)

$$\bar{\beta} = 0.7028$$

$$Ri = 10.87$$
 [-]

$$Ri [-] = \frac{gh[\rho_m(y=a) - \rho_m(y=h)]}{\bar{\rho}_m \cdot u_*^2}$$

Remarks: Group a-1 (Erodible flat sediment layer on the bottom => capacity-flow)  
 Laboratory channel, aspect ratio=  $B/h = 5.0$   
 Small reference concentration  $\bar{c}_s^m = 28.07$  [kg/m³] =  $0.011$  [m³/m³] <  $0.05$  [m³/m³] => Rouse eq.  
 Instantaneous velocity and concentration measured with the APFP ultrasonic instrument  
 The calibration of the APFP instrument has been made measuring by suction the concentration distribution (shown here).  
 Thickness of the sediment layer  $\approx 2$  [mm]  
 Subcritical flow

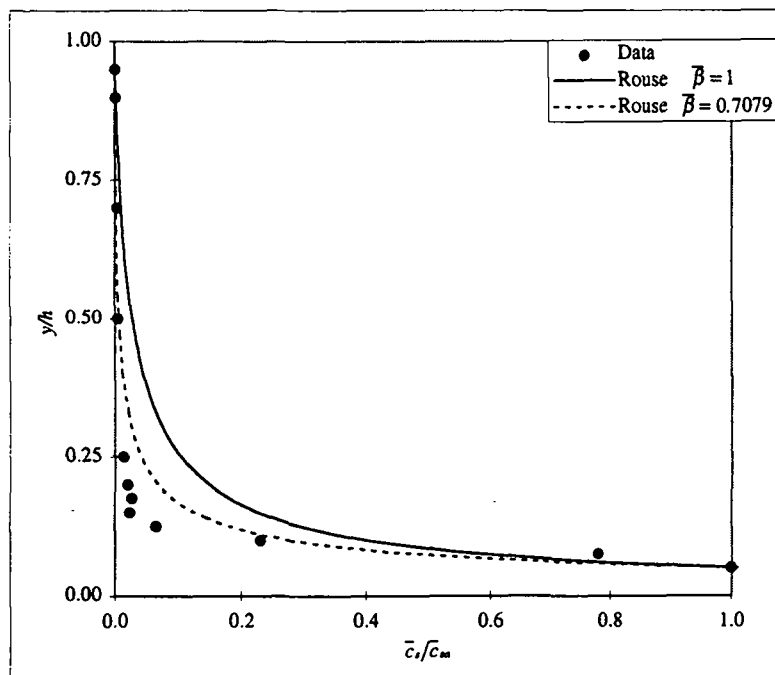
EPFL, (1998)

## Sediment concentration distribution

Run	Q57S0175_II	Sand particles	$d = 0.230$ [mm]	Group	a-1
-----	-------------	----------------	------------------	-------	-----

$y$ [cm]	$y/h$ [-]	$\bar{c}_s$ [kg/m³]	$\bar{c}_s$ (volum.) [%]	Measured		Calculated			
				$\bar{c}_s/\bar{c}_{sa}$ [-]	Rouse eq. $\beta=1$ $\bar{c}_s/\bar{c}_{sa}$ [-]	Rouse eq. $\beta \neq 1$ $\bar{c}_s/\bar{c}_{sa}$ [-]	Hunt eq. $\beta \neq 1$ $\bar{c}_s/\bar{c}_{sa}$ [-]	$\bar{c}_s \cdot y/h$ [kg/m³]	$\rho_m$ [kg/m³]
0.60	0.05	24.77	0.93	1.000	1.000	1.000	1.000	1.24E+00	1015.43
0.90	0.08	19.31	0.73	0.779	0.590	0.475	0.478	4.83E-01	1012.02
1.20	0.10	5.72	0.22	0.231	0.402	0.276	0.278	1.43E-01	1003.56
1.50	0.13	1.62	0.06	0.065	0.295	0.179	0.181	4.05E-02	1001.01
1.80	0.15	0.60	0.02	0.024	0.228	0.124	0.126	1.50E-02	1000.37
2.10	0.18	0.67	0.03	0.027	0.182	0.090	0.091	1.67E-02	1000.42
2.40	0.20	0.49	0.02	0.020	0.149	0.068	0.069	1.22E-02	1000.30
3.00	0.25	0.34	0.01	0.014	0.105	0.041	0.042	1.68E-02	1000.21
6.00	0.50	0.11	0.00	0.004	0.027	0.006	0.006	2.69E-02	1000.07
8.40	0.70	0.07	0.00	0.003	0.010	0.001	0.001	1.34E-02	1000.04
10.80	0.90	0.02	0.00	0.001	0.002	0.000	0.000	4.15E-03	1000.01
11.40	0.95	0.02	0.00	0.001	0.001	0.000	0.000	1.23E-03	1000.02

Depth aver.	$\bar{C}_s = 2.01$ [kg/m³]
Depth aver.	$\rho_m = 1001.25$ [kg/m³]



$h = 0.12$ [m]
$S$ (Bed slope) = $1.75E-3$ [-]
$u_* = 0.043$ [m/s]
$\kappa = 0.4$ [-]
$U = 0.8357956$ [m/s]
$Fr = 0.77$ [-]
$a$ (refer.) = 0.006 [m]
$\bar{c}_{sa} = 24.77$ [kg/m³]
$\bar{c}_{sa} = \bar{c}_s / \rho_m = 0.009$ [m³/m³]
$\rho_m = 2650$ [kg/m³]
$v_u = 0.021$ [m/s]
$z = v_u / (a u^2) = 1.221$ [-]

Best fitting on  $\beta$  (Rouse equation)

$$\bar{\beta} = 0.7079$$

$Ri = 9.80$ [-]
$Ri [-] = \frac{gh[\rho_m(y=a) - \rho_m(y=h)]}{\bar{\rho}_m \cdot u_*^2}$

Remarks: Group a-1 (Erodible flat sediment layer on the bottom => capacity-flow)  
 Laboratory channel, aspect ratio =  $B/h = 5.0$   
 Small reference concentration  $\bar{c}_s = 24.77$  [kg/m³] = 0.009 [m³/m³] < 0.05 [m³/m³] => Rouse eq.  
 Instantaneous velocity and concentration measured with the APPF ultrasonic instrument  
 The calibration of the APPF instrument has been made measuring by suction the concentration distribution (shown here).  
 Thickness of the sediment layer  $\geq 2$  [mm]  
 Subcritical flow

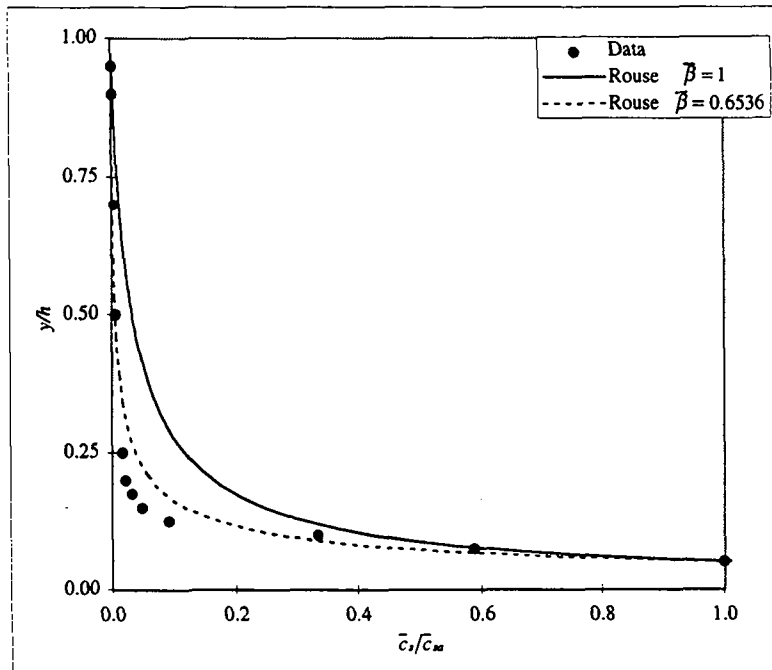
EPFL, (1998)

## Sediment concentration distribution

Run	Q60S02_II	Sand particles	d= 0.230 [mm]	Group	a-1
-----	-----------	----------------	---------------	-------	-----

y [cm]	y/h [-]	$\bar{c}_s^*$ [kg/m³]	$\bar{c}_s$ (volum.) [%]	Measured		Calculated			
				$\bar{c}_s/\bar{c}_{s*}$ [-]	Rouse eq. $\beta = 1$ $\bar{c}_s/\bar{c}_{s*}$ [-]	Rouse eq. $\beta \neq 1$ $\bar{c}_s/\bar{c}_{s*}$ [-]	Hunt eq. $\beta \neq 1$ $\bar{c}_s/\bar{c}_{s*}$ [-]	$\bar{c}_s^* \cdot y/h$ [kg/m³]	$\rho_m$ [kg/m³]
0.60	0.05	23.29	0.88	1.000	1.000	1.000	1.000	1.16E+00	1014.50
0.90	0.08	13.68	0.52	0.587	0.607	0.466	0.469	3.42E-01	1008.52
1.20	0.10	7.78	0.29	0.334	0.421	0.267	0.269	1.95E-01	1004.85
1.50	0.13	2.16	0.08	0.093	0.315	0.171	0.173	5.41E-02	1001.35
1.80	0.15	1.14	0.04	0.049	0.247	0.118	0.119	2.85E-02	1000.71
2.10	0.18	0.75	0.03	0.032	0.200	0.085	0.086	1.88E-02	1000.47
2.40	0.20	0.51	0.02	0.022	0.165	0.064	0.064	1.28E-02	1000.32
3.00	0.25	0.40	0.01	0.017	0.118	0.038	0.039	1.98E-02	1000.25
6.00	0.50	0.15	0.01	0.006	0.033	0.005	0.006	3.63E-02	1000.09
8.40	0.70	0.09	0.00	0.004	0.012	0.001	0.001	1.70E-02	1000.05
10.80	0.90	0.03	0.00	0.001	0.003	0.000	0.000	6.47E-03	1000.02
11.40	0.95	0.03	0.00	0.001	0.001	0.000	0.000	1.30E-03	1000.02

Depth aver.  $\bar{C}_s^* = 1.90$  [kg/m³]  
 Depth aver.  $\rho_m = 1001.18$  [kg/m³]



$h = 0.12$  [m]  
 $S (\text{Bed slope}) = 2.00E-3$  [-]  
 $u_* = 0.045$  [m/s]  
 $\kappa = 0.4$  [-]  
 $U = 0.8496344$  [m/s]  
 $Fr = 0.78$  [-]  
 $a (\text{refer.}) = 0.006$  [m]  
 $\bar{c}_s^* = 23.29$  [kg/m³]  
 $\bar{c}_{s*} = \bar{c}_s^*/\rho_m = 0.009$  [m³/m³]  
 $\rho_m = 2650$  [kg/m³]  
 $v_u = 0.021$  [m/s]  
 $z = v_u/(\kappa u) = 1.156$  [-]

Best fitting on  $\beta$  (Rouse equation)

$$\beta = 0.6536$$

$Ri = 8.26$  [-]

$$Ri [-] = \frac{gh[\rho_m(y=a) - \rho_m(y=h)]}{\bar{\rho}_m \cdot u_*^2}$$

Remarks: Group a-1 (Erodible flat sediment layer on the bottom => capacity-flow)  
 Laboratory channel, aspect ratio=  $B/h = 5.0$   
 Small reference concentration  $\bar{c}_{s*} = 23.29$  [kg/m³] = 0.009 [m³/m³] < 0.05 [m³/m³] => Rouse eq.  
 Instantaneous velocity and concentration measured with the APFP ultrasonic instrument  
 The calibration of the APFP instrument has been made measuring by suction the concentration distribution (shown here).  
 Thickness of the sediment layer  $\approx 2$  [mm]  
 Subcritical flow

EPFL, (1998)

## Sediment concentration distribution

Run Q65S0225\_II

Sand particles

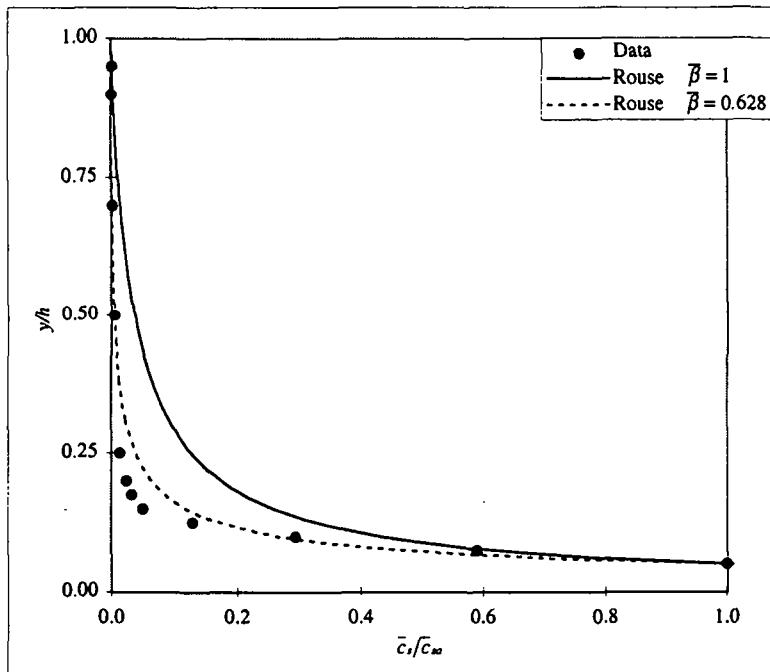
d= 0.230 [mm]

Group a-1

y [cm]	y/h [-]	$\bar{c}_s^m$ [kg/m³]	$\bar{c}_s$ (volum.) [%]	$\bar{c}_s/\bar{c}_{s0}$ [-]	Calculated				
					Rouse eq. $\beta = 1$ $\bar{c}_s/\bar{c}_{s0}$ [-]	Rouse eq. $\beta \neq 1$ $\bar{c}_s/\bar{c}_{s0}$ [-]	Hunt eq. $\beta \neq 1$ $\bar{c}_s/\bar{c}_{s0}$ [-]	$\bar{c}_s^m \cdot y/h$ [kg/m³]	$\rho_m$ [kg/m³]
0.60	0.05	34.36	1.30	1.000	1.000	1.000	1.000	1.72E+00	1021.40
0.90	0.08	20.27	0.77	0.590	0.617	0.464	0.469	5.07E-01	1012.62
1.20	0.10	10.10	0.38	0.294	0.434	0.265	0.269	2.52E-01	1006.29
1.50	0.13	4.44	0.17	0.129	0.328	0.169	0.172	1.11E-01	1002.76
1.80	0.15	1.72	0.06	0.050	0.259	0.116	0.118	4.29E-02	1001.07
2.10	0.18	1.11	0.04	0.032	0.211	0.084	0.085	2.78E-02	1000.69
2.40	0.20	0.81	0.03	0.024	0.175	0.063	0.064	2.03E-02	1000.51
3.00	0.25	0.48	0.02	0.014	0.127	0.038	0.038	2.38E-02	1000.30
6.00	0.50	0.18	0.01	0.005	0.037	0.005	0.005	4.45E-02	1000.11
8.40	0.70	0.08	0.00	0.002	0.014	0.001	0.001	1.55E-02	1000.05
10.80	0.90	0.05	0.00	0.001	0.003	0.000	0.000	1.01E-02	1000.03
11.40	0.95	0.05	0.00	0.001	0.001	0.000	0.000	2.25E-03	1000.03

$$\text{Depth aver. } \bar{c}_s^m = 2.78 \text{ [kg/m}^3\text{]}$$

$$\text{Depth aver. } \bar{\rho}_m = 1001.73 \text{ [kg/m}^3\text{]}$$



$$\begin{aligned}
 h &= 0.12 \text{ [m]} \\
 S (\text{Bed slope}) &= 2.25E-3 \text{ [-]} \\
 u_* &= 0.047 \text{ [m/s]} \\
 \kappa &= 0.4 \text{ [-]} \\
 U &= 0.865246 \text{ [m/s]} \\
 Fr &= 0.80 \text{ [-]} \\
 a (\text{refer.}) &= 0.006 \text{ [m]} \\
 \bar{c}_{s0} &= 34.36 \text{ [kg/m}^3\text{]} \\
 \bar{c}_s &= \bar{c}_{s0}/\rho_m = 0.013 \text{ [m}^3/\text{m}^3\text{]} \\
 \rho_m &= 2650 \text{ [kg/m}^3\text{]} \\
 v_u &= 0.021 \text{ [m/s]} \\
 z &= v_u/(104) = 1.117 \text{ [-]}
 \end{aligned}$$

Best fitting on  $\beta$  (Rouse equation)

$$\bar{\beta} = 0.628$$

$$\begin{aligned}
 Ri &= 11.37 \text{ [-]} \\
 Ri [-] &= \frac{gh[\rho_m(y=a) - \rho_m(y=h)]}{\bar{\rho}_m \cdot u_*^2}
 \end{aligned}$$

Remarks: Group a-1 (Erodible flat sediment layer on the bottom => capacity-flow)  
Laboratory channel, aspect ratio=  $B/h = 5.0$   
Small reference concentration  $\bar{c}_{s0} = 34.36 \text{ [kg/m}^3\text{]} = 0.013 \text{ [m}^3/\text{m}^3\text{]} < 0.05 \text{ [m}^3/\text{m}^3\text{]} =>$  Rouse eq.  
Instantaneous velocity and concentration measured with the APFP ultrasonic instrument  
The calibration of the APFP instrument has been made measuring by suction the concentration distribution (shown here).  
Thickness of the sediment layer  $\approx 2 \text{ [mm]}$   
Subcritical flow

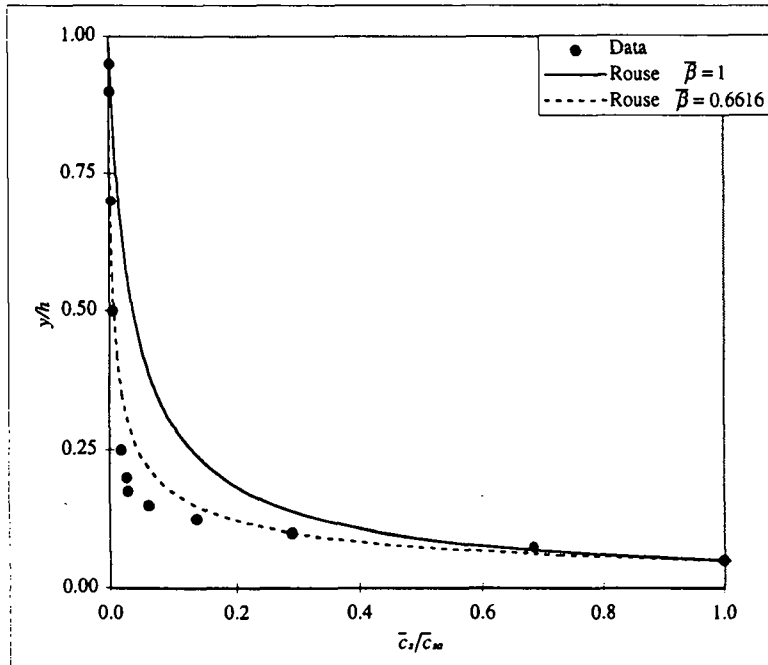
EPFL, (1998)

## Sediment concentration distribution

Run	Q70S025 II	Sand particles	$d = 0.230$ [mm]	Group	a-1
-----	------------	----------------	------------------	-------	-----

$y$ [cm]	$y/h$ [-]	$\bar{c}_s^m$ [kg/m³]	$\bar{c}_s$ (volum.) [%]	Measured		Calculated			
				$\bar{c}_s/\bar{c}_{so}$ [-]	Rouse eq. $\beta = 1$ $\bar{c}_s/\bar{c}_{so}$ [-]	Rouse eq. $\beta \neq 1$ $\bar{c}_s/\bar{c}_{so}$ [-]	Hunt eq. $\beta \neq 1$ $\bar{c}_s/\bar{c}_{so}$ [-]	$\bar{c}_s^m \cdot y/h$ [kg/m³]	$\rho_m$ [kg/m³]
0.60	0.05	33.83	1.28	1.000	1.000	0.487	0.491	1.69E+00	1021.06
0.90	0.08	23.17	0.87	0.685	0.621	0.439	0.288	5.79E-01	1014.43
1.20	0.10	9.82	0.37	0.290	0.137	0.332	0.189	0.292	2.46E-01
1.50	0.13	4.64	0.18	0.063	0.063	0.263	0.133	0.192	1.16E-01
1.80	0.15	2.13	0.08	0.030	0.030	0.215	0.098	0.100	2.57E-02
2.10	0.18	1.03	0.04	0.019	0.019	0.179	0.074	0.076	2.34E-02
2.40	0.20	0.93	0.04	0.015	0.015	0.131	0.046	0.047	1.00E-02
3.00	0.25	0.63	0.02	0.005	0.005	0.039	0.007	0.008	4.22E-02
6.00	0.50	0.17	0.01	0.002	0.002	0.003	0.002	0.002	1000.11
8.40	0.70	0.11	0.00	0.001	0.001	0.003	0.000	0.002	1000.07
10.80	0.90	0.05	0.00	0.001	0.001	0.003	0.000	0.000	1000.03
11.40	0.95	0.04	0.00	0.001	0.002	0.000	0.000	0.000	2.24E-03

Depth aver.	$\bar{c}_s^m = 2.84$ [kg/m³]
Depth aver.	$\rho_m = 1001.77$ [kg/m³]



$h = 0.12$ [m]
$S$ (Bed slope) = $2.50E-3$ [-]
$u_* = 0.048$ [m/s]
$\kappa = 0.4$ [-]
$U = 0.8683168$ [m/s]
$Fr = 0.80$ [-]
$a$ (refer.) = 0.006 [m]
$\bar{c}_s^m = 33.83$ [kg/m³]
$\bar{c}_{so} = \bar{c}_s^m / \rho_s = 0.013$ [ $m^3/m^3$ ]
$\rho_s = 2650$ [kg/m³]
$v_n = 0.021$ [m/s]
$z = v_n / (\kappa U) = 1.103$ [-]

Best fitting on  $\beta$  (Rouse equation)

$$\beta = 0.6616$$

$Ri = 10.91$ [-]
$Ri [-] = \frac{gh[\rho_m(y=a) - \rho_m(y=h)]}{\bar{\rho}_m \cdot u_*^2}$

Remarks: Group a-1 (Erodible flat sediment layer on the bottom => capacity-flow)  
Laboratory channel, aspect ratio =  $B/h = 5.0$   
Small reference concentration  $\bar{c}_{so} = 33.83$  [kg/m³] = 0.013 [ $m^3/m^3$ ] < 0.05 [ $m^3/m^3$ ] => Rouse eq.  
Instantaneous velocity and concentration measured with the APFP ultrasonic instrument  
The calibration of the APFP instrument has been made measuring by suction the concentration distribution (shown here).  
Thickness of the sediment layer ≈ 2 [mm]  
Subcritical flow

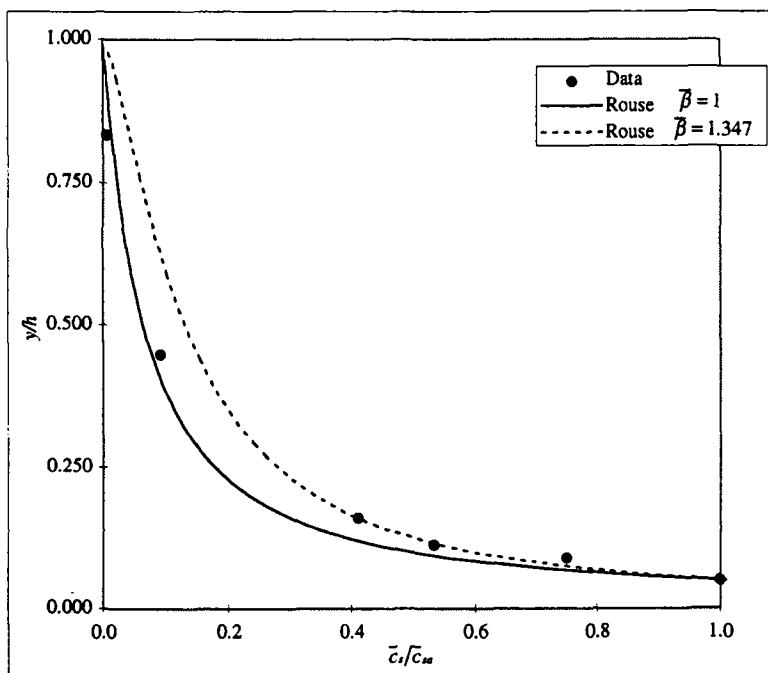
EPFL, (1997)

## Sediment concentration distribution

Run BF\_S015 Sand particles  $d = 0.135 \text{ [mm]}$ 

$y$ [cm]	$y/h$ [-]	$\bar{c}_r^*$ [kg/m³]	$\bar{c}_r$ (volum.) [%]	$\bar{c}_r/\bar{c}_{sa}$ [-]	Calculated				$\rho_m$ [kg/m³]
					Rouse eq. $\beta = 1$ $\bar{c}_r/\bar{c}_{sa}$ [-]	Rouse eq. $\beta \neq 1$ $\bar{c}_r/\bar{c}_{sa}$ [-]	Hunt eq. $\beta \neq 1$ $\bar{c}_r/\bar{c}_{sa}$ [-]	$\bar{c}_r^* \cdot y/h$ [kg/m³]	
0.55	0.050	21.47	0.81	1.000	1.000	1.000	1.000	1.07E+00	1013.37
0.97	0.088	16.12	0.61	0.751	0.567	0.656	0.657	6.13E-01	1010.04
1.23	0.112	11.46	0.43	0.534	0.441	0.544	0.546	2.75E-01	1007.13
1.76	0.160	8.82	0.33	0.411	0.299	0.409	0.410	4.23E-01	1005.49
4.93	0.448	1.93	0.07	0.090	0.077	0.149	0.150	5.57E-01	1001.20
9.15	0.832	0.12	0.00	0.006	0.014	0.042	0.043	6.80E-02	1000.08

$$\begin{aligned} \text{Depth aver. } \bar{c}_r^* &= 3.01 \text{ [kg/m³]} \\ \text{Depth aver. } \bar{\rho}_m &= 1001.87 \text{ [kg/m³]} \end{aligned}$$



$$\begin{aligned} h &= 0.11 \text{ [m]} \\ S (\text{Bed slope}) &= 1.50E-03 \text{ [-]} \\ u_* &= 0.032 \text{ [m/s]} \\ \kappa &= 0.4 \text{ [-]} \\ U &= 0.575 \text{ [m/s]} \\ Fr &= 0.55 \text{ [-]} \\ a (\text{refer.}) &= 0.0055 \text{ [m]} \\ \bar{c}_r^* &= 21.47 \text{ [kg/m³]} \\ \bar{c}_{sa} &= \bar{c}_r^*/\bar{\rho}_m = 0.008 \text{ [m³/m³]} \\ \rho_s &= 2650 \text{ [kg/m³]} \\ v_u &= 0.012 \text{ [m/s]} \\ z &= v_u / (\kappa u) = 0.938 \text{ [-]} \end{aligned}$$

Best fitting on  $\beta$  (Rouse equation)

$$\bar{\beta} = 1.347$$

$$Ri = 13.98 \text{ [-]}$$

$$Ri [-] = \frac{g h [\rho_m(y=a) - \rho_m(y=h)]}{\bar{\rho}_m \cdot u_*^2}$$

Remarks: Group a-2 (Erodible sediment layer on the bottom => capacity-flow)  
 Laboratory channel, aspect ratio =  $B/h = 5.5$   
 Small reference concentration  $\bar{c}_r^* = 21.47 \text{ [kg/m³]} = 0.008 \text{ [m³/m³]} < 0.05 \text{ [m³/m³]} \Rightarrow \text{Rouse eq.}$   
 Instantaneous velocity and concentration measured with the APFP ultrasonic instrument  
 The calibration of the APFP instrument has been made measuring by suction the concentration distribution (shown here).  
 Thickness of the sediment layer:  $\approx 2 \text{ [mm]}$   
 Subcritical flow

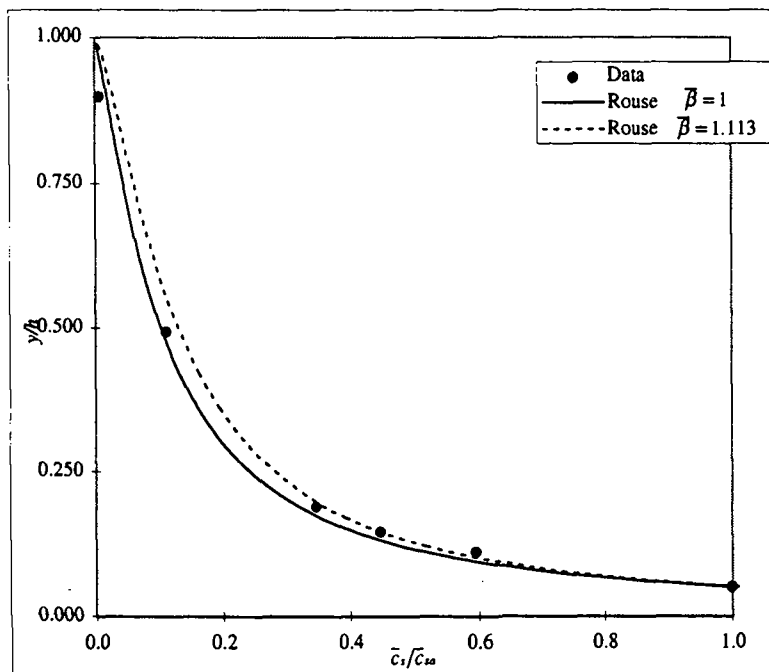
EPFL, (1997)

## Sediment concentration distribution

Run BF\_S02 | Sand particles |  $d = 0.135$  [mm]

$y$ [cm]	$y/h$ [--]	$\bar{c}^*$ [kg/m³]	$\bar{c}_s$ (volum.) [%]	Measured		Calculated			
				$\bar{c}_s/\bar{c}_{\infty}$ [--]	Rouse eq. $\beta = 1$ $\bar{c}_s/\bar{c}_{\infty}$ [--]	Rouse eq. $\beta \neq 1$ $\bar{c}_s/\bar{c}_{\infty}$ [--]	Hunt eq. $\beta \neq 1$ $\bar{c}_s/\bar{c}_{\infty}$ [--]	$\bar{c}^* \cdot y/h$ [kg/m³]	$\rho_m$ [kg/m³]
0.59	0.050	12.69	0.48	1.000	1.000	1.000	1.000	6.34E-01	1007.90
1.30	0.110	7.55	0.28	0.595	0.519	0.554	0.556	4.53E-01	1004.70
1.71	0.145	5.69	0.21	0.449	0.406	0.445	0.446	2.00E-01	1003.55
2.22	0.188	4.38	0.17	0.345	0.320	0.359	0.360	1.88E-01	1002.73
5.82	0.493	1.42	0.05	0.112	0.106	0.133	0.134	4.34E-01	1000.89
10.62	0.900	0.07	0.00	0.006	0.019	0.029	0.029	3.03E-02	1000.05

$$\begin{aligned} \text{Depth aver. } \bar{C}^* &= 1.94 \text{ [kg/m³]} \\ \text{Depth aver. } \bar{\rho}_m &= 1001.21 \text{ [kg/m³]} \end{aligned}$$



$$\begin{aligned} h &= 0.118 \text{ [m]} \\ S (\text{Bed slope}) &= 2.00E-03 \text{ [--]} \\ u_* &= 0.039 \text{ [m/s]} \\ x &\approx 0.4 \text{ [--]} \\ U &= 0.609 \text{ [m/s]} \\ Fr &= 0.57 \text{ [--]} \\ a (\text{refer.}) &= 0.0059 \text{ [m]} \\ \bar{c}_\infty &= 12.69 \text{ [kg/m³]} \\ \bar{c}_s &= \bar{c}_\infty / \rho_i = 0.005 \text{ [m³/m³]} \\ \rho_i &= 2650 \text{ [kg/m³]} \\ v_\mu &= 0.012 \text{ [m/s]} \\ z = v_u / (a u_*) &= 0.769 \text{ [--]} \end{aligned}$$

Best fitting on  $\beta$  (Rouse equation)

$$\beta = 1.113$$

$$Ri = 4.02 \text{ [--]}$$

$$Ri [-] = \frac{gh[\rho_m(y=a) - \rho_m(y=h)]}{\bar{\rho}_m \cdot u_*^2}$$

Remarks: Group a-2 (Erodible sediment layer on the bottom => capacity-flow)  
 Laboratory channel, aspect ratio =  $B/h = 5.5$   
 Small reference concentration  $\bar{c}_\infty = 12.69 \text{ [kg/m³]} = 0.005 \text{ [m³/m³]} < 0.05 \text{ [m³/m³]}$  => Rouse eq.  
 Instantaneous velocity and concentration measured with the APFP ultrasonic instrument  
 The calibration of the APFP instrument has been made measuring by suction the concentration distribution (shown here).  
 Thickness of the sediment layer  $\approx 2 \text{ [mm]}$   
 Subcritical flow



## APPENDIX C

### Velocity and concentration profiles in non-capacity condition

#### C1 Introduction

The distribution of sediments as suspended load is commonly obtained by consideration of the diffusion-convection equation, (see *Graf*, 1984, §8.3). Assuming steady-state condition and one-dimensionality – no change of concentration with respect to the time,  $t$ , to the longitudinal,  $x$ , and to the lateral,  $z$ , direction – the following equation is obtained:

$$v_{ss} \bar{c}_s + \varepsilon_s \frac{\partial \bar{c}_s}{\partial y} = Cte = 0 \quad (C1)$$

The constant of integration is taken as  $Cte=0$ , which does imply that at the water surface,  $\bar{c}_s = 0$ , for  $\varepsilon_s = 0$ . Note that eq. C1 remains reasonably valid for small concentrations, say  $\bar{c}_s < 0.05 \left[ \text{m}^3/\text{m}^3 \right] \cong 132 \left[ \text{kg/m}^3 \right]$ .  $v_{ss}$  is the settling velocity,  $\bar{c}_s(y) = c_s - c'_s$  is the mean suspended particle concentration, where  $c'_s$  is the fluctuation component and  $\varepsilon_s \left[ \text{m}^2/\text{s} \right]$  is the diffusion coefficient of the solid particles;  $y$  is the distance from the bed along the vertical direction.

Above eq. C1 implies that the downward flux due to the gravitational settling,  $v_{ss} \bar{c}_s$ , and the upward sediment flux due to the turbulence of the flow,  $\bar{c}'_s v'$ , are in equilibrium; the latter is commonly expressed as:

$$\bar{c}'_s v' = -\varepsilon_s \frac{\partial \bar{c}_s}{\partial y} \quad (C2)$$

Usually it is admitted the sediment diffusion coefficient,  $\varepsilon_s$ , and the momentum diffusion coefficient – which is nothing else than the turbulent (eddy) viscosity –,  $\varepsilon_m = v_t$ , are closely related, such as:

$$\varepsilon_s = \bar{\beta} \cdot \varepsilon_m \quad (C3)$$

where  $\varepsilon_m$  is defined – using the shear stress,  $-\rho \cdot \overline{u'v'}$  – by:

$$\overline{u'v'} = -\varepsilon_m \frac{\partial \bar{u}}{\partial y} \quad (C4)$$

and  $\bar{\beta}$  is the depth-averaged value of  $\beta(y) = \varepsilon_s(y)/\varepsilon_m(y)$ .

For uniform and unidirectional open-channel flow the vertical distribution of the momentum diffusion coefficient is given (see *Graf*, 1984, p. 173) by:

$$\varepsilon_m = \kappa \cdot u_* \cdot \frac{y}{h} (h - y) \quad (C5)$$

where  $h$  is the flow depth and  $u_*$  is the shear velocity.

Upon substitution of eq. C3 and eq. C5 into the diffusion-convection equation, eq. C1, after separation of the variables and upon integration in parts between the limits,  $a < y < h$ , the well known solution - often referred to as Rouse equation - is obtained, or:

$$\frac{\bar{c}_s}{\bar{c}_{sa}} = \left( \frac{h-y}{y} \frac{a}{h-a} \right)^z \quad (C6)$$

where the Rouse number is defined such as:

$$z = \frac{v_{ss}}{\kappa u_*} \quad \text{or} \quad z' = \frac{v_{ss}}{\beta \kappa u_*} = \frac{z}{\beta} \quad (C7)$$

The reference concentration,  $\bar{c}_{sa}$ , is usually evaluated at  $a = 0.05 \cdot h$ , which represents a vertical position in the flow and falls within the bed-load layer. With such a definition of the reference concentration, the resulting sediment transport as suspended load is in full *capacity* (saturation).

A sediment-laden flow is defined as *capacity* flow when a layer of sediment, composed of the same sediment as is in suspension, is present on the bed. When flow transports the full capacity of sediment - at saturation - one may consider the flow to be in a sedimentary equilibrium, this means that deposited particles can be readily replaced by eroded ones. Any further addition of sediments to the flow leads to a deposition of sediments on the channel bed without an increase of the suspended sediment concentration. If a flow is in *non-capacity* condition there is no active sediment layer on the bed. All the sediments added to the flow are kept suspended. A further addition of sediment to the flow leads to an increase of the sediment concentration without a deposition on the bed. The measurements reported by *Coleman* (1986), made with sediment-laden flow of different concentrations, have shown the importance of the capacity condition.

Data on capacity flow are treated in another part of this investigation (see *Cellino* and *Graf*, 1997, and ch. 3). Interesting results can also be obtained investigating flows carrying only a part of their capacity. Herewith the results of an investigation of flows in non-capacity condition are reported.

The 8 flows investigated varied from clear-water to the capacity (saturated) flow. For each run the instantaneous vertical concentration and velocity profiles are measured by a non-intrusive sonar (APFP) instrument (see *Shen* and *Lemmin*, 1996), while the vertical mean concentration profiles have been also measured by the suction method. Special attention is paid on the evolution of the turbulence characteristics due to an increase of the sediment concentration. The velocity measured appears to be the one of the water/sediment mixture (see *Shen*, 1997 and ch. 3).

## C2 Experimental procedure

The measurements were made in a recirculating tilting channel, 16.8[m] long and 0.60[m] wide. The measurements were performed at the centerline of the measuring section, located

13[m] from the entrance of the channel, where the boundary layer is assumed to be established. The instantaneous velocity and concentration profiles have been measured simultaneously with the APFP instrument (see *Shen* and *Lemmin*, 1996, and *Shen*, 1997) at measuring frequency of 16 [Hz]. In addition, a special (tristatic) configuration of the instrument (see Appendix A) has been used to increase the measuring frequency of the turbulence measurements only, reaching 39 [Hz]. To calibrate the APFP instrument the mean concentration profiles have been measured by the suction method. The samples were drawn with a velocity equal to the one of the fluid surrounding the probe's entrance, thus is isokinetic condition. The sample's mixture was then filtered to obtain the sediment concentration.

Starting with a clear-water flow (run CW\_S015), the measurements were made each after 4[h] of the injection of a certain amount of sediments ( $\approx 10$  [kg]) to the flow (runs SLF1\_S015 up to SLF6\_S015). The channel bed was a plate with an artificial bed, made up of grains of  $d=4.8$  [mm], which was gradually covered with the sediments studied (Sand I) of  $d_{50} = 0.135$  [mm]. The investigation ended when the capacity of the flow was achieved. This last run, SAT\_S015, refers to a capacity flow with presence on the bed of a sand layer nearly 2 [mm] thick. If additional sand is added, the thickness of the bed layer would increase.

In Table C1 are summarized the hydraulic and sediment characteristics as well as the results of the 8 runs. The flow discharge,  $Q$  [ $m^3/s$ ], measured approximately by a magnetic flowmeter, was adjusted to maintain constant the flow depth,  $h$  [m]=0.12 [m]. The aspect ratio,  $B/h$  [-], where  $B=0.6$  [m] is the channel width, is large enough to assume two-dimensional flow. The depth-averaged longitudinal (streamwise) velocity was obtained by integrating the mean velocity profiles,  $\bar{u}(y)$ , over the flow depth,  $U$  [ $m/s$ ]= $\frac{1}{h} \int_0^h \bar{u}(y) \cdot dy$ . The mean velocity profiles (measured at the centerline of the measuring section), were obtained by averaging the instantaneous velocity,  $u$ , over the time; in this way the fluctuating velocity,  $u'$ , is defined, such as  $\bar{u}(y)=u-u'$ . For all runs the bed slope,  $S_b$  [-], was kept constant. The Reynolds numbers,  $Re$  [-]= $\frac{4UR_h}{v_m}$ , where  $R_h$  [m] is the hydraulic radius and  $v_m$  [ $m^2/s$ ] is the kinematic mixture viscosity computed with a formula proposed by Einstein,  $v_m = v \cdot (1 + 2.5 \cdot C_s) \frac{\rho_w}{\rho_m}$  (see

*Graf*, 1984, p. 65), show that all the flows investigated were turbulent. The Froude numbers,  $Fr$  [-]= $U/\sqrt{gh}$ , always less than unity, indicate that the flows were subcritical. The shear velocity,  $u_*$  [ $m/s$ ], was obtained by extrapolating the measured Reynolds-stress profiles towards the bed. The Coles wake strength,  $\Pi$  [-], was obtained by best fitting Coles velocity-defect law (see *Coleman*, 1986, p. 1381, *Hinze*, 1975, p. 697, and *Liggett*, 1994, p.251), given by:

$$\frac{\bar{u}_c - \bar{u}}{u_*} = -\frac{1}{\kappa} \ln\left(\frac{y}{\delta}\right) + \frac{2\pi}{\kappa} \cos^2\left(\frac{\pi \cdot y}{2 \cdot \delta}\right)$$

to the measured velocity profiles. The maximum velocity,  $\bar{u}_c$ , was measured at  $y = \delta$ . The Karman constant was assumed to be  $\kappa[-] = 0.4$  for clear-water and for suspension flow according to the findings of *Coleman*, 1986, p. 1382. The Weisbach-Darcy friction factor,  $f [-] = 8(u_*/U)^2$ , was used to compute the equivalent roughness,  $k_s$  [mm], using the Colebrook and White formula, given as:

$$\sqrt{\frac{1}{f}} = -2 \cdot \log \left( \frac{k_s/R_h}{a_f} + \frac{b_f}{Re \sqrt{f}} \right)$$

with the coefficients  $a_f = 11.5$ ,  $b_f = 3$ , chosen for similar flows (see *Silberman* et al., 1963, pp. 97-143). The particle Reynolds numbers,  $5 < u_* k_s / v_m < 70$ , indicate that the flows were in transitional condition. The sand used in the experiments had a nominal particle diameter of  $d_{50} = 0.135$  [mm] and a density of  $\rho_s = 2650$  [kg/m<sup>3</sup>]. The settling velocity,  $v_{ss}$  [m/s], was taken in still, clear water (see *Graf*, 1984, p.45). The depth-averaged suspended concentration,  $C_s^m$  [kg/m<sup>3</sup>], as well as the reference concentration,  $\bar{C}_{sa}^m$  [kg/m<sup>3</sup>], were measured with the suction method. The depth-averaged mixture density was calculated according to  $\bar{\rho}_m$  [kg/m<sup>3</sup>] =  $\rho_w + C_s^m \cdot (1 - \rho_w / \rho_s)$ . The classical Rouse number,  $z [-] = \frac{v_{ss}}{\kappa \cdot u_*}$ , can be modified introducing the  $\bar{\beta}$ -values, leading to the modified Rouse number:  $z' [-] = \frac{v_{ss}}{\kappa \cdot u_* \cdot \bar{\beta}} = \frac{z}{\bar{\beta}}$ . In this study  $\bar{\beta}_{APFP}$  was gotten from measurements with the APFP instrument and  $\bar{\beta}_{SM}$  was gotten from the measurements with the suction method by best-fitting the Rouse equation, eq. C6, using the modified Rouse number<sup>1</sup>.

Author	run	$Q$	$h$	$B/h$	$\delta$	$\bar{u}_c$	$U$	$S_b$	$Re \cdot 10^5$	$Fr$	$u_*$	$\Pi$	$f$	$k_s$	$\frac{u_* k_s}{v_m}$
		[m <sup>3</sup> /s]	[m]	[-]	[m]	[m/s]	[m/s]	[%]	[-]	[-]	[m/s]	[-]	[-]	[mm]	[-]
EPFL	CW_S015	0.050	0.120	5.0	0.105	0.805	0.726	0.150	2.489	0.67	0.045	0.250	0.031	1.201	54.0
EPFL	SLF1_S015	0.050	0.120	5.0	0.110	0.813	0.734	0.150	2.516	0.68	0.044	0.247	0.028	0.953	41.5
EPFL	SLF2_S015	0.051	0.120	5.0	0.105	0.824	0.740	0.150	2.537	0.68	0.043	0.325	0.026	0.697	29.6
EPFL	SLF3_S015	0.051	0.120	5.0	0.110	0.832	0.748	0.150	2.562	0.69	0.045	0.330	0.028	1.061	47.2
EPFL	SLF4_S015	0.053	0.120	5.0	0.105	0.845	0.768	0.150	2.631	0.71	0.045	0.303	0.028	0.956	43.0
EPFL	SLF5_S015	0.055	0.120	5.0	0.105	0.865	0.796	0.150	2.729	0.73	0.045	0.286	0.025	0.631	28.1
EPFL	SLF6_S015	0.056	0.120	5.0	0.105	0.895	0.823	0.150	2.820	0.76	0.045	0.297	0.023	0.482	21.4
EPFL	SAT_S015	0.061	0.120	5.0	0.104	0.911	0.853	0.150	2.922	0.79	0.045	0.331	0.022	0.403	18.1

run	$d_{50}$	$\rho_s$	$v_{ss}$	$v_{ss}/u_*$	$C_s^m$	$\bar{C}_{sa}^m$	$\bar{\rho}_m$	$Ri$	$z = \frac{v_{ss}}{\kappa \cdot u_*}$ (best fit)	$z'$ (best fit)	$\bar{\beta}_{SM}$ (best fit)	$\bar{\beta}_{APFP}$ (APFP)
	[mm]	[kg/m <sup>3</sup> ]	[mm/s]	[-]	[kg/m <sup>3</sup> ]	[kg/m <sup>3</sup> ]	[kg/m <sup>3</sup> ]	[-]	[-]	[-]	[-]	[-]
CW_S015	0.135	2650	12.0	0.27	0.00	0.00	1000.00	--	--	--	--	--
SLF1_S015	0.135	2650	12.0	0.28	0.23	1.59	1000.14	0.607	0.690	1.239	0.557	--
SLF2_S015	0.135	2650	12.0	0.28	0.43	3.28	1000.27	1.359	0.706	1.052	0.671	--
SLF3_S015	0.135	2650	12.0	0.27	0.99	7.62	1000.62	2.740	0.674	1.215	0.555	--
SLF4_S015	0.135	2650	12.0	0.27	1.11	7.81	1000.69	2.700	0.667	1.351	0.493	0.627
SLF5_S015	0.135	2650	12.0	0.27	1.60	11.30	1001.00	4.002	0.674	1.209	0.558	0.523
SLF6_S015	0.135	2650	12.0	0.27	2.48	19.24	1001.55	6.838	0.674	1.266	0.532	0.516
SAT_S015	0.135	2650	12.0	0.27	3.93	41.09	1002.45	15.047	0.667	1.542	0.432	0.487

Table C1: Summary of data

<sup>1</sup> The mean concentration profiles,  $\bar{C}_s(y)$ , measured with the suction method, are listed on pages C-15 - C-21.

### C3 Velocity and turbulence-intensity profiles

In Fig. C1a are shown the velocity-defect profiles, which do not exhibit discernible changes when adding particles to the flow, even when the *capacity* condition is reached; this is particularly evident in the outer zone,  $y/h > 0.2$ . The Coles defect law, with an average wake-strength coefficient of  $\bar{\Pi} \approx 0.3$  and a Karman constant of  $\kappa = 0.4$ , fits well all the experimental data. The maximum velocity,  $\bar{u}_c$ , was measured at the height  $y = \delta$ . The shear velocity,  $u_*$ , was obtained by extrapolating the measured Reynolds-stress profiles towards the bed, see Fig. C1b.

The Reynolds-stress profiles, given in Fig. C1b, retain their linear trend – well documented in clear-water flow – both in *non-capacity* and *capacity* conditions. This result is consistent with the findings of other authors (see *Muste and Patel*, 1997).

In Figs. C2a and C2b are plotted the longitudinal and vertical turbulence-intensity profiles. The clear-water data are plotted, having a rather similar trend as was proposed by *Nezu and Nakagawa*, 1993, and confirmed by *Song, Graf and Lemmin*, 1994. Data for the non-capacity as well as capacity flow show deviations from the clear-water data. Upon increasing the concentration of the sediments the following is to be noticed: i) the longitudinal turbulence intensity slightly increases and subsequently decreases till the capacity condition is reached; ii) the vertical turbulence intensity decreases continuously, reaching a significant decreased value at the capacity condition. Solid particles which are in suspension seem to damp the turbulence of the flow; addition of polymer to the flow is known (see *Best*, 1993) to have the same effect.

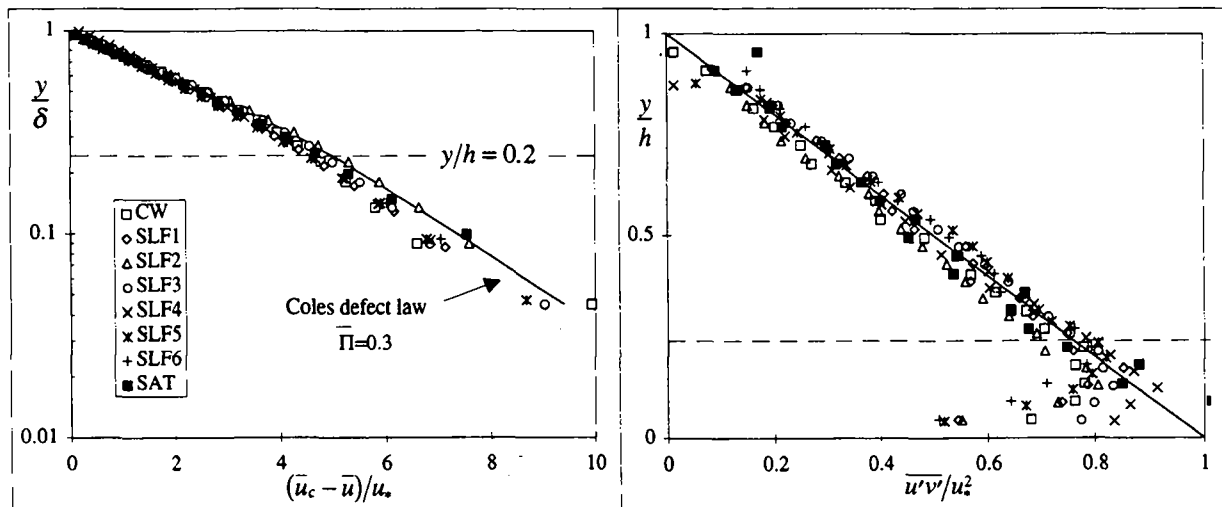


Fig. C1a,b: Velocity profiles and Reynolds-stress profiles

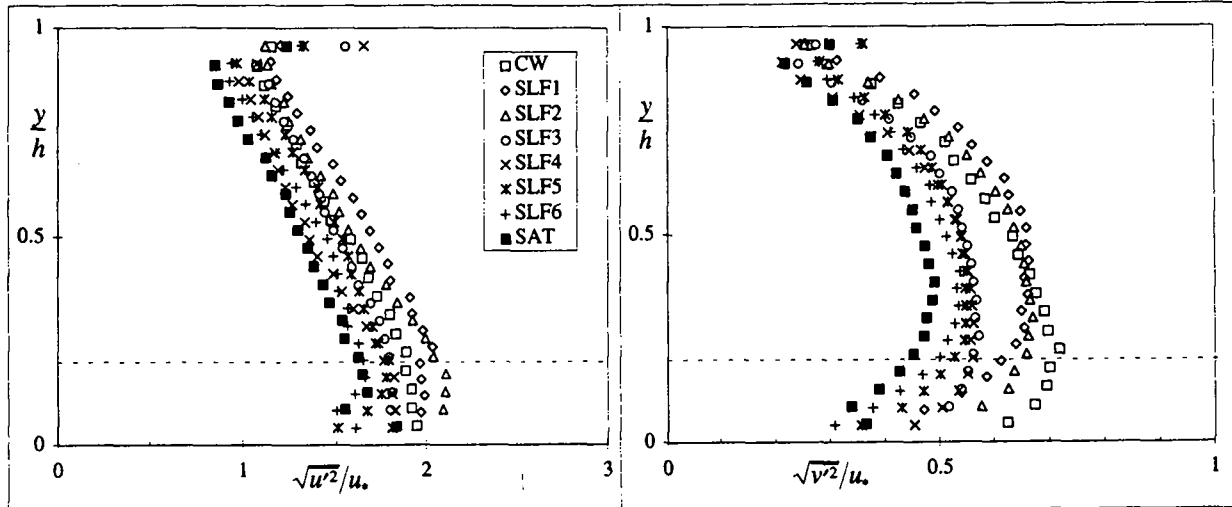


Fig. C2a,b: Longitudinal and vertical turbulence intensity profiles

#### C4 Turbulence spectra

The analysis of the turbulence spectra is an useful tool to understand how the energy is modulated by the introduction of particles to the flow. The spectra,  $E(n)$ , provide information on how the kinetic energy associated to  $u'$  or  $v'$  is distributed with respect to the frequency,  $n$ , of the turbulent eddies. The spectra have been obtained taking the Fourier transform of the complex random wave form of the turbulent motion. To evaluate the turbulence spectra the instrument has been used in a special (tristatic) configuration, allowing to increase the measuring frequency up to 39 [Hz].

The integral of the turbulence spectra is equal to the mean square value of the fluctuating velocity. For the vertical direction, for example, one can write:

$$\int_0^{\infty} E_v(n) dn = \bar{v'^2}$$

The spectra is usually normalized such as:

$$\int_0^{\infty} F(n) dn = 1$$

In our analysis the spectra have been computed analyzing only the *vertical* fluctuating velocity signals at three locations: near the bed, near the surface and in the middle of the flow depth. In Fig. C3 are presented the spectra of 5 runs with different depth-averaged suspended concentration varying from 0 (clear water, CW\_S015) up to 3.93 [kg/m<sup>3</sup>] (capacity flow, SAT\_S015); the measurements at these different positions in the flow depth are compared.

The spectral distribution in the inertial subrange follows the form of  $F(n) \propto n^{-5/3}$ , suggested by Kolmogoroff for locally-isotropic turbulence (see Hinze, 1975, p.228). Regrettably, it was not possible to observe the spectral distribution for the larger frequencies;  $n > 30$  [Hz].

It is to be noted that by adding suspended particles, in approaching the capacity condition, the energy spectra decrease slightly towards smaller frequencies. To the same conclusion came

*Tsuji and Morikawa, 1982, and Tsuji, Morikawa and Shiomi, 1984.* In their experiments the two-phase flow was composed of air and solid particles moving in a horizontal and vertical pipe. They noticed that the tendency of the small frequency spectra to decrease was evident only in case of very fine particles; for coarse particles the spectra were more and less unaffected.

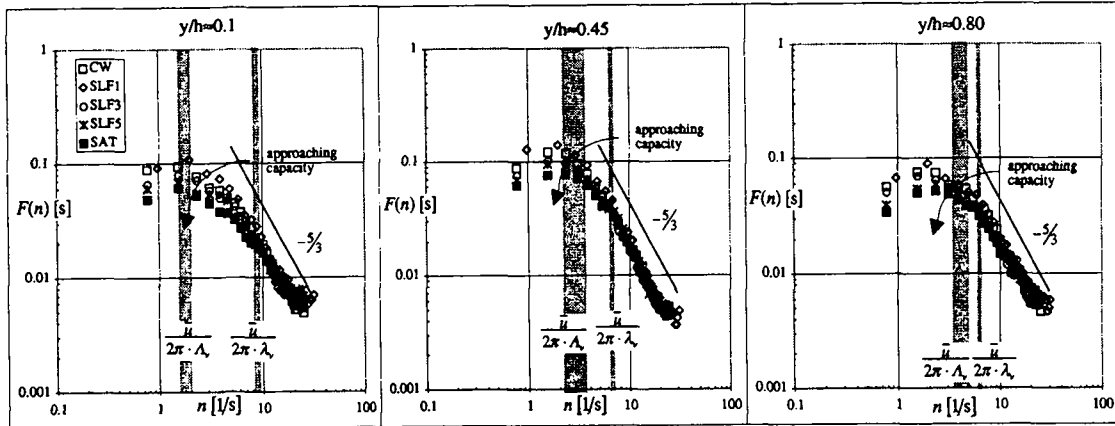


Fig. C3: Trend of the turbulence spectra adding suspended sediments.

## C5 Micro and Macro turbulence scale

The turbulence may be thought of as a group of various sizes of eddies. It is possible to compute characteristic scales of turbulence, i.e. characteristic sizes of eddies, knowing the correlation coefficients of a time series of longitudinal or vertical velocity fluctuations.

The correlation coefficients are computed measuring in two points – being a horizontal distance,  $r$ , apart – both the fluctuating longitudinal and vertical velocities, such as:

$$R_u(r) = \frac{\overline{u'_1 \cdot u'_2}}{\sqrt{\overline{u'^2_1} \cdot \sqrt{\overline{u'^2_2}}}}; \quad R_v(r) = \frac{\overline{v'_1 \cdot v'_2}}{\sqrt{\overline{v'^2_1} \cdot \sqrt{\overline{v'^2_2}}}} \quad (C8)$$

The integral of the correlation coefficients gives the macro (integral) scale of turbulence,  $\Lambda$ ; it represents the characteristic size of the eddies containing the turbulent energy. The longitudinal and vertical macro scales are defined and computed as:

$$\Lambda_u = \int_0^\infty R_u(r) dr; \quad \Lambda_v = \int_0^\infty R_v(r) dr \quad (C9)$$

Another characteristic length is the micro scale,  $\lambda$ , which represents the size of the eddies responsible of the energy dissipation. The longitudinal and vertical micro scales are defined as:

$$\frac{1}{\lambda_u^2} = -\frac{1}{2} \cdot \frac{\partial^2}{\partial r^2} R_u(r) \Big|_{r \rightarrow 0}; \quad \frac{1}{\lambda_v^2} = -\frac{1}{2} \cdot \frac{\partial^2}{\partial r^2} R_v(r) \Big|_{r \rightarrow 0} \quad (C10)$$

Since it is difficult to compute the micro scales according to these definitions from the data obtained with our APFP-instrument, the definition of the micro scale given by Nezu and Nakagawa, 1993, pp. 73, will be used:

$$\lambda_u = \frac{\sqrt{u'^2}}{\sqrt{(\partial u / \partial x)^2}}; \quad \lambda_v = \frac{\sqrt{v'^2}}{\sqrt{(\partial v / \partial x)^2}} \quad (C11)$$

Invoking the Taylor's frozen turbulence hypothesis, eqs. C11 can be written as:

$$\lambda_u = \bar{u} \cdot \frac{\sqrt{u'^2}}{\sqrt{\left(\frac{\partial u}{\partial t}\right)^2}}; \quad \lambda_v = \bar{u} \cdot \frac{\sqrt{v'^2}}{\sqrt{\left(\frac{\partial v}{\partial t}\right)^2}} \quad (C11a)$$

The longitudinal and vertical micro and macro scale profiles computed with eqs. C9 and eqs. C11a are presented in Fig. C4. The depth-averaged values of the micro and the macro scales were also calculated, such as:

$$\bar{\lambda}_u = \frac{1}{h} \int_{y=0}^{y=h} \lambda_u dy, \quad \bar{\lambda}_v = \frac{1}{h} \int_{y=0}^{y=h} \lambda_v dy; \quad \bar{\Lambda}_u = \frac{1}{h} \int_{y=0}^{y=h} \Lambda_u dy \text{ and } \bar{\Lambda}_v = \frac{1}{h} \int_{y=0}^{y=h} \Lambda_v dy \quad (C12)$$

They are summarized for the 8 runs in Table C2. The range of the turbulence scales is shown in the turbulence spectra (see Fig. C3).

run	$C_s^m$	$\bar{c}_{sa}^m$	$\frac{\sqrt{v'^2}}{u_*}$	$\Delta\sqrt{v'^2}$	$\bar{\lambda}_u$	$\bar{\lambda}_v$	$\bar{\Lambda}_u$	$\bar{\Lambda}_v$
	[kg/m³]	[kg/m³]	[—]	[%]	[cm]	[cm]	[cm]	[cm]
CW	0.00	0.00	0.558	0.0	2.17	1.60	13.40	4.60
SLF1	0.23	1.59	0.541	-3.0	2.20	1.58	13.53	4.20
SLF2	0.43	3.28	0.547	-2.0	2.41	1.79	12.39	3.99
SLF3	0.99	7.62	0.475	-14.9	2.33	1.68	15.29	4.60
SLF4	1.11	7.81	0.456	-18.3	2.30	1.74	14.26	4.61
SLF5	1.60	11.30	0.465	-16.6	2.25	1.76	13.12	3.91
SLF6	2.48	19.24	0.440	-21.0	2.37	1.87	12.72	3.73
SAT	3.93	41.09	0.397	-28.8	2.43	1.92	15.83	4.84

Table C2: Effect of particles on the rms. fluctuating vertical velocities and turbulence scales

Our experiments show that by adding particles to the flow, i.e. approaching the capacity condition, the micro and the macro scales – both their vertical profiles (see Fig. C4) and their average values (see Table C2) – seem to increase. However this tendency is unquestionable only for the micro scales. Subsequently the change in the turbulence due to the suspended particles transport was calculated, such as:

$$\Delta\sqrt{v'^2} = \frac{\sqrt{v'^2_{SLFx}} - \sqrt{v'^2_{CW}}}{\sqrt{v'^2_{CW}}} \cdot 100 \quad (C13)$$

where  $\sqrt{v'^2_{SLFx}}$  is the depth-averaged value of the rms. fluctuating vertical velocity measured in

sediment-laden flow:  $\sqrt{v'^2_{SLFx}} = \frac{1}{h} \int_{y=0}^{y=h} \sqrt{v'^2}(y) dy$  (runs SLFx and SAT) and

where  $\sqrt{v'^2_{CW}}$  is the depth-averaged value of the rms. fluctuating vertical velocity measured in

clear-water flow:  $\sqrt{v'^2_{CW}} = \frac{1}{h} \int_{y=0}^{y=h} \sqrt{v'^2}(y) dy$  (run CW)

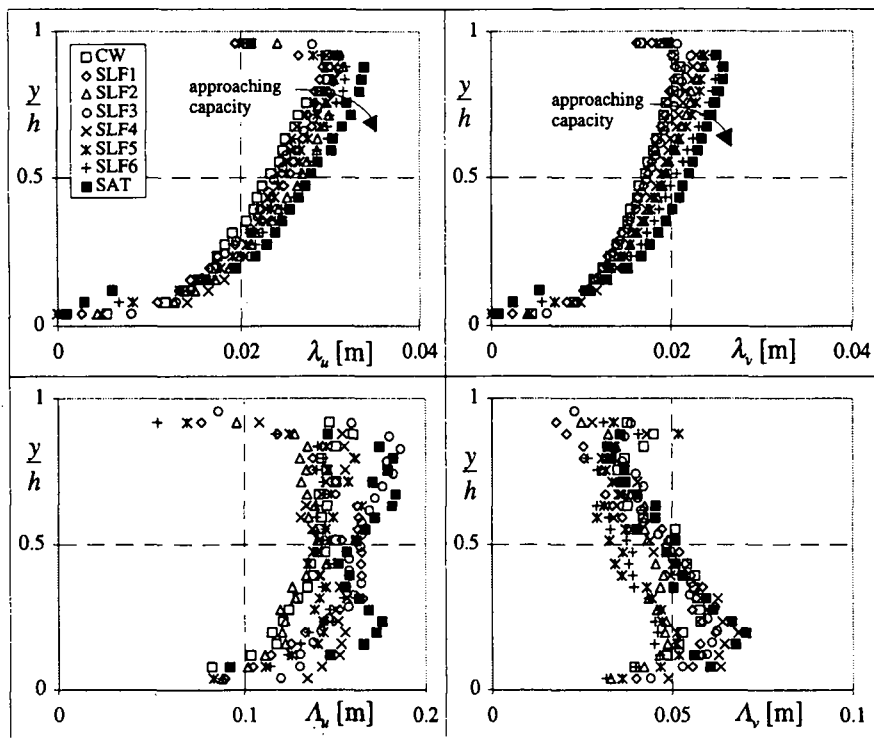


Fig. C4: Vertical profiles of the micro and macro scales

In Table C2 are summarized the results of these computations, where it is rather evident that the turbulence is suppressed by adding particles to the flow. This can clearly be seen in Fig. C5, where the change in turbulence,  $\Delta\overline{v'^2}$ , is plotted against the depth-averaged concentration,  $C_s^m$ , and the dimensionless particle diameter, using the turbulence scales,  $\overline{\Lambda}_v$  and  $\overline{\lambda}_v$ .

This conclusion corroborates with findings by *Gore and Crowe*, 1989, who summarized experimental data obtained with air-solid, liquid-solid and liquid-air suspensions. Even for such a variety of different mixture flows it was evident that for values of  $d/\Lambda < 0.1$  the turbulence is suppressed.

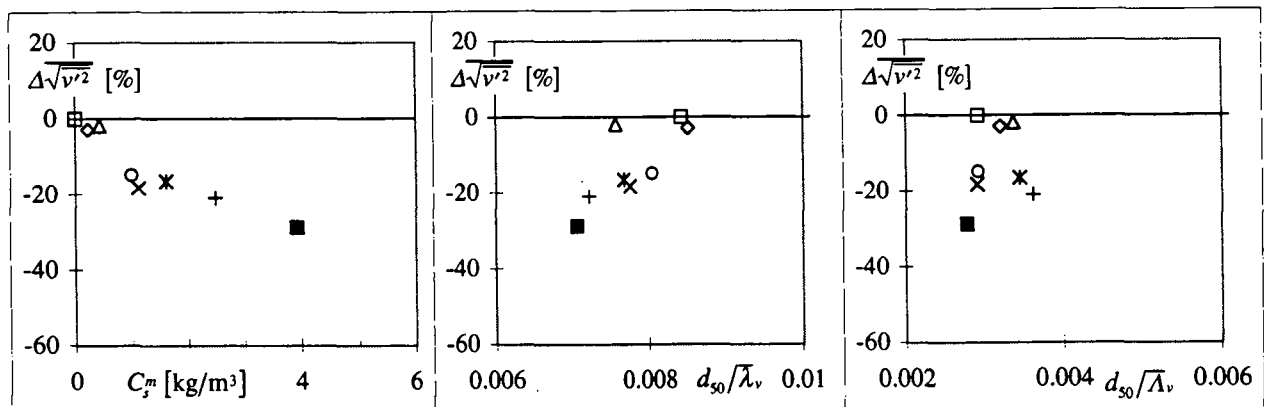


Fig. C5: Relationship between turbulence suppression, depth-averaged concentration and dimensionless particle diameter

## C6 Concentration profiles

Comparing the vertical mean sonar's echo-intensity profile and the vertical mean concentration profile the calibration curves have been obtained (see *Cellino and Graf*, 1997). With these curves it is possible to translate the instantaneous echo-intensity signals into instantaneous suspended concentrations. In Fig. C6a are presented the vertical mean concentration profiles measured by the suction method. The dimensionless fluctuating concentration profiles, measured using the APFP-instrument, are presented in Fig. C6b. They show a zone of high values of the fluctuating concentration close to the bottom ( $y/h < 0.25$ ); in the upper part of the flow the fluctuating concentration remains rather constant. Approaching the capacity condition these dimensionless profiles decrease, but this is also due to an increase of the reference concentration,  $\bar{c}_{sa}^m$ , approaching the capacity condition (see Table C1). The sediment-flux profiles are plotted in Fig. C6c, being normalized with its value at the bed. For all runs the trend is similar and the tendency of a decrease towards the capacity condition is somehow evident.

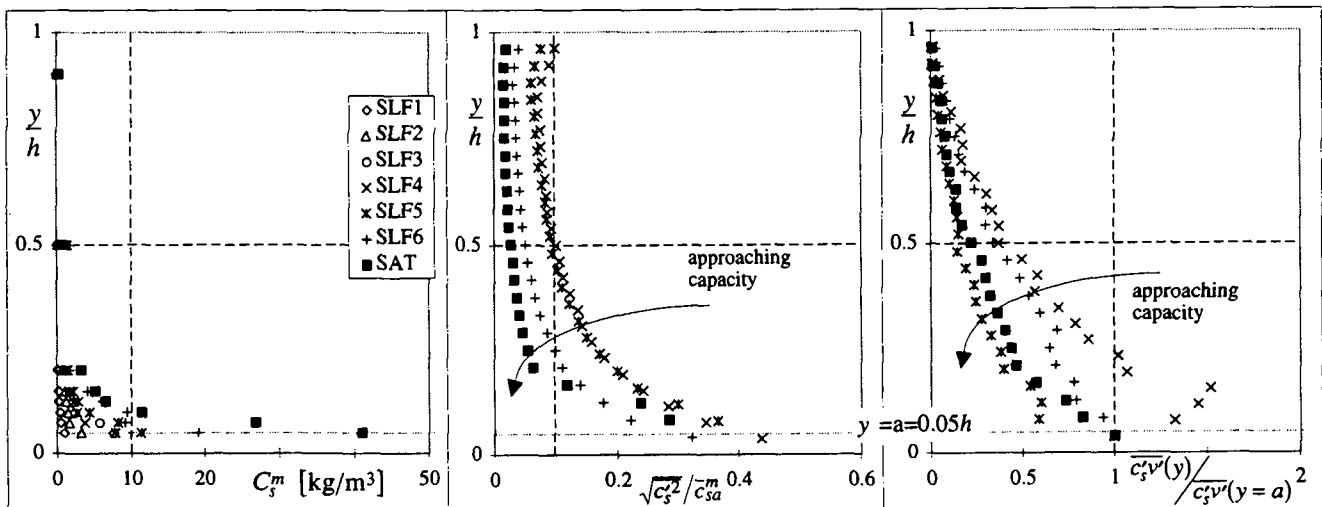


Fig. C6a,b,c: Vertical mean concentration profiles measured by the suction method, fluctuating concentration and sediment flux profiles measured by the APFP instrument

The dimensionless vertical mean concentration profiles – measured by the suction method – can now be used to obtain best-fit  $\bar{\beta}_{SM}$ -values. The data points are shown in Fig. C7 and the corresponding  $\bar{\beta}_{SM}$ -values are listed in Table C1. The  $\bar{\beta}_{SM}$ -values obtained have a tendency to decrease approaching the capacity condition. This is also evidenced in *Coleman's*, 1986, measurements, elaborated in Appendix B. The dotted line in Fig. C7 represents the Rouse equation, eq. C6, that best fits the vertical concentration profile measured in capacity condition, (run SAT\_S015); its value is found to be  $\bar{\beta}_{SM} = 0.432$ , being considerable different from the “theoretical” value of  $\bar{\beta} = 1$ , plotted as a dark full line.

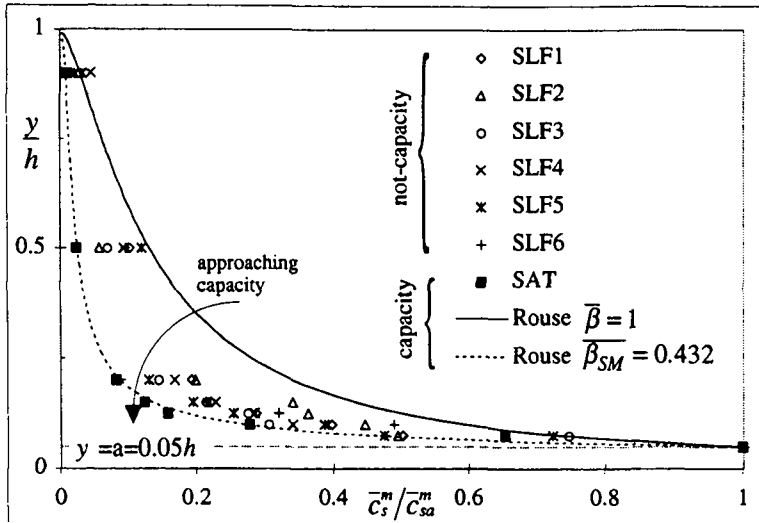


Fig. C7: Dimensionless concentration profiles for the 8 runs

## C7 Diffusion coefficients

In Fig. C8a,b experimental – obtained with the APFP-instrument – sediment diffusion coefficient, eq. C2, profiles (black symbols) are compared with the experimental (gray symbols), eq. C4, and the theoretical momentum diffusion coefficient, eq. C5, (full line) profiles.

In Fig. C8a the experimental momentum diffusion coefficient profiles,  $\varepsilon_m(y/h)$ , are compared with the corresponding sediment diffusion coefficient profiles,  $\varepsilon_s(y/h)$ , for some individual runs. Close to the bed – where the concentration is very high – the momentum diffusion coefficient is always larger than the sediment diffusion coefficient. The largest difference between the momentum and the sediment diffusion coefficient is observed close to the middle of the flow depth. Near the surface the diffusion coefficients are rather similar.

In Fig. C8b the dimensionless experimental momentum diffusion coefficient profiles (gray points) are plotted; they do not distinguishably change when approaching the capacity condition. They are, however always smaller than the theoretical profile (full line). The shape of the sediment diffusion coefficient profiles are very similar to each other. Close to the bed, in approaching the capacity condition, their values become smaller. Near the surface, where the concentration is always small, by increasing the concentration the sediment diffusion coefficient profiles do not exhibit discernible changes.

The ratio between the sediment and the momentum diffusion coefficient defines the  $\beta(y)$ -value (see eq. C2 and eq. C4) or:

$$\beta(y) = \frac{\varepsilon_s(y)}{\varepsilon_m(y)} = \frac{c'_s v' / (\partial c_s / \partial y)}{u' v' / (\partial u / \partial y)}(y) \quad (C14)$$

The vertical distributions of the  $\beta_{APFP}(y)$ -values – the index recalls that the data are taken with the APFP instrument – are plotted in Fig. C9 for the runs investigated. The  $\beta_{APFP}(y)$ -values seem to increase with the distance from the bed when the flow is close to capacity; for non-

capacity (smaller concentrations) this trend is less evident. In these plots is also shown the depth-averaged value,  $\overline{\beta}_{APFP}$ . Approaching the capacity flow the  $\overline{\beta}_{APFP}$ -values decrease. This is in agreement with the trend of the  $\overline{\beta}_{SM}$ -values, obtained by best-fitting the mean concentration profiles as measured by the suction method (see Fig. C7 and Table C1).

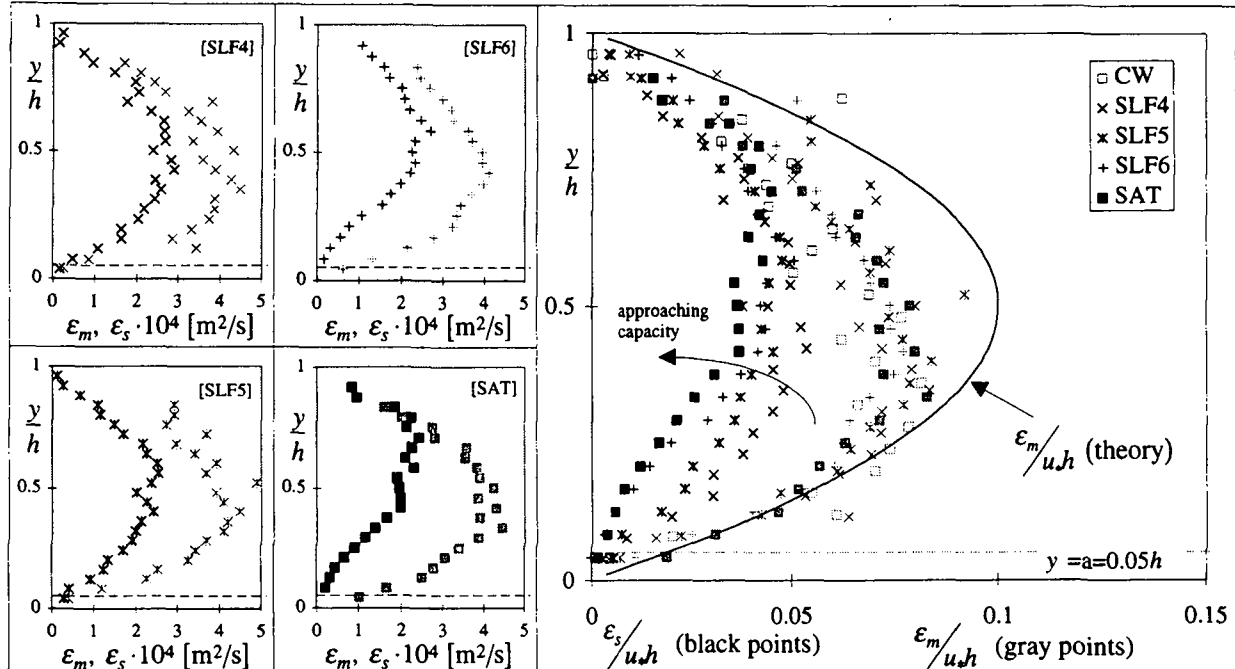


Fig.C8a,b: [Dimensionless] sediment,  $\epsilon_s$ , and momentum,  $\epsilon_m$ , diffusion coefficient profiles

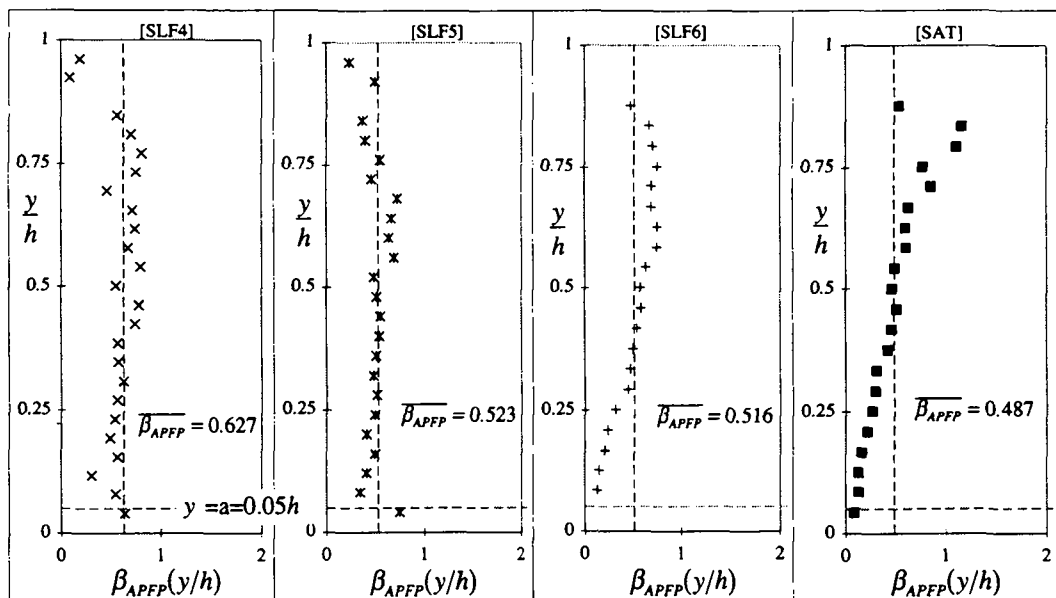


Fig. C9: Vertical profile of the  $\overline{\beta}_{APFP}$ -values

The concentration profiles are presented in Fig. C10. The Rouse equation, eq. C6, is shown, using the  $\overline{\beta}_{APFP}$ -values – obtained with the diffusion-coefficients, eq. C14 – as well as the best-fit  $\overline{\beta}_{SM}$ -values (see Fig. C7). In either case is the agreement to be considered as rather good. Also evident is that a “theoretical”  $\overline{\beta}$ -values of  $\overline{\beta}=1$ , is not justified.

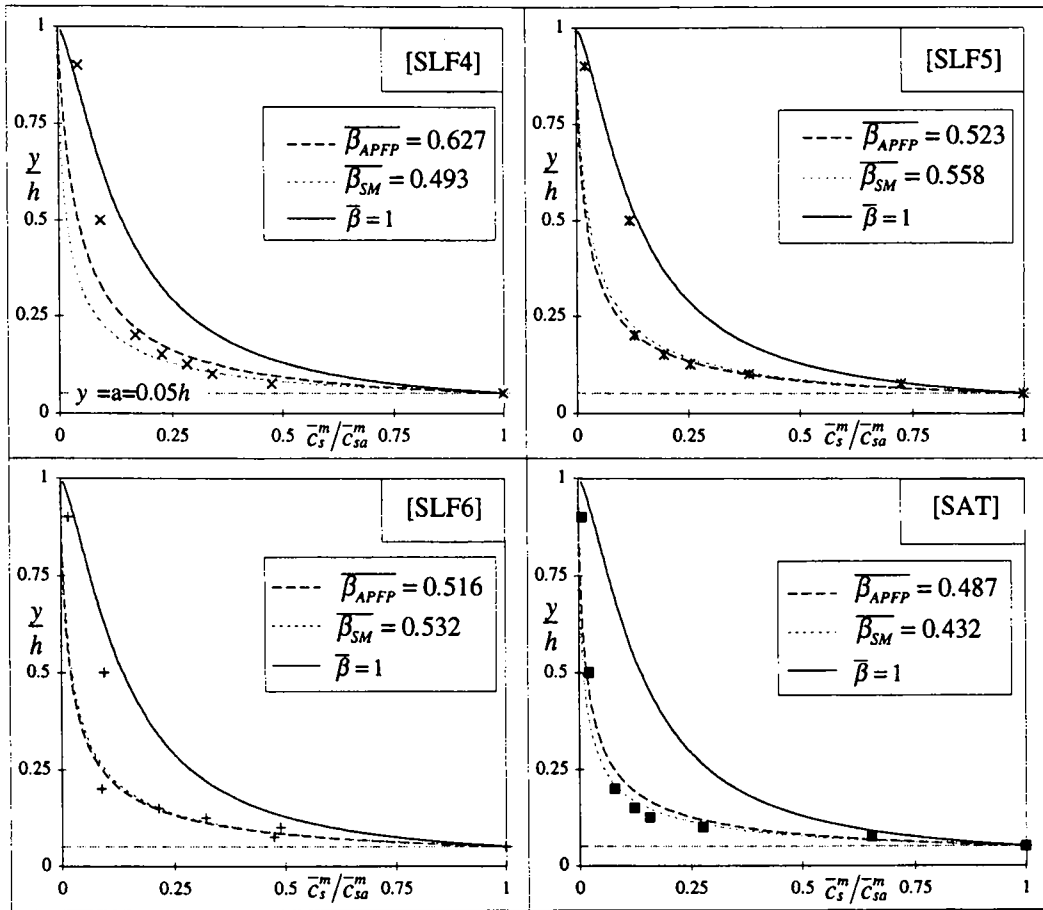


Fig. C10: Dimensionless concentration profiles, compared with the Rouse equation using the  $\overline{\beta}_{APFP}$ -values as well as the  $\overline{\beta}_{SM}$ -values.

## C8 Conclusions

An experimental study was performed to investigate the influence of suspended particles on the flow in an open channel under *non-capacity* and *capacity* conditions. *Capacity* flow is herewith defined when a layer of sediments, composed of the same particles as are in suspension, is available on the bed.

Concentration measurements were performed using the suction method and the non-intrusive sonar (APFP) instrument; the latter was also used to measure the velocity and turbulence profiles.

For both *non-capacity* and *capacity* flow the Rouse equation, eq. C6, was used to describe the vertical concentration distribution. The study focused on the determination of the Rouse number, eq. C7, notably on its  $\beta$ -value.

For the present experiments, done with particles having a small diameter,  $d_{50} = 0.135$  [mm], the  $\beta$ -values are always less than unity,  $\beta < 1$ . These  $\beta$ -values have a pronounced tendency to decrease going from non-capacity to capacity flow, as is evident in Table C1 and Fig. C7.

The effect of particles in the flow is such that the flow's turbulence is suppressed; this is shown in Fig. C2 and Table C2.

Both momentum and sediment diffusion coefficients were evaluated from data obtained with the APFP instrument (see Fig. C8). The momentum diffusion coefficient equation, eq. C4, is little influenced by the studied concentrations, but is always smaller than the theoretical value, eq. C5. The sediment diffusion coefficient, eq. C2, is always smaller than the momentum diffusion coefficient, and is influenced by the sediment concentration in the flow.

## C9 References

- BEST, J. L. (1993), "On the interactions between turbulent flow structure, sediment transport and bedform development: some considerations from recent experimental research", in *Turbulence, Perspectives on Flow and Sediment Transport*, Wiley & Sons Ltd., Chichester, UK, pp.61-92.
- CELLINO, M. and GRAF, W. H., (1997) "Measurements of suspension flow in open channels", Proceedings of XXVII IAHR Congress., vol. 1, pp. 179-184, San Francisco.
- COLEMAN, N. L. (1986). "Effects of Suspended Sediment on the Open-Channel Velocity Distribution." *Water Resources Research*, vol. 22 (No. 10), pp. 1377-1384.
- GORE, R. A. and CROWE, C. T. (1989). "Effect of particle size on modulating turbulent intensity." *Int. J. Multiphase Flow*, Vol. 15, No. 2, pp. 279-285.
- GRAF, W. H. (1984). *Hydraulics of Sediment Transport*, McGraw-Hill, New York.
- HINZE, J. O. (1975). *Turbulence*, McGraw-Hill, New York.
- LIGGETT, J. A. (1994). *Fluid Mechanics*, McGraw-Hill, New York.
- MUSTE, M. and PATEL, V. C. (1997). "Velocity profiles for particles and liquid in open-channel flow with suspended sediment." *J. Hydr. Engr., ASCE*, vol. 123, No. 9, pp.742-751.
- NEZU, I. and NAKAGAWA, H. (1993). *Turbulence in Open-Channel Flows*, IAHR Monograph Series, A.A. Balkema, Rotterdam.
- SHEN, W. and LEMMIN, U. (1996). "Ultrasonic measurements of suspended sediments: a concentration profiling system with attenuation compensation." *Meas. Sci. Technol.*, Vol. 7, pp. 1191-1194.
- SHEN, W. (1997). "An acoustic instantaneous sediment flux profiler for turbulent flow." *Doctoral dissertation*, No. 1630, Ecole Polytechnique Fédérale, Lausanne.
- SILBERMAN, E. et al. (1963). "Friction Factors in Open Channels." *Proc. Am. Soc. Civil Engrs.*, vol. 90, N° HY1, USA.
- SONG, T., GRAF, W.H. and LEMMIN, U. (1994). "Uniform flow in open channels with movable gravel bed." *J. of Hydr. Res.*, Vol. 32, No. 6, pp. 861-876
- TSUJI, Y. and MORIKAWA, Y. (1982). "LDV measurements of an air-solid two-phase flow in a horizontal pipe." *J. Fluid Mech.*, vol. 120, pp. 385-409.
- TSUJI, Y., MORIKAWA, Y., and SHIOMI, H. (1984). "LDV measurements of an air-solid two-phase flow in a vertical pipe." *J. Fluid Mech.*, vol. 139, pp. 417-434.

EPFL, (1997)

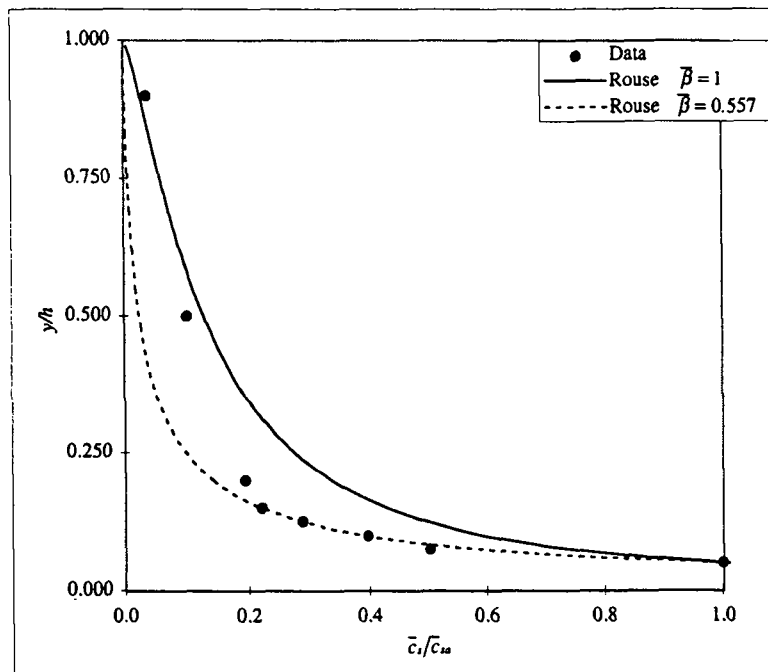
## Sediment concentration distribution

Run SLF1\_S015 | Sand particles       $d = 0.135$  [mm]

$y$ [cm]	$y/h$ [-]	$\bar{c}_s^*$ [kg/m³]	$\bar{c}_s$ (volum.) [%]	Measured		Calculated			
				$\bar{c}_s/\bar{c}_{ss}$ [-]	Rouse eq. $\beta = 1$ $\bar{c}_s/\bar{c}_{ss}$ [-]	Rouse eq. $\beta \neq 1$ $\bar{c}_s/\bar{c}_{ss}$ [-]	Hunt eq. $\beta \neq 1$ $\bar{c}_s/\bar{c}_{ss}$ [-]	$\bar{c}_s^* \cdot y/h$ [kg/m³]	$\rho_m$ [kg/m³]
0.60	0.050	1.59	0.06	1.000	1.000	0.740	0.582	7.96E-02	1000.99
0.90	0.075	0.80	0.03	0.503	0.503	0.582	0.582	2.00E-02	1000.50
1.20	0.100	0.63	0.02	0.398	0.594	0.392	0.392	1.58E-02	1000.39
1.50	0.125	0.46	0.02	0.288	0.498	0.286	0.286	1.15E-02	1000.29
1.80	0.150	0.35	0.01	0.221	0.430	0.220	0.220	8.80E-03	1000.22
2.40	0.200	0.31	0.01	0.194	0.337	0.142	0.142	1.54E-02	1000.19
6.00	0.500	0.16	0.01	0.102	0.128	0.025	0.025	4.88E-02	1000.10
10.80	0.900	0.06	0.00	0.038	0.028	0.002	0.002	3.01E-02	1000.04

$$\text{Depth aver. } \bar{C}_s^* = 0.23 \text{ [kg/m}^3\text{]}$$

$$\text{Depth aver. } \bar{\rho}_m = 1000.14 \text{ [kg/m}^3\text{]}$$



$$\begin{aligned}
 h &= 0.12 \text{ [m]} \\
 S (\text{Bed slope}) &= 1.50E-03 \text{ [-]} \\
 u_* &= 0.043 \text{ [m/s]} \\
 \kappa &= 0.4 \text{ [-]} \\
 U &= 0.734 \text{ [m/s]} \\
 Fr &= 0.68 \text{ [-]} \\
 a (\text{refer.}) &= 0.006 \text{ [m]} \\
 \bar{c}_s^* &= 1.59 \text{ [kg/m}^3\text{]} \\
 \bar{c}_{ss} &= \bar{c}_s^*/\rho_m = 0.001 \text{ [m}^3\text{/m}^3\text{]} \\
 \rho_i &= 2650 \text{ [kg/m}^3\text{]} \\
 v_n &= 0.012 \text{ [m/s]} \\
 z &= v_n/(\kappa u_*) = 0.698 \text{ [-]}
 \end{aligned}$$

Best fitting on  $\beta$  (Rouse equation)

$$\beta = 0.557$$

$$Ri = 0.61 \text{ [-]}$$

$$Ri [-] = \frac{gh[\rho_m(y=a) - \rho_m(y=h)]}{\bar{\rho}_m \cdot u_*^2}$$

Remarks: Group c  
 Laboratory channel, aspect ratio=  $B/h = 5.0$   
 Small reference concentration  $\bar{c}_{ss} = 1.59 \text{ [kg/m}^3\text{]} = 0.001 \text{ [m}^3\text{/m}^3\text{]} < 0.05 \text{ [m}^3\text{/m}^3\text{]} \Rightarrow \text{Rouse eq.}$   
 Instantaneous velocity and concentration measured with the APFP ultrasonic instrument  
 The calibration of the APFP instrument has been made measuring by suction the concentration distribution (shown here).  
 No sediment layer on the bed  
 Subcritical flow

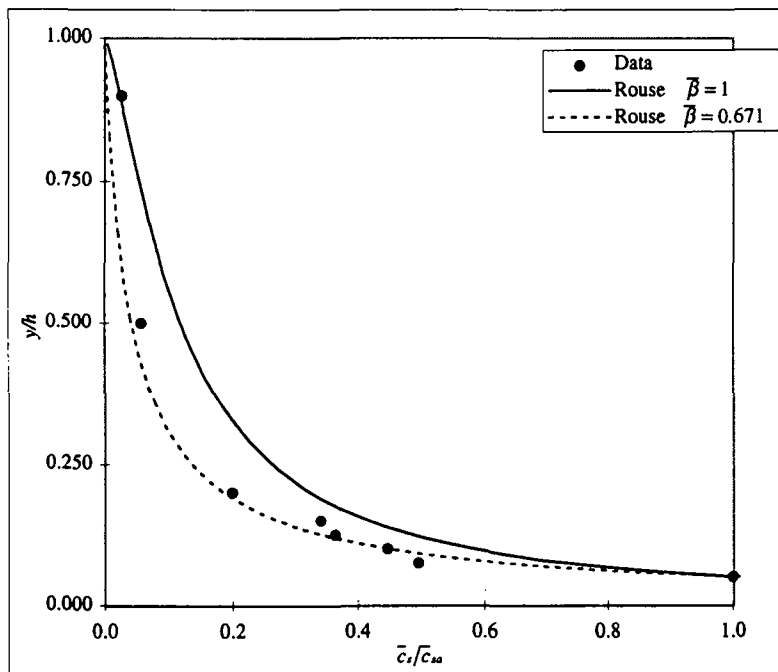
EPFL, (1997)

## Sediment concentration distribution

Run SLF2\_S015 | Sand particles       $d = 0.135$  [mm]

$y$ [cm]	$y/h$ [--]	$\bar{c}_s^m$ [kg/m³]	$\bar{c}_s$ (volum.) [%]	$\bar{c}_s/\bar{c}_{sa}$ [--]	Calculated				
					Rouse eq. $\beta = 1$ $\bar{c}_s/\bar{c}_{sa}$ [--]	Rouse eq. $\beta \neq 1$ $\bar{c}_s/\bar{c}_{sa}$ [--]	Hunt eq. $\beta \neq 1$ $\bar{c}_s/\bar{c}_{sa}$ [--]	$\bar{c}_s^m \cdot y/h$ [kg/m³]	$\rho_m$ [kg/m³]
0.60	0.050	3.28	0.12	1.000	1.000	1.000	1.000	1.64E-01	1002.04
0.90	0.075	1.63	0.06	0.496	0.732	0.628	0.628	4.07E-02	1001.01
1.20	0.100	1.47	0.06	0.447	0.583	0.447	0.447	3.66E-02	1000.91
1.50	0.125	1.19	0.05	0.364	0.486	0.341	0.341	2.98E-02	1000.74
1.80	0.150	1.12	0.04	0.341	0.417	0.272	0.272	2.80E-02	1000.70
2.40	0.200	0.65	0.02	0.199	0.324	0.187	0.187	3.26E-02	1000.41
6.00	0.500	0.19	0.01	0.057	0.119	0.042	0.042	5.63E-02	1000.12
10.80	0.900	0.09	0.00	0.027	0.024	0.004	0.004	4.39E-02	1000.05

$$\begin{aligned} \text{Depth aver. } \bar{c}_s^m &= 0.43 \text{ [kg/m}^3\text{]} \\ \text{Depth aver. } \bar{\rho}_m &= 1000.27 \text{ [kg/m}^3\text{]} \end{aligned}$$



$$\begin{aligned} h &= 0.12 \text{ [m]} \\ S (\text{Bed slope}) &= 1.50E-03 \text{ [--]} \\ u_* &= 0.042 \text{ [m/s]} \\ \kappa &= 0.4 \text{ [--]} \\ U &= 0.74 \text{ [m/s]} \\ Fr &= 0.68 \text{ [--]} \\ a (\text{refer.}) &= 0.006 \text{ [m]} \\ \bar{c}_s^m &= 3.28 \text{ [kg/m}^3\text{]} \\ \bar{c}_{sa} &= \bar{c}_s^m / \rho_s = 0.001 \text{ [m}^3\text{/m}^3\text{]} \\ \rho_s &= 2650 \text{ [kg/m}^3\text{]} \\ v_g &= 0.012 \text{ [m/s]} \\ z = v_g / (\kappa u) &= 0.723 \text{ [--]} \end{aligned}$$

Best fitting on  $\beta$  (Rouse equation)

$$\bar{\beta} = 0.671$$

$$Ri = 1.36 \text{ [--]}$$

$$Ri [-] = \frac{gh[\rho_m(y=a) - \rho_m(y=h)]}{\bar{\rho}_m \cdot u_*^2}$$

Remarks: Group c  
 Laboratory channel, aspect ratio =  $B/h = 5.0$   
 Small reference concentration  $\bar{c}_s^m = 3.28 \text{ [kg/m}^3\text{]} = 0.001 \text{ [m}^3\text{/m}^3\text{]} < 0.05 \text{ [m}^3\text{/m}^3\text{]} \Rightarrow$  Rouse eq.  
 Instantaneous velocity and concentration measured with the APFP ultrasonic instrument  
 The calibration of the APFP instrument has been made measuring by suction the concentration distribution (shown here).  
 No sediment layer on the bed  
 Subcritical flow

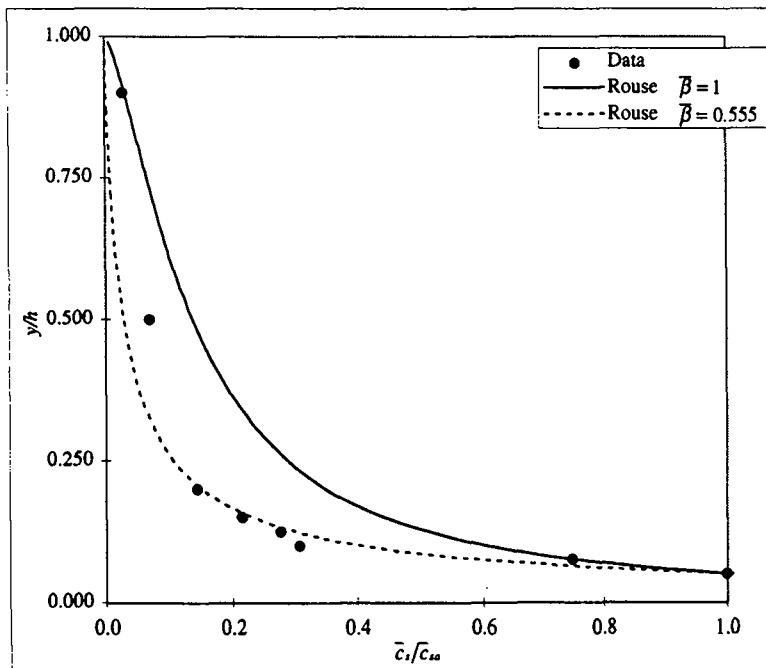
EPFL, (1997)

## Sediment concentration distribution

Run SLF3 S015 Sand particles  $d = 0.135$  [mm]

$y$ [cm]	$y/h$ [-]	$\bar{c}_s^m$ [kg/m³]	$\bar{c}_s$ (volum.) [%]	$\bar{c}_s/\bar{c}_{so}$ [-]	Calculated				
					Rouse eq. $\beta = 1$ $\bar{c}_s/\bar{c}_{so}$ [-]	Rouse eq. $\beta \neq 1$ $\bar{c}_s/\bar{c}_{so}$ [-]	Hunt eq. $\beta \neq 1$ $\bar{c}_s/\bar{c}_{so}$ [-]	$\bar{c}_s^m \cdot y/h$ [kg/m³]	$\rho_m$ [kg/m³]
0.60	0.050	7.62	0.29	1.000	1.000	1.000	1.000	3.81E-01	1004.75
0.90	0.075	5.70	0.21	0.747	0.747	0.592	0.593	1.42E-01	1003.55
1.20	0.100	2.33	0.09	0.305	0.604	0.403	0.405	5.82E-02	1001.45
1.50	0.125	2.10	0.08	0.275	0.510	0.297	0.298	5.24E-02	1001.31
1.80	0.150	1.63	0.06	0.214	0.442	0.230	0.231	4.09E-02	1001.02
2.40	0.200	1.10	0.04	0.144	0.350	0.151	0.151	5.50E-02	1000.68
6.00	0.500	0.53	0.02	0.069	0.137	0.028	0.028	1.58E-01	1000.33
10.80	0.900	0.21	0.01	0.028	0.031	0.002	0.002	1.07E-01	1000.13

$$\begin{aligned} \text{Depth aver. } \bar{c}_s^m &= 0.99 \text{ [kg/m³]} \\ \text{Depth aver. } \bar{\rho}_m &= 1000.62 \text{ [kg/m³]} \end{aligned}$$



$$\begin{aligned} h &= 0.12 \text{ [m]} \\ S (\text{Bed slope}) &= 1.50E-03 \text{ [-]} \\ u_* &= 0.045 \text{ [m/s]} \\ \kappa &= 0.4 \text{ [-]} \\ U &= 0.748 \text{ [m/s]} \\ Fr &= 0.69 \text{ [-]} \\ a (\text{refer.}) &= 0.006 \text{ [m]} \\ \bar{c}_s^m &= 7.62 \text{ [kg/m³]} \\ \bar{c}_s &= \bar{c}_s^m / \rho_s = 0.003 \text{ [m³/m³]} \\ \rho_s &= 2650 \text{ [kg/m³]} \\ v_s &= 0.012 \text{ [m/s]} \\ z &= v_s / (a u_*) = 0.674 \text{ [-]} \end{aligned}$$

Best fitting on  $\beta$  (Rouse equation)

$$\beta = 0.555$$

$$Ri = 2.74 \text{ [-]} \\ Ri [-] = \frac{gh[\rho_m(y=a) - \rho_m(y=h)]}{\bar{\rho}_m \cdot u_*^2}$$

Remarks: Group c Light deposition very close to walls  
 Laboratory channel, aspect ratio =  $B/h = 5.0$   
 Small reference concentration  $\bar{c}_s^m = 7.62 \text{ [kg/m³]} = 0.003 \text{ [m³/m³]} < 0.05 \text{ [m³/m³]}$  => Rouse eq.  
 Instantaneous velocity and concentration measured with the APFP ultrasonic instrument  
 The calibration of the APFP instrument has been made measuring by suction the concentration distribution (shown here).  
 No sediment layer on the bed  
 Subcritical flow

EPFL, (1997)

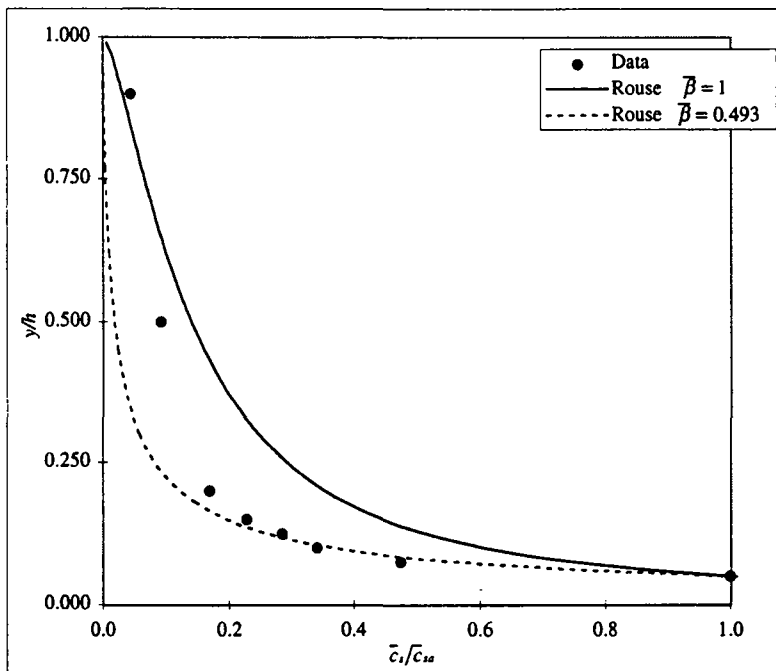
## Sediment concentration distribution

Run SLF4\_S015 | Sand particles  $d = 0.135$  [mm]

$y$ [cm]	$y/h$ [--]	$\bar{c}_s^m$ [kg/m³]	$\bar{c}_s$ (volum.) [%]	Measured		Calculated			
				$\bar{c}_s/\bar{c}_{ss}$ [--]	Rouse eq. $\beta = 1$	Rouse eq. $\beta \neq 1$	Hunt eq. $\beta \neq 1$	$\bar{c}_s \cdot y/h$ [kg/m³]	$\rho_m$ [kg/m³]
0.60	0.050	7.81	0.29	1.000	1.000	1.000	1.000	3.91E-01	1004.87
0.90	0.075	3.72	0.14	0.476	0.750	0.558	0.559	9.29E-02	1002.31
1.20	0.100	2.66	0.10	0.341	0.608	0.364	0.366	6.66E-02	1001.66
1.50	0.125	2.22	0.08	0.285	0.514	0.259	0.261	5.56E-02	1001.39
1.80	0.150	1.78	0.07	0.228	0.446	0.195	0.196	4.45E-02	1001.11
2.40	0.200	1.32	0.05	0.168	0.354	0.122	0.122	6.58E-02	1000.82
6.00	0.500	0.73	0.03	0.093	0.140	0.019	0.019	2.19E-01	1000.45
10.80	0.900	0.35	0.01	0.045	0.032	0.001	0.001	1.75E-01	1000.22

$$\text{Depth aver. } \bar{c}_s^m = 1.11 \text{ [kg/m}^3\text{]}$$

$$\text{Depth aver. } \bar{\rho}_m = 1000.69 \text{ [kg/m}^3\text{]}$$



$$\begin{aligned} h &= 0.12 \text{ [m]} \\ S (\text{Bed slope}) &= 1.50E-03 \text{ [--]} \\ u_* &= 0.045 \text{ [m/s]} \\ \kappa &= 0.4 \text{ [--]} \\ U &= 0.768 \text{ [m/s]} \\ Fr &= 0.71 \text{ [--]} \\ a (\text{refer.}) &= 0.006 \text{ [m]} \\ \bar{c}_s^m &= 7.81 \text{ [kg/m}^3\text{]} \\ \bar{c}_{ss} &= \bar{c}_s^m / \rho_i = 0.003 \text{ [m}^3\text{/m}^3\text{]} \\ \rho_i &= 2650 \text{ [kg/m}^3\text{]} \\ v_u &= 0.012 \text{ [m/s]} \\ z = v_u / (\rho_i U) &= 0.667 \text{ [--]} \end{aligned}$$

Best fitting on  $\beta$  (Rouse equation)  
 $\beta = 0.493$

$$Ri = 2.70 \text{ [--]}$$

$$Ri [-] = \frac{gh[\rho_m(y=a) - \rho_m(y=h)]}{\bar{\rho}_m \cdot u_*^2}$$

Remarks: Group c Deposition close to walls  
 Laboratory channel, aspect ratio =  $B/h = 5.0$   
 Small reference concentration  $\bar{c}_{ss}^m = 7.81 \text{ [kg/m}^3\text{]} = 0.003 \text{ [m}^3\text{/m}^3\text{]} < 0.05 \text{ [m}^3\text{/m}^3\text{]} \Rightarrow$  Rouse eq.  
 Instantaneous velocity and concentration measured with the APFP ultrasonic instrument  
 The calibration of the APFP instrument has been made measuring by suction the concentration distribution (shown here).  
 No sediment layer on the bed  
 Subcritical flow

EPFL, (1997)

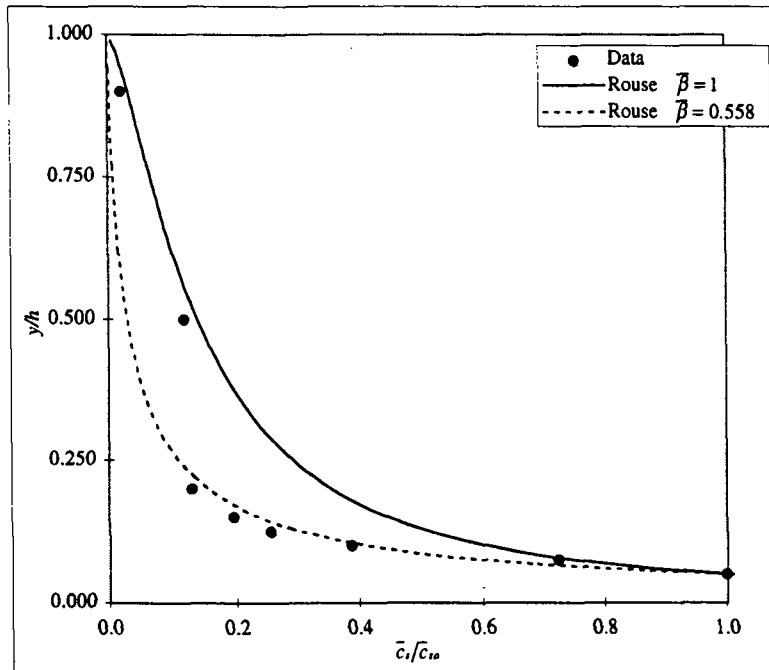
## Sediment concentration distribution

Run SLF5\_S015 | Sand particles |  $d = 0.135$  [mm]

$y$ [cm]	$y/h$ [--]	$\bar{c}_s^m$ [kg/m³]	$\bar{c}_s$ (volum.) [%]	$\bar{c}_s/\bar{c}_{ss}$ [-]	Calculated				
					Rouse eq. $\beta = 1$ $\bar{c}_s/\bar{c}_{ss}$ [-]	Rouse eq. $\beta \neq 1$ $\bar{c}_s/\bar{c}_{ss}$ [-]	Hunt eq. $\beta \neq 1$ $\bar{c}_s/\bar{c}_{ss}$ [-]	$\bar{c}_s^m \cdot y/h$ [kg/m³]	$\rho_m$ [kg/m³]
0.60	0.050	11.30	0.43	1.000	1.000	1.000	1.000	5.65E-01	1007.04
0.90	0.075	8.19	0.31	0.725	0.750	0.597	0.598	2.05E-01	1005.10
1.20	0.100	4.37	0.16	0.387	0.608	0.409	0.411	1.09E-01	1002.72
1.50	0.125	2.88	0.11	0.255	0.514	0.303	0.305	7.20E-02	1001.79
1.80	0.150	2.21	0.08	0.196	0.446	0.235	0.237	5.53E-02	1001.38
2.40	0.200	1.48	0.06	0.131	0.354	0.155	0.156	7.38E-02	1000.92
6.00	0.500	1.35	0.05	0.120	0.140	0.030	0.030	4.06E-01	1000.84
10.80	0.900	0.23	0.01	0.021	0.032	0.002	0.002	1.17E-01	1000.15

$$\text{Depth aver. } \bar{C}_s^m = 1.60 \text{ [kg/m}^3\text{]}$$

$$\text{Depth aver. } \bar{\rho}_m = 1001.00 \text{ [kg/m}^3\text{]}$$



$h = 0.12$  [m]  
 $S(\text{Bed slope}) = 1.50E-03$  [--]  
 $u_* = 0.045$  [m/s]  
 $\kappa = 0.4$  [-]  
 $U = 0.796$  [m/s]  
 $Fr = 0.73$  [-]  
 $a(\text{refer.}) = 0.006$  [m]  
 $\bar{c}_s^m = 11.30$  [kg/m³]  
 $\bar{c}_s = \bar{c}_s^m / \rho_s = 0.004$  [m³/m³]  
 $\rho_s = 2650$  [kg/m³]  
 $v_u = 0.012$  [m/s]  
 $z = v_u / (\kappa U) = 0.667$  [-]

Best fitting on  $\beta$  (Rouse equation)

$$\beta = 0.558$$

$$Ri = 4.00 \text{ [--]}$$

$$Ri [-] = \frac{gh[\rho_m(y=a) - \rho_m(y=h)]}{\bar{\rho}_m \cdot u_*^2}$$

Remarks: Group b Deposition close to walls  
 Laboratory channel, aspect ratio =  $B/h = 5.0$   
 Small reference concentration  $\bar{c}_s^m = 11.30 \text{ [kg/m}^3\text{]} = 0.004 \text{ [m}^3/\text{m}^3\text{]} < 0.05 \text{ [m}^3/\text{m}^3\text{]} \Rightarrow \text{Rouse eq.}$   
 Instantaneous velocity and concentration measured with the APFP ultrasonic instrument  
 The calibration of the APFP instrument has been made measuring by suction the concentration distribution (shown here).  
 No sediment layer on the bed  
 Subcritical flow

EPFL, (1997)

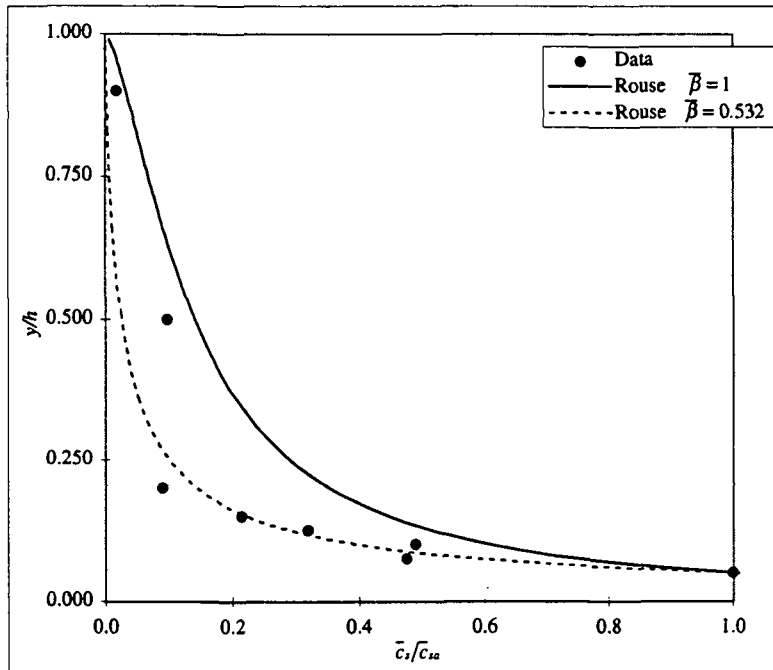
## Sediment concentration distribution

Run SLF6\_S015 Sand particles  $d = 0.135$  [mm]

y [cm]	y/h [-]	$\bar{c}_s^*$ [kg/m³]	$\bar{c}_s$ (volum.) [%]	Measured		Calculated				
				$\bar{c}_s/\bar{c}_{ia}$ [-]	Rouse eq. $\beta = 1$ $\bar{c}_s/\bar{c}_{ia}$ [-]	Rouse eq. $\beta \neq 1$ $\bar{c}_s/\bar{c}_{ia}$ [-]	Hunt eq. $\beta \neq 1$ $\bar{c}_s/\bar{c}_{ia}$ [-]	$\bar{c}_s^* \cdot y/h$ [kg/m³]	$\rho_m$ [kg/m³]	
0.60	0.050	19.24	0.73	1.000	1.000	0.750	0.582	0.585	9.62E-01	1011.98
0.90	0.075	9.14	0.35	0.475	0.475	0.582	0.582	0.585	2.29E-01	1005.69
1.20	0.100	9.43	0.36	0.490	0.608	0.392	0.396	0.396	2.36E-01	1005.87
1.50	0.125	6.16	0.23	0.320	0.514	0.286	0.289	0.289	1.54E-01	1003.84
1.80	0.150	4.12	0.16	0.214	0.446	0.220	0.222	0.222	1.03E-01	1002.57
2.40	0.200	1.71	0.06	0.089	0.354	0.142	0.144	0.144	8.53E-02	1001.06
6.00	0.500	1.84	0.07	0.096	0.140	0.025	0.025	0.025	5.53E-01	1001.15
10.80	0.900	0.33	0.01	0.017	0.032	0.002	0.002	0.002	1.63E-01	1000.20

$$\text{Depth aver. } \bar{c}_s^* = 2.48 \text{ [kg/m}^3\text{]}$$

$$\text{Depth aver. } \bar{\rho}_m = 1001.55 \text{ [kg/m}^3\text{]}$$



$h = 0.12$  [m]  
 $S (\text{Bed slope}) = 1.50E-03$  [-]  
 $u_* = 0.045$  [m/s]  
 $\kappa = 0.4$  [-]  
 $U = 0.823$  [m/s]  
 $Fr = 0.76$  [-]  
 $a (\text{refer.}) = 0.006$  [m]  
 $\bar{c}_s^* = 19.24$  [kg/m³]  
 $\bar{c}_{ia} = \bar{c}_s^*/\rho_i = 0.007$  [m³/m³]  
 $\rho_s = 2650$  [kg/m³]  
 $v_d = 0.012$  [m/s]  
 $z = v_d/(\alpha U) = 0.667$  [-]

Best fitting on  $\beta$  (Rouse equation)

$$\beta = 0.532$$

$$Ri = 6.84 \text{ [-]}$$

$$Ri [-] = \frac{gh[\rho_m(y=a) - \rho_m(y=h)]}{\bar{\rho}_m \cdot u^2}$$

Remarks: Group b Deposition close to walls  
 Laboratory channel, aspect ratio =  $B/h = 5.0$   
 Small reference concentration  $\bar{c}_{ia} = 19.24 \text{ [kg/m}^3\text{]} = 0.007 \text{ [m}^3/\text{m}^3\text{]}$   $< 0.05 \text{ [m}^3/\text{m}^3\text{]}$  => Rouse eq.  
 Instantaneous velocity and concentration measured with the APFP ultrasonic instrument  
 The calibration of the APFP instrument has been made measuring by suction the concentration distribution (shown here).  
 Sediment layer near the walls  
 Subcritical flow

EPFL, (1997)

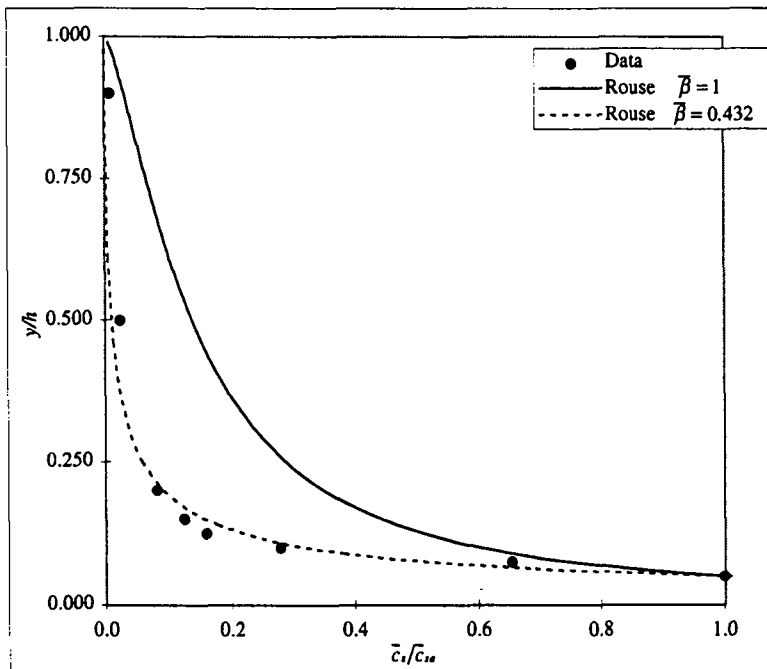
## Sediment concentration distribution

Run SAT\_S015 Sand particles  $d = 0.135$  [mm]

$y$ [cm]	$y/h$ [-]	$\bar{c}_s^*$ [kg/m³]	$\bar{c}_s$ (volum.) [%]	Measured		Calculated			
				$\bar{c}_s/\bar{c}_{so}$ [-]	Rouse eq. $\beta = 1$ $\bar{c}_s/\bar{c}_{so}$ [-]	Rouse eq. $\beta \neq 1$ $\bar{c}_s/\bar{c}_{so}$ [-]	Hunt eq. $\beta \neq 1$ $\bar{c}_s/\bar{c}_{so}$ [-]	$\bar{c}_s^* \cdot y/h$ [kg/m³]	$\rho_m$ [kg/m³]
0.60	0.050	41.09	1.55	1.000	1.000	0.747	0.510	2.05E+00	1025.59
0.90	0.075	26.89	1.01	0.654	0.654	0.510	0.519	6.72E-01	1016.74
1.20	0.100	11.41	0.43	0.278	0.604	0.312	0.320	2.85E-01	1007.10
1.50	0.125	6.51	0.25	0.158	0.510	0.211	0.217	1.63E-01	1004.05
1.80	0.150	5.10	0.19	0.124	0.442	0.152	0.156	1.28E-01	1003.18
2.40	0.200	3.31	0.13	0.081	0.350	0.088	0.091	1.66E-01	1002.06
6.00	0.500	0.96	0.04	0.023	0.137	0.010	0.011	2.88E-01	1000.60
10.80	0.900	0.34	0.01	0.008	0.031	0.000	0.000	1.71E-01	1000.21

$$\text{Depth aver. } \bar{c}_s^* = 3.93 \text{ [kg/m}^3\text{]}$$

$$\text{Depth aver. } \bar{\rho}_m = 1002.45 \text{ [kg/m}^3\text{]}$$



$$\begin{aligned}
 h &= 0.12 \text{ [m]} \\
 S (\text{Bed slope}) &= 1.50E-03 \text{ [-]} \\
 u_* &= 0.045 \text{ [m/s]} \\
 \kappa &= 0.4 \text{ [-]} \\
 U &= 0.853 \text{ [m/s]} \\
 Fr &= 0.79 \text{ [-]} \\
 a (\text{refer.}) &= 0.006 \text{ [m]} \\
 \bar{c}_s^* &= 41.09 \text{ [kg/m}^3\text{]} \\
 \bar{c}_{so} &= \bar{c}_s^*/\rho_s = 0.016 \text{ [m}^3\text{/m}^3\text{]} \\
 \rho_s &= 2650 \text{ [kg/m}^3\text{]} \\
 v_s &= 0.012 \text{ [m/s]} \\
 z &= v_{fl}/(a u_*) = 0.674 \text{ [-]}
 \end{aligned}$$

Best fitting on  $\beta$  (Rouse equation)

$$\beta = 0.432$$

$$Ri = 15.05 \text{ [-]}$$

$$Ri [-] = \frac{gh[\rho_m(y=a) - \rho_m(y=h)]}{\bar{\rho}_m \cdot u_*^2}$$

Remarks: Group a-1 (Erodible flat sediment layer on the bottom => capacity-flow)  
Laboratory channel, aspect ratio =  $B/h = 5.0$   
Small reference concentration  $\bar{c}_s^* = 41.09 \text{ [kg/m}^3\text{]} = 0.016 \text{ [m}^3\text{/m}^3\text{]} < 0.05 \text{ [m}^3\text{/m}^3\text{]} \Rightarrow \text{Rouse eq.}$   
Instantaneous velocity and concentration measured with the APFP ultrasonic instrument  
The calibration of the APFP instrument has been made measuring by suction the concentration distribution (shown here).  
Thickness of the sediment layer  $\geq 2 \text{ [mm]}$   
Subcritical flow



## APPENDIX D

### Suspension flow over bed forms

#### D1 Introduction

Free-surface flow over a mobile bed is usually accompanied by entrainment of sediment and by formation of bed forms; both in turn will influence the flow and its sediment carrying capacity. Here is proposed to study the influence of fixed bed forms on the suspended-load transport.

The bed forms of the mobile bed, appearing as dunes and mini dunes, consist of spatially periodic irregularities. However, indicative and useful relationships – determined on an empirical basis – were proposed by Yalin (see *Graf*, 1984, p. 283); they are:

$$\frac{\lambda}{h} \approx 5 \quad \frac{\Delta H}{h} < \frac{1}{6} \quad (\text{D1})$$

where  $\lambda$  and  $\Delta H$  are respectively the bed-form length and height and  $h$  is the flow depth.

The main effect of bed forms on flow is a flow separation behind the bed-form crest; there the flow is spatially decelerating. In this region recirculation takes place and local enhancement of turbulence is usually observed. Consequently, an influence on the vertical distribution of the suspended sediment concentration in the presence of bed forms and in particular behind the bed-form crest is to be expected.

For steady and uniform flow the vertical distribution of the suspension concentration,  $\bar{c}_s(y)$ , according to the diffusion-convection theory by Rouse (see *Graf*, 1984, p. 173), is given by:

$$\frac{\bar{c}_s}{\bar{c}_{sa}} = \left( \frac{h-y}{y} \frac{a}{h-a} \right)^z \quad (\text{D2})$$

with the Rouse number,  $z$ , defined as:

$$z = \frac{v_{ss}}{\kappa u_*} \quad \text{or} \quad z' = \frac{v_{ss}}{\beta \kappa u_*} = \frac{z}{\beta} \quad (\text{D3})$$

where  $y$  represents the distance from the top of the sediment layer (see Fig. D1),  $h$  is the flow depth,  $a=0.05h$  is the reference level where the reference concentration,  $\bar{c}_{sa}$ , is measured,  $v_{ss}$  is the settling velocity of the particles in still clear water,  $\kappa$  is the Karman constant – assumed to be  $\kappa = 0.4$  for clear-water and for suspension flows – and  $u_*$  is the shear velocity.

The  $\beta$ -value in eq. D3 is the depth-averaged value of  $\beta$ , representing the ratio of the sediment diffusion,  $\epsilon_s$ , and the momentum diffusion coefficient,  $\epsilon_m$ ; its vertical distribution is:

$$\beta(y) = \frac{\text{sediment diffusion coefficient}}{\text{momentum diffusion coefficient}} = \frac{\epsilon_s(y)}{\epsilon_m(y)} = \frac{\overline{c_s v'(y)} / \frac{\partial \bar{c}_s(y)}{\partial y}}{\overline{u' v'(y)} / \frac{\partial \bar{u}(y)}{\partial y}} \quad (\text{D4})$$

where  $\overline{c'_s v'}(y)$  is the sediment flux and  $\overline{u'v'}(y)$  is the turbulent flux. Subsequently a depth-averaged  $\bar{\beta}$ -value can be obtained:

$$\bar{\beta} = \frac{1}{h-a} \int_a^h \beta(y) dy \quad (D5)$$

A set of data from the Rio Grande river, presented by *Nordin and Dempster*, 1963, has been evaluated by *Cellino*, 1998, who obtained (by best fitting) large  $\bar{\beta}$ -values,  $0.7 < \bar{\beta} < 5$ . Carefully performed experiments by *Lyn*, 1988, *Sumer et al.*, 1996 and *Cellino and Graf*, 1997 under capacity condition without the presence of bed forms, showed rather small  $\bar{\beta}$ -values,  $\bar{\beta} < 1$ . Consequently, it seems reasonable to think that the bed forms – usually present in river flows – are at least partially responsible for these large  $\bar{\beta}$ -values. The present study tries to shed some light onto this discrepancy.

In order to compute the  $\bar{\beta}$ -values, the sediment,  $\varepsilon_s(y)$ , and the momentum,  $\varepsilon_m(y)$ , diffusion coefficients have to be obtained. While studies on the diffusion coefficients have been done in the past (see *Jobson and Sayre*, 1970, p. 715, *Coleman*, 1970, p. 807), good measurements of the sediment diffusion coefficient are still a challenging task. It is particularly the direct determination of the sediment flux,  $\overline{c'_s v'}(y)$ , which poses an almost insurmountable problem. The recent development of the APFP sonar instrument (see *Shen and Lemmin*, 1996, and *Shen*, 1997) has allowed us to make an interesting contribution along this line.

In our research, we shall accept the concentration distribution given with the relation of Rouse, eq. D2, and shall try to express the effect of bed forms through the depth-averaged  $\bar{\beta}$ -value. This implies that the flow over bed forms is quasi-uniform. It would of course be desirable to study the evolution of the flow structure, of the concentration distribution and consequently of the  $\bar{\beta}$ -value evolution over one or two entire bed forms. However, our measuring equipment, the APFP instrument, is limited to measure the concentration distribution only at one single section where we were able to make detailed measurements. Nevertheless we find it worthwhile to report also our measurements on evolution of the flow structure over part of a bed form; for reader in a hurry, this part of the paper could readily be skipped.

## D2 Experimental facilities and flow conditions

The measurements have been made in a recirculating tilting channel, 16.8[m] long and  $B=0.60[m]$  wide. Sediments were added slowly to the uniform flow; the measurements started only after 4[h] of flow circulation when the presence of a sediment layer ( $\approx 2$  [mm] thick) on the bed is assured. The layer's thickness, measured periodically ( $\approx 0.5$  [h]) using manual limnimeters, was reasonably constant in time. The measuring section (n° 9) is located 13[m] from the entrance of the channel where the flow is assumed to be established; all measurements were performed at the centerline of the cross section.

Three artificial plastic (PVC) bed forms have been fixed on the channel floor in vicinity of the measuring section (see Fig. D1). The bed-form length,  $\lambda$ , and height,  $\Delta H$ , have been

calculated with eq. D1 and are given in Table D1. This artificial geometry was slightly modified, when sediment deposited downstream of the crest.

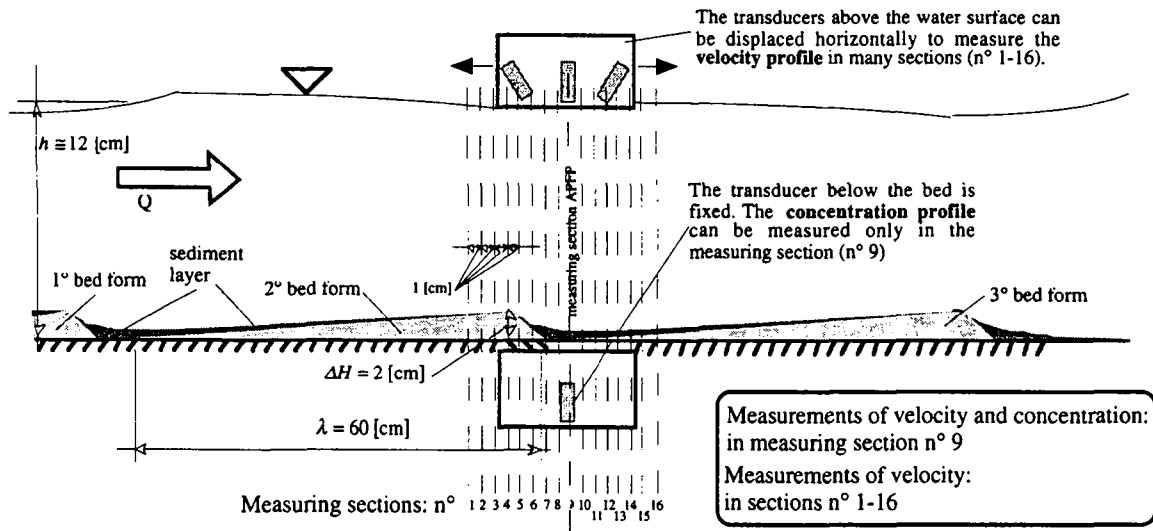


Fig. D1: Schematic of the bed forms

The velocity and concentration measurements have been made with a sonar instrument, the APFP. With this instrument one obtains the instantaneous velocities profile by measuring the back-scattered echo signals (see *Lhermitte and Lemmin, 1994*). The measured velocity appears to be the one of the water/sediment mixture (see *Shen, 1997* and *Cellino, 1998, ch.3*). In addition, by measuring the forward and backward echo signals an echo intensity is obtained (see *Shen and Lemmin, 1996* and *Shen, 1997*) being indicative of the sediment concentration. To get this concentration a calibration – using the suction-sampling method – was performed. The sonar transducers of the APFP are placed in water-filled housings in contact with the water surface and the channel bed (see Fig. D1); the resulting flow perturbation is thus minimized.

The measurements were performed with the sediment-laden flow in capacity condition, notably when a layer of sediment, composed of the same sediment as is in suspension, is always present on the bed.

The measuring section (n° 9) was located between the second and third bed form, thus being close to the downstream face of a bed form. In this section the vertical transducer above the water surface is coaxial with the one below the bed. The vertical transducers operate alternatively emitting and receiving the ultrasonic echoes, which are proportional to the local suspension concentration. Since the transducer below the bed is fixed, thus it cannot be displaced, the APFP can be used to measure the concentration only in one measuring section (n°9). The point velocity,  $u(y, t)$ , and its corresponding concentration,  $c_s(y, t)$ , are extracted, with a frequency of 16 [Hz], from a cylinder-shaped measuring volume having a diameter of  $\Phi \approx 13$  [mm] and height of  $\Delta d \approx 5$  [mm] (see *Shen, 1997*, and *Cellino, 1998*) corresponding to a volume of nearly  $Vol \approx 7 \cdot 10^{-7}$  [ $m^3$ ]. For spherical-shaped sand particles of diameter  $d_{s0} = 0.135$  [mm], a measuring volume contains  $\approx 26$  particles for  $c_s^* = 1$  [ $kg/m^3$ ] up to  $\approx 130$

particles for  $c_s^m = 15$  [kg/m<sup>3</sup>]. In this measuring volume the instantaneous concentration and velocity are supposed to be homogeneous.

The velocity profile is obtained measuring the Doppler frequencies of the backscattered signals coming from the insonified water column. In a special configuration of the APFP instrument, the emitting and receiving transducers are all located in the housing above the water surface (the bed transducer is inactive during the velocity measurements). Thus, it was possible to displace horizontally the instrument. A tristatic configuration has been used to investigate the velocity profiles in many sections (n° 1-n° 16) along the bed forms. In the tristatic configuration the velocity measuring frequency could be increased up to 39 [Hz].

Two flows have been investigated, runs BF\_S015 and BF\_S02, whose hydraulic characteristics are summarized in Table D1. In addition, run BF\_S015 was repeated and a series of 16 velocity measurements around the bed-form crest have been performed to put into evidence the spatial evolution of the flow and its turbulence characteristics.

Author	run	$Q$	$h$	$B/h$	$\lambda/h$	$\Delta H/h$	$U$	$S_f$	$Re \cdot 10^4$	$Fr$	$u_* \equiv u_{*r}$	$u_{*s}$
		[m <sup>3</sup> /s]	[m]	[--]	[--]	[--]	[m/s]	[%]	[--]	[--]	[m/s]	[m/s]
EPFL	BF_S015	0.038	0.110	5.5	5.5	0.18	0.575	0.150	6.322	0.55	0.032	0.040
EPFL	BF_S02	0.043	0.118	5.1	5.1	0.17	0.609	0.200	7.189	0.57	0.039	0.048

run	$d_{50}$	$\rho_s$	$v_{ss}$	$C_s^m$	$\bar{c}_{sa}^m$	$\bar{\rho}_m$	$\overline{\beta_{SM}}$ (best fit)	$\overline{\beta_{APFP}}$ (APFP)
	[mm]	[kg/m <sup>3</sup> ]	[mm/s]	[kg/m <sup>3</sup> ]	[kg/m <sup>3</sup> ]	[kg/m <sup>3</sup> ]	[--]	[--]
BF_S015	0.135	2650	12.0	3.01	21.47	1001.87	1.347	1.142
BF_S02	0.135	2650	12.0	1.94	12.69	1001.21	1.113	1.116

Table D1: Summary of data, for runs BF\_S015 and BF\_S02

The discharge,  $Q$ , has been evaluated as  $Q = U \cdot B \cdot h$ , where the depth-averaged velocity,  $U$ , is obtained by integrating over the depth the longitudinal velocity profile,  $\bar{u}(y)$ ; the flow depth,  $h$ , was measured using limnimeters. The flow depth,  $h$ , is the distance from the top of the sediment layer to the water surface (see Fig. D1). The aspect ratio,  $B/h$ , was high enough to consider the flow as bidimensional. The channel slope,  $S_f$ , refers to the bottom on which the artificial bed forms have been fixed. The Reynolds number,  $Re = U \cdot h / v$ , – where  $v$  is the kinematic viscosity of clear water – and the Froude number,  $Fr = U / \sqrt{g \cdot h}$ , numbers show the flow to be turbulent and subcritical. The shear velocity,  $u_{*r}$ , has been obtained by extrapolating the Reynolds-stress distribution – measured in the upper part of the flow,  $y/h > 0.5$  – towards the bed (see Fig. D4e); this value represents a local estimation of the shear velocity. Subsequently, the shear velocity,  $u_{*s}$ , was also calculated using  $u_{*s} = \sqrt{ghS_f}$ . Both methods (especially the second one) are questionable for obvious reason, but for lack of a better method the shear velocity,  $u_*$ , used for any further calculation is taken as  $u_* \equiv u_{*r}$ .

The sediment used was sand having a characteristic diameter,  $d_{50} = 0.135$  [mm] and a density,  $\rho_s = 2650$  [kg/m<sup>3</sup>]. The settling velocity,  $v_{ss}$ , defined in still clear water, has been calculated (see *Graf*, 1984, p. 45). The depth-averaged concentration,  $C_s^m$ , and the reference

concentration,  $\bar{c}_{sa}^m$ , have been measured with the suction method. The reference concentration,  $\bar{c}_{sa}$ , is evaluated at  $a = 0.05 \cdot h$ , which represents a vertical position in the flow. Defining  $a$  one implicitly assumes that above,  $y > a$ , the sediments are transported in suspension while below,  $y < a$ , the sediments are transported in bedload mode. Since the bedload layer exists only if the flow is in capacity condition, with such a definition of the reference concentration the resulting sediment transport as suspended load is in full *capacity* (saturation). The depth-averaged density,  $\bar{\rho}_m$ , is computed with the depth-averaged concentration.

The  $\overline{\beta}_{SM}$ -values have been obtained by best fitting eq. D2 – using the Rouse number defined in eq. D3 – to the measured dimensionless concentration distributions. Using the definition of eq. D4, the  $\beta(y)$ -values can be evaluated also experimentally using the data obtained with the APFP instrument. Subsequently the depth-averaged  $\overline{\beta}_{APFP}$ -values are obtained.

### D3 Velocity measurements

For both, runs BF\_S015 and BF\_S02, the measurement of the velocities and concentration profiles are obtained using the APFP instrument, positioned fixed in section n° 9 (see Fig. D1). The longitudinal mean velocity profiles, in dimensional,  $\bar{u}$  [m/s], and in dimensionless form,  $\bar{u}/U$ , are plotted in Fig. D2a,b. They are compared to the velocity profiles measured in comparable plane-bed suspension flows (runs Q55S015 and Q60S02 refer to the same channel slope,  $S_f$ , while run Q40S003 had a similar discharge,  $Q$ ) which were reported in *Cellino, 1998 ch. 3*. The thick dashed gray line represents the height of the bed-form crest,  $\Delta H = 0.02$  [m] (see Fig. D1). The thin gray lines represent the upper,  $y_{uv}$ , and lower level,  $y_{dv}$ , of the high vorticity region observed close to the bed-form crest (see Fig. D8a). In the upper part of the flow ( $y > y_{uv}$ ) all the profiles have similar tendencies while close to the bed ( $y < y_{uv}$ ), the ones measured in presence of bed forms fall to zero faster. Note the very small velocities close to the bed ( $y/h < 0.2$ ), which are probably due to the effect of the recirculating region within sections n° 7 and n° 9. Similar observations, both for the  $\bar{u}$  and  $\bar{v}$  profiles, have been communicated by *Mendoza and Shen, 1990*, p. 466, and *Yoon and Patel, 1996*, p. 15, performing mathematical models and by *Lyn, 1993*, p. 312, and *Bennett and Best, 1995*, p. 499, in experimental studies. In Fig. D2c the dimensionless vertical mean velocity profiles are shown. The high values of the downward vertical velocity (black symbols,  $\bar{v}/U \approx -0.07$ ) have to be associated to the reattachment of the flow to the bed behind the bed form. In case of plane-bed suspension flow (gray symbols) the vertical velocities were small and often directed upward.

The longitudinal and vertical components of the turbulence intensity plotted in Fig. D3a,b show the same trend obtained by *Yoon and Patel, 1996*, p. 15, with a numerical model and by *Nelson, McLean and Wolfe, 1993*, p. 3942, in an experimental study. In particular, the presence of a peak close to the bed-form crest reveals the presence of a developing shear layer caused by the separation of the flow.

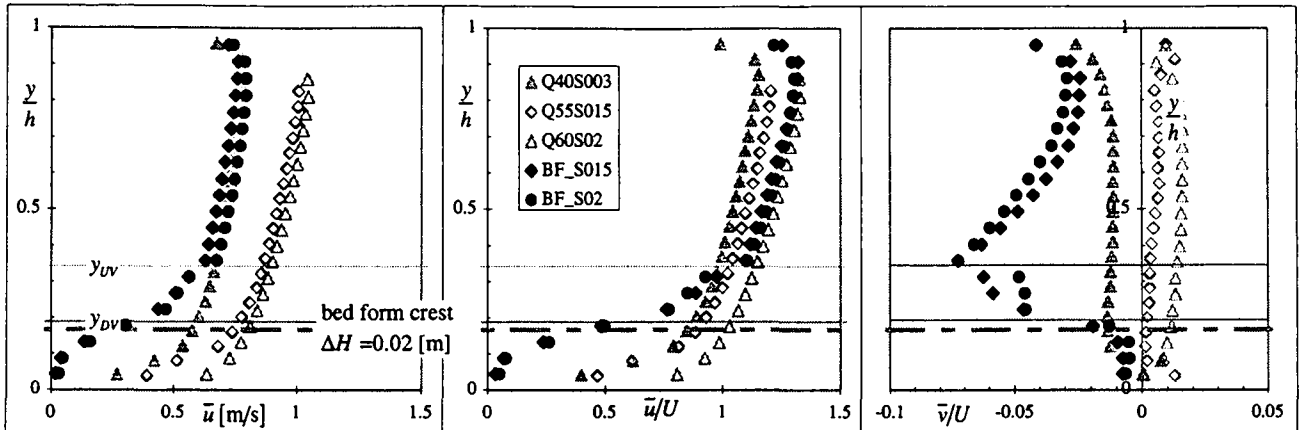


Fig. D2a,b,c: Longitudinal and vertical mean velocity profiles, measured in section n° 9

For  $y > y_{UV}$  the magnitude of the both longitudinal and vertical component of the turbulence intensity (black points) is rather similar to the one observed in a comparable plane-bed suspension flows (gray points). Also the 16 profiles measured around the bed form show somehow the same tendency (see Fig. D4c,d).

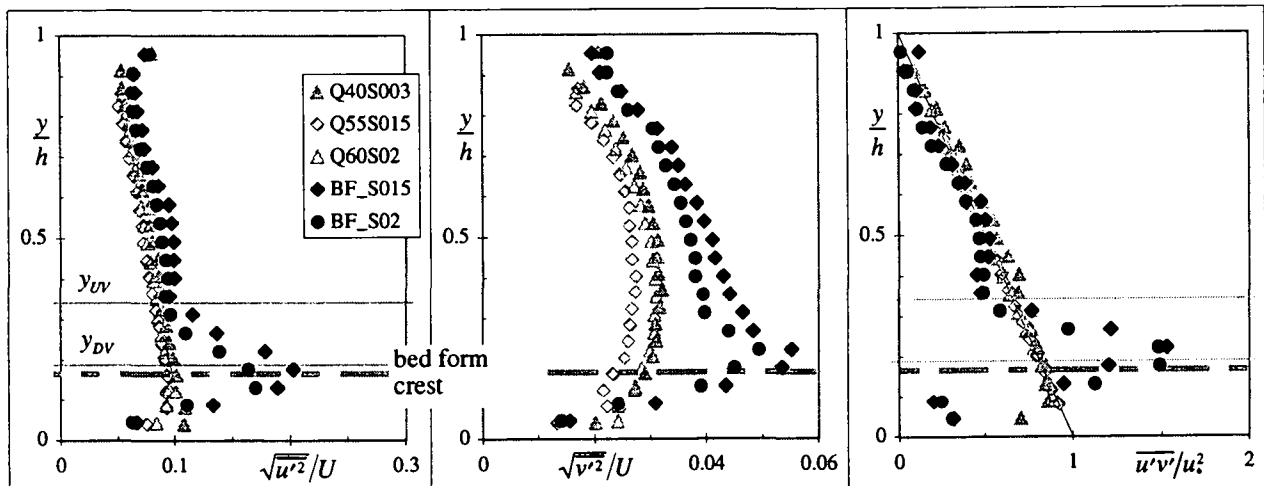


Fig. D3a,b,c: Turbulence-intensity and Reynolds-stress profiles, measured in section n° 9

The dimensionless Reynolds-stress profiles (see Fig. D3c) show a clear peak in the vicinity of the bed-form crest ( $y/h \approx 0.17$ ) which was also evident in the numerical studies of *Mendoza and Shen*, 1990, p. 467, and *Yoon and Patel*, 1996, p. 15. The fact that the Reynolds-stress profiles are close to be linear in the upper part of the flow,  $y/h > 0.5$ , is consistent with the findings of *Lyn*, 1993, p. 318. The Reynolds stress at the wall is considerably lower than the one at the bed-form crest. This fact illustrates the role which turbulence, thus the shear stress, will have on the particle dynamics. Sediment particles which arrive at the bed-form crest (due to previously accelerating flow) will readily remain suspended due to the high degree of turbulence in the flow's free-shear layer. However when particles settle, they will probably remain rather long as part of the bed.

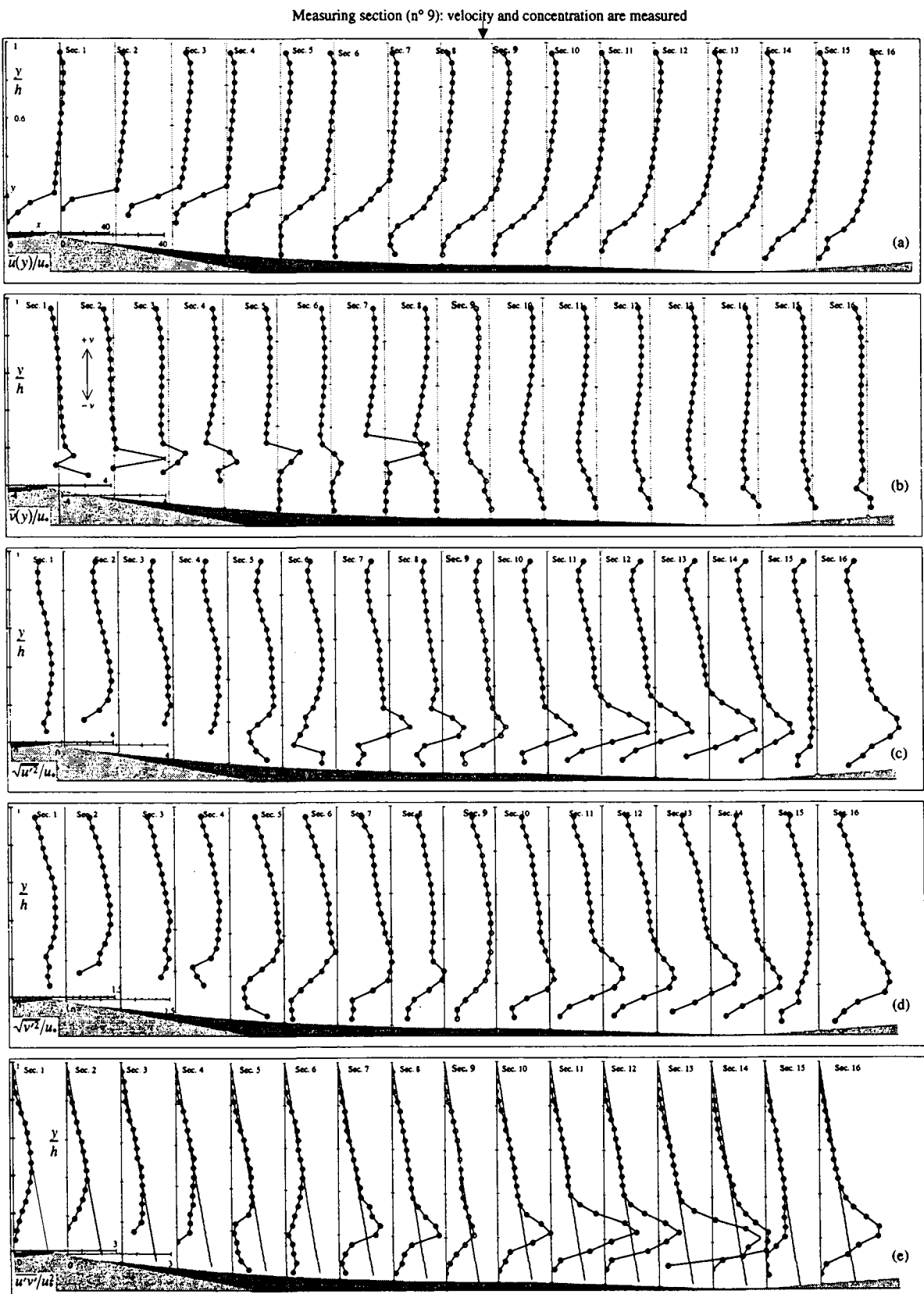


Fig. 4a,b,c,d,e: Velocity, turbulence intensity and Reynolds stress profiles

## D4 Spatial evolution of the flow structure

For the two runs, BF\_S015 and BF\_S02, the APPF instrument has been used to measure both the velocity and concentration profiles, but only in the measuring section n° 9 (see Fig. D1). In addition, for the same hydraulic conditions as existed in run BF\_S015 the velocity field around a bed form has been measured in 16 sections, spaced at 1 [cm]. This investigation has been carried out to study the longitudinal evolution of the flow.

While the overall characteristics of the flow are given in Table D1, the characteristics of the flow's evolution are summarized in Table D2 for the 16 sections investigated. The distance from the bed,  $y$ , refers to the sediment layer on bed forms. The flow depth,  $h$ , represents the distance from the top of the sediment layer to the water surface (see Fig. D1).

In Fig. D4 are plotted the dimensionless distributions of the longitudinal (a) and the vertical (b) velocity, their turbulence intensities (c, d) and the Reynolds stresses (e); the shear velocity is always taken as  $u_* \equiv u_{*r}$ .

The longitudinal velocity profiles (see Fig. D4a) seem to be strongly affected by the presence of the bed form. In some sections (from n° 5 to n° 8) it is even possible to observe negative values of the velocity (directed towards upstream) generated by a flow recirculation behind the bed-form crest. The vertical velocity profiles (see Fig. D4b) show negative values (velocity directed towards the bed) behind the bed-form crest. This is due to the tendency of the flow to reattach itself towards the bed downstream of the bed-form crest. The longitudinal (see Fig. D4c) and vertical (see Fig. D4d) turbulence intensity profiles show, behind the bed-form crest (from section n° 5 to n° 16), the presence of peaks associated with the existence of a separating shear layer. The dimensionless Reynolds-stress profiles have been plotted in Fig. D4e. Only in the upper part of the flow ( $y/h > 0.5$ ) the measured Reynolds-stress profiles follow reasonably the linear trend. Closer to the bed ( $y/h < 0.5$ ) the development of a shear layer is confirmed by the presence of peaks.

Sect.	$h$	$\delta$	$\bar{u}_c$	$U$	$Fr$	$u_* = u_{*r}$	$u_{*s}$	$f$	$Re \cdot 10^4$	$k_s$	$u_* \cdot k_s / v$	$\Pi$
	[m]	[m]	[m/s]	[m/s]	[-]	[m/s]	[m/s]	[-]	[-]	[mm]	[-]	[-]
1	0.092	0.080	0.834	0.677	0.71	0.037	0.037	0.024	6.23	0.366	13.64	0.253
2	0.095	0.083	0.839	0.651	0.67	0.032	0.037	0.020	6.19	0.089	2.87	0.268
3	0.102	0.089	0.840	0.654	0.65	0.033	0.039	0.020	6.67	0.136	4.47	0.320
4	0.105	0.092	0.832	0.612	0.60	0.034	0.039	0.024	6.42	0.397	13.31	0.336
5	0.107	0.093	0.835	0.589	0.57	0.033	0.040	0.025	6.30	0.447	14.57	0.504
6	0.107	0.093	0.823	0.585	0.57	0.038	0.040	0.033	6.26	1.541	58.24	0.517
7	0.108	0.094	0.811	0.584	0.57	0.031	0.040	0.023	6.30	0.324	10.16	0.407
8	0.109	0.095	0.811	0.598	0.58	0.030	0.040	0.020	6.52	0.113	3.36	0.555
9	0.110	0.096	0.800	0.601	0.58	0.031	0.040	0.021	6.62	0.200	6.21	0.576
10	0.111	0.097	0.799	0.595	0.57	0.030	0.040	0.021	6.60	0.171	5.17	0.723
11	0.112	0.098	0.783	0.582	0.55	0.031	0.041	0.023	6.52	0.345	10.79	0.664
12	0.113	0.099	0.781	0.577	0.55	0.031	0.041	0.023	6.52	0.361	11.24	1.007
13	0.116	0.101	0.780	0.569	0.53	0.029	0.041	0.020	6.60	0.150	4.31	1.185
14	0.115	0.100	0.778	0.578	0.54	0.029	0.041	0.020	6.65	0.151	4.42	1.100
15	0.112	0.098	0.772	0.593	0.57	0.030	0.041	0.020	6.64	0.133	3.94	0.979
16	0.110	0.096	0.774	0.595	0.57	0.031	0.040	0.022	6.55	0.264	8.26	1.032
average	0.108	0.094	0.806	0.603	0.59	0.032	0.040	0.023	6.47	0.324	10.94	0.652

Table D2: Summary of data for run BF\_S015

The overall tendency of the flow's evolution over a bed form, as shown in Fig. D4, is rather similar to the one observed behind a bed-form crest by *Nelson, McLean and Wolfe*, 1993, p. 12734, *McLean, Nelson and Wolfe*, 1994, p. 3939 and *Bennett and Best*, 1995, p. 502, as well as behind a back-facing step by *Etheridge and Kemp*, 1978, p. 552, *Nakagawa and Nezu*, 1987, p. 69, and *Wang and Fontijn*, 1993, p. 306.

The friction factor,  $f$ , has been computed by  $f = 8(u_*/U)^2$  (see Table D2). Using the Colebrook-White formula (with the values  $a_f = 11.5$  and  $b_f = 1.5$ ; given by *Silberman et al.*, 1963, pp. 97-143) the values of the equivalent bed roughness,  $k_s$ , have been calculated. Note, that  $f$  and  $k_s$  have to be considered local values being calculated from the local estimation of the shear velocity,  $u_* \equiv u_{*r}$ . The particle Reynolds number,  $u_* k_s / v$ , shows that the bed is not hydraulically rough,  $u_* k_s / v < 70$ . The  $\Pi$ -values have been obtained fitting the theoretical Coles' defect law to the measured profiles, but applied only in the upper part of the flow,  $y/h > 0.5$ , to exclude the recirculation region close to the bed.

The measured longitudinal velocity profiles plotted in defect form,  $(\bar{u}_c - \bar{u})/u_*$  vs  $y/\delta$ , where  $\bar{u}_c$  is the maximum velocity observed at  $y = \delta$ , are shown in Fig. D5a. Also shown is the theoretical Coles' defect law plotted using an average value of the wake strength,  $\Pi = 0.652$  (see Table D2). A value  $\Pi > 0.2$ , would indicate that the flow is a decelerating one (see *Graf and Altinakar*, 1991, p.60) being caused by the reattachment of the flow to the bed. The Coles' defect law describes somehow the experimental profiles only for  $y/\delta > 0.3$ . Close to the bed,  $y/\delta < 0.3$ , the experimental points deviate strongly from the theoretical distribution; this corroborates the observations done by *Lyn*, 1993, p.313. The magnitude of the averaged  $\Pi$ -value agrees with the tendency shown experimentally by *Coleman*, 1981, p. 221.

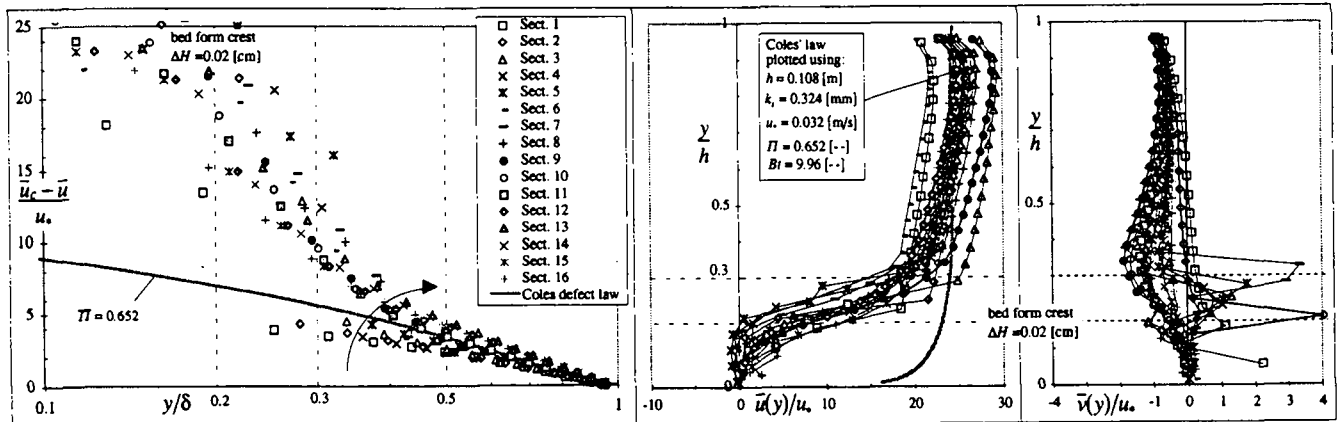


Fig. D5a,b,c: Velocity mean profiles

In Fig. D5b are plotted all the dimensionless longitudinal mean velocities,  $\bar{u}(y)/u_*$ , against the dimensionless coordinate,  $y/h$ . Apart some scatter all the profiles are similar. The gray full line in Fig. D5b represents the Coles law plotted using the spatially averaged hydraulic parameters (see Table D2), namely:  $h = 0.108$  [m],  $k_s = 0.324$  [mm],  $u_* = 0.032$  [m/s] and  $\Pi = 0.652$  [-]. Coles' law and the experimental profiles are very similar in the upper part of

the flow,  $y/h > 0.3$ , while closer to the bed,  $y/h < 0.3$ , the presence of a recirculating region attenuates strongly the experimental profiles. Note also the presence of weak negative velocities (directed towards upstream) below the bed-form crest. These results confirm the tendency observed investigating only section n° 9 (see Fig. D2a,b).

In Fig. D5c are presented the vertical mean velocity profiles,  $\bar{v}(y)/u_*$ . Except for a few profiles (from sections n° 1 to n° 7 and close to the bed) the vertical velocities are always negative (directed towards the bed). This confirms – as shown in Fig. D2c investigating section n° 9 only – that behind section n° 7 the flow reattaches itself towards the bed.

In Fig. D6a are presented the Reynolds-stress profiles compared with the theoretical linear distribution,  $\overline{u'v'}(y) = u_*^2(1 - y/h)$ . In the upper part of the flow ( $y/h > 0.4$ ), the Reynolds stress distribution seems to be linear; this result is consistent with the findings of Lyn, 1993, pp. 318. Close to the bed, the measured Reynolds-stress profiles are perturbed; in particular pronounced peaks are observed which can be associated to the development of a shear layer behind the bed-form crest caused by a separated flow.

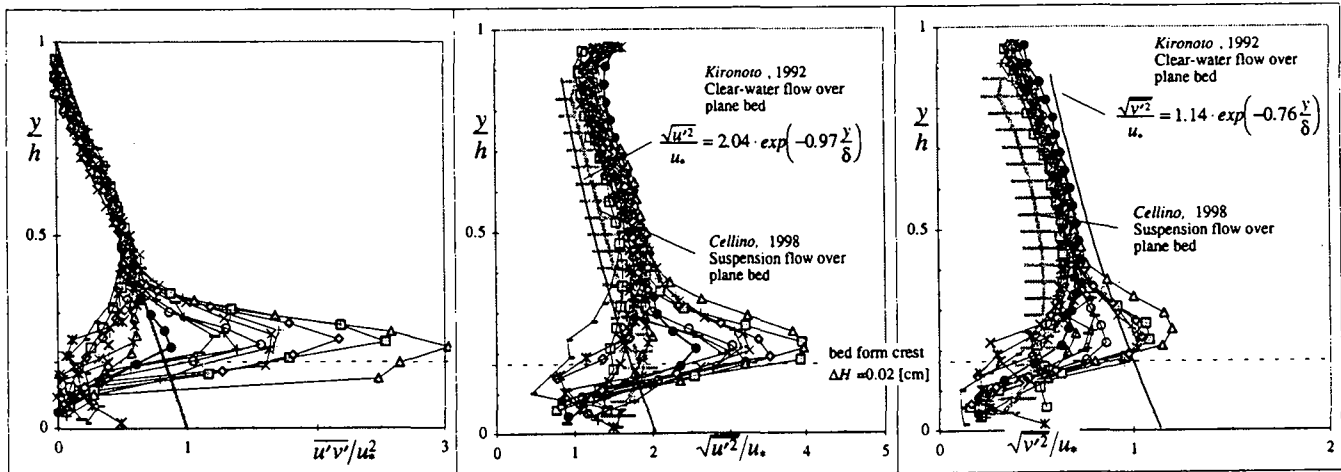


Fig. D6a,b,c: Dimensionless Reynolds-stress, longitudinal and vertical turbulence intensity profiles

In Fig. D6b,c the longitudinal,  $\sqrt{u'^2}/u_*$ , and the vertical,  $\sqrt{v'^2}/u_*$ , component of the turbulence intensity are presented. These intensity profiles are self similar and comparable to the ones measured in suspension flow over plane bed (see gray lines). An important difference is represented by the peak values, caused by the developing shear layer, detected close to the bed ( $y/h < 0.4$ ) in case of flow over bed forms. Again, this is qualitatively consistent with the measurements of Lyn, 1993, p. 316. The full lines in Fig. D6b,c represent the universal expression of the components of the turbulence intensity (in clear water) proposed by Nezu and Nakagawa, 1993, p. 53, using the empirical coefficients obtained by Kironoto, 1992, p. 3.18. The longitudinal component of the turbulence intensity in both type of suspension flow (over a plane bed – gray patterns – and over bed forms – experimental symbols) seems to be slightly enhanced. On the other hand, the vertical component of the turbulence intensity seems to be suppressed over the entire flow depth and especially very close to the bed ( $y/h < 0.1$ ).

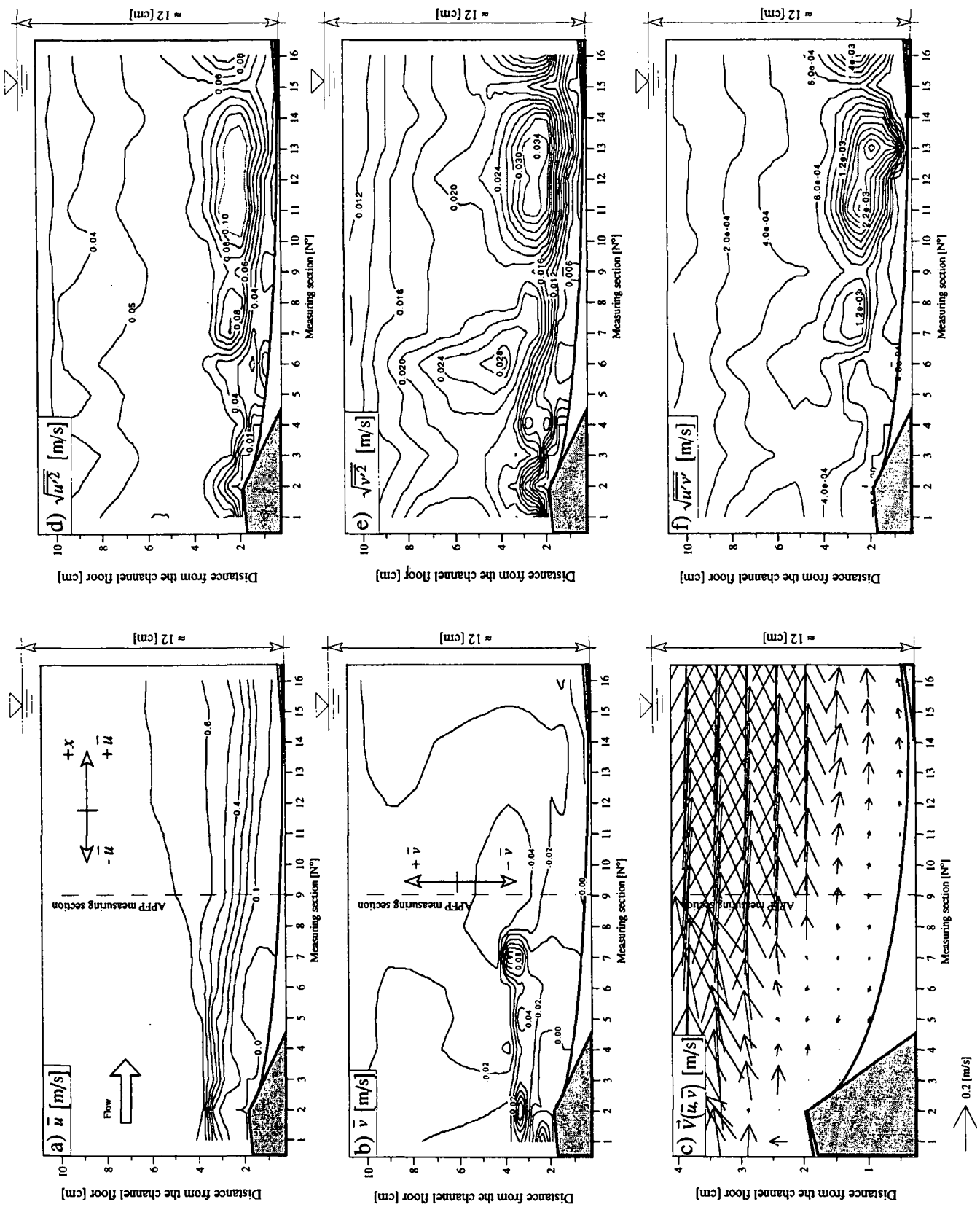


Fig. D7: Contour plots of  
 a): Longitudinal mean velocity  
 b): Vertical mean velocity  
 c): Vector plot of mean velocity  
 d): Longitudinal turbulent fluctuations  
 e): Vertical turbulent fluctuations  
 f): Reynolds stress

Using the data displayed in Figs. D4 contour plots were obtained. In Fig. D7a,b the contour plots of the longitudinal and vertical mean velocity are presented. The contour plot of the longitudinal velocity,  $\bar{u}$ , shows that between sections n° 1 and n° 8 the iso-velocity lines are closely spaced, reflecting the strong vertical gradient of the velocity profiles. Behind section n° 8 the iso-velocity lines become more distant. The contour plot of the vertical velocity,  $\bar{v}$ , shows that between sections n° 1 and n° 7 and close to the bed, the direction of the flow is towards the surface, while behind section n° 7 the direction of the flow is towards the bed. This implies that the reattachment of the flow towards the bed starts behind section n° 8. The contour plot of the velocity vectors,  $\vec{V}(\bar{u}, \bar{v})$ , is given with Fig. D7c. It reveals the presence of a weak reverse flow between sections n° 4 and n° 7 behind the bed-form crest, the separation of the flow between sections n° 2 and n° 8 and finally the reattachment of the flow to the bed behind section n° 8.

In Fig. D7d,e are given the contour plots of the longitudinal and vertical turbulence intensity. The presence of the bed forms generates zones of high turbulence intensity between sections n° 8 and n° 16, where the flow reattaches itself towards the bed. The contour plots of the Reynolds stress, given in Fig. D7f, show a strong enhancement between the sections n° 8 and n° 16, notably close to the bed. The enhancement of both turbulence intensity and Reynolds stress is caused by the developing shear layer due to the separated flow. These results are consistent with numerical and experimental observations made by *Yoon and Patel*, 1996, p. 13, by *Lyn*, 1993, p. 318 and by *Bennett and Best*, 1995 p. 502; for flow over a backward-facing step, *Etheridge and Kemp*, 1978, p. 555 and *Nakagawa and Nezu*, 1987, p. 76, made similar observations.

Subsequently, the mean transverse vorticity,  $\omega_z$ , has been computed from the mean longitudinal and vertical velocity component:

$$\omega_z = \frac{1}{2} \left( \frac{\partial \bar{u}}{\partial y} - \frac{\partial \bar{v}}{\partial x} \right) \quad (\text{D3})$$

The derivative terms,  $\partial \bar{u} / \partial y$  and  $\partial \bar{v} / \partial x$ , have been calculated using a center-finite difference approximation. The corresponding contours of constant  $\omega_z$  are plotted in Fig. D8a. These contour lines show that a high positive (clockwise) vorticity region develops above the bed-form crest, whose magnitude diminishes towards the downstream. A low negative vorticity region develops at the bed-form crest up to the reattachment point at section n° 8. Also indicated are the upper,  $y_{UV}$ , and lower,  $y_{DV}$ , limit of the high vorticity region.

Mean streamlines have been constructed from the velocity profiles in form of lines of constant  $\Psi / (u_c \cdot h)$ , where the stream function is given by:

$$\Psi = \int_0^y \bar{u}(y) \cdot dy$$

This is plotted in Fig. D8b, where around the section n° 6, a reverse-flow region is evident, delimited by  $\Psi = 0$ . Reattachment of the flow is reached at the section n° 8.

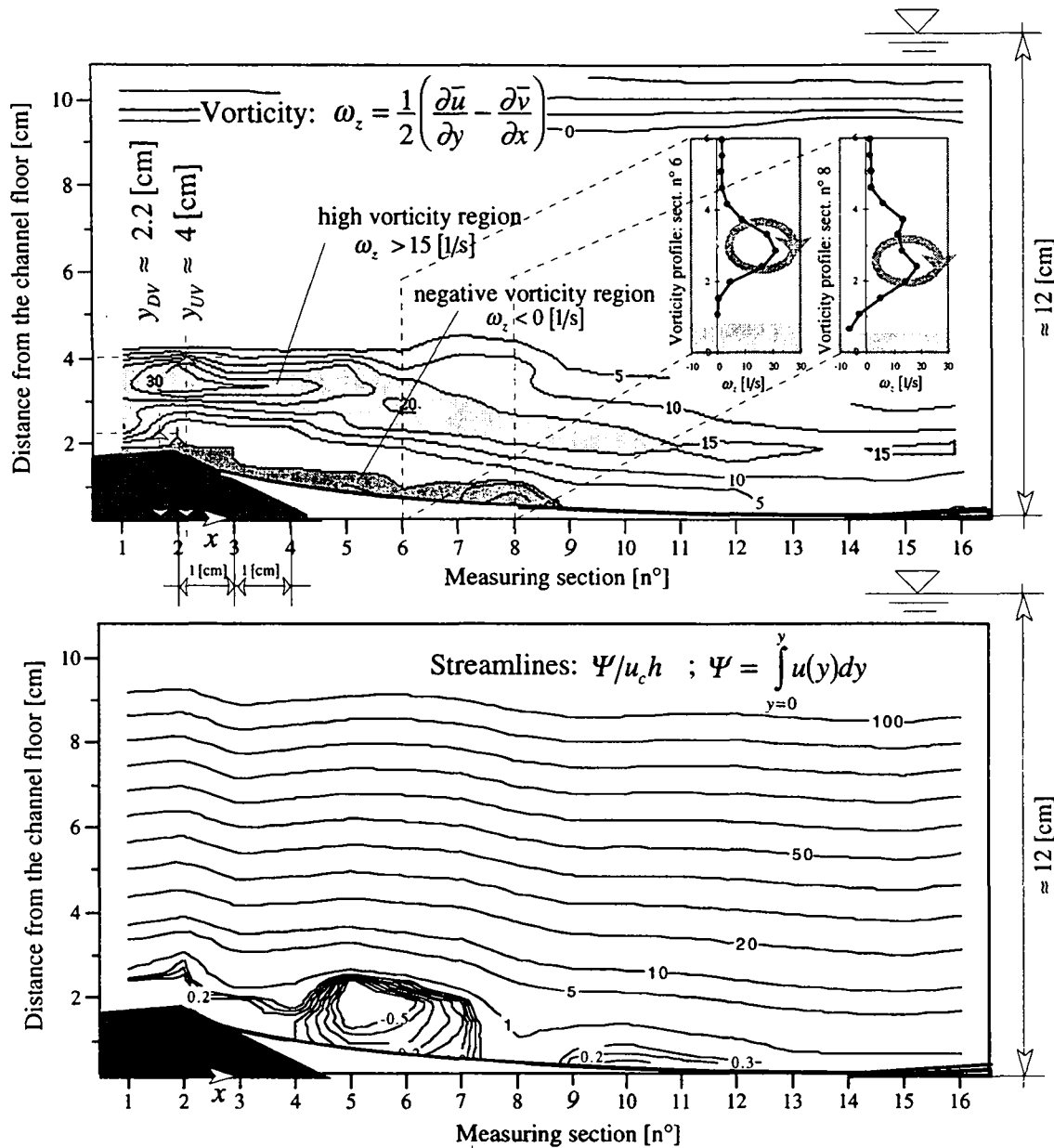


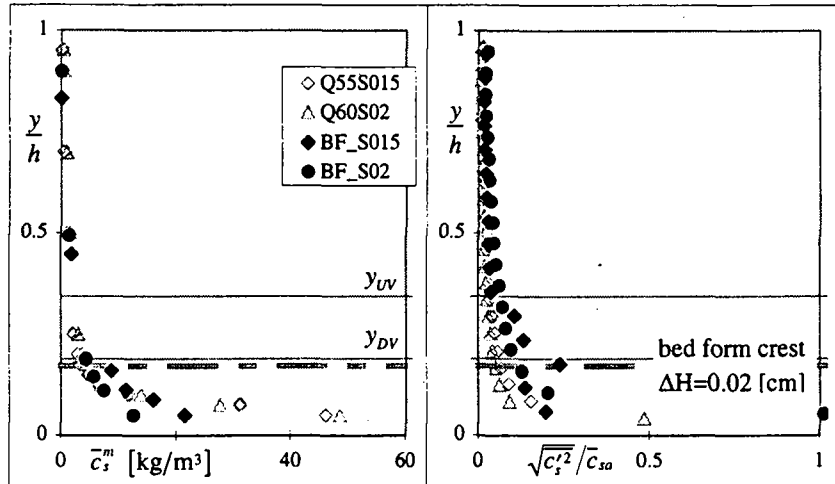
Fig. D8a,b: Contour plot of the vorticity and streamlines

## D5 Concentration measurements

As was explained earlier, concentration measurements could only be performed at one single section, notably section n° 9, since the APFP instrument could only be operated as a fixed installation.

The mean concentration profiles,  $\bar{c}_s^m(y)$  – measured with the suction method – as well as the profiles of the dimensionless fluctuating sediment concentration,  $\sqrt{\bar{c}_s'^2}/\bar{c}_{sa}$  – measured with the APFP instrument – are plotted in Fig. D9a,b. The reference concentration,  $\bar{c}_{sa}$ , evaluated at  $a = 0.05 \cdot h$  with the suction method (see Table D1) has been used as a scaling parameter; it represents the largest concentration of sediments transported in suspension. The depth-averaged concentration,  $C_s^m$ , is obtained integrating the mean concentration profile,  $\bar{c}_s^m(y)$ , over the flow depth. The dimensionless fluctuating concentration profiles,  $\sqrt{\bar{c}_s'^2}/\bar{c}_{sa}$ , (see Fig. D9b) have their

maximum values close to the bed ( $y/h < 0.25$ ); in the upper part of the flow ( $y/h > 0.25$ ) the fluctuating concentrations decrease quite rapidly. The vertical distribution of mean concentration (see Fig. D9a) and fluctuating concentration (see Fig. D9b) are comparable to the ones measured in plane-bed suspension flows (gray symbols in Fig. D9a,b).



Figs D9a,b: Vertical mean and fluctuating concentration profiles

The profiles of the sediment flux,  $\bar{c}_s'v'$  – obtained with the APFP and normalized with their values at the bed – are plotted on Fig. D10. While some scatters is evident, in both cases a peak close to the height of the bed-form crest is noticeable. Apart of these peaks the tendency is similar to the one observed in comparable plane-bed suspension flows (gray symbols).

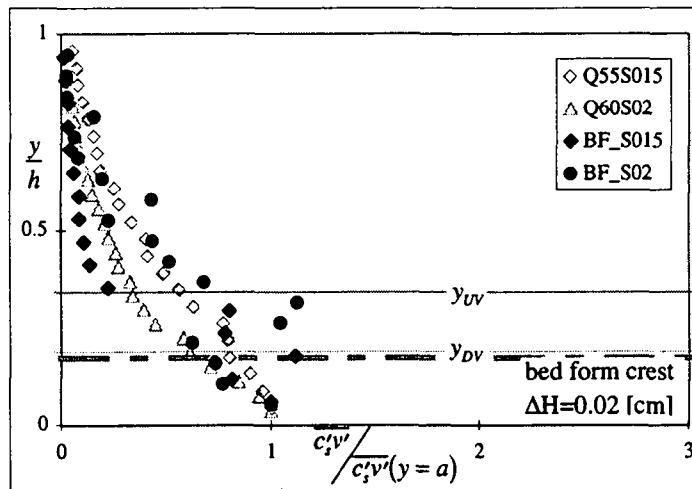


Fig. D10: Sediment flux normalized with its value at the bed

The momentum,  $\epsilon_m(y)$ , as well as the sediment diffusion coefficient,  $\epsilon_s(y)$ , can be evaluated from the measured data set – obtained with the APFP instrument – using their definition given with eq. D4.

The dimensionless momentum,  $\epsilon_m/(u_*h)$ , and sediment,  $\epsilon_s/(u_*h)$ , diffusion coefficient profiles are plotted in Fig. D11a,b. For the first (BF\_S015 in Fig. D11a) and for the second run (BF\_S02 in Fig. D11b) the dimensionless momentum and sediment-diffusion coefficient

profiles show in both cases a peak close to the same location, namely at  $y/h \approx 0.3$ , situated above the bed-form crest. In the case of suspension flows over a plane bed (see gray points in Fig. D11a,b) no pronounced peak is distinguishable.

The dimensionless sediment diffusion coefficients,  $\epsilon_s/(u.h)$ , measured in flows over bed forms, are larger – between  $0.25 < y/h < 0.70$  – than the ones measured in suspension flows over plane bed. This means that the particles are diffused more efficiently by the high turbulence region generated by the bed-form. Close to the water surface –  $y/h > 0.70$  – the coefficients are similar probably because the effect of the bed forms becomes negligible. Close to the bed –  $y/h < 0.25$  – the sediment diffusion coefficients measured in suspension flows over bed forms fall to zero more rapidly becoming smaller than the ones measured in flows over plane bed. This effect is related to the small velocities, turbulence intensities and shear stress measured close to the bed.

The dimensionless momentum diffusion coefficients,  $\epsilon_m/(u.h)$ , measured in flows over bed forms, are smaller than the ones measured in flows over plane bed in the upper region of the flow (above the upper level of the turbulent region,  $y_{uv}$  or  $y/h \approx 0.36$ ). Below this level, where the peaks have been observed, the coefficients measured over bed forms are slightly larger than the ones measured in plane-bed flows. Close to the bed –  $y/h < 0.25$  – they become smaller, falling to zero more rapidly than the ones measured over plane bed. Such a tendency was also reported by Lyn, 1993, p. 321, and by Thorne et al., 1996, p.351.

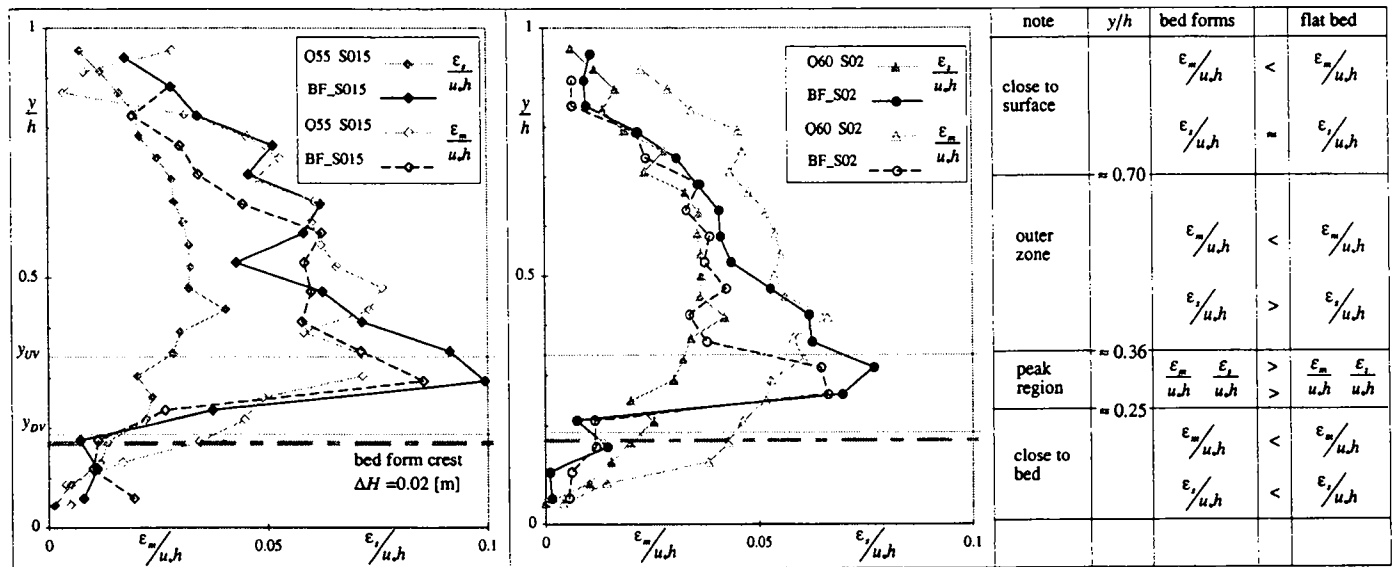


Fig. D11a,b: Dimensionless sediment and momentum diffusion coefficient profiles

The enhancement of the sediment diffusion coefficients over a large part of the flow depth and the partial suppression of the momentum diffusion coefficients can be interpreted as being due to the effect of the shear layer – generated by the bed-form crest – that diffuses more efficiently the particles in the flow and that partially inhibits the diffusion of momentum.

The ratio of the sediment and momentum diffusion coefficient defines the  $\beta(y)$ -values, given with eq. D4; it is shown in Fig. D12a,b. Also shown is the depth-averaged value,  $\overline{\beta}_{APFP}$ , being

close to the unity (see Table D1). For suspension flows over plane bed (gray symbols), it has been shown (see *Cellino*, 1998, §3 and Appendix B) that the experimental  $\beta(y)$ -values – obtained using the APFP instrument – are always smaller than unity. Such an increase is mainly due to the effect of the high turbulence region – generated by the bed-form crest – when the sediment diffusion coefficient is considerably enhanced and the momentum diffusion coefficient is suppressed, leading to an augmentation of the  $\bar{\beta}$ -values.

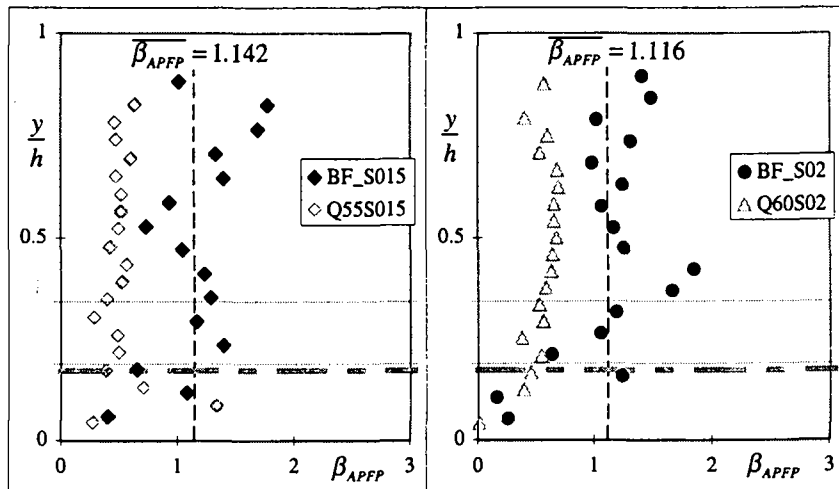


Fig. D12a,b: Profiles of  $\beta$ -values

The concentration profiles – measured with the suction method – are shown for both runs in Fig. D13a,b, using black symbols. For sake of comparison the Rouse equation is shown, using the “theoretical”  $\bar{\beta}$ -value of  $\bar{\beta}=1$  (full line). Also shown is the Rouse equation plotted using the  $\bar{\beta}_{APFP}$ -values (obtained with the diffusion coefficients, dashed line) as well as the best-fit  $\bar{\beta}_{SM}$ -values (obtained by best fitting the Rouse equation, eq. D2, to the vertical concentration profiles measured using the suction method, dotted line, see *Cellino*, 1998, Appendix B). The agreement between the measured concentration profiles (black symbols) and the one using the  $\bar{\beta}_{APFP}$ -values (dashed line) is in both cases satisfactory.

With the present experiments, we believe to shed some light on the long-standing argument (see *Graf*, 1984, p. 174) whether or not the  $\bar{\beta}$ -value is larger or smaller than unity. For the same sediment particles – to be considered as fine particles,  $v_{ss}/u_* < 0.5$  – the  $\bar{\beta}$ -value is  $\bar{\beta} < 1$  for flow over plane bed, however in the presence of bed form, the  $\bar{\beta}$ -value is  $\bar{\beta} > 1$ . This would in a way explain the field data obtained on the Rio Grande river reported by *Nordin* and *Dempster*, 1963, where the presence of bed forms is undeniable and consequently the reported  $\bar{\beta}$ -values are rather large,  $0.7 < \bar{\beta} < 5$ . Note, that other data from Enoree river reported by *Anderson*, 1942, and from the Niobrara river by *Colby et al.*, 1955, (see *Graf*, 1984, p. 177) show the very same tendency.

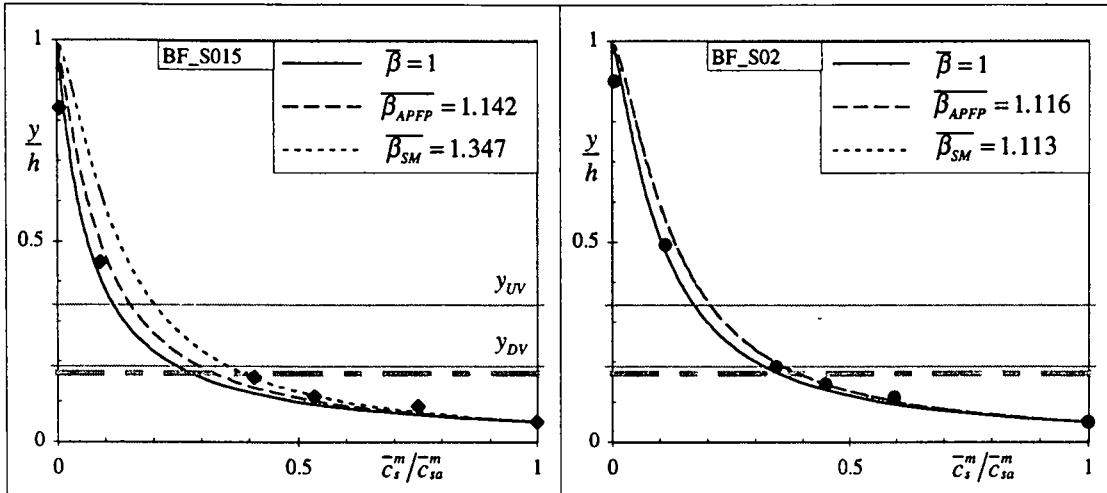


Fig. D13a,b: Vertical mean concentration profiles

## D6 Conclusions

Suspension flows over bed forms have been investigated using a non-intrusive sonar APFP instrument. The measurements were performed with the flow in capacity condition.

In the main part of the paper, we studied the diffusion coefficients of the flow over a bed form. Due to the limitation in the use of the APFP instrument to measure the concentration profiles, only one single section – section n° 9 – could be investigated. The longitudinal and vertical mean velocity profiles, measured in this section, confirms the separation of the flow. The longitudinal and vertical components of the turbulence intensity as well as the Reynolds-stress profiles show pronounced peaks close to the bed-form crest; this is in agreement with the flow structure shown in another part of the paper. The vertical mean concentration profiles, measured at this section – using the suction method – as well as the fluctuating concentration profiles – measured using the APFP instrument – are similar to the ones measured in suspension flow over plane bed (see Fig. D9a,b). The sediment fluxes profiles – measured with the APFP instrument – show peaks located close to the bed-form crest (see Fig. D10). Apart of these peaks, the tendency is rather similar to the one observed in comparable suspension flow over plane bed.

The dimensionless sediment diffusion coefficient profiles,  $\varepsilon_s(y)$ , compared to the ones measured in suspension flow over plane bed, are enhanced over a large portion of the flow depth. On the contrary, the momentum diffusion coefficient profiles,  $\varepsilon_m(y)$ , are partially suppressed (see Fig. D11a,b). This can be interpreted as being due to the effect of the shear layer, generated by the bed-form crest, that diffuses more efficiently the particles in the flow, but partially inhibits the diffusion of momentum.

The depth-averaged  $\overline{\beta(y)}$ -values measured experimentally (being calculated as the ratio of the sediment and the momentum diffusion coefficients), are larger than unity,  $\overline{\beta_{APFP}} > 1$  (see Fig. D12a,b). In the same figure they are compared to the values measured in a comparable suspension flow over plane bed; here it is evident that  $\overline{\beta_{APFP}} < 1$  (see Cellino, 1998). The

agreement between the measured concentration distributions, using the suction method, and the Rouse equation, eq. D4, using the  $\overline{\beta}_{APFP}$ -values measured using the APFP instrument, is considered to be very good (see Fig. D13a,b).

Thus, the presence of bed forms affects the suspension flows, leading to larger  $\overline{\beta}$ -value,  $\overline{\beta} > 1$ , than the ones observed in suspension flow over plane bed, where  $\overline{\beta} < 1$ .

In another part of the paper the spatial evolution of the flow structure was studied. The longitudinal and vertical mean velocity profiles, measured in sections located between two bed forms and close to the bed-form crest, show the separation of the flow and its successive reattachment to the bed (see Fig. D4a,b and D5a,b,c). The longitudinal and vertical components of the turbulence intensity as well as the Reynolds-stress profiles show pronounced peaks close to the bed-form crest,  $y/h \approx 0.17$  (see Fig. D4c,d,e and D6a,b,c). These peaks are generated by the developing shear layer caused by the separation of the flow. The resulting vorticity contour lines show that a high positive (clockwise) vorticity region develops on top of the bed-form crest; its magnitude diminishes towards the downstream. Underneath and beginning at the bed-form crest a weak negative (anti-clockwise) vorticity region develops; it extends up to the reattachment of the flow (see Fig. D8a).

## D7 References

- BENNETT, S. J. and BEST, J. L. (1995). "Mean flow and turbulence structure over fixed, two-dimensional dunes: implications for sediment transport and bedform stability." *Sedimentology*, vol. 42, pp. 491-513.
- CELLINO, M. and GRAF, W. H., (1997) "Measurements of suspension flow in open channels", Proceedings of XXVII IAHR Congress., vol. 1, pp. 179-184, San Francisco.
- CELLINO, M. (1998). "Suspension Flow in Open Channel." *Doctoral dissertation*, Ecole Polytechnique fédérale de Lausanne.
- COLEMAN, N. L. (1970). "Flume Studies of the Sediment Transfer Coefficient." *Water Resour. Res.*, Vol. 6, N°. 3, pp. 801-809.
- COLEMAN, N. L. (1981). "Velocity profiles with suspended sediment." *J. Hydr. Res.*, vol. 19, N° 3, pp. 211-229.
- ETHERIDGE, D.W. and KEMP, P.H. (1978). "Measurements of turbulent flow downstream of a rearward-facing step" *J. Fluid Mech.*, vol. 86, N° 3, pp. 545-566.
- GRAF, W. H. (1984). *Hydraulics of Sediment Transport*. Water Resource Publications, Littleton, CO.
- GRAF, W. H. and ALTINAKAR, M. S. (1991). *Hydrodynamique*. Eyrolles, Paris.
- JOBSON, H. E. and SAYRE, W. W. (1970). "Vertical Transfer in Open Channel Flow." *Proc., Am. Soc. Civil Engrs.* , vol. 96, N° HY3, pp. 703 - 724.
- KIRONOTO, B. (1992). "Turbulence characteristics of non-uniform Flow in rough Open-channel." *Doctoral dissertation N° 1094*, Ecole Polytechnique Fédérale de Lausanne.

- LHERMITTE, R. and LEMMIN, U. (1994). "Open-Channel Flow and Turbulence Measurements by High-Resolution Doppler Sonar." *J. Atmospheric and Oceanic Tech.*, vol. 11, N° 5, pp. 1295-1308.
- LYN, D. A. (1988). "A similarity approach to turbulent sediment-laden flows in open channels." *J. Fluid Mech.*, Vol. 193, pp. 1-26.
- LYN, D. A. (1993). "Turbulence Measurements in Open-Channel Flows over Artificial Bed Forms." *J. Hydr. Engr.*, vol. 119, N° 3, pp. 306-326.
- MCLEAN, S. R., NELSON, J. M. and WOLFE, S. R. (1994). "Turbulence structure over two-dimensional bed forms: Implications for sediment transport." *J. Geophysical Res.*, vol. 99, n° C6, pp.12729-12747,
- MENDOZA, C. and SHEN, H. W. (1990). "Investigation of Turbulent Flow over Dunes." *J. Hydr. Eng.*, vol. 116, N° 4, pp. 459-477.
- NAKAGAWA, H. and NEZU, I. (1987). "Experimental investigation on turbulent structure of backward-facing step flow in an open channel." *J. Hydr. Res.*, vol. 25, N° 1, pp. 67-88.
- NELSON, J. M., McLEAN, S. R. and WOLFE, S. R. (1993). "Mean Flow and Turbulence Fields over two-dimensional Bed Forms." *Water Resour. Res.*, vol. 29, N° 12, pp.3935-3953.
- NEZU, I. and NAKAGAWA, H. (1993). *Turbulence in open-channel flows*. A. A. Balkema, Rotterdam.
- NORDIN, C. F. and DEMPSTER, G. R. (1963). "Vertical Distribution of Velocity and Suspended Sediment Middle Rio Grande New Mexico." US Geol. Survey; Professional Paper 462-B.
- SHEN, W. (1997). "An acoustic instantaneous sediment flux profiler for turbulent flow." *Doctoral dissertation, No. 1630*, Ecole Polytechnique Fédérale de Lausanne.
- SHEN, W. and LEMMIN, U. (1996). "Ultrasonic measurements of suspended sediments. A concentration profiling system with attenuation compensation." *Meas. Sci. Tecn.*, vol. 7, pp. 1191-1194
- SILBERMAN, E. et al. (1963). "Friction Factors in Open Channels." *Proc., Am. Soc. Civil Engrs.*, vol. 90 HY1, USA.
- SUMER, B. M. et al. (1996). "Velocity and Concentration Profiles in Sheet-Flow Layer of Movable Bed." *J. Hydr. Engr.*, vol. 122, N°. 10, pp. 549-558.
- THORNE, P.D. et al. (1996). "Observation of Near-bed Suspended Sediment Turbulence Structures using Multifrequency Acoustic Backscattering" in: *Coherent Flow Structures in Open Channels*, Wiley & Sons Ltd., Chichester, UK.
- WANG, X. and FONTIJN, H.L. (1993). "Experimental study of the hydrodynamic forces on a bed element in an open channel with a backward-facing step" *J. Fluids and Struct.*, vol. 7, pp. 299-318.
- YOON, J. Y. and PATEL, V. C. (1996). "Numerical model of turbulent flow over sand dune." *J. Hydr. Engr.*, vol. 122, N° 1, pp. 10-18.



## APPENDIX E

### Velocity-concentration correlations

#### E1 Introduction

Many open-channel flow experiments have shown that the region of the flow near the bed is composed of two sub-regions each of which has its own character (*Sumer* and *Oguz*, 1978, p.121); these regions are: the viscous sublayer,  $y u_* / v < 5$ , and the generation region,  $5 < y u_* / v < 70$ . In the viscous sublayer, the motion is characterized by a lateral variation of the longitudinal (streamwise) component of the fluid velocity. In the generation region, most of the turbulence generation and dissipation takes place. The remaining flow depth,  $y u_* / v > 70$ , which is called the outer region, includes the log and the wake regions.

The repetitive nature of the turbulent flow in the generation region has been widely accepted. It appears that a deterministic sequence of events occurs, even if the motion is basically chaotic and random in space and time. The characteristic sequence of events is called a **Burst** (or burst cycle). The **Ejections** and the **Sweeps** are the two most important phases of the burst. During ejection, assumed here to be the first part of one typical burst event, a three-dimensional disturbance, composed of low-speed fluid, is pushed away from the bed into the flow whereas in the sweep phase, high-speed fluid moves down towards the bed. It is widely accepted that in the ejection phase, low-speed fluid is ejected upward and at the same time a local convected recirculation cell will form below the lifted streak. Both the low-speed streak and the recirculation cell are pushed far from the bed where the cell size starts to grow. In the lower part of the convected cell, the velocity direction is opposite with respect to an observer moving with the convection speed of the recirculating cell. Thus, a local adverse pressure gradient is temporarily present. When this structure passes over another low-speed wall streak, a new lift-up (ejection event) can appear (see *Sumer* and *Oguz*, 1978). Some fluid from a burst event returns to the wall hitting the bottom and spreading out sideways. If suspended particles are present, this leads to the formation of longitudinal streaks on the bed. A picture of the streaks observed by *Grass*, 1982, is shown in Fig. E1. The transversal distance between wall streaks,  $\lambda$ , is roughly  $\lambda = 100 \cdot v/u_*$ . (see *Sumer* and *Oguz*, 1978) where  $v$  is the fluid viscosity and  $u_*$  is the shear velocity. Spreading fluids push the particles in their immediate vicinity to the adjacent low-speed wall streak. A settling particle is expected to meet the next lifting low-speed streak and it will eventually have another upward motion (ejection). Close to the bed, this process would make it possible for heavy particles to stay in suspension and be transported by the flow.

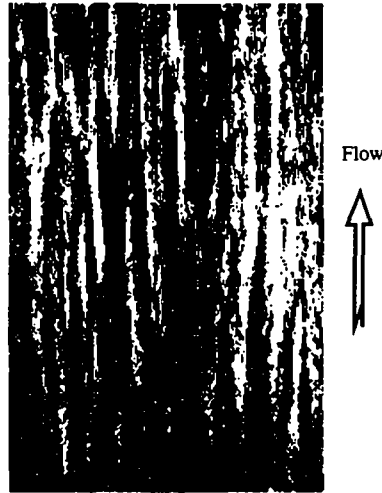


Fig. E1 Sediment parallel streaks observed on the channel bed (*Grass*, 1982)

Another interesting description of the cyclic process (burst) comes from *Hinze*, 1975, p.683. He suggests that the repetitive events are similar to the laminar-turbulent transition process. He assumed that the formation of a horseshoe-shaped vortex close to the bed represents the first step of a burst (see Fig. E2).

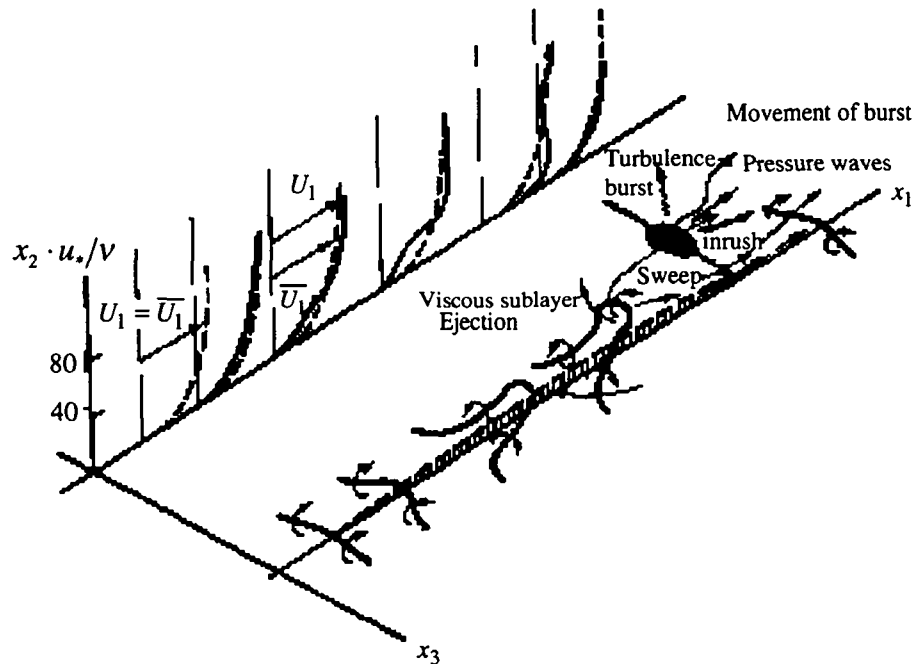


Fig. E2: Conceptual model of the bursting process (*Hinze*, 1975, p.683)

The horseshoe-shaped vortex is elongated by the flow in the longitudinal (streamwise) direction. The tip of the vortex loop moves upward into the region of greater velocities due to a self-induction process. Below the vortex tip, a local deceleration of the fluid appears.

This ejection process, as will be shown later, transports low-momentum fluid away from the wall producing a marked contribution to the shear stress. The local inflectional instability and the collapse of the flow surrounding the original tip of the vortex produces a turbulence burst, similar to that observed during the laminar-turbulent transition process. The burst growing in size moves away from the bed, is convected in an accelerated fluid and swept downstream. The pressure waves associated with the turbulence burst may add to the movement of the fluid towards the bed resulting in a sweep-inrush flow. Both the ejection and the sweep events contribute strongly to the shear stress; experimental measurements of this contribution will be presented later. The longitudinal movement due to the sweep, retarded by the bed, may generate another horseshoe vortex leading to another burst event. The near-wall coherent structures may evolve in the log-wake region (outer edge of the boundary layer) to a larger scale producing the intermittent bulges. These large-scale structures do not govern but affect the near-wall production processes (*Robinson*, 1991).

The introduction of particles into the flow does not seem to affect the overall qualitative cycle of a burst, but may change the frequency and the velocity of the ejections and/or sweep within a burst. In this way, the presence of particles may affect the transport mechanism of turbulent energy from the wall region to the bulk flow (*Rashidi, Hetsroni and Banerjee*, 1990). On the other hand, the burst cycle may influence the sediment suspension mechanism through the ejection and sweep events. The purpose of this Appendix is to shed some light on the complex mutual interaction between coherent structures by analyzing ejections and sweeps and suspended sediment transport.

The investigation of coherent structures, such as the burst cycle, presents several difficulties related to the three-dimensionality and to the event structure of the phenomenon. Flow visualization employing dye, bubbles and smoke has played a major role in the preliminary study of turbulent coherent motions. The quantitative investigation is generally more difficult. This quantification has been successful only in two-dimensional planes of turbulent flows.

In this Appendix, the results of the investigation of coherent structures in capacity suspension flows (Q50S01 sand I, see Table 3.1, and Q50S01\_II sand II, see Table 3.2) and in clear-water flow (CW\_S015, see Table C1) using the APFP instrument, described in detail in Appendix A, are presented. This instrument measured the instantaneous velocity and concentration profiles on the centerline of the measuring cross section located 13 [m] from the entrance of the channel, where the boundary layer is assumed to be established. For more information about the experimental facilities, see Ch. 2. The instantaneous velocity and concentration profiles measured with the APFP instrument have been

correlated and filtered to obtain information about the two main phases composing the burst cycle, namely the ejection and sweep events. Even if the ejection and sweep are defined in the generation region,  $5 < yu_*/v < 70$ , the filtration has been carried out in the whole flow depth.

## **E2 Four-quadrant analysis**

The qualitative description reported above indicates that ejections and sweeps are the two main events composing the burst cycle. The ejection event is schematically characterized by an upward movement of a retarded fluid, while the sweep is a downward movement of an accelerated fluid towards the bed. Thus, it is possible to distinguish these two events by analyzing the direction of the fluctuating velocity components. In other words, it is possible to detect an ejection event if a decelerated fluid,  $u' < 0$ , and an upward velocity,  $v' > 0$ , are observed simultaneously. In the same way, the sweep is characterized by the simultaneous occurrence of an accelerated fluid,  $u' > 0$ , and a downward velocity,  $v' < 0$ . To perform this analysis the longitudinal,  $u' = u - \bar{u}$ , and the vertical,  $v' = v - \bar{v}$  fluctuating velocities will be decomposed following their sign. This approach represents the  $u'v'$  quadrant-splitting scheme (*Lu and Willmarth, 1973, p.495*). The instantaneous  $u'v'$  plane is composed of four quadrants each of which represents an idealized event. In Fig. E3 the  $u'v'$  plane is plotted and the following four quadrants are shown:

**Quadrant I)      *Outward interaction event:***

This event takes place when a positive longitudinal velocity fluctuation,  $u' > 0$ , and a positive vertical velocity fluctuation,  $v' > 0$ , are observed simultaneously.

**Quadrant II)    *Ejection event:***

This event is characterized by the upward movement,  $v' > 0$ , of a low-speed fluid,  $u' < 0$ .

**Quadrant III)   *Inward interaction event:***

In this case a low-speed fluid,  $u' < 0$ , is pushed toward the bed by a negative vertical velocity fluctuation,  $v' < 0$ .

**Quadrant IV)   *Sweep event:***

This event is characterized by a high-speed fluid,  $u' > 0$ , pushed towards the bed by a downward vertical velocity,  $v' < 0$ .

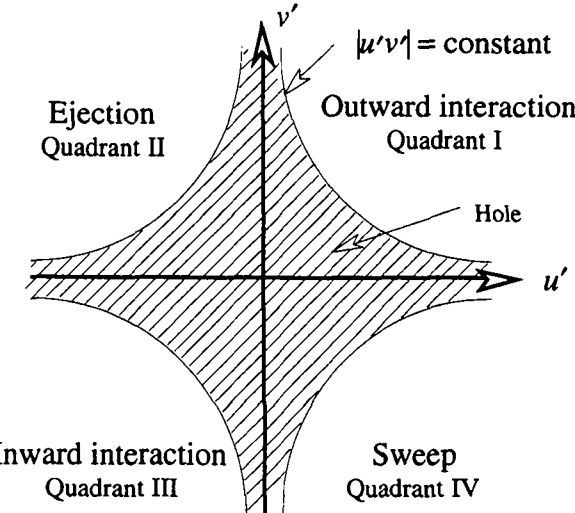


Fig. E3: Sketch of the  $u'v'$  plane

In Fig. E3 the cross-hatched region, called 'hole', is bounded by the curves:

$$|u'v'| = H\sqrt{u'^2}\sqrt{v'^2} \quad (\text{E1})$$

where  $H$  is the hole size representing a threshold level. The four quadrants, excluding the hole are the region contributing to the events. The hole size value,  $H$ , permits to distinguish between strong and weak events for small values of the hole size and strong events only for large values of the hole size.

The instantaneous ( $u$ ,  $v$ ), mean ( $\bar{u}$ ,  $\bar{v}$ ) and fluctuating ( $u' = u - \bar{u}$ ,  $v' = v - \bar{v}$ ) velocities, as well as the Reynolds stress ( $u'v'$ ) and sediment flux ( $c'_sv'$ ) have been filtered using the four-quadrants technique to compute the contribution coming from each quadrant. The filtration has been performed introducing the discriminating variable,  $I_H^i(y, t)$ , defined as follows:

$$I_H^i(y, t) = \begin{cases} 1, & \text{if } [u'(y, t), v'(y, t)] \text{ is in quadrant } i \text{ and if } |u'(y, t)v'(y, t)| > H\sqrt{u'^2}\sqrt{v'^2} \\ 0, & \text{otherwise} \end{cases} \quad (\text{E2})$$

The use of the discriminating variable,  $I_H^i(y, t)$ , as a function of time,  $t$ , and depth,  $y$ , greatly simplifies the filtration procedure.

### E3 Filtration of the instantaneous velocity

The longitudinal and vertical fluctuating velocities,  $u'$  and  $v'$ , measured at four levels over the flow depth, namely at  $y/h \approx 0.05, 0.125, 0.50, 0.90$ , for a run with sand I

(Q50S01) and one with sand II (Q50S01-II), have been plotted into the  $u'v'$ -plane. In Fig. E4, approximately 2900 values of the measured fluctuating velocities,  $(u', v')$ , are shown. In this analysis the hole size has been set at  $H = 0$ ; meaning that all the fluctuating velocities are taken. Note, that most of the velocities fall into Quadrant II (ejection) and Quadrant IV (sweep).

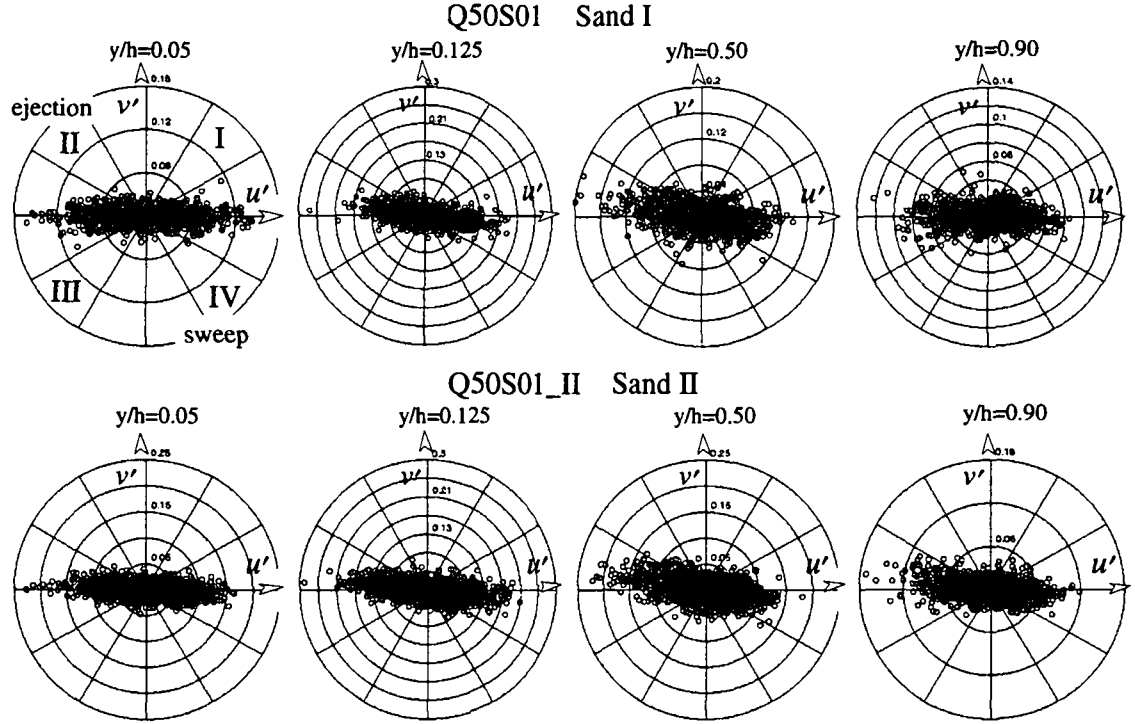


Fig. E4: Quadrant distribution

The number of times (also called occurrence) that the fluctuating velocity falls into the quadrant  $i$ ,  $N_H^i$ , is computed as follows:

$$N_H^i = \sum_{t=0}^{t=T_{MEAS}} I_H^i(y, t) \quad (E3)$$

where  $T_{MEAS}$  is the measurement time length (see Appendix A, p. A-12). Subsequently, the occurrence probability of each event,  $P_H^i$ , is computed dividing  $N_H^i$  by the total number of events, as follows:

$$P_H^i = \frac{\sum_{t=0}^{t=T_{MEAS}} I_H^i(y, t)}{\sum_{t=0}^{t=T_{MEAS}} [I_H^{i=1}(y, t) + I_H^{i=2}(y, t) + I_H^{i=3}(y, t) + I_H^{i=4}(y, t)]} \quad (E4)$$

The occurrence probability profiles are shown in Fig. E5. The computation has been performed four times by first taking all the events ( $H=0$ ), and then progressively

eliminating the weaker ones ( $H=1,2,3$ ) respectively. It is surprising that for the same hole size value,  $H$ , the occurrence-probability profiles for clear-water and suspension flows (sand I and II) are rather similar. Thus, for the size of particles investigated here, the occurrence probabilities are not affected by suspended sediments.

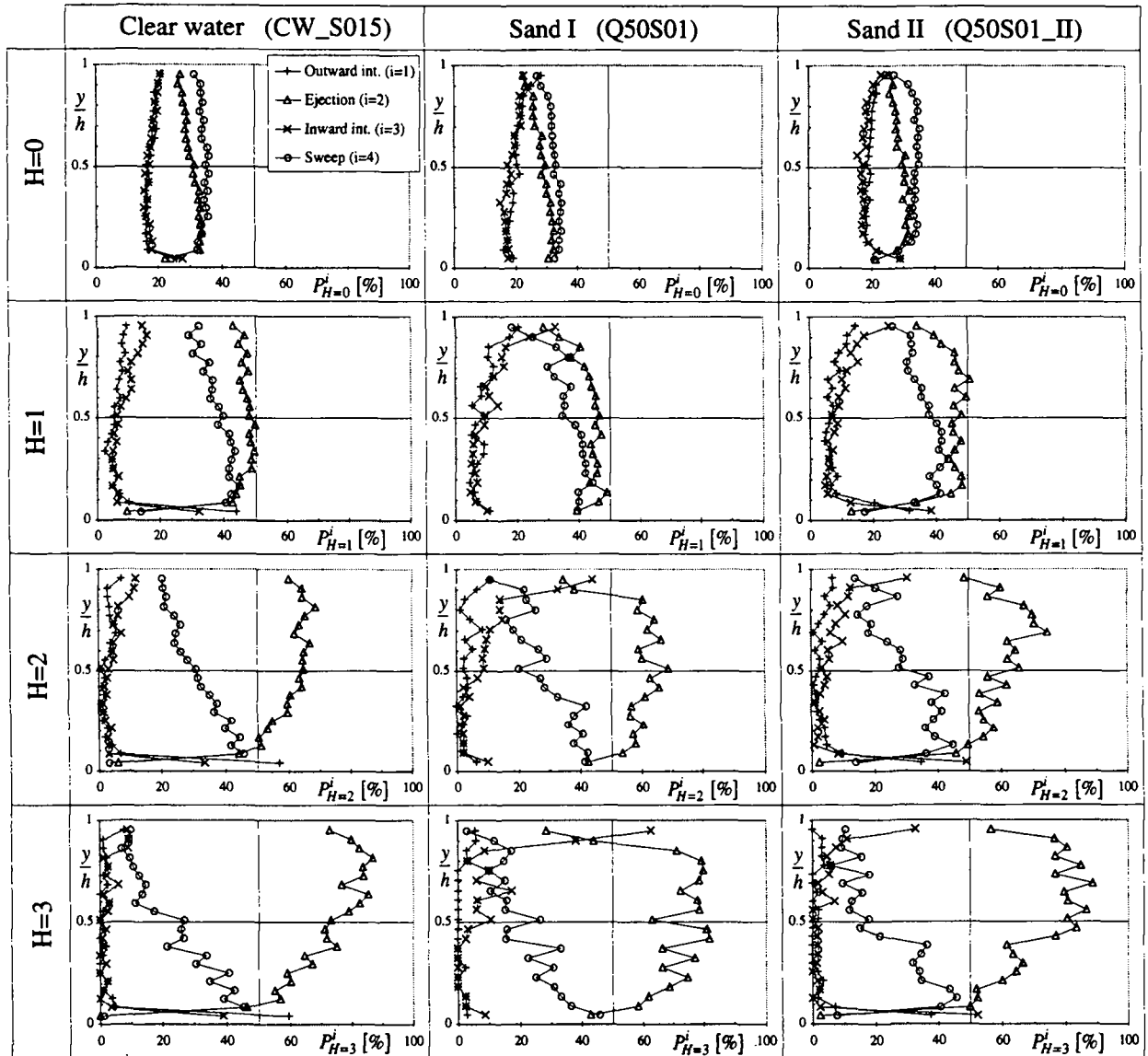


Fig. E5: Event occurrence probability for clear-water and suspension flows (sand I and sand II) for different hole sizes,  $H$ .

For  $H=0$ , the highest probabilities are found for the sweep events,  $P_{H=0}^{i=4}$ , followed by the ejection ones,  $P_{H=0}^{i=2}$ . The other events, namely the outward,  $P_{H=0}^{i=1}$ , and the inward,  $P_{H=0}^{i=3}$  interactions, have the same small occurrence probability. By increasing the hole size value,  $H=1$ , i.e. eliminating the weakest events (for which  $|\mu'v'| < H\sqrt{u'^2}\sqrt{v'^2}$ ), the probability of

observing an ejection,  $P_{H=1}^{i=2}$ , increases rapidly, becoming larger than that of the sweep one,  $P_{H=1}^{i=4}$ . The highest sweep occurrence probability is located close to the bed,  $y/h \approx 0.1$ ; it decreases rapidly going towards the surface. The ejection occurrence probability is rather constant all over the depth. The outward and inward interaction probabilities increase towards the surface but always remain smaller than the ejection and sweep ones.

For  $H=2,3$ , i.e. taking into account only the strongest events, the ejection occurrence probability increases towards the surface where the maximum value is usually observed. The highest sweep occurrence probability has been detected close to the bed at  $y/h \approx 0.1$ ; its value decreases rapidly towards the water surface. The probability of observing outward and inward interactions decreases rapidly with increasing the hole-size value.

The depth-averaged values of the occurrence probabilities, for each hole size,  $H$ , are shown in Table E1. Note, that the probability of the same event for the same hole size,  $H$ , is similar for clear-water and for suspension flows. By increasing the hole size, the ejection occurrence probability increases rapidly. By eliminating the weakest events ( $H=2,3$ ) the inward interaction probability is slightly larger than the outward one; however, both of them are always very small.

	Clear water (CW_S015)				Sand I (Q50S01)				Sand II (Q50S01_II)			
	H=0	H=1	H=2	H=3	H=0	H=1	H=2	H=3	H=0	H=1	H=2	H=3
Outward (N° 1)	18.2	8.3	5.7	4.6	20.6	9.96	4.01	1.61	20.3	9.66	5.07	3.08
Ejection (N°2)	30.0	45.0	58.5	69.5	28.2	42.2	56.3	65.8	28.6	43.2	56.7	68
Inward (N°3)	18.4	10.1	6.5	4.7	19.1	12.6	12	12.3	18.8	12.1	9.91	7.84
Sweep (N°4)	33.5	36.6	29.3	21.2	32.1	35.3	27.7	20.3	32.3	35.1	28.3	21.1
Depth-averaged occurrence probability, $\bar{P}_H^i$ [%]												

Table E1: Depth-average occurrence probability

#### E4 Filtration of the longitudinal mean velocity

The filtration of the longitudinal mean velocity profiles into the  $u'v'$ -plane has also been performed. Let us consider the time series of the longitudinal,  $u(t, y)$ , and the vertical,  $v(t, y)$ , instantaneous velocities measured at a given depth,  $y$ . These series are filtered in the  $u'v'$ -plane by using the corresponding fluctuating longitudinal,  $u'(t, y) = u(t, y) - \bar{u}(y)$ , and vertical,  $v'(t, y) = v(t, y) - \bar{v}(y)$ , velocities as discriminants. The filtration has been carried out by using the discriminating variable,  $I_H^i$ , according to the following equation:

$$\bar{u}_H^i(y) = \frac{\sum_{t=0}^{T_{MEAS}} u(y, t) \cdot I_H^i(y, t) \cdot \Delta t_{MEAS}}{\sum_{t=0}^{T_{MEAS}} I_H^i(y, t) \cdot \Delta t_{MEAS}} \quad (E5)$$

where  $\Delta t_{MEAS}$  is the time lag between two consecutive velocity acquisitions. In other words, with eq. E5, one time-averages only those instantaneous longitudinal velocities,  $u(y, t)$ , which fall into a given quadrant and which obey  $|u'(y, t)v'(y, t)| > H\sqrt{u'^2}\sqrt{v'^2}$ .

In addition, the instantaneous velocity has also been filtered using only the vertical fluctuating velocity as a criterion. In this way, it is possible to average only the instantaneous longitudinal velocity referring to upward,  $v' > 0$  (Quadrant I or II), or downward,  $v' < 0$  (Quadrant III or IV), fluctuating velocities. These criteria are obtained by modifying eq. E5 as follows:

$$\bar{u}_H^{up}(y) = \frac{\sum_{t=0}^{T_{MEAS}} u(y, t) \cdot [I_H^{i=1}(y, t) + I_H^{i=2}(y, t)] \cdot \Delta t_{MEAS}}{\sum_{t=0}^{T_{MEAS}} [I_H^{i=1}(y, t) + I_H^{i=2}(y, t)] \cdot \Delta t_{MEAS}} \quad (E6)$$

$$\bar{u}_H^{down}(y) = \frac{\sum_{t=0}^{T_{MEAS}} u(y, t) \cdot [I_H^{i=3}(y, t) + I_H^{i=4}(y, t)] \cdot \Delta t_{MEAS}}{\sum_{t=0}^{T_{MEAS}} [I_H^{i=3}(y, t) + I_H^{i=4}(y, t)] \cdot \Delta t_{MEAS}} \quad (E7)$$

In Fig. E6 the longitudinal mean velocity profiles, filtered into the four quadrants, are shown. In this case all the events have been taken in consideration, i.e.  $H=0$ .

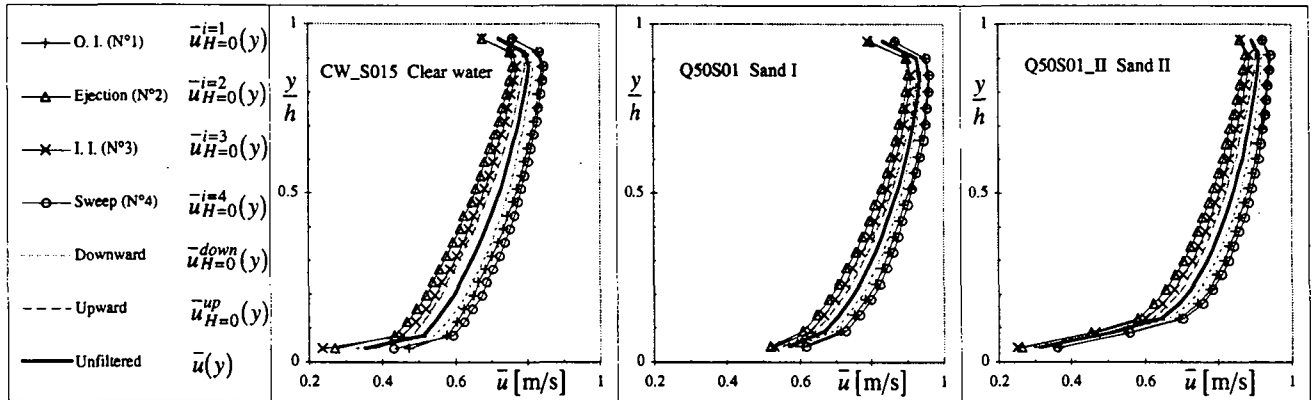


Fig. E6: Filtered longitudinal mean velocity profiles.

Note, that the longitudinal mean velocity, referring to upward movements,  $\bar{u}_{H=0}^{up}(y)$ , is smaller than the unfiltered one,  $\bar{u}(y)$ . This confirms that the fluid ejected upwards,  $v' > 0$ , is a low-speed fluid, or:  $\bar{u}_{H=0}^{up}(y) < \bar{u}(y)$ . This observation has also been made by *Grass*, 1982, p. 14. A more precise indication comes from the longitudinal mean velocity profiles referring to the ejection event:  $\bar{u}_{H=0}^{i=2}(y)$ ; it is evident that the ejection event occurs in the presence of low-speed fluid,  $\bar{u}_{H=0}^{i=2}(y) < \bar{u}(y)$ . On the other hand, the sweep occurs in the presence of high-speed fluid,  $\bar{u}_{H=0}^{i=4}(y) > \bar{u}(y)$ . More generally, it is the downward movement,  $v' < 0$ , that occurs in the presence of high-speed fluid,  $\bar{u}_{H=0}^{down}(y) > \bar{u}(y)$ . One obtains the same results by filtering clear-water longitudinal mean velocity profiles.

## E5 Filtration of the fluctuating velocities

The characteristic values of the fluctuating velocities in the horizontal and the vertical direction are represented by the root mean square (rms.) values. Thus, the rms. values of the fluctuating velocities filtered in the  $u'v'$ -plane represent the characteristic magnitudes of the fluctuating velocities associated with each event. Using the same notation as in eq. E3, the rms values of the filtered longitudinal and the vertical fluctuating velocities have been calculated according to the eqs. E8 and E9, as follows:

$$\sqrt{\bar{u'^2}}_H^i(y) = \frac{\sum_{t=0}^{t=T_{MEAS}} [u'(y, t)]^2 \cdot I_H^i(y, t) \cdot \Delta t_{MEAS}}{\sum_{t=0}^{t=T_{MEAS}} I_H^i(y, t) \cdot \Delta t_{MEAS}} \quad (E8)$$

$$\sqrt{\bar{v'^2}}_H^i(y) = \frac{\sum_{t=0}^{t=T_{MEAS}} [v'(y, t)]^2 \cdot I_H^i(y, t) \cdot \Delta t_{MEAS}}{\sum_{t=0}^{t=T_{MEAS}} I_H^i(y, t) \cdot \Delta t_{MEAS}} \quad (E9)$$

The characteristic values of the fluctuating velocity directed upward and downward have been computed as well. The equations used are:

$$\sqrt{\bar{u'^2}}_H^{up}(y) = \frac{\sum_{t=0}^{t=T_{MEAS}} [u'(y, t)]^2 \cdot [I_H^{i=1}(y, t) + I_H^{i=2}(y, t)] \cdot \Delta t_{MEAS}}{\sum_{t=0}^{t=T_{MEAS}} [I_H^{i=1}(y, t) + I_H^{i=2}(y, t)] \cdot \Delta t_{MEAS}} \quad (E10)$$

$$\sqrt{u'^2}_{H=0}^{down}(y) = \frac{\sum_{t=0}^{t=T_{MEAS}} [u'(y, t)]^2 \cdot [I_H^{i=3}(y, t) + I_H^{i=4}(y, t)] \cdot \Delta t_{MEAS}}{\sum_{t=0}^{t=T_{MEAS}} [I_H^{i=3}(y, t) + I_H^{i=4}(y, t)] \cdot \Delta t_{MEAS}} \quad (E10bis)$$

$$\sqrt{v'^2}_{H=0}^{up}(y) = \frac{\sum_{t=0}^{t=T_{MEAS}} [v'(y, t)]^2 \cdot [I_H^{i=1}(y, t) + I_H^{i=2}(y, t)] \cdot \Delta t_{MEAS}}{\sum_{t=0}^{t=T_{MEAS}} [I_H^{i=1}(y, t) + I_H^{i=2}(y, t)] \cdot \Delta t_{MEAS}} \quad (E11)$$

$$\sqrt{v'^2}_{H=0}^{down}(y) = \frac{\sum_{t=0}^{t=T_{MEAS}} [v'(y, t)]^2 \cdot [I_H^{i=3}(y, t) + I_H^{i=4}(y, t)] \cdot \Delta t_{MEAS}}{\sum_{t=0}^{t=T_{MEAS}} [I_H^{i=3}(y, t) + I_H^{i=4}(y, t)] \cdot \Delta t_{MEAS}} \quad (E11bis)$$

In Fig. E7 the profiles of the rms. longitudinal velocity fluctuations, filtered in the  $u'v'$ -plane, taking all the events in consideration,  $H=0$ , are shown. These profiles,  $\sqrt{u'^2}_{H=0}^{i=1,2,3,4}(y)$ , as well as the ones associated with upward,  $\sqrt{u'^2}_{H=0}^{up}(y)$ , and with downward,  $\sqrt{u'^2}_{H=0}^{down}(y)$ , fluctuating velocities, and the unfiltered,  $\sqrt{u'^2}(y)$ , ones are rather similar in clear-water and in suspension flows using sand I and sand II. In all the cases the rms. values of the fluctuating velocities associated with Quadrant II,  $\sqrt{u'^2}_{H=0}^{i=2}(y)$ , (ejection) are larger than the ones associated with the other three quadrants. This means that the largest characteristic fluctuating velocities are observed during the ejection events. The longitudinal fluctuating velocities associated with upward movements,  $\sqrt{u'^2}_{H=0}^{up}(y)$ , are larger than the ones related to downward movements,  $\sqrt{u'^2}_{H=0}^{down}(y)$ ; this has been observed in both clear-water and suspension flows. Note, that the fluctuating velocities of each quadrant are not additive because of the square in the rms. definition.

In summary, the upward event in general and the ejection event in particular are characterized by large values of the longitudinal fluctuating velocities. Close to the surface, the fluctuating velocities associated with all four quadrants are similar. This is probably due to the turbulence isotropy. The profiles are also similar close to the bed; in this region the ejection events transfer fluid momentum to the sediments on the bed leading to an apparent diminution of their characteristic longitudinal velocity fluctuations. This is confirmed by the absence of the same suppression observed in case of clear-water flow.

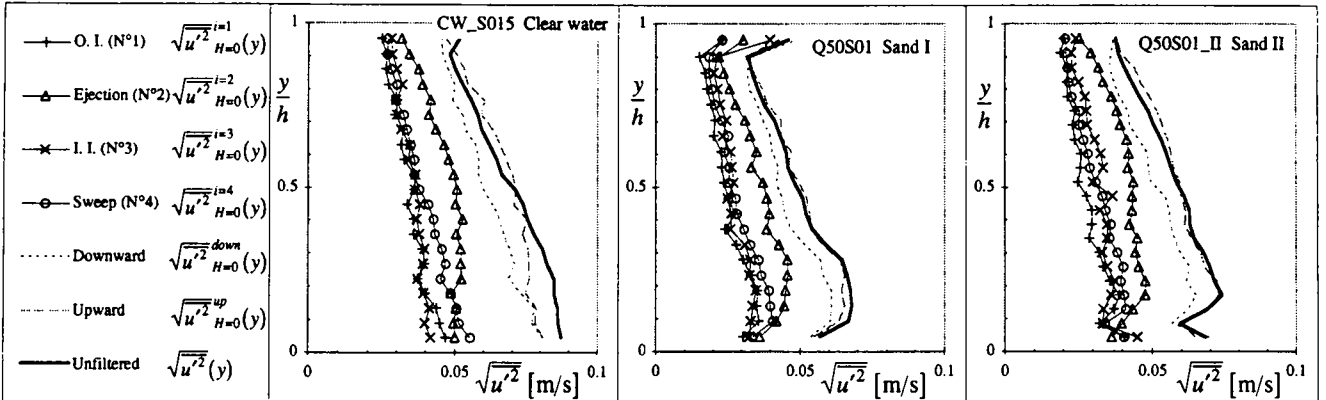


Fig. E7: Filtered longitudinal fluctuating velocity profiles

The profiles obtained by filtering the fluctuating vertical velocities into the four quadrants, are shown in Fig. E8. First of all, the presence of a turbulence damping is evident comparing the suspension flows and the clear-water flow profiles. The turbulence damping associated with the presence of suspended sediment has been the object of a detailed study in Appendix C and Ch. 3 of this thesis. The rms. values of the fluctuating vertical velocities associated with the ejection events,  $\sqrt{v'^2}_{H=0}(y)$ , are larger than the ones related to the other three quadrants. Close to the surface and close to the bed, the profiles become rather similar to each other as was already observed for the longitudinal direction. In this case, the partial suppression of the rms. values of the ejection events observed close to the bed is due to the momentum transfer from the fluid to the sediment particles on the bed. Again, note the absence of this suppression in the case of clear-water flow.

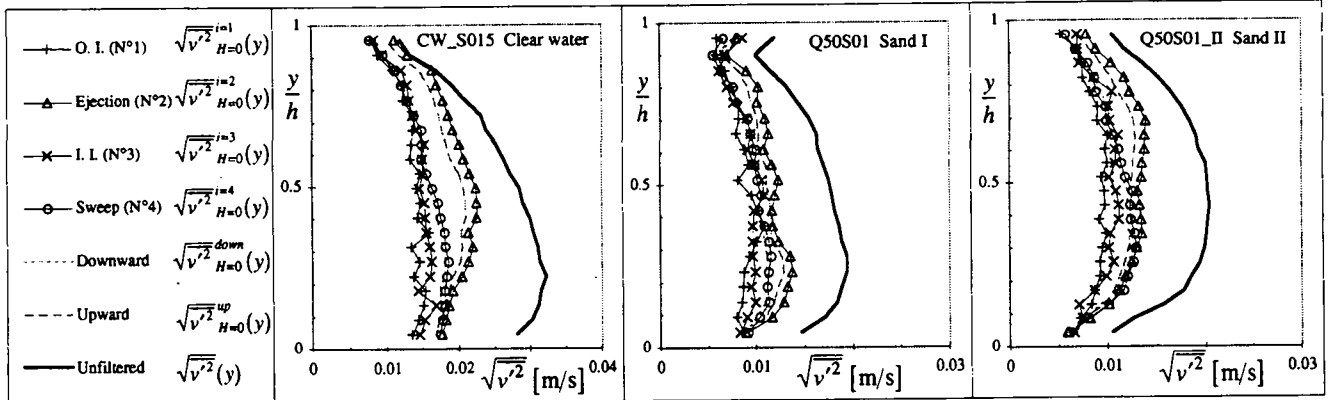


Fig. E8: Filtered vertical fluctuating velocity profiles

Fig. E7 and E8 clearly show that the ejection events are characterized by high longitudinal and vertical fluctuating velocities. This indicates that the erosion of sediment

particles from the bed and maintaining them in suspension can be attributed mainly to the ejection events.

## E6 Filtration of the Reynolds stress

The filtration of the Reynolds-stress profiles,  $\overline{u'v'}(y)$ , into the four quadrants provides information about the contribution coming from each event. This can be particularly interesting because the Reynolds stress is strictly related to the beginning of motion of the sediment particles on the bed and their subsequent suspension in the flow. In the filtering procedure, all the events have been considered,  $H=0$ . The equation used to compute the filtered Reynolds-stress profiles is the following:

$$\overline{u'v'}_H^i(y) = \frac{\sum_{t=0}^{T_{MEAS}} u'(y, t)v'(y, t) \cdot I_H^i(y, t) \cdot \Delta t_{MEAS}}{\sum_{t=0}^{T_{MEAS}} I_H^i(y, t) \cdot \Delta t_{MEAS}} \quad (E12)$$

In Fig. E9 the filtered and the unfiltered Reynolds-stress profiles are shown. Again, the contribution to the Reynolds stress coming from the ejection event,  $\overline{u'v'}_{H=0}^{i=2}(y)$ , is the most important one for both clear-water and suspension flows. The second most important contribution comes from the sweep event,  $\overline{u'v'}_{H=0}^{i=4}(y)$ . The outward (N° 1) and the inward interaction (N° 3) make similar small negative contributions.

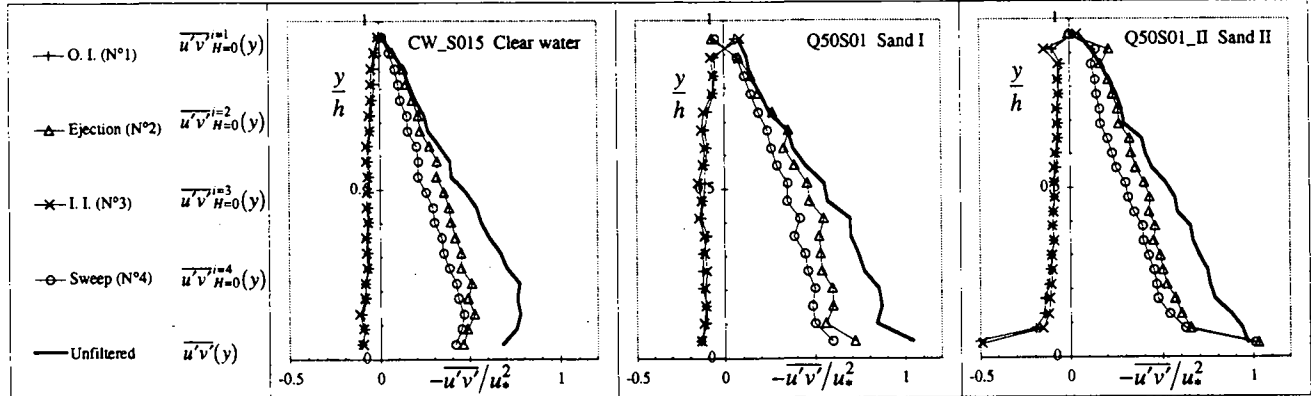


Fig. E9: Filtered Reynolds-stress profiles

The contributions to the Reynolds stress coming from each of the quadrants are additive. Thus, it is possible to compute the fractional contribution profiles of each quadrant as shown in Fig. E10. In both clear-water and suspension flows, the fractional contributions coming from ejection, (N° II), and sweep, (N° IV), events increase from the bed towards

the surface. The contribution coming from the ejection event, N° II, is about 80%, while the sweep-event one is about 60% for both clear-water and suspension flows. Nakagawa and Nezu, 1977, p. 120, Nakagawa and Nezu, 1981 and Lu and Willmarth, 1973, p. 497 obtained similar results investigating the contribution to the Reynolds stress in clear water flows close to the bed.

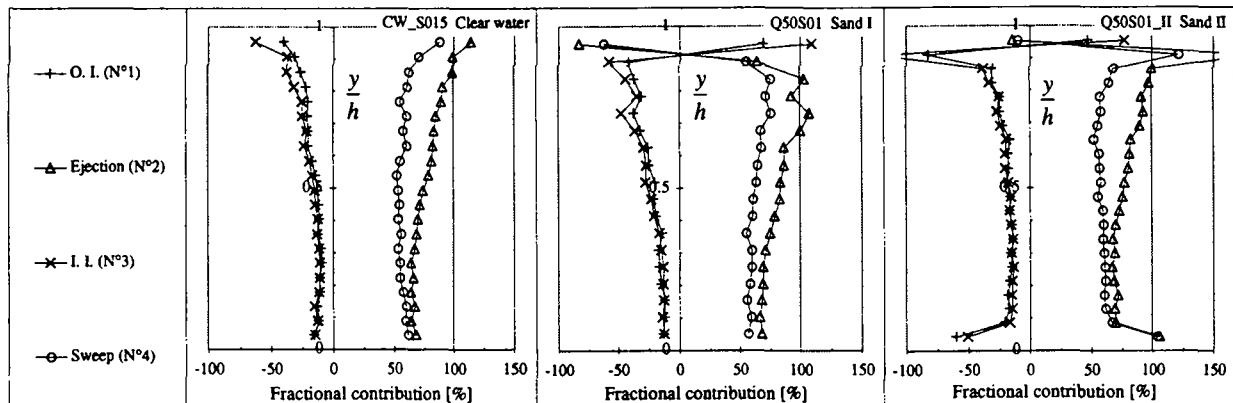


Fig. E10: Fractional contribution to the Reynolds stress

The largest contribution comes from the ejections and sweeps, showing again the importance of these events. The strong influence of these events on the erosion, deposition and suspension of sediments is confirmed.

As said above, the ejection and sweep events are the main phases composing the burst cycle. The first step of the bursting development can be represented by the ejection event, while the collapse of the coherent structure can be represented by the sweep event. Therefore, a strong correlation between the burst cycle and suspended sediment transport is expected. When the ejection event occurs, one should observe high longitudinal and vertical fluctuating velocities providing a strong contribution to the shear stress. This leads to an erosion of the bed or to the re-suspension of sediment particles. To confirm this argument, the filtration of the sediment flux,  $\bar{c}_s'v'$ , into the four quadrants has been performed.

## E7 Filtration of the sediment flux

The sediment flux,  $\bar{c}_s'v'$ , represents the upward flux of sediment generated by the fluctuating vertical velocity which compensates the downward flux of sediment caused by the gravitational settling,  $\bar{c}_s \cdot v_{ss}$ , where  $v_{ss}$  is the settling velocity. The solution of the equation obtained by imposing the equilibrium of these two fluxes leads to the Rouse equation (see Ch. 1) expressing the vertical mean concentration distribution.

If, as was shown by the filtration of velocities, the ejection event is the principal contributor to the upward fluctuating velocities and to the Reynolds stress, the sediment flux will also be principally generated by the ejection event. To verify this argument the filtration of the sediment flux into the  $u'v'$ -plane has been performed taking all events into account,  $H=0$ , as follows:

$$\overline{c'_s v'}_H^i(y) = \frac{\sum_{t=0}^{T_{MEAS}} c'_s(y, t) v'(y, t) \cdot I_H^i(y, t) \cdot \Delta t_{MEAS}}{\sum_{t=0}^{T_{MEAS}} I_H^i(y, t) \cdot \Delta t_{MEAS}} \quad (E13)$$

In Fig. E11, the filtered and the unfiltered sediment-flux profiles are shown. As expected, the largest contribution to the sediment flux comes from the ejection events,  $\overline{c'_s v'}_{H=0}^{i=2}(y)$ . The second largest contribution comes from the sweep event,  $\overline{c'_s v'}_{H=0}^{i=4}(y)$ , but in this case the sediment flux is directed towards the bed. The contributions coming from the outward (N° I) and inward (N° III) interactions are negligible.

Therefore, the ejection events can be considered as an injector of sediments into the main flow. Since the ejection events are not continuous, it is of interest to compute the mean-time period separating two successive ejection events.

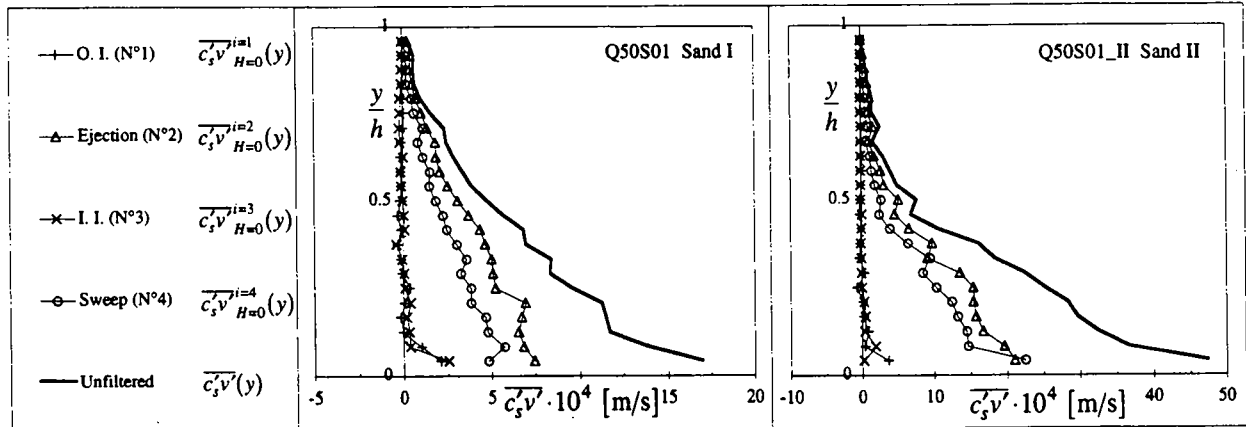


Fig. E11: Filtered sediment-flux profiles

## E8 Mean event intervals

In Fig. E5 the occurrence probability distributions of the four event types are shown. These profiles have been computed as the ratio of the occurrence number of the event- $i$ ,  $N^i$ , and the total number of events,  $N_H^{tot} = N_H^{i=1} + N_H^{i=2} + N_H^{i=3} + N_H^{i=4}$ . Similarly, by

dividing the measurement time length,  $T_{MEAS} \approx 180$  [s], by the occurrence number of each event,  $N_H^i$ , one obtains the mean-time interval separating two  $i$ -events as follows:

$$\Delta T_H^i = T_{MEAS} / N_H^i \quad (\text{E14})$$

In Fig. E12 the mean-time interval distributions for the ejection and sweep events, for different hole sizes,  $H$ , are shown.

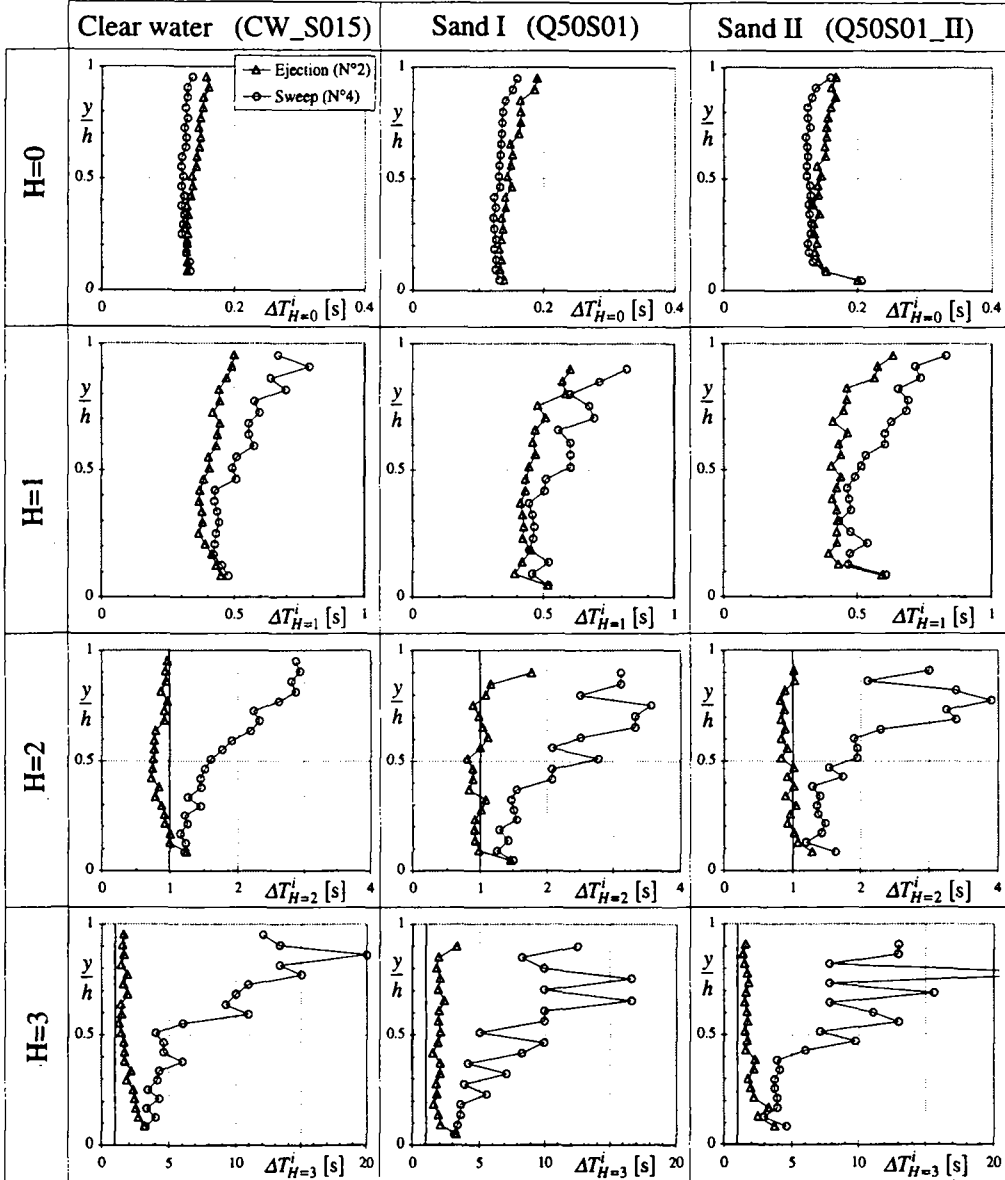


Fig. E12: Mean time interval distribution for ejection and sweep events

For the same hole size,  $H$ , the mean-time interval distributions measured in clear-water and suspension flows are very similar. By increasing the hole size,  $H$ , the time intervals of both the ejection,  $\Delta T_H^{i=2}$ , and the sweep,  $\Delta T_H^{i=4}$ , events increase (note the change in the  $x$ -

axis scales). When taking all the events into account,  $H=0$ , a sweep and ejection event is normally observed every  $\Delta T_{H=0}^{i=2}$  [s]  $\approx \Delta T_{H=0}^{i=4}$  [s]  $\approx 0.13$  [s]. Note, that a strong ejection event, for example  $H=2$ , occurs every  $\Delta T_{H=2}^{i=2}$  [s]  $\approx 1$  [s], while the observation of a sweep event of the same magnitude occurs every  $\Delta T_{H=2}^{i=4}$  [s]  $\approx 2$  [s]. These profiles also show that the mean-time interval, referring to ejection event,  $\Delta T_{H=2}^{i=2}$  [s]  $\approx 1$  [s], is nearly constant all along the depth while the sweep one,  $\Delta T_{H=2}^{i=4}$  [s]  $\approx 2$  [s], increases towards the surface.

Almost every second a strong ejection event,  $H=2$ , occurs. This means that in this time period the particles are eroded from the bed and injected into the flow and/or kept suspended. In Table E2 the depth-averaged values of the ejection and sweep mean-time intervals for the different hole sizes are summarized. Note, that these values are merely indicative due to the depth dependence of the interval distributions (especially the sweep ones).

The outward and inward interactions are weak phenomena; thus, by filtering out the smallest events,  $H>0$ , they become too rare to give reliable values. On the other hand, the sweep but especially the ejection events are strong and rather frequent.

	Clear water (CW_S015)				Sand I (Q50S01)				Sand II (Q50S01_II)			
	H=0	H=1	H=2	H=3	H=0	H=1	H=2	H=3	H=0	H=1	H=2	H=3
Outward (N° 1)	0.23	3.19	too rare	too rare	0.21	2.44	too rare	too rare	0.21	2.57	too rare	too rare
Ejection (N°2)	<b>0.13</b>	<b>0.43</b>	<b>0.91</b>	<b>1.94</b>	<b>0.15</b>	<b>0.48</b>	<b>1.12</b>	<b>2.22</b>	<b>0.15</b>	<b>0.47</b>	<b>0.97</b>	<b>2.02</b>
Inward (N°3)	0.23	2.41	too rare	too rare	0.23	2.14	too rare	too rare	0.23	2.21	too rare	too rare
Sweep (N°4)	<b>0.12</b>	<b>0.53</b>	<b>1.91</b>	<b>8.06</b>	<b>0.13</b>	<b>0.59</b>	<b>2.32</b>	<b>8.49</b>	<b>0.13</b>	<b>0.59</b>	<b>2.15</b>	<b>8.73</b>
Mean time interval, $\Delta T^i$ [s], between the same event <i>i</i>												

Table E2: Depth-averaged mean time interval

### E9 Visual correlation between velocity and suspended concentration

The APFP instrument measures simultaneously and continuously the velocity and the suspended concentration of the flow at the centerline of the measuring section. Interesting observations can be made by visually comparing the instantaneous velocity and concentration profiles. In fact, if one plots these profiles against time, it becomes possible to observe the temporal evolution of the measured velocity and concentration with their mutual correlation.

It is important to note that the velocity and the suspended concentration profiles have been obtained in two independent ways from the same signal. The velocity has been measured by the analysis of the Doppler frequency, whereas the concentration has been

measured by recording the ultrasonic echo intensity (see Appendix A). The measuring frequency of the APFP instrument was equal to 16[Hz] for both velocity and concentration.

In Figs E13 and E14 the velocity and concentration profiles measured for runs Q50S01 and Q55S015 (both with sand I) are plotted. In order to obtain readable plots, only the profiles measured during three seconds have been considered. In Figs. E13a,b and E14a,b the instantaneous longitudinal and vertical velocities are shown respectively. Note the chaotic sequence of high and low longitudinal and vertical velocities; this shows the irregular motion of the flow. The plot of the instantaneous suspended concentration is very interesting (see Figs. E13c and E14c). Close to the bed,  $y/h < 0.2$ , the high concentration region (yellow color) is particularly evident. Although this region is thin and always located close to the bed, in certain cases it approaches and exceeds  $y/h \approx 0.3$ . A sediment “cloud” is generated very close to the bed and is subsequently diffused towards the surface. The existence of a correlation between these sediment clouds and the instantaneous velocity will be put into evidence later.

In Fig. E15 and E16 the suspended concentration profiles (see Fig. E15b and E16b) are compared to the instantaneous velocity profiles filtered into the upward (see Fig. E15a and E16a) and downward (see Fig. E15c and E16c) components taking all events into account,  $H=0$ . The event labeled E1 (E for Erosion) in Fig. E15a is correlated with the sediment cloud (also labeled E1) in Fig. E15b. The upward movement in E1 transports fluid rich in sediment (high concentration region located close to the bed) towards the surface; as a consequence a sediment cloud appears. On the other hand, the downward event called D1 in Fig. E15c (D for Deposition) produces the opposite effect. The movement towards the bed transports fluid poor in sediment (low concentration region) towards the bed. As a consequence the sediment clouds vanish (see Fig. E15b). The very same observations can be made for run Q55S015 (sand I). The sediment clouds called E2 and E3 (see Fig. E16b) are correlated with the upward velocity movements E2 and E3 (see Fig. E16a) while the downward movement D2 (see Fig. E16a) is correlated with the low concentration region called D2 (see Fig. E16b).

The fluctuating vertical velocity profiles have been filtered into the  $u'v'$ -plane taking all the events into account,  $H=0$ . In Fig. E17 and E18 the suspended concentration profiles are compared to the filtered fluctuating vertical velocities. The sediment cloud labeled E1 (see Fig. E17a) is correlated to the ejection events E1 (see Fig. E17c) while the sediment clouds E2 and E3 (see Fig. E18a) are correlated to the ejection events E2 and E3 (see Fig. E17c). This confirms that the erosion of sediment from the bed and its diffusion in the flow are mainly caused by ejection events. The disappearance of sediment clouds, region D1 in Fig. E17a and region D2 in Fig. E18a, is however associated with sweep events (see Fig. E17e

and Fig. E18e). The outward (see Fig. E16b and Fig. E17b) and inward (see Fig. E17d and Fig. E18d) interactions are weak events not well correlated to the suspended concentration profiles. From Fig. E17 and Fig. E18 the importance of the ejection and sweep events on the suspension mechanics is clearly evident.

In Figs. E19 and E20 the instantaneous suspended concentration profiles are compared to the instantaneous Reynolds stress. In Fig. E19a the large Reynolds-stress regions called E1 and D1 are correlated to the sediment cloud E1 and to the low concentration region D1 respectively. In the same way, the sediment clouds E2 and E3 and the low concentration region D2 in Fig. E20b are correlated to the high Reynolds-stress region E2, E3 and D2 in Fig. E20a. Note, that the Reynolds stress associated with ejection and sweep events are not distinguishable being  $-\rho u'v' > 0$  in both the cases. The discrimination has to be made through the sign of  $u'$  and  $v'$ .

## E10 Conclusions

The coherent structure called burst has been the subject of much research. Unfortunately, the complex mutual interaction between bursts and suspended particles is far from being clearly understood. The results reported here were obtained by investigating the burst cycle in suspension flows. The analysis has been carried out by filtering the instantaneous longitudinal and vertical velocity profiles as well as the suspended concentration profiles according to the classical four quadrant  $u'v'$ -plane (see Fig. E3) decomposition. The purpose of this Appendix is to shed some light on the correlation between the two most important phases of the burst cycle, namely the ejection (assumed here to be the initial event of the burst cycle) and the sweep events (final event), and the suspended transport.

The ejection event, characterized by the simultaneous occurrence of an upward movement,  $v' > 0$ , of a decelerated fluid,  $u' < 0$ , and the sweep event, characterized by the downward movement,  $v' < 0$ , of an accelerated fluid,  $u' > 0$ , are observed more frequently than the other two events, namely the outward and the inward interactions (see Fig. E4). This discrepancy increases when the weakest events are filtered out (see Fig. E5). The occurrence probability profiles of each event measured in clear-water and in suspension flows are similar. This means that the statistical distribution of the events in the suspension flow is not affected by adding the suspended sediments used in this study.

The mean longitudinal velocity profiles,  $\bar{u}(y)$ , filtered in the  $u'v'$ -plane, clearly show that the ejection and sweep events are associated with a decelerated and accelerated fluid respectively (see Fig. E6). Generally speaking, the upward,  $v' > 0$ , and the downward

vertical fluctuating velocities,  $v' < 0$ , seem to mainly involve decelerated and accelerated fluid respectively.

The filtered rms. values (interpreted as characteristic values) of the longitudinal,  $\sqrt{u'^2}$ , (see Fig. E7) and vertical,  $\sqrt{v'^2}$ , fluctuating velocities (see Fig. E8), show that the strongest velocity fluctuations occur during the ejection event. Thus, this event will be strongly involved in suspended transport since the particles are eroded and/or suspended predominantly by strong turbulent velocity fluctuations.

The Reynolds stress,  $\overline{u'v'}$ , has been filtered (see Fig. E9) and the contribution coming from each event (see Fig. E10) has been computed. Again, it is evident that the ejection event contributes the most to the unfiltered Reynolds stress. The second most important contribution comes from the sweep event. Thus, the critical Reynolds stress, normally used as a threshold level for the motion of the particles on the bed, could be effectively replaced by an equivalent critical ejection level.

The sediment flux,  $\overline{c'_s v'}$ , (representing the upward flux of sediment that compensates the downward one,  $\overline{c_s v_{ss}}$ , due to the gravitational settling), is mainly generated by the ejection events (see Fig. E10). The contribution of the sweep events, directed towards the bed and always smaller than the ejection ones, can not be neglected.

The mean-time interval between two successive ejection and sweep events have been computed (see Fig. E11 and Table E2). The strongest ejection events occur with a frequency of nearly 1 [s] while the equivalent sweep events are rarer, being of nearly 2 [s].

The comparison of the instantaneous velocities and suspended concentration profiles confirms the importance of the ejection and sweep events on the suspended transport mechanics. The appearance of sediment clouds eroded from the bed (see Fig. E13 and E14) is strictly correlated to a strong upward vertical fluctuating velocity in general (see Figs. E15 and E16) and a strong ejection event in particular (see Figs. E17 and E18). However, these sediment clouds disappear in the presence of a vertical downward fluctuating velocity or a sweep event. The correlation between the instantaneous Reynolds stress and the suspended concentration profiles is also very strong (see Fig. E19 and E20).

In summary, the burst cycle plays an important role in sediment suspension mechanics. In particular, the ejection event, the initial phase of a burst cycle, represents the main cause of the erosion and/or the suspension of particles, whereas the sweep event, the final phase of a burst cycle, can be associated with the sediment deposition.

### Q50S01 Sand I

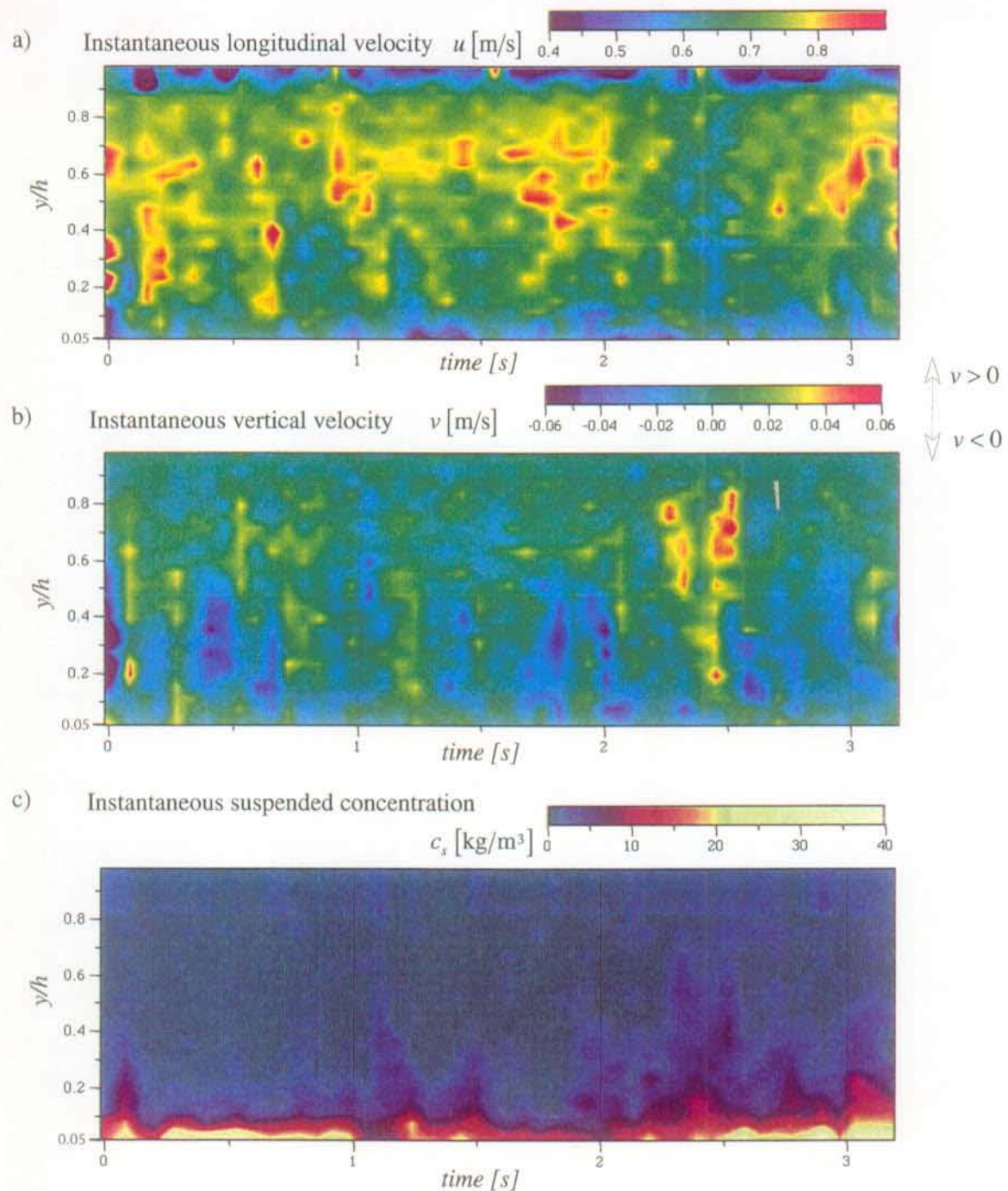


Fig. E13: Instantaneous velocity and concentration profiles

Q55S015 Sand I

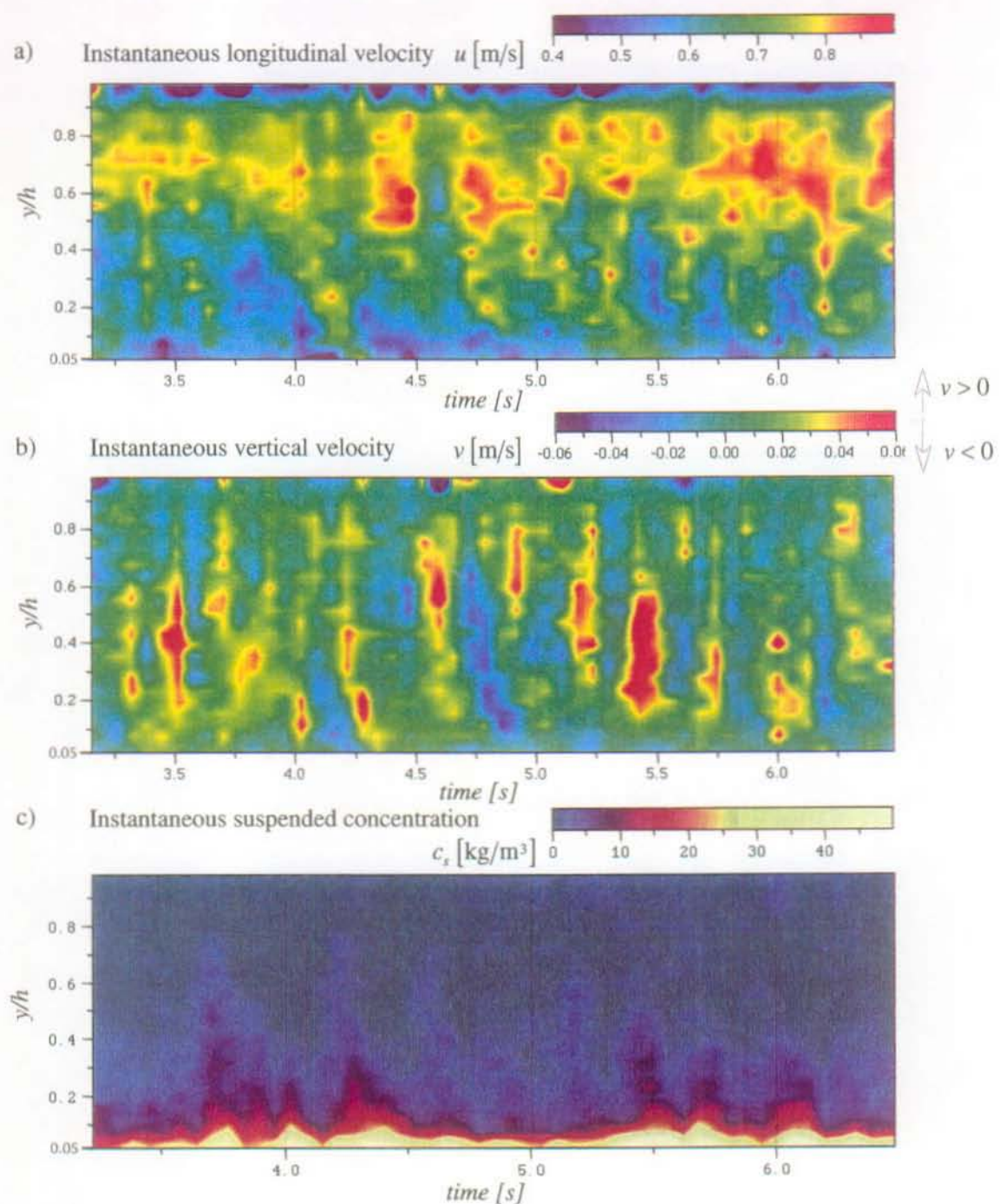


Fig. E14: Instantaneous velocity and concentration profiles

Q50S01 Sand I

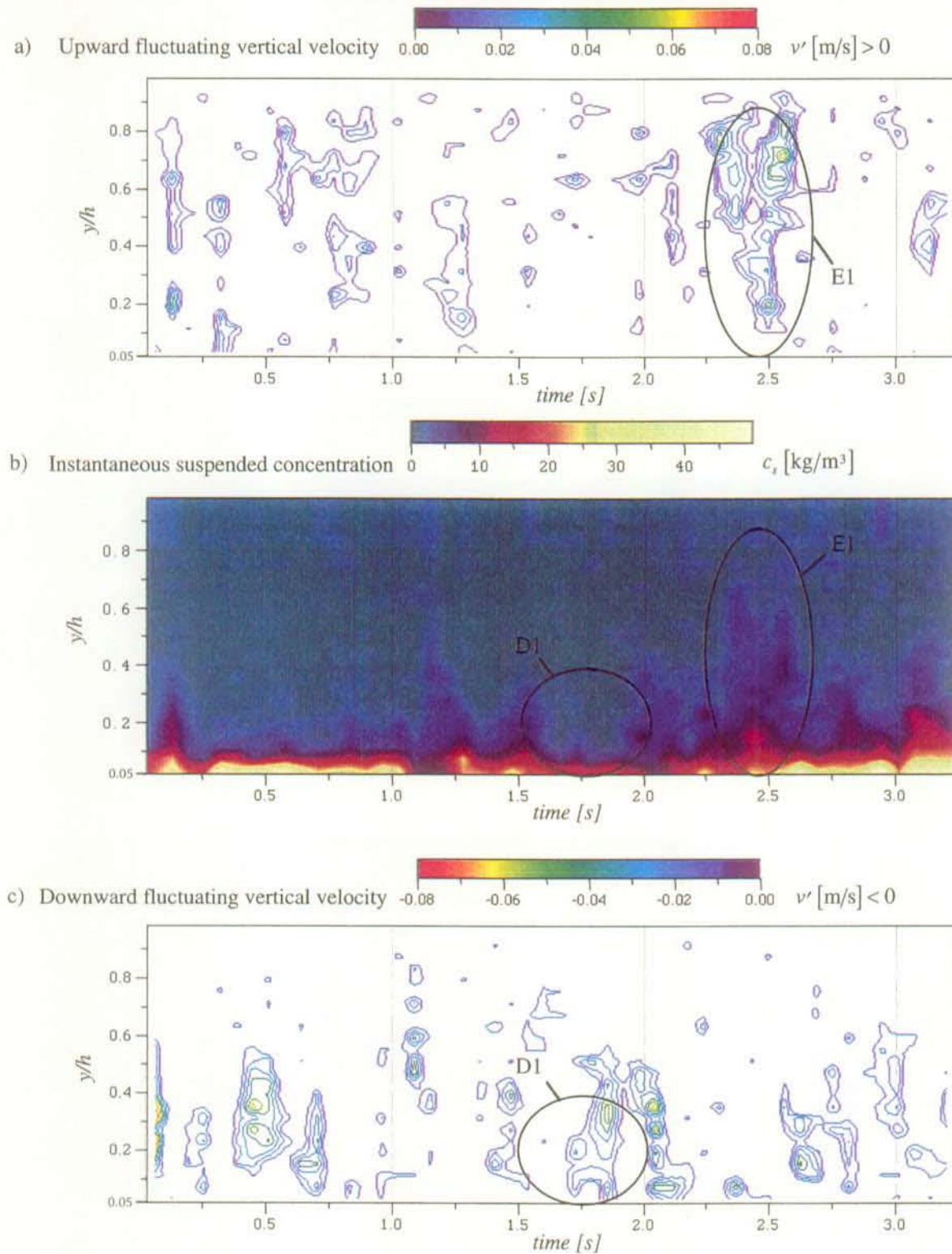


Fig. E15: Correlation between the concentration and the fluctuating vertical velocity

Q55S015 Sand I

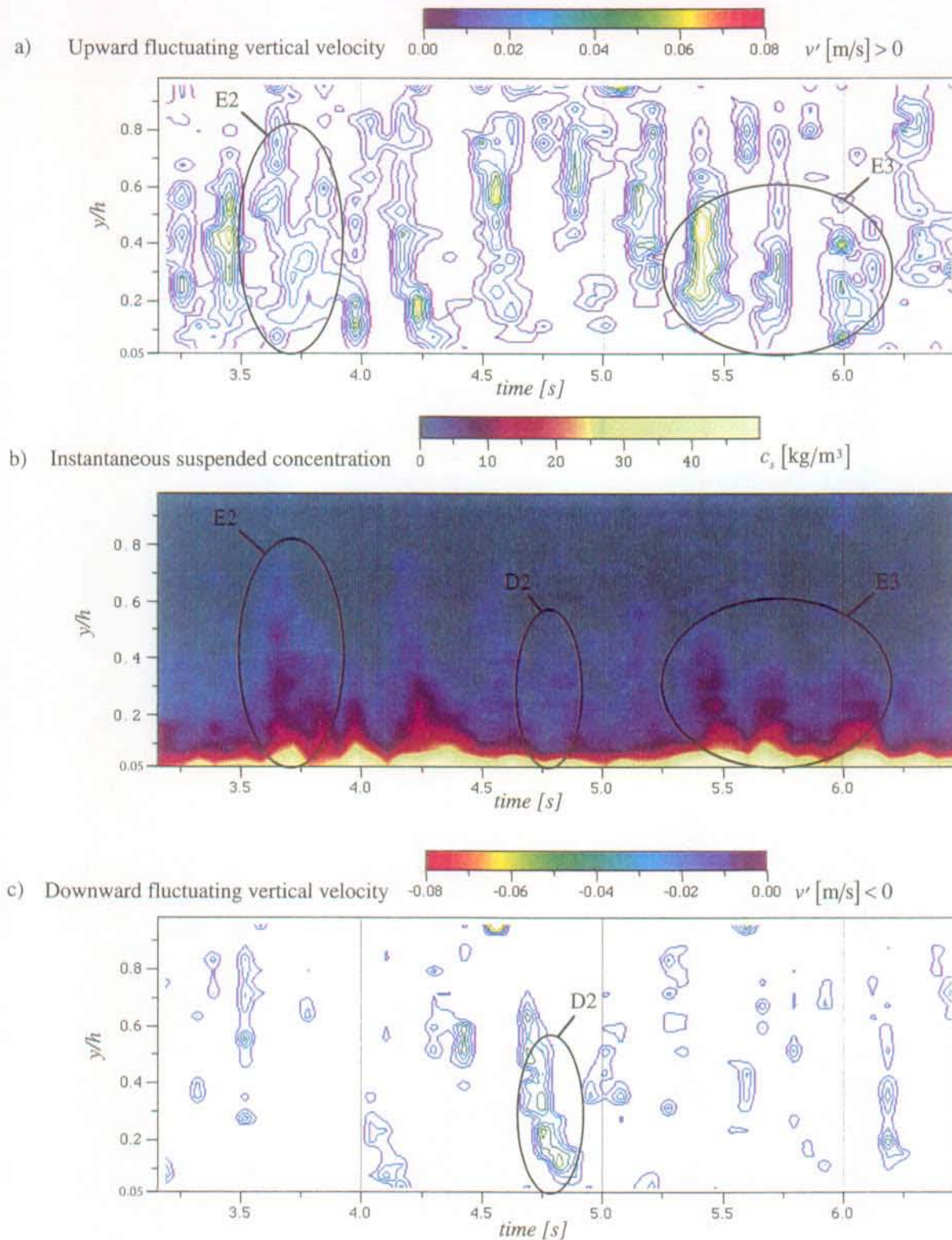
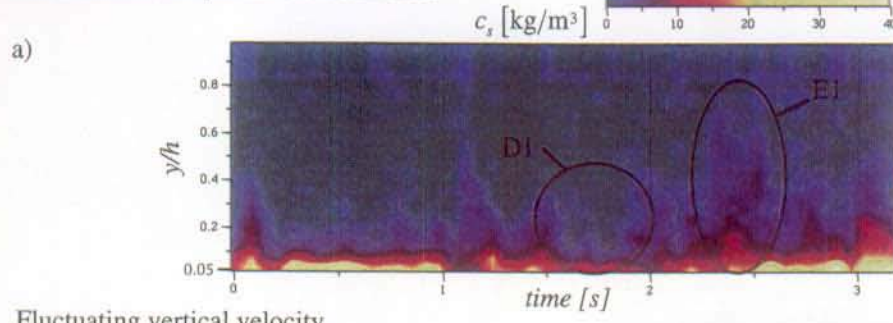


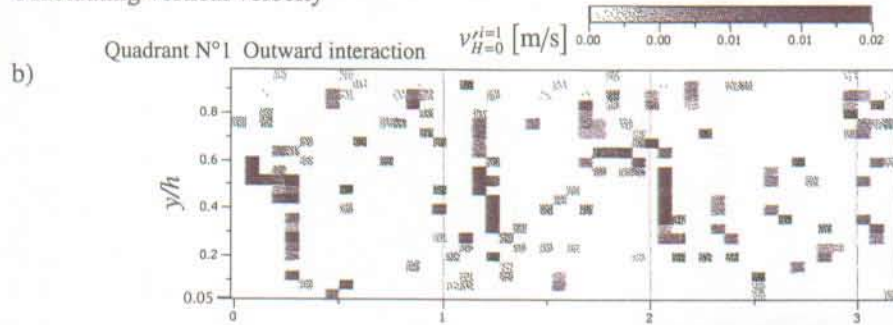
Fig. E16: Correlation between the concentration and the fluctuating vertical velocity

### Q50S01 Sand I

Instantaneous suspended concentration



Fluctuating vertical velocity



c)

Quadrant N°2 Ejection  $v_{H=0}^{i=2} [\text{m}/\text{s}]$

$y/h$

time [s]

$v_{H=0}^{i=2} [\text{m}/\text{s}]$

E1

d)

Quadrant N°3 Inward interaction  $v_{H=0}^{i=3} [\text{m}/\text{s}]$

$y/h$

time [s]

$v_{H=0}^{i=3} [\text{m}/\text{s}]$

e)

Quadrant N°4 Sweep  $v_{H=0}^{i=4} [\text{m}/\text{s}]$

$y/h$

time [s]

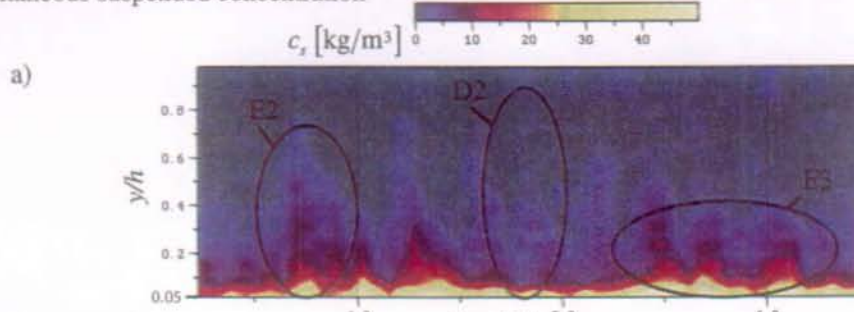
$v_{H=0}^{i=4} [\text{m}/\text{s}]$

D1

Fig. E17: Correlation between the concentration and the filtered fluctuating vertical velocity

### Q55S015 Sand I

Instantaneous suspended concentration



Fluctuating vertical velocity

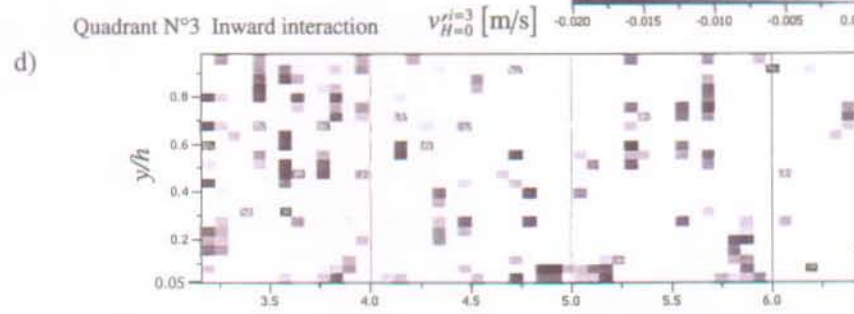
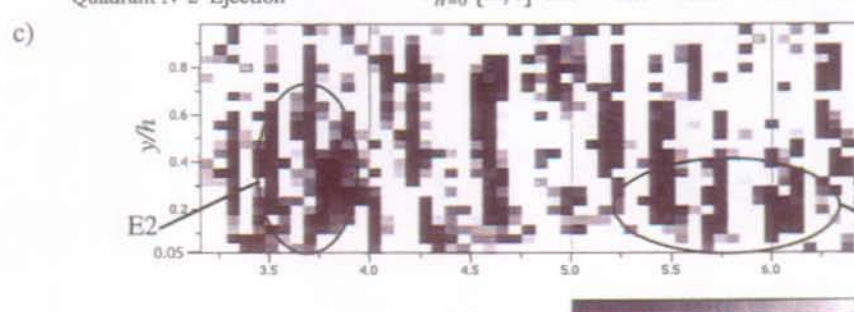
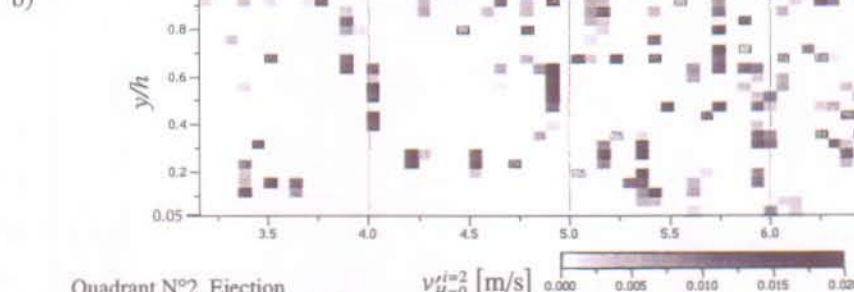
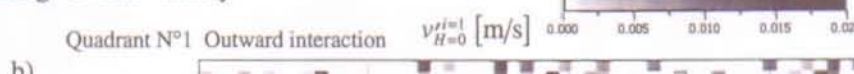


Fig. E18: Correlation between the concentration and the filtered fluctuating vertical velocity

Q50S01 Sand I

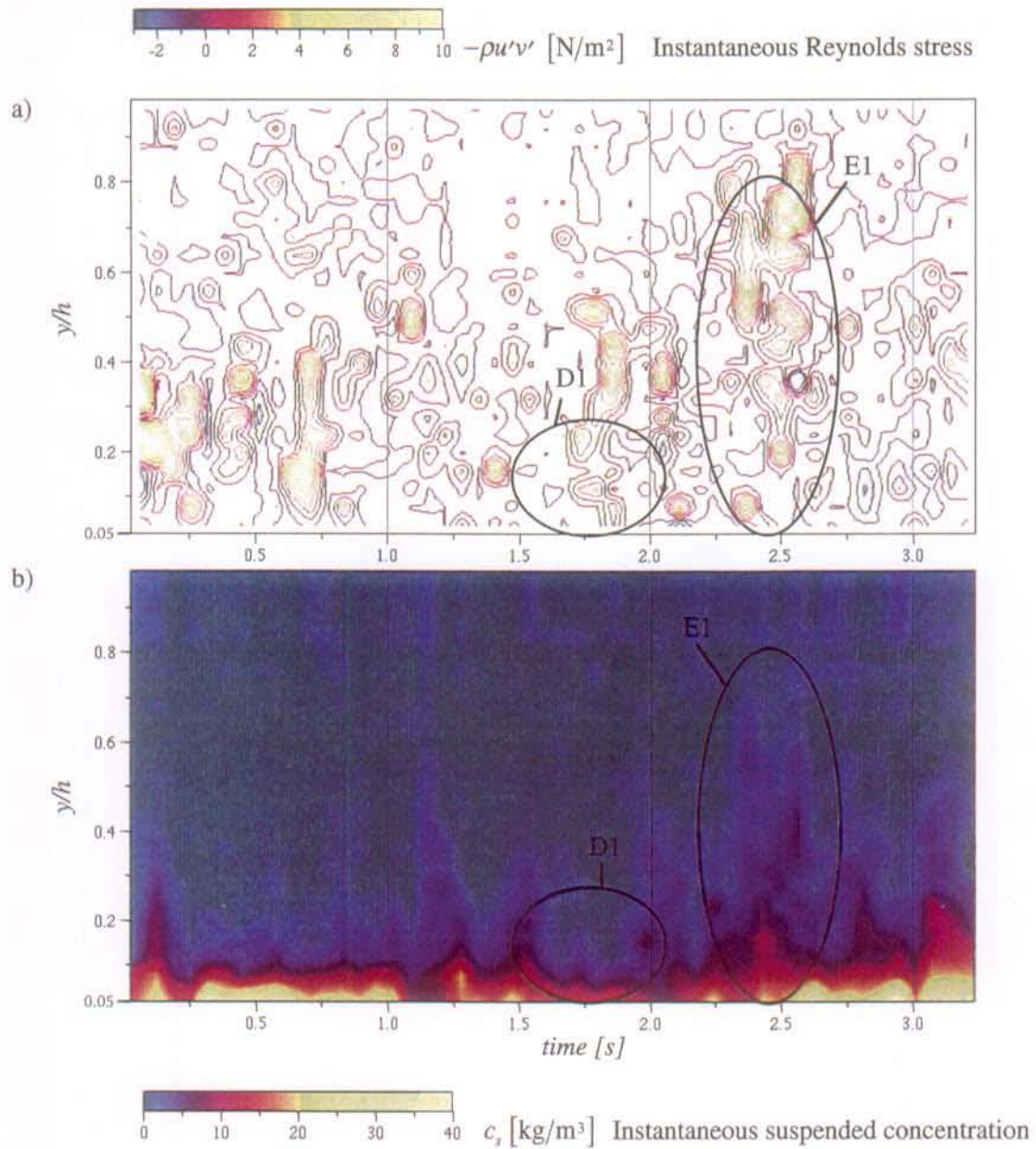
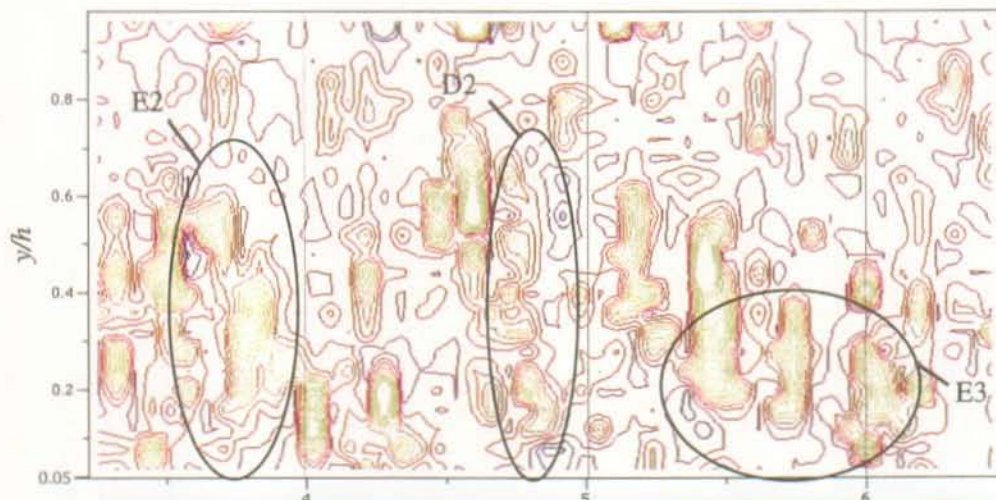


Fig. E19: Correlation between the concentration and the Reynolds stress

Q55S015 Sand I

$-\rho u'v'$  [N/m<sup>2</sup>] Instantaneous Reynolds stress

a)



b)

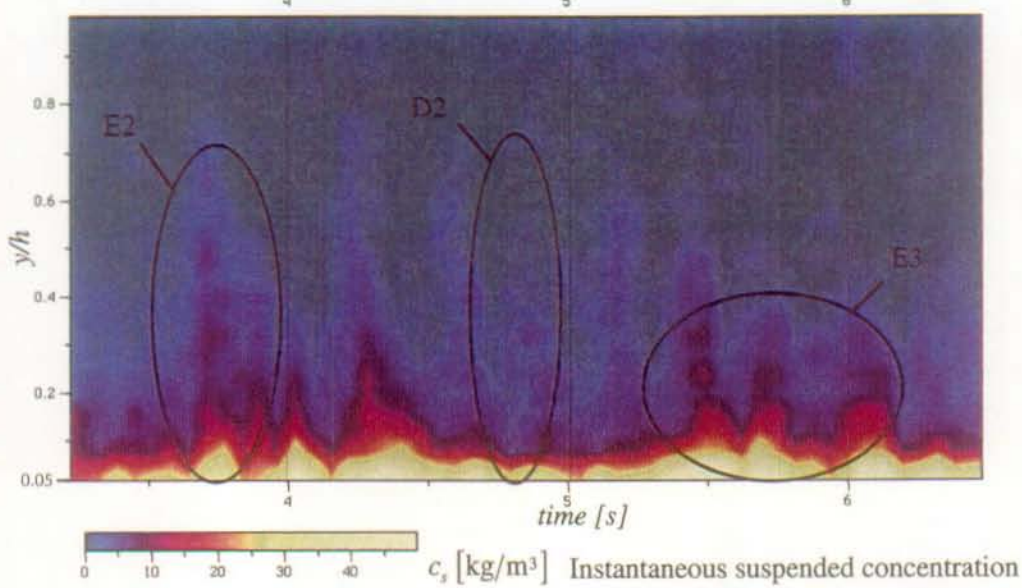


Fig. E20: Correlation between the concentration and the Reynolds stress

## E11 References

- GRASS, A. J. (1982). "The influence of boundary layer turbulence on the mechanics of sediment transport", *Euromech 156: Mechanics of Sediment Transport*, Istanbul, pp. 3-17.
- HINZE, J. O. (1975). *Turbulence*. McGraw-Hill, New York.
- LU, S. S. and WILLMARTH, W. W. (1973). "Measurements of the structure of the Reynolds stress in a turbulent boundary layer", *J. Fluid Mech.*, vol. 60, part 3, pp. 481-511.
- NAKAGAWA, H. and NEZU, I. (1977). "Prediction of the contributions to the Reynolds stress from bursting events in open-channel flows." *J. Fluid Mech.*, vol. 80, part 1, pp. 99-128.
- NAKAGAWA, H. and NEZU, I. (1981). "Structure of space-time correlations of bursting phenomena in an open-channel flow." *J. Fluid Mech.*, vol. 104, pp. 1-43.
- RASHIDI, M., HETSRONI, G. and BANERJEE, S. (1990). "Particle-turbulence interaction in a boundary layer", *Int. J. Multiphase Flow*, vol. 16, N°. 6, pp. 935-949.
- ROBINSON, S. K. (1991). "Coherent motions in the turbulent boundary layer." *Annual Rev. Fluid Mech.*, vol. 23, pp. 601-639.
- SUMER, B. M. and OGUZ, B. (1978). "Particle motions near the bottom in turbulent flow in an open channel." *J. Fluid Mech.*, vol. 86, part 1, pp. 109-127.

The experimental data were stored on a CD-ROM, which is obtainable from the Laboratoire de Recherches Hydraulique, EPFL, DGC-EPFL, 1015 Lausanne.

# CURRICULUM VITAE

Nom: **CELLINO**  
Prénom: **Massimo**  
Date de naissance: 2 Septembre 1969 à Turin (Italie)  
Nationalité: Italienne  
Adresse en Suisse/Italie: av. des Jordils, 4 via Governolo, 19  
1006 Lausanne 10128 Torino  
(079) 6078605 (011) 500494  
Téléphone:  
E-mail: massimo.cellino@epfl.ch  
Situation de famille: Célibataire

**Domaines d'expertise:** Hydraulique générale, hydraulique fluviale (transport de sédiments, laves torrentielles), analyse numérique.

## Formation:

- 1988 Diplôme de Géomètre, ITG C. e A. di Castellamonte, Grugliasco (Turin).
- 1988-1993 Faculté de Ingénierie civile de l'Ecole Polytechnique de Turin.  
Spécialisation en Ingénierie Hydraulique.
- 1993 Titre de la thèse de diplôme (Laurea in ingegneria idraulica):  
"Modello matematico per lo studio della propagazione dei debris-flow".  
Note finale du diplôme: 110/110 (Décembre 1993).
- 1993-1994 Mécanique des fluides (Monkewitz), Aérodynamique et Hydrodynamique, Calcul numérique (Deville), Hydraulique fluviale et cotière (Graf).
- 1993-1998 Travail de doctorat à l'Ecole Polytechnique Fédérale de Lausanne, EPFL  
Titre de la thèse:  
"Experimental Study of Suspension Flow in Open Channels"  
Titre décerné: Dr ès sciences techniques.

## Emplois:

- 1992-1993 Bourses d'études pour activités didactiques à l'Ecole Polytechnique de Turin.
- 1994 Consultation avec le bureau d'ingénierie: Ing. Alonzo (Turin)  
Calcul de l'adduction et du réseau de distribution pour un quartier de la ville de Pioggiasco (Italie) (environ 1000 habitants).  
Calcul de la structure métallique du stand FIAT au salon de l'auto de Frankfurt.
- 1994 Collaboration avec l'Ecole Polytechnique de Turin (Prof. Bianco).  
Dimensionnement d'une épi résistante aux ondes de debris-flows.  
(Dans le cadre de la thèse de diplôme de M. P. Berthod "Risques, prévisions et contrôle des "debris-flow" sur le territoire de la vallée d'Aoste", 1994).
- 1994 Simulation numérique d'une lave torrentielle dans le torrent Canalone (Susa, Italie) pour la protection de la centrale hydroélectrique de Pont Ventoux.  
Mandataire: Soc. Pont-Ventoux, Ecole Polytechnique de Turin.
- 1994-1998 Assistant / doctorant au Laboratoire de Recherches Hydraulique, EPFL.
- Juillet 1998 - présent Bonnard & Gardel Ingénieurs-conseils SA, Ingénieur civil au Service "Alimentation en eau". Avenue de Cour 61, Lausanne.

## Langues:

- Italien: Langue maternelle  
Français: Lu, écrit et parlé  
Anglais: Lu, écrit et parlé

**Publications:**

M. CELLINO

*Modello matematico per lo studio della propagazione dei debris-flow*

Tesi di Laurea, Politecnico di Torino, Torino, 1993

Relatori: Prof. G. PEZZOLI, Prof. G. BIANCO, Ing. M. ROSSO, Ing. M. ARATTANO

M. CELLINO, G. BIANCO, M. ARATTANO, M. ROSSO

*Modello cinematico per lo studio della propagazione in alvei naturali di debris-flow con notevole variazione del volume in moto*

IV Convegno internazionale di Geoingegneria

Torino, 1994

M. CELLINO, W. SHEN, U. LEMMIN, W.H. GRAF

*Measurements of instantaneous sediment flux profiles in sediment laden flows*

XXV Convegno di Idraulica e Costruzioni Idrauliche, Torino, 1996

M. CELLINO, W.H. GRAF

*Measurements on Suspension Flow in Open Channels*

XXVII IAHR Congress, San Francisco, 10-15 August 1997

M. CELLINO, W.H. GRAF

*Discussion on "Velocity Profiles for Particles and Liquid in Open-Channel Flow with Suspended Sediment"*

To be published in: J. Hydraulic Engineering

M. CELLINO, W.H. GRAF

*Suspended sediment-laden Flow in Open Channels under non-Capacity and Capacity Condition*

Submitted for publication

M. CELLINO, W.H. GRAF

*Experiments on Suspension Flow in Open Channels with Bed Forms*

Submitted for publication

W.H. GRAF, M. CELLINO

*Suspension Flows in Open Channels; Experimental Study*

Submitted for publication

W.H. GRAF, M. CELLINO

*Turbulence suppression in Suspension Flow*

XXVIII IAHR Congress, Graz, 10-15 August 1999